Identification of EFNB1 as a key immune modulator in brain with a dual role in T cell co-stimulation and glial cell immune resistance

DISSERTATION ZUR ERLANGUNG DES DOKTORGRADES DER NATURWISSENSCHAFTEN (DR. RER. NAT.) DER FAKULTÄT FÜR BIOLOGIE UND VORKLINISCHE MEDIZIN DER UNIVERSITÄT REGENSBURG

vorgelegt von

Ayse Nur Menevse, M. Sc.

aus

Istanbul, Türkei

im Jahr

2020

Identification of EFNB1 as a key immune modulator in brain with a dual role in T cell co-stimulation and glial cell immune resistance

DISSERTATION ZUR ERLANGUNG DES DOKTORGRADES DER NATURWISSENSCHAFTEN (DR. RER. NAT.) DER FAKULTÄT FÜR BIOLOGIE UND VORKLINISCHE MEDIZIN DER UNIVERSITÄT REGENSBURG

vorgelegt von

Ayse Nur Menevse, M. Sc.

aus

Istanbul, Türkei

im Jahr

2020

Das Promotionsgesuch wurde eingereicht am:

23.07.2020

Die Arbeit wurde angeleitet von:

Prof. Philipp Beckhove

Unterschrift:

Acknowledgments

If we imagine scientific career as life, making PhD resembles primary school times where you learn the basics essential for your entire life, while you can still play games with your friends. I would like to start by thanking those who made the "primary school" stage of my scientific life perfect and filled it with many good memories.

Foremost, I would like to start by thanking my supervisor Prof. Philipp Beckhove for being a supportive teacher and strong leader. I didn't hesitate when I left a worldwide known research institute in order to follow him and haven't regretted my decision a single day. Thank you Philipp for giving me the opportunity to perform my PhD in this great team with a very interesting project. As a future PI, the leadership skills I have learned from you were more valuable than your scientific guidance.

I am also very thankful to my PhD mentors Prof. Gunter Meister and PD. Dr. Klaus Dornmair for their supervision and valuable comments. Their suggestions during the research progress meetings helped shaping this project.

A special gratitude goes to all the AG-Beckhove members, my lab-family. I can't image how hard the past 4 years would have been without their presence and continuous support. Therefore I would like to thank Vale, my lab-sister, for guiding me through the "immune checkpoint" way. She is the one who made me often burst into laughter, which forced our other group members to come to our room and say "Ayse we can here you from the other side of the corridor" or ask "how much fun can you girls have in this PhD office". Special thanks go to Slava not only for being my unofficial PhD supervisor, but also for being our lab-mum and taking care of literally everything. It was great to have someone whose name you can cry out at any moment like you are calling for an ambulance. I would like to express my gratitude to Till for the bioinformatic analyses and his suggestions. Thanks to him, I did not need to be afraid of R. I would also like to extend my deepest gratitude to my master thesis supervisor, "boss", Antonio who actually had taught me most of the methods I needed for my PhD work. I am not only grateful for his scientific support but also for the cheerful memories he left to us. I'm extremely grateful to my "FACS & mouse work teacher" Chih-Yeh for being so nice, patient and helpful. If I am not afraid of the FACS machine anymore it is because of him.

Next, I would like to thank our technicians, the golden girls. Sometimes I had to spend long hours in the cell culture, but this was not a problem at all if Birgitta was sitting at the next hood. Thank you Birgitta for all the energy and support you give us. I want to thank Jasmin for her help especially during my busiest moments. Whenever I went to her with a guilty smiling face and a blood "Kegel" in my hand she always helped me, doesn't matter how busy she was. I also would like to thank Karin for taking care of the mice, which was the scariest part of this PhD for me. I would particularly like to thank my PhD colleagues Franzi and Julian for the cheer and fresh energy they brought into our family. The moments I shared with them always will make me smile. I also wish to thank our IT-hero Heiko for his constant support and his unique humor. Many thanks to Maria and Anchana for their suggestions and mature advises. I would also like to thank Nisit for preparing the soil of the HTP-screen and for the productive discussions at iOmx. I would like to express many thanks to our former colleagues Janine, Eva, Katja, Kathi, Mattea, Lilli and Wenke. My gratitude goes also to my dear Sabine Termer and Sabine Repp for their continuous administrative help at RCI. Special thanks to the members of AG-Abken and AG-Feuerer for being part of this friendly atmosphere.

Endless thanks go to my master's student Antonia Engelhorn, my bachelor's students Ursula Spirk, Hannnes Linder, Melanie Gimpl and my practical students Michaela Raab, Juliana Hünergardt, Tamara Woppman and Gabriela Zuleger. Despite the hard-work and sometimes frustrating results they kept their motivation high and contributed to this work enormously.

I would like to thank all our scientific collaborators, Prof. Dr. Peter Hau, Prof. Dr. Markus Riemenschneider, Prof. Dr. Martin Proescholdt, Dr. Arabel Vollmann-Zwerenz, Birgit Jachnik, and Dr. Tanja Rothhammer-Hampl for their constant support. I'd like to acknowledge the help of Prof. Michael Rehli, Dr. Nicholas Strieder and Dr. Claudia Gebhard for the RNA-Sequencing; Irina Fink and Rüdiger Eder for the FACS-sorting; and Carina Mirbeth for the radioactive experiments.

Above all, my greatest gratitude from the bottom of my heart goes humbly to my family, my mum Meltem, my dad Alpaslan, my brother Mehmet Eren Menevşe, and my grandma Güngör Gedik, for their love, prayers, sacrifices, continuous encouragement and support. Your trust and faith in me, is the source of motivation for fulfilling my dreams and continuing to walk on this path. May Allah not separate us.

Dedicated to my mum, dad, brother

and my dear grandmas

Abstract

Dysregulation of immune checkpoint molecule (ICM) signaling is one of the immune evasion mechanisms exerted by many tumors such as glioma. Despite the ongoing clinical trials for gliomas, targeting central nervous system (CNS) tumors remains a challenge due to its difficulties to balance the immune response while preventing autoimmune reactions. The severest autoimmune disease of the CNS is Multiple Sclerosis (MS). Similar to tumor reactive T cells uncovered in gliomas, myelin-specific cytotoxic CD8+ T cells were found in the brains of MS patients, which were indicated to play an important role in the immunopathology of MS.

I hypothesized that dysregulated ICM signaling on oligodendrocytes can contribute to glioma immune evasion and modulate autoreactive CD8+ T cell activity in MS patients. Our aim is to identify novel ICMs as therapeutic targets on oligodendrocytes that could potentially play a role in the immunopathology of glioma and MS.

To identify novel MS-glioma associated ICMs, I performed a high-throughput screen by co-culturing Flu-specific CD8+ T cells with the human oligodendrocyte cell line MO3.13-A2-Luc transfected with a siRNA library consisting 4155 genes. The impact of gene knockdown on T-cell cytotoxicity was measured using a luciferase readout system. I selected 56 HITs and performed a secondary screen both using oligodendrocytes and primary glioma cells. Among them, one of the ligands of the Ephrin receptor, EFNB1 was selected for further validation. I showed that, EFNB1 on glial cells induces effector cytokine secretion by T cells through the Akt-mTOR pathway and increases the T cell mediated killing of target cells. Besides, EFNB1 reverse signaling modulates glial cells' intrinsic immune resistance by inducing PD-L1 expression and the TGFβ pathway.

Taken together, I established an *in vitro* co-culture model for MS and glioma to identify novel ICM molecules that play a role in the antigen-specific CD8+ T cell mediated glial cell killing in a high-throughput manner. EFNB1 was identified as a promising immune modulatory target with a dual role in T cell co-stimulation and glial cell immune resistance.

Zusammenfassung

Die Dysregulation von Immun-Checkpoint-Molekülen (ICM) ist einer der Mechanismen, die von vielen Tumoren, wie z.B. Gliomen, eingesetzt werden, um Antworten des Immunsystems zu umgehen. Zurzeit laufen einige klinische Studien zu Immuntherapien von Gliomen, jedoch besteht bei der Behandlung von Tumoren des ZNS die Hauptherausforderung darin, die Immunantwort so auszubalancieren, dass Autoimmunreaktionen verhindert werden. Die schwerste Autoimmunerkrankung des ZNS ist die Multiple Sklerose (MS). So wie beim Gliom tumorreaktive T-Zellen auftreten, wurden ebenso in den Gehirnen von MS-Patienten myelinspezifische zytotoxische CD8+ T-Zellen gefunden, denen eine wichtige Rolle in der Immunpathologie bei MS zugewiesen wurde.

Ich stelle die Hypothese auf, dass fehlregulierte ICM-Signale auf Oligodendrozyten zur Umgehung der Immunantwort beim Gliom beitragen und diese ebenfalls die Aktivität autoreaktiver CD8+ T-Zellen bei MS-Patienten modulieren können. Unser Ziel ist es, neue therapeutische Ziele auf Oligodendrozyten zu identifizieren, die möglicherweise eine Rolle in der Immunpathologie von Gliom und MS spielen könnten.

Um neue MS-Gliom-assoziierte ICMs zu identifizieren, führten I ein Hochdurchsatzscreening durch, indem ich Flu-spezifische CD8+ T-Zellen mit humanen Oligodendrozytenzellen der Linie MO3.13-A2-Luc ko-kultivierte, welche mit einer siRNA-Bibliothek aus 4155 Genen transfiziert sind. Der Einfluss des Herunterregulierens der Gene auf die T-Zell-Zytotoxizität wurde mit einem Luciferase-Auslesesystem gemessen. Aus den 126 besten HITs wählte ich 56 HITs aus und führte ein sekundäres Screening sowohl mit Oligodendrozyten als auch mit primären Gliomzellen durch. Von ihnen wurde einer der Liganden der Eph-Rezeptoren, EFNB1, zur weiteren Validierung ausgewählt. I zeigten, dass EFNB1 auf Gliazellen die Sekretion von Effektorzytokinen durch T-Zellen über den Akt-mTOR-Signalweg aktiviert und die T-Zell-vermittelte Abtötung von Zielzellen erhöht. Gleichzeitig moduliert EFNB1 die intrinsische Immunresistenz von Gliazellen, indem es die Expression von PD-L1 und den TGFβ Signalweg induziert.

Insgesamt haben I ein *in vitro* Ko-Kulturmodell für MS und das Gliom etabliert, um neue ICM-Moleküle zu identifizieren, die bei der antigenspezifischen CD8+ T-Zell-vermittelten Abtötung von Gliazellen im Hochdurchsatzverfahren eine Rolle spielen. EFNB1 wurde als ein vielversprechendes immunmodulierendes Ziel identifiziert, das sowohl bei der Kostimulation von T-Zellen, als auch in der Immunresistenz bei Gliazellen eine Rolle spielt.

Table of Contents

1 Introduction

1.1 Immune Checkpoint Signaling in Health and Disease

1.1.1 The physiological role of immune checkpoint signaling in T cells

T cells represent a very important and potent effector component of the immune system. Proper activation of naïve T cells requires stimuli from at least two signals. Signal 1 is triggered after the engagement of the T cell receptor (TCR) with the cognate antigenic peptide presented by the major histocompatibility complex (MHC) on antigen presenting cells (APCs) [1]. For full T cell activation a co-stimulation signal (signal 2) is required through the interaction between co-stimulatory ligands expressed on APCs and their counter receptors on T cells [2]. Following activation, T cells induce the expression of co-inhibitory receptors as a negative feedback mechanism [3]. These co-stimulatory and co-inhibitory receptors (immune checkpoint molecules) cluster with the TCR at the immunological synapse, where they interfere with downstream signaling cascades to fine-tune the magnitude of the T cell response and play an essential role in T cell differentiation, survival and function. T cells exert strong effector mechanisms against cells infected with pathogens, however, this effector function may also result in potential self-tissue damages [4]. In order to prevent such autoimmune reactions and to restore quiescence after inflammation, TCR signaling is strictly controlled and regulated by tolerance mechanisms [5].

Self-tolerance refers to the unresponsiveness of the immune system to self-antigens (self-Ags) [1]. During their development, autoreactive T cells are controlled by central tolerance mechanisms in the thymus, where medullary thymic epithelial cells (MTECs) express tissue-restricted antigens and thereby facilitate the negative selection of autoreactive T cell clones [6, 7]. However the ectopic gene expression in the thymus can be dysregulated, which may lead to escape of autoreactive T cells from the negative selection and their subsequent entry into the periphery [8]. In the periphery, inappropriate responses of autoreactive T cells are prevented by co-inhibitory ligands expressed on self-tissues [4].

The repertoire of immune checkpoint molecules expressed on T cells is regulated in a spatiotemporal manner and highly versatile [2]. The balance between co-stimulatory

and co-inhibitory receptors has a crucial role in T cell activation and in preserving self-tolerance, as this determines the functional outcome of the TCR signaling [2]. In recent years, a large number of immune checkpoint molecules have been identified and functionally characterized (Figure I). Most of these molecules belong to immunoglobulin superfamily (IgSF) and tumor necrosis factor receptor superfamily (TNFRSF) [2].

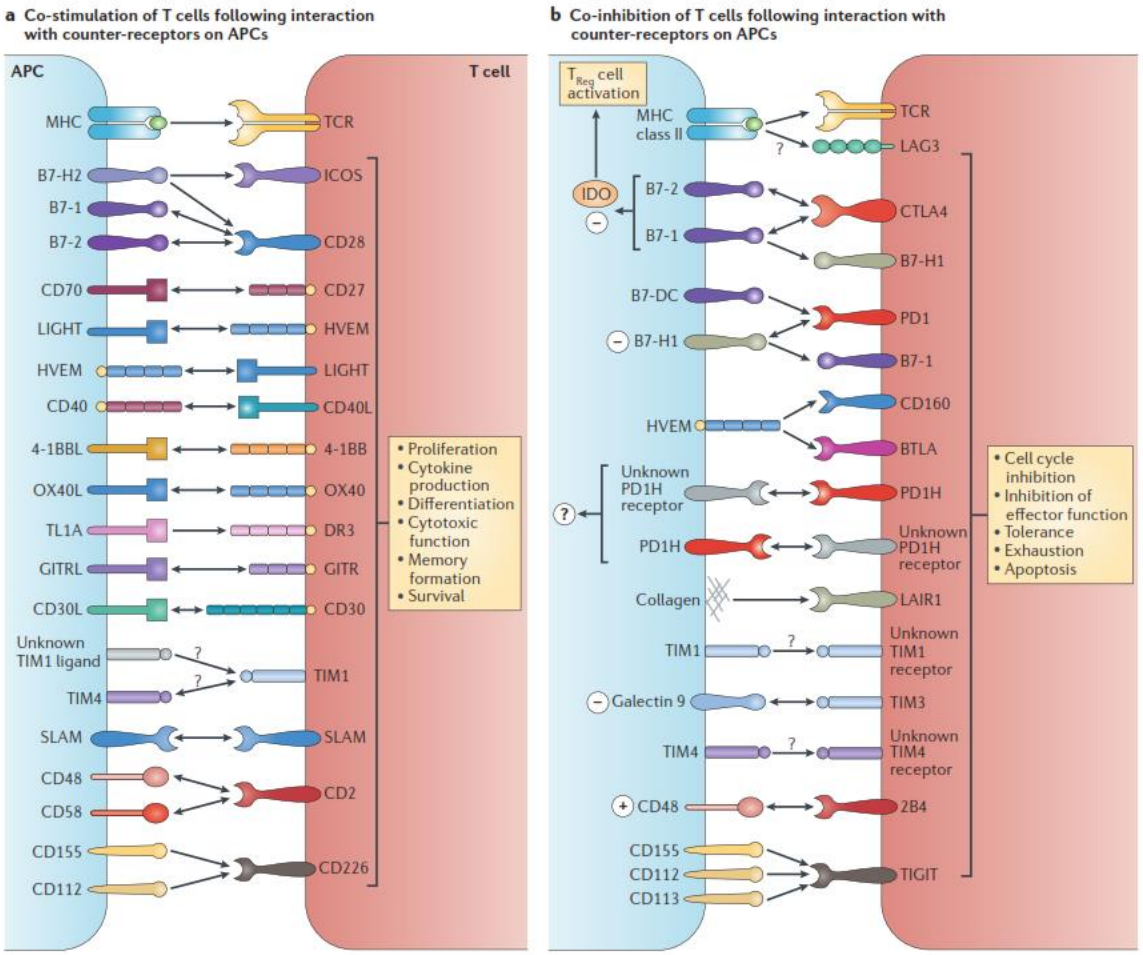

Figure I: Co-stimulatory (A) and co-inhibitory (B) receptor-ligand interactions between T cells and antigen presenting cells. Coupled to TCR signaling, the repertoire of immune checkpoint molecules expressed on T cells plays an important role in proliferation, effector function, differentiation, tolerance and survival (Adapted from [2]).

1.1.1.1 Co-stimulatory immune checkpoint molecules

CD28 is one of the most well-described IgSF member co-stimulatory receptor expressed on T cells. The two-signal model of T cell activation has been proposed after the identification of CD28 on T cells and its ligand CD80 (B7-1) on APCs [2]. Constitutive expression of CD28 on $CD4^+$ and $CD8^+$ T cells provides a strong and rapid co-stimulatory

signal for T cell growth and survival [9]. CD28 mediates its co-stimulatory functions through YMNM and PYAP motifs in its cytoplasmic domain [10]. YMNM motif interacts with the p85 subunit of phosphatidylinositol 3-kinase (PI3K), which in turn activates the Akt signaling pathway. The CD28-PI3K-Akt axis promotes T cell proliferation and survival by activating nuclear factor-κB (NF-κB), nuclear factor of activated T cells (NFAT), BCL-XL, mammalian target of rapamycin (mTOR) and several other downstream targets [10]. Additionally, through its PYAP motif, CD28 associates with the lymphocyte cell-specific protein-tyrosine kinase (Lck) and the growth factor receptor-bound protein 2 (GRB2), thereby promoting NFAT nuclear translocation and enhanced IL-2 production [11].

ICOS (Inducible T cell co-stimulator) is another important T cell co-stimulatory receptor belonging to the IgSF superfamily. ICOS stimulates T cells upon ligation to B7-H2 (ICOSLG) whose expression can be induced on peripheral tissues. Although CD28 can also interact with B7-H2, ICOS has a higher affinity for B7-H2 [12]. ICOS is expressed by activated $CD4^+$ and $CD8^+$ T cells [13]. Upon ligand binding ICOS recruits both p85 and p50α subunits of PI3K and thereby promotes a stronger AKT signaling compared to CD28 [14]. ICOS-PI3K-AKT axis induces IL-4, IL-10 and IL-21 production, which is essential for development of $CD4^+$ T helper 2 cells (T_H2) and T follicular helper cells (T_{FH}). However, due to the lack of interaction with GRB2 and LCK, ICOS cannot induce IL-2 production as CD28 [15].

4-1BB (also known as CD137 or TNFRSF9) and ***OX40*** (also known as TNFSF4) are members of the TNFRSF and augment the TCR-CD3 signaling to promote cell cycle progression, cytokine production and T cell survival [16]. They are expressed on activated $CD4^+$ and $CD8^+$ T cells, where their ligands 4-1BBL (also known as CD137L) and OX40L are expressed on activated macrophages, dendritic cells (DCs) and B cells [13]. After TCR engagement, the expressions of 4-1BB and OX40 are upregulated on T cells and they interact with their ligands on APCs in a trimerized manner. Upon trimerization TNF receptor-associated factor (TRAF) adaptor proteins are recruited to their cytoplasmic domains and thereby activate multiple signaling molecules such as NF-κB, JNK and MAPK [16]. 4-1BB can recruit TRAF1-3, whereas OX40 binds TRAF2, TRAF3 and TRAF5 [17, 18]. Co-stimulation mediated by 4-1BB and OX40 leads to upregulation of anti-apoptotic factors such as BCL-2 and BCL-XL thereby promoting T cell survival.

Additionally 4-1BB and OX40 downstream signaling activate Akt and promote cell cycle progression [16].

1.1.1.2 Co-inhibitory immune checkpoint molecules

CTLA-4 (Cytotoxic T-lymphocyte protein 4) plays a crucial role in suppressing T cell response following activation [9]. It binds to the same ligands (CD80 and CD86) as the co-stimulatory molecule CD28, but with a higher affinity. By out-competing CD28, CTLA-4 dampens the stimulatory signaling provided by the CD28-CD80/86 axis. Accumulation of CTLA-4 in the immunological synapse, excludes CD28 from TCR proximity, which in turn prevents the recruitment and activation of PKCθ [19]. CTLA-4 also disrupts the stimulatory signaling by recruiting phosphatases such as SHP2 and PP2A to the immunological synapse, which dephosphorylate key TCR and CD28 downstream signaling components such as Lck and Akt [9, 20]. This leads to decreased IL-2 production and T cell anergy [21]. As naïve and resting memory T cells lack CTLA-4 expression on their surface, CD28-mediated co-stimulation dominates upon antigen recognition. Upon one hour antigen engagement, CTLA-4 is shuttled to the cell surface from intracellular protein vesicles, and initiates feedback inhibition [22]. Studies with *Ctla-4* knockout mice demonstrated the fundamental role of this feedback mechanism in immune tolerance, since mice lacking Ctla-4 presented a lethal systemic immune hyperactivation phenotype as well as and multiorgan destruction [23].

PD-1 (Programmed cell death-1, CD279) is another well-described co-inhibitory receptor of the IgSF family and is expressed on activated T cells, B cells, Natural killer T (NKT) cells, activated monocytes and DCs [13, 24]. Its ligand PD-L1 (also known as B7-H1 and CD274) is widely expressed on non-hematopoietic parenchymal cells as well as on hematopoietic cells. PD-L2 (B7-DC, CD273), another ligand of PD-1, is only expressed by DCs and myeloid cells [5]. Upon ligation by its ligands, PD-1 becomes phosphorylated on intracellular tyrosine residues: the immunoreceptor tyrosine-based inhibitory motif (ITIM) and the immunoreceptor tyrosine-based switch motif (ITSM) [25]. Consequently, the phosphorylated ITSM domain recruits and activates protein phosphatases such as SHP-1 and SHP-2, which inhibit proximal TCR downstream signaling [26]. Similar to CTLA-4, PD-1 cluster with TCR at the immunological synapse, and thereby can induce dephosphorylation of CD3ζ, ZAP70 and PKCθ and shuts down TCR signaling after activation [27, 28].

LAG3 (Lymphocyte activation gene 3, CD223) is expressed on T cells 3-4 days after activation, and plays an important role as an inhibitory immune checkpoint molecule. It belongs to the immunoglobulin superfamily (IgSF) and co-localizes with the CD3/ TCR complex [29]. The only described ligand for LAG-3 is MHC-II [30] and this interaction prevents the binding of CD4-TCR to the same MHC molecule and thereby hinders TCR signaling [31]. LAG-3 also exerts inhibitory function on $CD8^+$ T cells. Studies in mice demonstrated that, LAG-3 knockout CD8 T cells have a higher proliferation and cytokine production rate [32]. However, the exact mode of action by which LAG-3 inhibits T cell function is not fully understood yet [33]. LAG-3 induces downstream signaling via its cytoplasmic KIEELE motif and suppresses $CD4^+$ and $CD8^+$ T cell expansion by preventing entry to the S-phase during the cell cycle [34]. Still, the interaction partners of KIEELE motif need to be identified [31].

TIM3 (T cell immunoglobulin and mucin domain 3) is one of the immunoglobulin superfamily (IgSF) member proteins and was first identified on IFN-γ producing $CD4^+$ and $CD8^+$ T cells. It is also expressed by NK cells, regulatory T cells (Tregs) and monocytes [2, 35]. Several different ligands such as galectin 9, phosphatidylserine (PtdSer), CEACAM1 and high mobility group protein B1 (HMGB1), have been identified to bind to different regions of TIM3 [35]. When TIM3 is not engaged to its ligands, its intracellular domain interacts with HLA-B-associated transcript 3 (BAT3), which recruits catalytically active Lck [36, 37]. Lck recruitment to TIM3 at the immunological synapse enhances T cell activation [35]. Upon binding to galectin 9 or CEACAM1, the cytoplasmic tail of TIM3 becomes phosphorylated, dissociates BAT3-Lck complex and recruits the tyrosine kinase FYN [38]. TIM3 acts as a co-inhibitory receptor by using FYN downstream signaling which dephosphorylates Lck, disrupts the immunological synapse and induces T cell anergy and apoptosis [36, 39].

Imbalances in immune checkpoint signaling in terms of insufficient co-inhibition and/or excessive co-stimulation are responsible to cause aberrant T cell activation and lead to autoimmunity. Conversely, lack of proper co-stimulation and excessive co-inhibition of immune cells are important mechanisms taken over by tumor cells to escape anti-tumor immunity (Figure II).

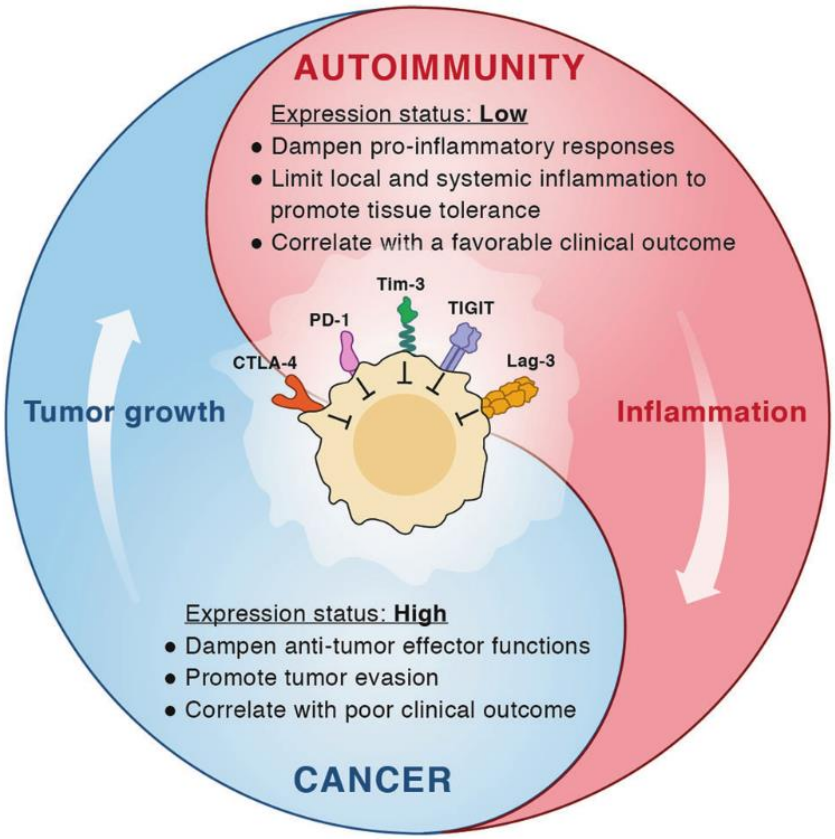

Figure II: Involvement of co-inhibitory receptors in autoimmunity and cancer as two different sides of a medallion. In the tumor, co-inhibitory immune checkpoints on T cells impair the function of tumor reactive T cells and thereby contribute to tumor immune evasion. Conversely, the same molecules play important roles in reducing tissue inflammation and maintaining self-tolerance in autoimmune diseases (Adapted from [5]).

1.1.2 Dysregulation of co-stimulatory and co-inhibitory receptors in autoimmune diseases

In both humans and mice dysregulation of immune checkpoint molecules has been demonstrated to play a crucial role in autoimmune diseases [1, 4]. Relevance of co-stimulatory receptor ligand interactions in autoimmune diseases have been studied with the help of mouse models. Mice deficient for CD28 delayed the development of lupus and displayed resistance to collagen induced arthritis (CIA, RA model in mice) [40, 41]. The CD28-B7 axis has been shown to be crucial for development of EAE (Experimental autoimmune encephalomyelitis, a multiple sclerosis model in mice). *CD28*$^{-/-}$ $MBP_{1\text{-}17}$ TCR transgenic mice abrogated developing spontaneous EAE [42]. Similarly, C57BL/6J mice deficient for B7.1 and B7.2 were resistant to develop $MOG_{35\text{-}55}$-induced EAE [43].

ICOS-ICOSL and OX40-OX40L pathways have been found to be activated during RA pathogenesis. Blockade of ICOSL alleviated CIA and decreased the level of auto-antibodies, whereas lack of OX40-OX40L signaling led to decreased IFN-γ levels and auto-antibody secretion and increased tissue integrity [44-46]. Within active lesions in both EAE and MS (multiple sclerosis) patients, OX40 expression has been found to be elevated on autoreactive T cells and depletion of $OX40^+$ T cells decreased EAE [47, 48]. Moreover, OX40L overexpressing transgenic mice developed more severe EAE [49]. Similar to B7.1 and B7.2 deficient mice, 4-1BBL deficient mice become resistant to MOG_{35-55}-induced EAE and showed decreased autoreactive T cell infiltration [50].

The role of co-inhibitory receptors such as CTLA-4, PD-1, TIM-3 and LAG-3 in T cell function was first discovered in the autoimmune disease models in mice, where lack or blockade of these molecules associated with development of autoimmune diseases [5].

Global *Ctla-4* knockout mice developed lethal autoimmunity characterized by lymphoblast infiltration into multiple organs such as liver and heart [23, 51]. In adult mice, deletion of *Ctla-4* was found to cause non-lethal autoimmune diseases in different organs [52]. Additionally, administration of monoclonal antibodies blocking CTLA-4 exacerbated the disease in relapsing-remitting EAE mice [53]. In vivo blockade of CTLA-4 in young diabetes-susceptible mice promoted rapid onset of diabetes [54]. In humans, an allelic variation in *CTLA-4* gene, responsible to increase CTLA-4 mRNA levels, was found to be associated with susceptibility to type 1 diabetes (T1D) [55].

Several studies showed that loss of *Pdcd-1* in mice causes autoimmune cardiomyopathy and lupus-like disease on BALB/c and C57BL/6 background, respectively [56, 57]. T1D susceptible NOD mice, that lack PD-1, presented earlier onset and increased incidence of diabetes [58]. Moreover, blockade of PD-1 in EAE models increased the progression and the severity of the disease. In humans, the susceptibility to a wide range of autoimmune diseases such as systemic lupus erythematosus (SLE), rheumatoid arthritis (RA), and MS is associated with polymorphisms in the *PDCD1* gene [59-63].

Similar to treatments with anti-PD-1 and anti-CTLA-4, in vivo blockade of TIM-3 exacerbated EAE and autoimmune diabetes [64, 65]. In MS patients, TIM-3 levels on T-cell clones isolated from cerebrospinal fluid (CSF) were found to be lower compared to clones from control subjects [66]. Remarkably, MS patients treated with IFNβ, an FDA-

approved drug for MS, showed restoration of TIM-3 expression and milder disease activity [67]. Similarly, decreased TIM-3 levels on $CD4^+$ and $CD8^+$ T cells are inversely correlated with severity of several autoimmune diseases such as RA, ulcerative colitis (UC) and psoriasis [68-70]. Similar to the *PDCD1* locus, polymorphisms in the *TIM-3* gene have been associated with several autoimmune diseases in humans [71].

In contrast to mice with germline deletions of CTLA-4 and PD-1, LAG-3 global knockout mice do not show increased susceptibility to autoimmune diseases unless bred to a permissive genetic background. LAG-3 deficient NOD mice accelerated T1D with an incidence of 100% [72].

The involvement of immune checkpoint molecules in several autoimmune diseases makes their manipulation as a promising immunotherapeutic strategy. As mentioned in the previous section (Figure II), an imbalance in the same signaling cascades play crucial role in tumor immune escape.

1.1.3 Immune checkpoint signaling in cancer immune escape

Cancer immunoediting refers to the 3E-phases of the interaction between the tumor cells and the immune system, where E's stand for elimination, equilibrium and escape. During the onset of tumor development, cancerous cells can be recognized and eliminated by the host's immune cells. However, in the equilibrium stage tumor cells develop resistance mechanisms against immune-mediated killing. Further shift in the balance in favor of tumor cells results in progression of cancer cells capable of escaping an immune attack [73]. One of the immune escape mechanisms developed by tumor cells is the expression/overexpression of co-inhibitory ligands, which impair the function of tumor infiltrating lymphocytes (TILs) upon interacting with their cognate receptors [22].

The first insights about the involvement of co-inhibitory receptors in tumor development arose from studies where the in vivo blockade of CTLA-4 showed tumor control and/or regression in mice models [74-76]. In human hematologic and solid tumors, CTLA-4 levels negatively correlate with clinical outcome [77, 78]. Blockade of CTLA-4 is the first in line treatment (FDA-approved checkpoint blockade therapy) for metastatic melanoma [79].

Interaction between T cells and tumor cells through the PD-1/PD-L1 axis is another important determinant in anti-tumor immune response. In several mice models, global knockout or in vivo blockade of PD-1 resulted in accelerated tumor clearance [80, 81]. In humans, treatment with anti-PD-1 antibodies promotes tumor regression in patients with melanoma, renal cancer, lung cancer and colon cancer [82]. By upregulating PD-L1 expression, tumor cells can directly inhibit the effector function of cytotoxic T cells [83]. In several tumor entities, levels of PD-1/PD-L1 have been associated with poor prognosis and can be used as a predictive marker of response to anti-PD-1/anti-PD-L1 therapy [84]. Moreover, several PD-1 polymorphisms associated with susceptibility to various types of cancers have been identified [85].

Beyond CTLA-4 and PD-1, the role of the co-inhibitory receptors TIM-3 and LAG-3 has been deciphered in cancer immune escape. The most dysfunctional population of $CD8^+$ TILs is characterized by elevated TIM-3 and PD-1 expression [86, 87]. In vivo blockade of TIM-3 showed reduction in tumor growth and improvement in tumor-specific $CD8^+$ T-cell function [37, 87]. In line, high expression levels of TIM-3 are associated with poor prognosis in colon, gastric, non-small cell lung, and clear cell renal carcinoma [88]. Similar to PD-1, polymorphisms in the *TIM-3* locus indicate higher risk of developing renal cell carcinoma, pancreatic cancer and non-small cell lung cancer [89-91]. So far, clinical trials assessing TIM-3 blockade showed promising results, especially when administered as combinatorial therapy with anti-PD-1 [92].

Another promising co-inhibitory target for anti-tumor immunotherapy is LAG-3, which is widely expressed by tumor-infiltrating lymphocytes in multiple tumor entities [93]. In preclinical models, the blockade of LAG-3 resulted in reduced growth of transplantable tumors [32]. Importantly, LAG-3 synergizes with PD-1 signaling to induce tumor progression [94, 95]. Promising results have been obtained from the ongoing clinical trials with LAG-3 blockade as monotherapy or in combination with anti-PD-1 [95].

As an immunotherapeutic strategy, immune checkpoint blockade hold promise for many solid tumors, yet so far the blockade of well characterized immune-modulators PD-1, PD-L1 and CTLA-4 showed limited clinical benefit in many different tumor entities and most of the patients do not respond to current checkpoint therapies.

Other important limitations of checkpoint blockade therapy are the immune related adverse events (irAEs). Patients treated with checkpoint inhibitors often develop a wide range of autoimmune related side effects affecting organs including the gut, skin, lung, liver, joints and pancreas [96]. These adverse reactions highlight the importance of maintaining the balance in immune checkpoint signaling for self-tolerance [4]. Based on that, identification of novel immune checkpoint molecules is of fundamental need in the field of immunotherapy to achieve a more effective tumor-specific immunity without inducing autoimmune-like side effects (Figure III).

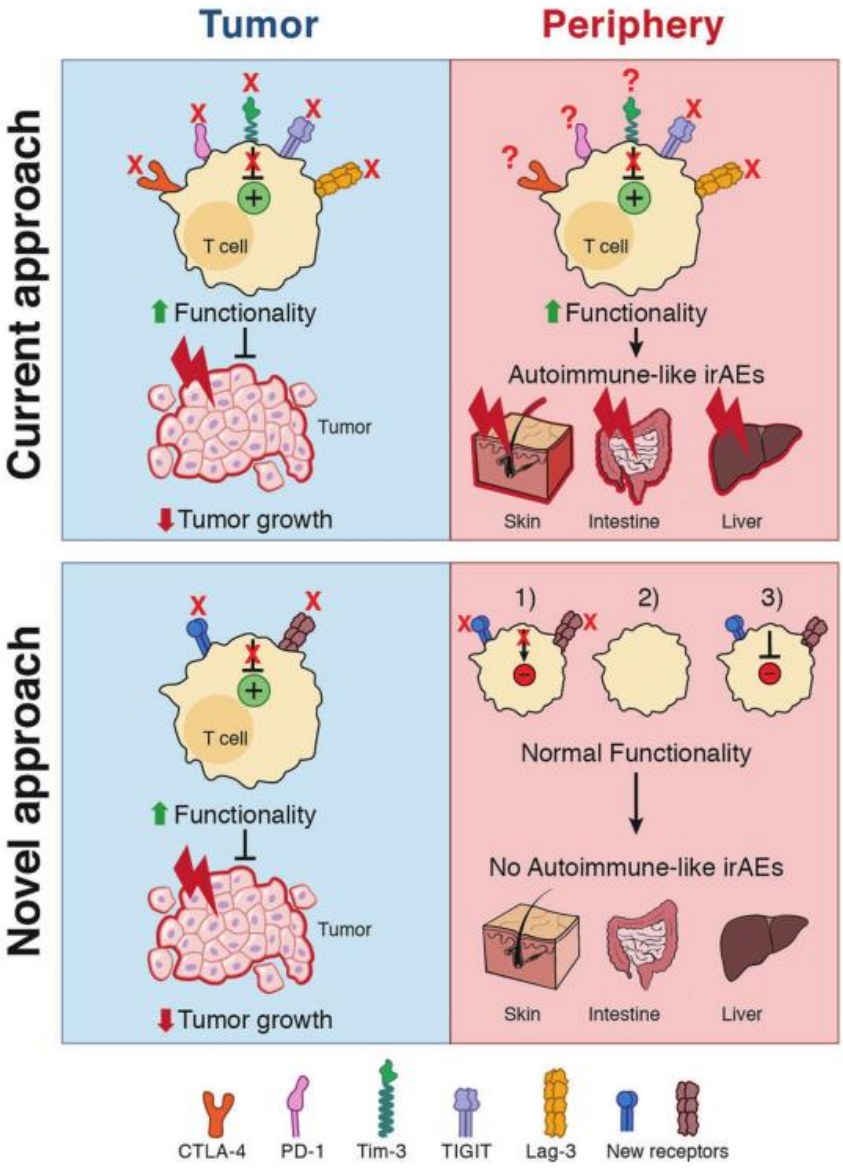

Figure III: Future perspectives for checkpoint blockade therapy to eliminate autoimmune-like immune related adverse events (irAEs). Top panel: Current approaches for checkpoint blockade enhance T cell function, induce anti-tumor immunity and reduce tumor growth. However, T cells with improved functionality induce at the same time severe autoimmune-like irAEs affecting tissues such

as skin, intestine and liver. Bottom panel: In future novel immune checkpoints targets should be identified, whose blockade mediate a strong immune response in the tumor, without inducing autoimmune-like toxicities (Adapted from [5]).

As described above, imbalances in immune checkpoint signaling can lead to development of autoimmune diseases or promote tumor immune escape. Brain is one of the organs where both of these immunopathological malignancies can develop either as glioma or as multiple sclerosis.

1.2 Multiple Sclerosis

1.2.1 Epidemiology, risk factors and pathology of MS

Being one of the most common and disabling diseases, multiple sclerosis (MS) is a chronic demyelinating, neuroinflammatory autoimmune disorder of the central nervous system (CNS) [97]. Approximately 2.3 million young adults are affected by MS worldwide, where the female to male ratio among the affected individuals is 3:1. The prevalence differs between countries and ranges from 2 per 100,000 individuals in Asia to 1 per 1,000 individuals in European countries [98].

Although the exact cause of MS still remains unknown, it is accepted to be an autoimmune disease. Importantly, genetic and environmental risk factors play a role in the development of the disease [97, 99]. Among the well-characterized environmental risk factors, Epstein–Barr virus (EBV) infection, active or passive smoking, low vitamin D levels, insufficient exposure to sun and obesity during adolescence play a key role [100]. These environmental risk factors can cooperate with genetic risk factors. More than 200 genes have been identified as risk variants for MS by Genome- wide association studies (GWAS). Varying combinations of these variants determine the genetic susceptibility of individual patients [101]. Most of these polymorphisms are found in genes involved in the adaptive and innate immunity such as HLA class I and HLA class II genes, IL2, IL7R and genes that modulate the tumor necrosis factor (TNF) [101-104]. Interestingly, genes identified in MS predisposition do not overlap with those involved in other neurodegenerative diseases [97].

MS is a heterogeneous disease in terms of pathology, disease progression, and outcome. Based on the clinical course MS is categorized into four subtypes: relapsing-remitting MS (RRMS), secondary progressive MS (SPMS), primary progressive MS (PPMS) and progressive relapsing MS (PRMS) [105]. RRMS is observed in 85% of MS patients and

characterized by reversible episodes of neurological symptoms ("relapses") lasting days to weeks, followed by complete or incomplete neurological recovery [106, 107]. With increasing age, most of the patients with RRMS will develop SPMS, which is characterized by prominent disability and neurological deficits [105]. The progressive disease PPMS can be observed in 10-15% of MS patients [105, 108], while PRMS is the rarest course of MS and from the onset the disease progresses with acute relapses and continue to worsen between relapses [105]. Based on the occurrence of relapses and lesions detected by MRI, each of the MS subtypes can be defined as active or not active [109].

The major pathological hallmark of MS is focal plaques throughout the CNS, which are lesions of demyelinated areas with disrupted blood-brain barrier (BBB). The initial cause of BBB disruption is still unknown however it has been shown that pro-inflammatory cytokines and chemokines (such as TNF, IL-6) that are secreted by endothelial cells and resident cells play a major role in the onset [110, 111]. Breakdown of the BBB increases the trafficking of activated T cells, B cells and macrophages into the CNS, which in turn causes further inflammation and demyelination. This is followed by loss of oligodendrocytes (myeling forming cells), reactive gliosis and degeneration of neurons [112, 113]. During disease progression, occurrence of remyelination has been suggested for the reason of clinical recovery following a relapse [114]. The rate of remyelination is dependent on the patient's age, the location of the lesion and the presence of oligodendrocyte progenitor cells [115]. Especially in younger individuals with RRMS, remyelination is frequent, whereas it is rare or absent in patients with PPMS and SPMS [116].

Several immunological mechanisms involve in the progression of MS and drive neurodegeneration.

1.2.2 Immunopathology of MS

From the early onset of MS, the CNS is infiltrated by different types of immune cells such as T cells, B cells and myeloid cells (Figure IV) [97]. Together with the CNS resident microglia and astrocytes, the infiltrating immune cells cause inflammation and demyelination by secreting inflammatory cytokines, chemokines and reactive oxygen species (ROS) [117]. The most prominent proinflammatory effector T cell populations

infiltrating into the CNS during MS are $CD4^+$ T_H17 cells and $CD8^+$ T cells. Although the exact mechanisms are still unknown, these autoreactive cells are thought to target directly neurons and oligodendrocytes [118-120].

Myelin-specific cytotoxic CD8+ T cells were shown to play an important role in the immunopathology of MS. In actively demyelinating brain lesions, CD8+ T cells outnumber CD4+ T cells and are clonally expanded [121]. It has also been demonstrated that autoreactive myelin-specific T cells are present in the normal T-cell repertoire of healthy individuals and are not harmful. Several myelin-derived peptides were identified, to which increased CD8+ T cell response was detected in MS patients compared to healthy individuals [122]. Although the role of myelin reactive CD8+ T cells in the induction of the CNS demyelination is clear in animal models, the cross-talk between CD8+ T cells and oligodendrocytes in MS patients still needs to be further investigated.

Based on their fundamental role in CNS injury, immune cell infiltrates have been targeted when developing immunotherapeutical strategies against MS.

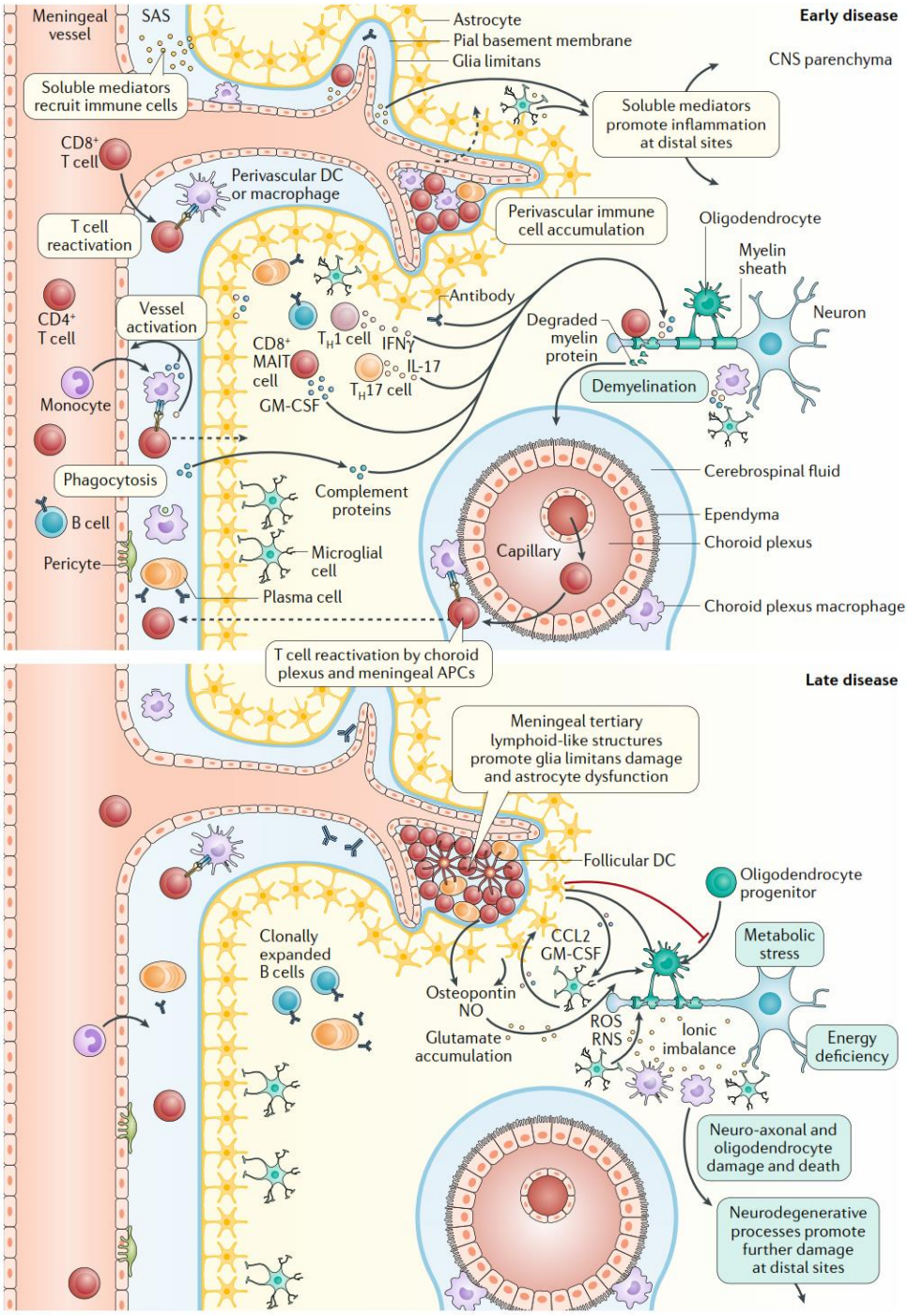

Figure IV: Involvement of the immune system compartments in early and late MS. During MS relapse, both innate and adaptive immune cells such as $CD8^+$ T cells, $CD4^+$ T cells and myeloid cells infiltrate into the CNS through the BBB. Together with the CNS resident activated microglia and astrocytes, these immune cells are involved in oligodendrocyte injury and consequently demyelination through direct cell contact and secretion of proinflammatory factors. During later MS stages, infiltration of immune cells is decreased however; chronic inflammation is boosted by the CNS- compartmentalized immune cells such as B cells and microglia. Astrocytes are involved in the recruitment and activation of microglia and prevent remyelination by inhibiting the differentiation of oligodendrocyte progenitor cells. (APC, antigen-presenting cell; DC, dendritic cell; MAIT, mucosal-

associated invariant T; NO, nitric oxide; RNS, reactive nitrogen species; ROS, reactive oxygen species; T_H1, T helper 1; T_H17, T helper 17. Adapted from [97, 117])

1.2.3 Treatment of MS

Due to its highly inflammatory nature, several immunotherapeutic approaches have been developed for the treatment of MS. However these treatment strategies are disease-modifying treatments (DMTs) that are not able to prevent the progression of MS into chronic stages, but rather reduce inflammation, decrease the relapse rate and ameliorate the disease symptoms such as fatigue and pain [97, 117, 123].

The first immunotherapeutic DMTs approved for MS were Interferon-β-1b and glatiramer acetate injections, which have been also used as first-line treatment options for RRMS. In particular, IFNβ treatment reduces annual relapse rates by 34%, but shows no prominent effect on disability progression. Glatiramer acetate, mixture of peptides, is thought to mimic myelin basic protein, thereby competitively blocking the recognition of myelin by immune cells. Glatiramer acetate treatment also reduces both the relapse rates and the disability progression. Although these therapies show good safety profiles, patients can suffer due to injection-related adverse effects such as injection site inflammation [124, 125].

The first monoclonal antibody approved for MS was natalizumab, which binds to α4β1 integrin expressed on lymphocytes and thereby prevent their interaction with VCAM1 on endothelial cells and reduce their infiltration through the blood brain barrier [125]. Although natalizumab treatment has been shown to be an effective treatment for MS patients, it can cause severe side effects such as progressive multifocal leukoencephalopathy (PML) and allergic reactions [126, 127].

The immunosuppressive oral drug fingolimod was approved for RRMS in 2010. Fingolimod is an antagonist of the sphingosine 1-phosphate (S1P) receptor expressed on leukocytes and acts by inhibiting the T cell exit from the lymph nodes. Thereby fingolimod therapy decreases the number of T cells migrated into the CNS [128]. Initial clinical trials with fingolimod demonstrated a reduction of 54% in the relapse rate, reduced number of enlarged lesions as well as probability of disability progression in RRMS patients [129, 130]. Both fingolimod and natalizumab have been tested in progressive forms of MS but did not show any clinical effect [131, 132].

Another FDA-approved monoclonal antibody for MS is alemtuzumab, which is an anti-CD52 antibody targeting lymphocytes, in particular it depletes circulating T and B cells. Compared to IFNβ treated patients, alemtuzumab treated patients experience less relapse but can suffer from other autoimmune side effects such as nephropathies or thyroid disorders [133].

Despite the development of several DMTs for the treatment of RRMS, the only treatment approved for the progressive forms of MS is ocrelizumab an anti-CD20 monoclonal antibody [97]. Depletion of B cells by ocrelizumab, have been shown to reduced MS disease activity and progression as well as decreased annual relapse rate. However patients showed increased risk of developing breast cancer and PML [134].

Taken together, current treatment strategies for MS have shown serious side effects and are not able to prevent the progression of MS into chronic stages. Thus, identification of novel immunotherapeutic targets for treatment of MS is essential.

1.3 Glioma

1.3.1 Tumor biology

Gliomas are the most common and malignant types of primary brain tumors and are considered to be derived from neuroglial stem cells, progenitor cells of astrocytes and oligodendrocytes [135].Compared to other CNS primary neoplasms, gliomas account for the majority of deaths. Based on the cellular origin and histology gliomas are classified as astrocytomas, oligodendrogliomas, mixed oligoastrocytic gliomas and ependymomas [136]. Despite anaplastic properties, such as mitotic activity and necrosis, gliomas are further classified according to the malignancy grade from the WHO grade I to IV. Grade I and II tumors exhibit high degree of cellular differentiation and have a low proliferative capacity, whereas grade III and IV tumors are highly mitotic and show recurrence after treatment [136]. Among all different types of gliomas, glioblastoma (WHO grade IV glioma) is the most malignant and common type, with a median survival of 15-17 months [137]. In the Unites States, the incidence of glioma is 6,6 per 100,000 individuals, where glioblastomas occur with an incidence of 5,6 per 100,000 [138, 139]. The incidence of gliomas highly correlates with the age; however the biological mechanism behind this correlation has not been understood yet [139]. So far, the only

environmental factor found to be causative for gliomas is the exposure to a therapeutic dose of ionizing radiation [140].

The complexity of gliomas is due to their highly heterogeneous nature both intratumorally and among different patients. Multiple molecular alterations associated with cell metabolism, proliferation, apoptosis and genome integrity are involved in the pathology of glioma [137]. Such alterations include the activation of Ras-MAPK and PI3K/mTOR pathways, genomic amplification of EGFR (epidermal growth factor receptor) and PDGFRA (platelet-derived growth factor receptor α), and loss of function mutations in the tumor suppressor genes PTEN (phosphatase and tensin homolog) and *p53* [141]. Another important loss of function mutation for glioma tumorigenesis occurs in *IDH1/2* locus. Mutated IDH enzymes lead to increased levels of R(-)-2-hydroxyglutarate, which inhibits the activity of histone demethylases and thereby increases the histone methylation and hypermethylation of multiple CpG islands. The status of IDH1 locus is a determinant of the type of glioblastoma, where primary glioblastomas harbor wildtype IDH1, whereas mutated IDH1 is a characteristic of secondary glioblastomas [142, 143].

The first line treatment for glioma is surgery followed by radiotherapy and chemotherapy with the alkylating agent temozolomide (TMZ) [144]. Recent clinical trials with the monoclonal anti-VEGF antibody Bevacizumab® in glioblastoma, resulted in increased progression free survival, without affecting the overall survival of patients [145]. Another targeted therapy options for glioma patients are small molecule inhibitors targeting MEK, IDH1, BRAF and mTOR [136].

Nevertheless, the above mentioned therapeutic strategies only targeting tumor cell proliferation have a limited effect on the overall survival and have adverse effects such as cognitive impairment and focal neurological deficits [136]. This encouraged the development of immunotherapeutic strategies for gliomas that exert effective tumor rejection without inducing serious side effects [137].

Besides molecular tumor-cell intrinsic mechanisms, the pathogenesis of glioma is also highly dependent on immune escape mechanisms developed by tumors to evade anti-tumor immune responses.

1.3.2 Immune escape mechanisms in Glioma

As studies showed that the CNS is not an 'immunologically privileged' site, several research groups revealed that escape mechanisms are important for the immune rejection of gliomas [146]. Glioma patients show an overall systemic immunosuppression, which resulted in reduced number of circulating $CD4^+$ cells in the blood, decreased proliferative capacity of PBMCs in response to T-cell antigens, defects in TCR/CD3 signaling and reduced antibody production [147]. The frequency of Tregs in glioma patients are increased, which correlates with $CD4^+$ T cell dysfunction [148].

The glioblastoma microenvironment also contributes to the tumor-associated immunosuppression [149]. Multiple cell types in glioblastoma can produce potent immunosuppressive factors, such as indoleamine 2,3-dioxygenase (IDO), IL-10, STAT-3, prostaglandin E2 and TGF-β [149-151]. Elevated levels of TGF-β promote Treg proliferation. Together with Tregs, CNS-resident microglia and myeloid-derived suppressor cells (MDSCs) also mediate T cell suppression in glioblastoma [137].

In glioblastoma, the blood-brain barrier has become permeable due to neoangiogenesis. In 20% of glioblastoma patients tumor cells were found to be circulating in the peripheral blood, which may lead to priming of anti-tumor immune responses in secondary lymphoid organs [152, 153]. However, even though priming can occur in lymphoid organs, due to the highly immunosuppressive microenvironment and defects in the antigen presentation machinery; in line the reactivation of tumor-antigen specific lymphocytes in glioblastoma tissue is inhibited [137].

$CD8^+$ T cells can be programmed to eliminate tumor cells via a cascade of steps (Figure III) [149]. As tumor cells undergoing apoptosis release antigens, APCs present them to T cells in the lymph nodes. Primed and activated tumor-antigen specific $CD8^+$ T cells infiltrate into the brain, where they recognize and target the tumor cells. Upon T-cell mediated tumor cell death, more antigens are released. During this cycle, the cross-talk between $CD8^+$ T cells and APCs in the lymph nodes and between $CD8^+$ T cells and tumor cells are highly regulated through the downstream signaling of immune checkpoint molecules [154].

Like other tumors, one of the most important immunosuppressive mechanism developed by glioblastoma to inhibit tumor infiltrating T cells is the expression or up-

regulation of co-inhibitory receptors and ligands such as PD-L1 [149]. PD-L1 is expressed in 88% of glioblastomas from newly diagnosed patients and in 72% of tissues from recurrent glioblastomas. However, no correlation between PD-L1 expression and survival could be found [155]. PD-L1 expression was found to be higher in glioblastomas compared to other tumor entities such as melanoma and NSCLC, where PD-L1 was detected in 30% and 25-36% of tumors, respectively [156, 157]. Importantly, in healthy CNS tissues PD-L1 levels are very low [155]. Different molecular subtypes of glioblastoma express different levels of PD-L1. Highest PD-L1 expression was detected in the mesenchymal subtype, which correlates with the highly immunogenic nature of that particular subtype [158, 159].

Functionally, ligation of PD-1 on tumor infiltrating lymphocytes with PD-L1 on glioma cells results in inhibition of T cell activation and reduced cytokine production such as IFN-γ and IL-2 [160, 161]. Not only glioma cells, but the microglia and tumor-infiltrating macrophages can inhibit T cell activation by upregulating PD-L1 expression [155, 162].

Overall, the clinical success of blocking the immune checkpoint signaling in other tumor types and the involvement of checkpoint molecules in glioma as an immune escape mechanism makes clinical trials with such agents promising for patients with gliomas.

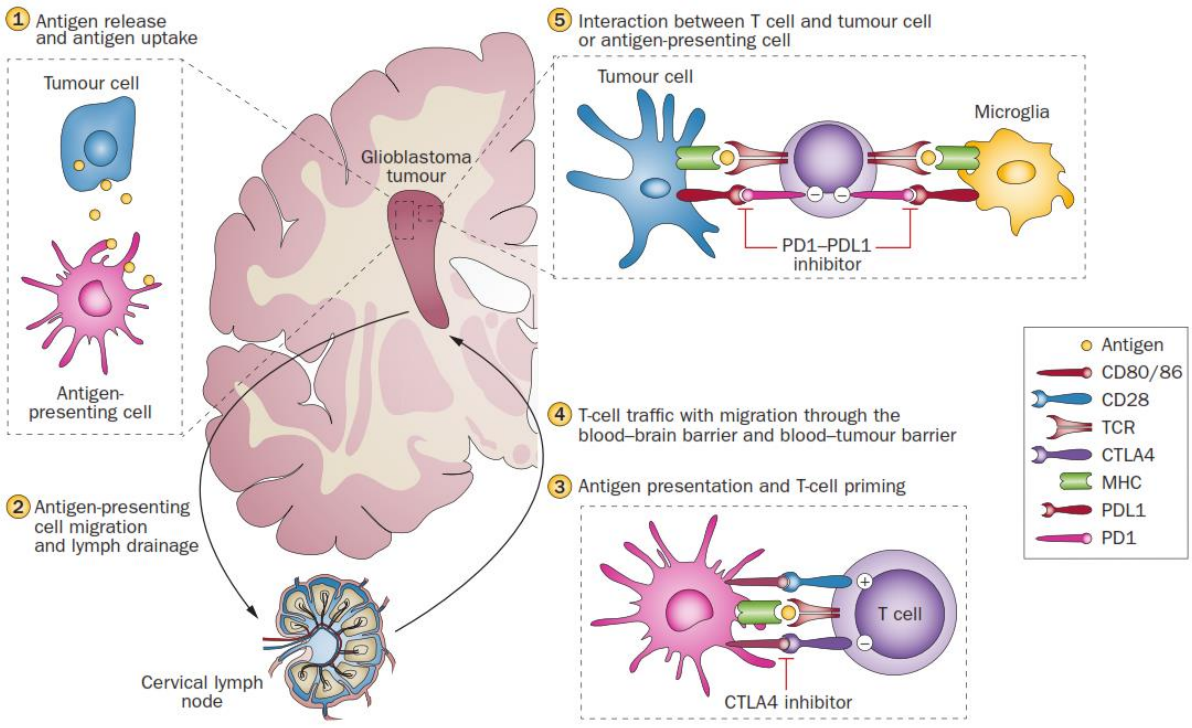

Figure V: Immune cycle of glioblastoma and involvement of immune checkpoint molecules. (1) Antigens released from apoptotic tumor cells are taken up by APCs such as the microglia and macrophages. (2) Tumor-antigen presenting APCs migrate to the cervical lymph node. (3) In lymphatic tissues, T-cells are primed by APCs. The interaction between APCs and primed T cells is highly regulated by co-inhibitory (CTLA-4) and co-stimulatory (CD80, CD86, CD28) receptors. (4) Activated T cells then migrate back and infiltrate into tumor tissue. (5) The ability of T cells to clear the tumor is inhibited by co-inhibitory checkpoints expressed by tumor cells such as PD-L1, which impede the T cell mediated killing upon binding to PD-1. Blockade of this interaction increases tumor cell lysis by tumor infiltrating T cells (Adapted from [149]).

1.3.3 Immunotherapy of Glioma using checkpoint inhibitors

Due to its highly immunosuppressive nature, multiple immunotherapeutic strategies such as adoptive cellular therapy, antibody-mediated therapy and vaccines have been developed for the treatment of gliomas. However, none of these immunotherapies have been approved up to now [163].

Preclinical studies using checkpoint inhibitors showed a certain level of success [164, 165]. Blockade of PD-1 and CTLA-4 in animal models of gliomas resulted in tumor regression and increased the long-term survival [165]. Combination of immune checkpoint blockade with radiation or combined treatment with anti-CTLA-4 and anti-PD-L1 prolonged survival [151, 166]. Additionally, treatments enhanced the immune function, resulting in increased TILs infiltration and an increased effector T cells to Tregs ratio [151, 166].

Given the involvement of immune checkpoint signaling in glioblastoma and the success in preclinical studies, several clinical trials determined the efficacy of PD-1, PD-L1 and CTLA-4 blockade in glioblastoma [149]. In one of the phase 1 trial, recurrent glioblastoma patients were treated with nivolumab (nivo) (anti-PD-1) alone or in combination with ipilimumab (ipi) (anti-CTLA-4). Combination of PD-1 and CTLA-4 blockade resulted in higher toxicity and comparable median overall survival (mOS) to nivo treatment alone [167]. Based on the safety of nivo monotherapy and increased mOS compared to controls, a phase 3 trial has initiated to compare nivo and bevacizumab. The interim analysis of patients in the cohort showed that nivo did not increase mOS compared to bevacizumab. However, it is important to note that among the responder patients, responses were found to be more durable in the nivo arm [163, 168].

Until now, there is not a prominent effect of a monotherapy of checkpoint blockade in the treatment of most of the glioblastoma patients. Therefore targeting multiple immune checkpoint molecules in combination with other immune stimulatory strategies are considered [163]. When targeting CNS tumors with checkpoint inhibitors the major concern is immune related adverse events (irAEs). Due to the limited regenerative potential of the CNS tissue, adverse events upon exacerbated inflammation would be deleterious [137]. Such fatal immune adverse events affecting CNS have been reported following checkpoint inhibition [167]. Therefore, identification of novel targets is crucial for achieving effective tumor rejection without autoimmunity.

1.4 High-throughput (HTP) RNAi-based screens to discover novel immune checkpoint molecules

RNA interference (RNAi) refers to an intracellular mechanism by which double stranded (ds) RNAs induce degradation of mRNAs containing identical sequences. After its discovery in *Caenorhabditis elegans*, gene silencing via RNAi have been widely used to reveal gene function in a high-throughput manner [168].

RNAi-based genetic screens have emerged as powerful approach to study gene function in a high-throughput fashion [169]. Small interfering RNAs (siRNAs) are among the major tools suitable for RNAi-based genetic screens. By RNAi screening in human cells, siRNAs of 21-23 nucleotides long are used for gene silencing [170]. Once transfected into cells, these duplex siRNAs are recognized by the RNA-induced silencing complex (RISC) which in turn integrates the anti-sense strand of the siRNA and direct it to the target mRNA with a complementary sequence. The mRNA sequence targeted by the complementary anti-sense siRNA is degraded by the RISC complex, which further leads to the transient knock-down of the corresponding gene in the cell [171]. The phenotype upon gene silencing is then assessed by appropriate readout assays. The readout of screen generates a primary HIT-list of candidate genes, whose knockdown shows the desired biological effect. Selected candidate genes are further validated by secondary screens to exclude false-positive and false-negative results [169].

In order to reveal novel candidate inhibitory immune checkpoint molecules expressed by tumor cells, Dr. Nisit Khandelwal from our group has developed a siRNA-based high-throughput RNAi screening approach where luciferase intensity is the final readout for

the measurement of T cell cytotoxicity [172]. In this set-up, stably luciferase-expressing tumor cells are transfected with a siRNA library enriched for surface proteins, G-protein coupled receptors (GPCRs) and protein kinases. After 48-72h of transfection, tumor cells are co-cultured with HLA-A2+ matched patient derived tumor-infiltrating lymphocytes or tumor-antigen specific T cell clones. After 20-24h of co-culture, residual luciferase intensity is measured to assess how the knockdown of a particular gene in tumor cells can alter the T cell mediated killing. So far, our group has performed HTP screens in breast cancer, pancreatic cancer, melanoma and multiple myeloma models and identified more than 500 candidate co-inhibitory and co-stimulatory immune checkpoint molecules (HITs).

1.5 Preliminary literature and database search on formerly identified cancer associated HITs

Based on the findings that, in cancer and autoimmune diseases, immune checkpoint molecules have dysregulated gene expression and/or polymorphisms linked to disease susceptibility, we performed a preliminary literature search to asses, whether the cancer-associated HITs identified in our group have a known association to autoimmune diseases. We therefore searched the literature and took advantage of databases to investigate about multiple sclerosis (MS), rheumatoid arthritis (RA), inflammatory bowel disease (IBD), graft versus host disease (GvHD) and vitiligo. We analyzed the expression data of HITs in patients with autoimmune diseases, HITs that have single nucleotide polymorphisms (SNPs) or variants linked to autoimmune diseases and HITs whose orthologues in mice were linked to autoimmunity. Remarkably, we were able to find PDAC HITs associated with IBD and also melanoma HITs that are associated with skin GvHD and vitiligo. We found the highest number of HITs-association for MS: 6 of the HITs have SNPs associated with MS, 2 co-stimulatory HITs were found to be upregulated in the brain of MS patients and 6 HITs whose knock-out / knock-in were shown to affect susceptibility of mice to EAE.

Another observation we had is that there are only few overlapping candidate immune checkpoint HITs even between different tumor entities. Therefore, a screen for glioma and multiple sclerosis will give us a broader and more disease relevant ICMs list.

2 Aims of the study

Co-inhibitory and co-stimulatory immune checkpoint molecules are the key players regulating the crosstalk between immune cells and non-immune cells. Imbalances in the immune checkpoint signaling can cause development of cancer and autoimmune diseases such as glioma and multiple sclerosis [117, 136]. MS and glioma are two different CNS diseases with potentially similar mechanisms involved in the disease immunopathology, but in a contrary manner.

Here I hypothesize that dysregulated immune checkpoint signaling in oligodendrocytes can occur as increased inhibition / reduced stimulation, which lead to the reduced brain infiltrating lymphocyte activity and contribute to the glioma immune evasion. On the other hand, this imbalance can appear as reduced inhibition / increased stimulation, which enhance the autoreactive $CD8^+$ T cell activity and contribute to the demyelination in MS patients.

So far developed immunotherapeutical strategies for both of these diseases had either shown serious side effects or were unable to prevent disease progression. The major aim of this work is to identify novel immune modulatory molecules that could be used as potential targets for the immunotherapy of MS and glioma.

Based on a *proof-of-concept* approach established in this laboratory [172], the aims of this study are to,

- Develop a high-throughput RNAi screen for the identification of novel immune checkpoint molecules on oligodendrocytes.
- Validate the role of selected HITs in mediating the communication between glial cells and antigen-specific cytotoxic T cells.
- Characterize the molecular mechanism underlying the immunomodulatory role of selected HITs.
- Provide the rationale for the applicability of selected candidate genes as novel targets for MS and glioma immunotherapy.

3 Results

3.1 High throughput (HTP) screen setup for the identification of novel Glioma-MS associated immune checkpoint molecules

In order to identify novel immune checkpoint molecules involved in the cross-talk between glial cells and antigen-specific CD8+ T cells, the human oligodendrocyte cell line MO3.13 was used as a model in this project. To discover potential co-stimulatory and co-inhibitory molecules on oligodendrocytes, a high-throughput (HTP) screen approach was developed. This method was previously established in our division by Dr. Nisit Khandelwal [172], and subsequently improved and adapted according to the aims of this project.

Briefly, stably HLA-A2 and firefly luciferase-expressing MO3.13-A2-Luc cells were reverse transfected with a siRNA library targeting 4155 genes encoding for the whole surfaceome, as well as protein kinases and metabolic proteins. After 72h of transfection, cells were pulsed with HLA-A2-matched Influenza (Flu) peptide GILGFVFTL for 1h. After pulsing, peptide-containing medium was removed and either Flu-specific CD8+ T cells (FluT) (*cytotoxicity setting*) or plain T cell media (*viability setting*) were added to the transfected oligodendrocytes. After 21h of co-culture, the supernatant (containing dead tumor cells and T cells) was removed, remaining oligodendrocytes were lysed and luciferase intensity was measured. Luciferase activity is proportional to the amount of remaining living cells in each well. The *cytotoxicity setting* allows to identify genes whose knockdown increases or decreases T cell mediated oligodendrocyte killing, whereas the *viability setting* allows the exclusion of genes whose knockdown has an impact on cell viability *per se*. Ideally, the knockdown of a co-inhibitory gene would result in a decreased luciferase activity in the cytotoxicity setting, whereas no difference in the viability setting should be seen compared to the non-targeting control siRNA. On the contrary, the knockdown of a co-stimulatory gene should result in higher luciferase activity compared to the non-targeting control siRNA in the cytotoxicity setting.

A schematic explanation of the method is depicted in Figure 1.

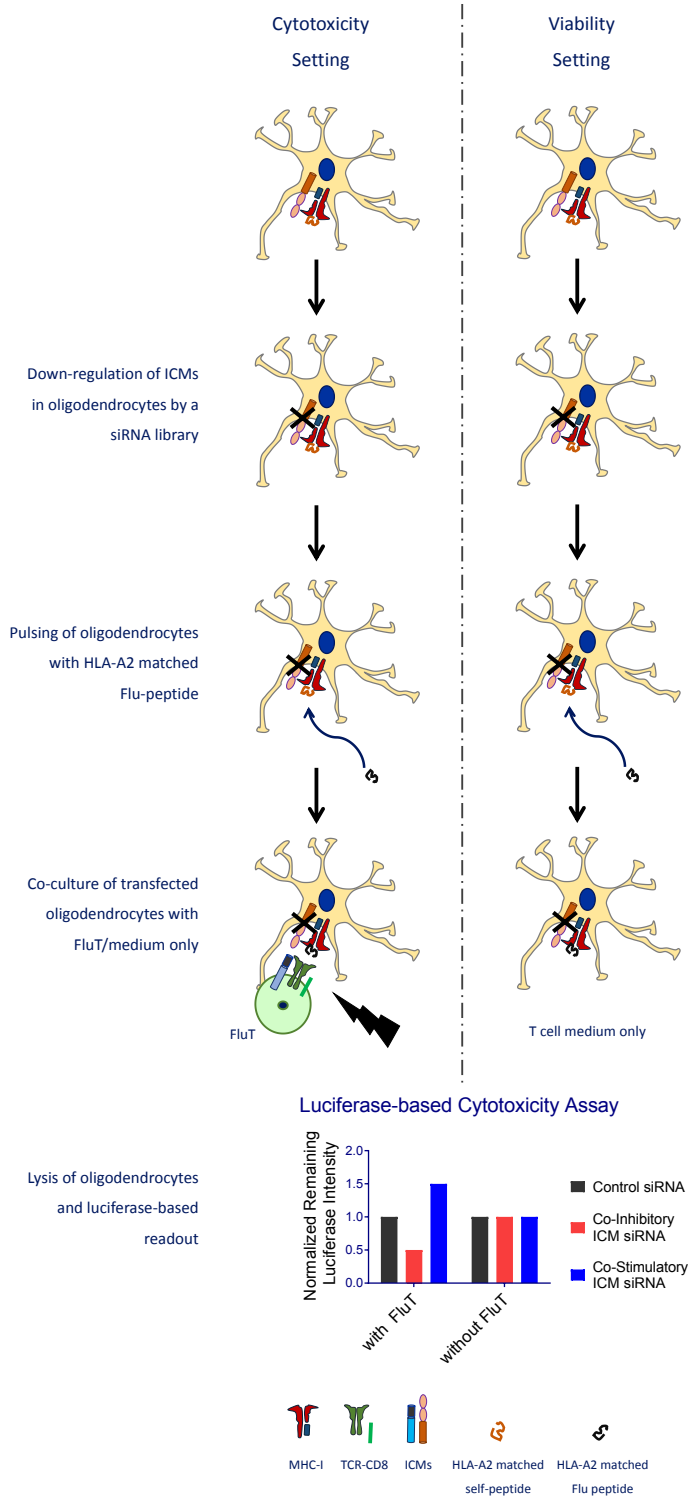

Figure 1: Experimental set-up of the primary siRNA-based high-throughput RNAi screen. Stably luciferase expressing HLA-A2+ human oligodendrocytes (MO3.13-A2-Luc) were reverse transfected with a siRNA library targeting 4155 genes. After 72h of transfection MO3.13-A2-Luc cells were pulsed with HLA-A2-matched Flu peptide for 1 hour. After pulsing, peptide-containing media is removed and MO3.13-A2-Luc cells were co-cultured with or without Flu-specific T cells (FluT) derived from HLA-A2+ healthy donors. Increased cytotoxicity upon gene silencing was quantified by using the difference between the luciferase intensity of residual MO3.13-A2-Luc co-cultured with or without FluT.

Before performing the HTP screen, in order to ensure the reliability and the robustness of the screen a series of adaption and optimization procedures regarding co-culture and transfection conditions were necessary. These procedures are described in further details in the next sections.

3.1.1 Generation of HLA-A2+ Luciferase+ human oligodendrocyte cell line

Since the HTP screen is based on a HLA-A2-matched co-culture of oligodendrocytes and FluT cells, I first investigated the expression of HLA-A2 on MO3.13 cells by FACS (Figure 2A). As MO3.13 cells resulted to be HLA-A2 negative, they were transfected with a HLA-A2 expression plasmid. After 2 weeks of antibiotic selection (0,8 mg/ml of G418), only 31,9% of the cells became HLA-A2+. In order to obtain a pure target cell population, MO3.13-A2 cells were FACS sorted and kept cultured in selection media.

As the final readout of the HTP screen is luciferase-based, stably luciferase expressing oligodendrocytes (MO3.13-A2-Luc) were generated. To this, MO3.13-A2 cells were transduced with a lentiviral vector encoding for the firefly-luciferase reporter gene fused with the green fluorescent protein (GFP). This construct enables FACS-sorting of the transduced cells based on the GFP expression, thereby assuring luciferase expression of the sorted cells. Moreover, the vector backbone contains the puromycin-resistance gene that allows the selection of transduced cells. After transduction, the cells were expanded under selection media containing 0,6 µg/ml of puromycin for 2 weeks and GFP percentage was determined by FACS analysis (Figure 2B). 64% of the cells expressed GFP. Although the transduction efficiency was high, GFP+ cells were sorted by FACS to enrich the luciferase positive population. HLA-A2 and GFP expression resulted to be stable in oligodendrocytes.

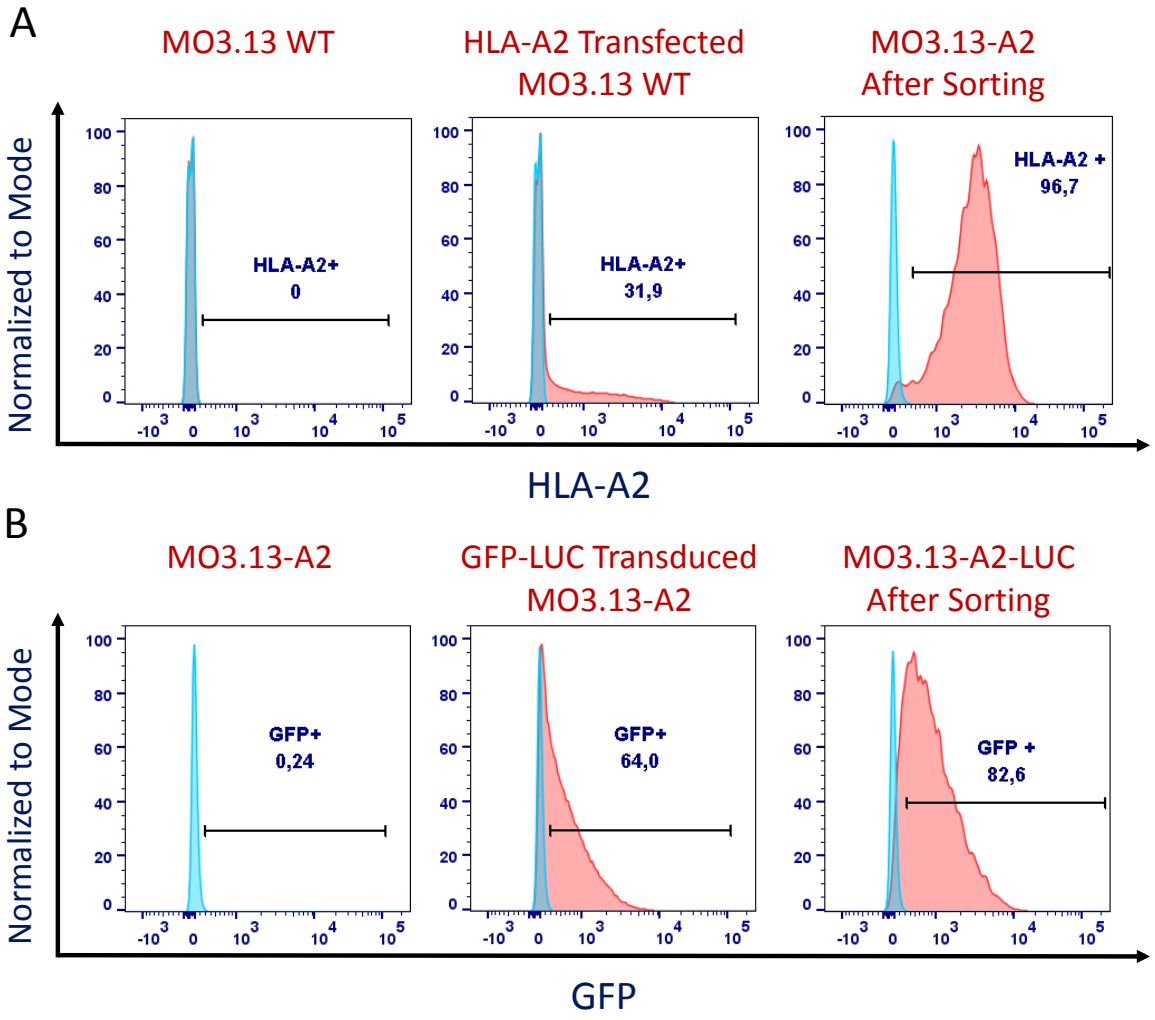

Figure 2: Generation of HLA-A2+ Luciferase+ human oligodendrocyte cell line. (A) FACS analysis for HLA-A2 expression on MO3.13 cells. Blue and red histograms indicate the isotype control and HLA-A2 antibody staining, respectively. Gate shows the percentage (%) of HLA-A2+ cells. From left to right: panels show the staining of wildtype MO3.13, HLA-A2 transfected cells after 2 weeks of selection and FACS sorted cells. **(B)** FACS analysis for GFP expression in MO3.13 cells. Blue and red histograms indicate untransduced and transduced MO3.13-A2 cells, respectively. Gate shows the percentage of GFP⁺ cells. From left to right: panels show the FACS data of untransduced MO3.13-A2 cells, GFP-Luc transduced cells after 2 weeks of selection and FACS sorted cells.

3.1.2 Generation of HLA-A2⁺ Flu-antigen specific T cells from healthy donors

Multiple sclerosis is characterized by infiltration of myelin-reactive T cells into the brain. To mimic autoreactive T cells in MS patients and study antigen-specific CD8⁺ T cell mediated killing of oligodendrocytes Flu-antigen specific T cells (FluT) were generated as effector cells from peripheral blood mononuclear cells (PBMCs) of HLA-A2⁺ healthy

donors. FluT were first generated using an antigen-specific expansion (ASE) protocol and subsequently further expanded by rapid expansion protocol (REP) established by Rosenberg *et al.* [173].

The percentage of Flu specificity was determined on day 7 and 14 of ASE by pentamer FACS staining (Figure 3A-C). On day 7 after ASE, the percentage of FluT derived from donor#11 was 21,6% but it increased to 43,2% on day 14. In the unpulsed control only 0,11 and 0,26% of FluT cells were detected on day 7 and 14, respectively.

During the antigen specific expansion, proliferation of T cells is induced by antigenic stimuli in the presence of low-dose IL-2 and IL-15. This enables the enrichment of a T cell population specific for a particular antigen, however quantitative increase is not sufficient to perform a HTP screen and further validation experiments. Therefore, following ASE, FluT were sorted by FACS and expanded using REP for further 14 days in the presence of high-doses of IL-2, agonistic anti-CD3 antibody (clone OKT3) and irradiated feeder cells from 3 different donors. Sorting of the cells ensures the expansion of a pure population and thereby decreases potential allogeneic reactions in the up-coming co-culture experiments. On day 14 of the REP the antigen specificity was monitored again by FACS-pentamer staining, which resulted in 96% of Flu-specific T cells (Figure 3D).

The expansion of FluT cells from 8 different HLA-A2$^+$ donors were tested. Based on the Flu specificity, the number of expanded cells, and the cell viability, FluT from Donor#11 were selected for the screen and further experiments.

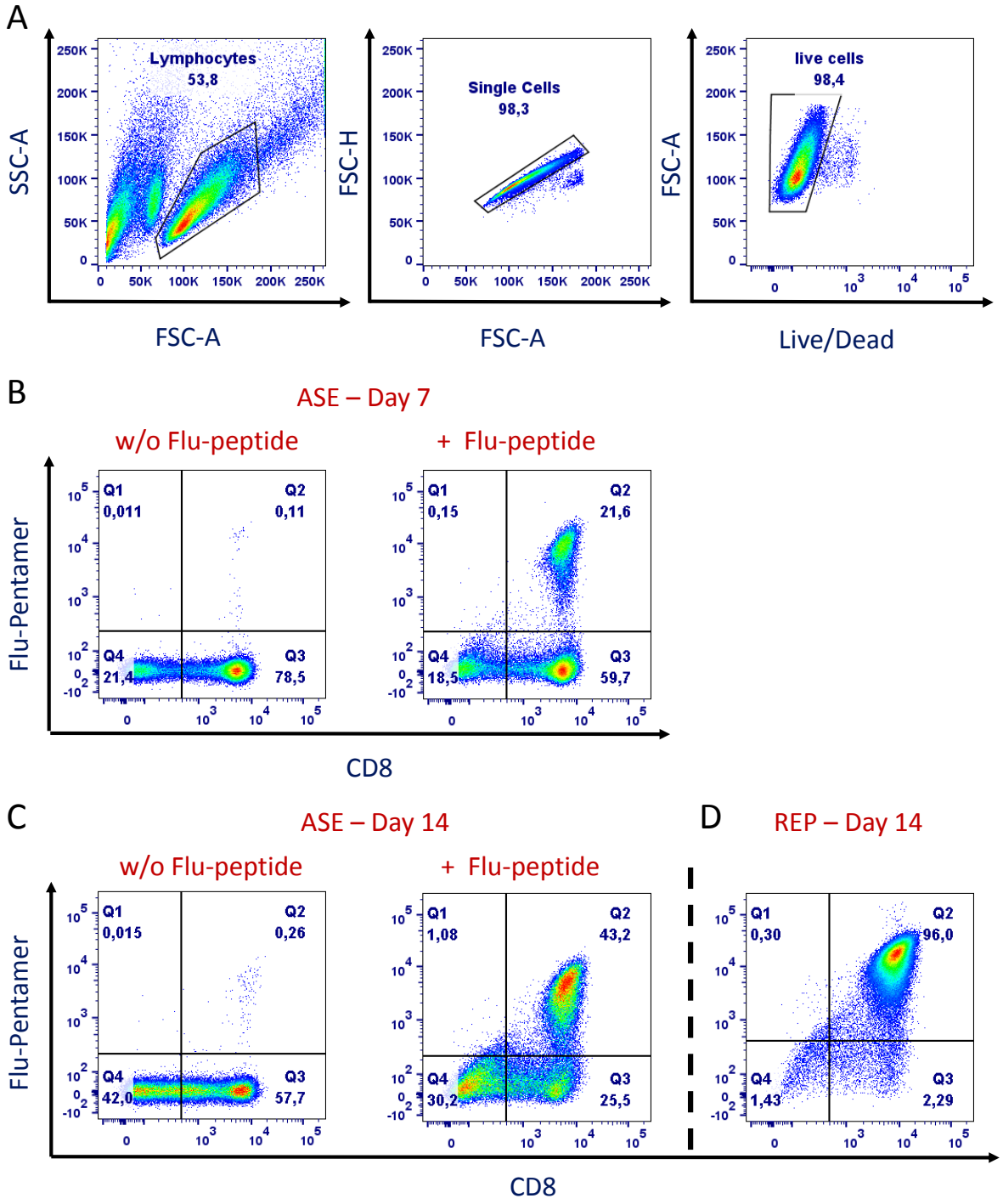

Figure 3: FACS analysis of FluT after ASE and REP. (A) All samples were gated on lymphocytes, single cells and live cells. **(B)** CD8 and Flu Pentamer staining on day 7 of ASE and **(C)** on day 14. Left panel shows unpulsed control; the right panel shows the staining of FluT expanded in the presence of Flu-peptide. **(D)** CD8 and Flu Pentamer staining on day 14 of REP.

3.1.3 Phenotypical and functional characterization of FluT

In order to characterize the phenotypes of FluT cell subsets, FACS analysis was performed and the expression of the surface markers CD45RO and CD62L were analyzed to distinguish between effector and memory subsets. As expected, no naïve T cells (TN) (CD62L+, CD45O-) were detected among the antigen experienced FluT cells. 87,6% of FluT cells were characterized as effector memory cells (T_{EM}) (CD62L-, CD45O+) and 11,8% as central memory (T_{CM}) subsets (CD62L+, CD45O+) (Figure 4A). The purity of MACS separation was confirmed by performing CD4 staining. More than 90% of $CD3^+$ cells were found to be $CD8^+$. Less than 1% of $CD3^+$ cells express CD4.

Next the expression of exhaustion markers on expanded FluT cells was investigated since elevated levels of such markers indicate impaired T cell function [174]. In the resting state 23,1%, 14,6% and 18,1% of FluT cells express PD-1, TIM-3 and LAG-3 respectively (Figure 4B-C). The low expression levels of exhaustion markers on FluT D11 indicate a good cytotoxic potential and capacity for further activation.

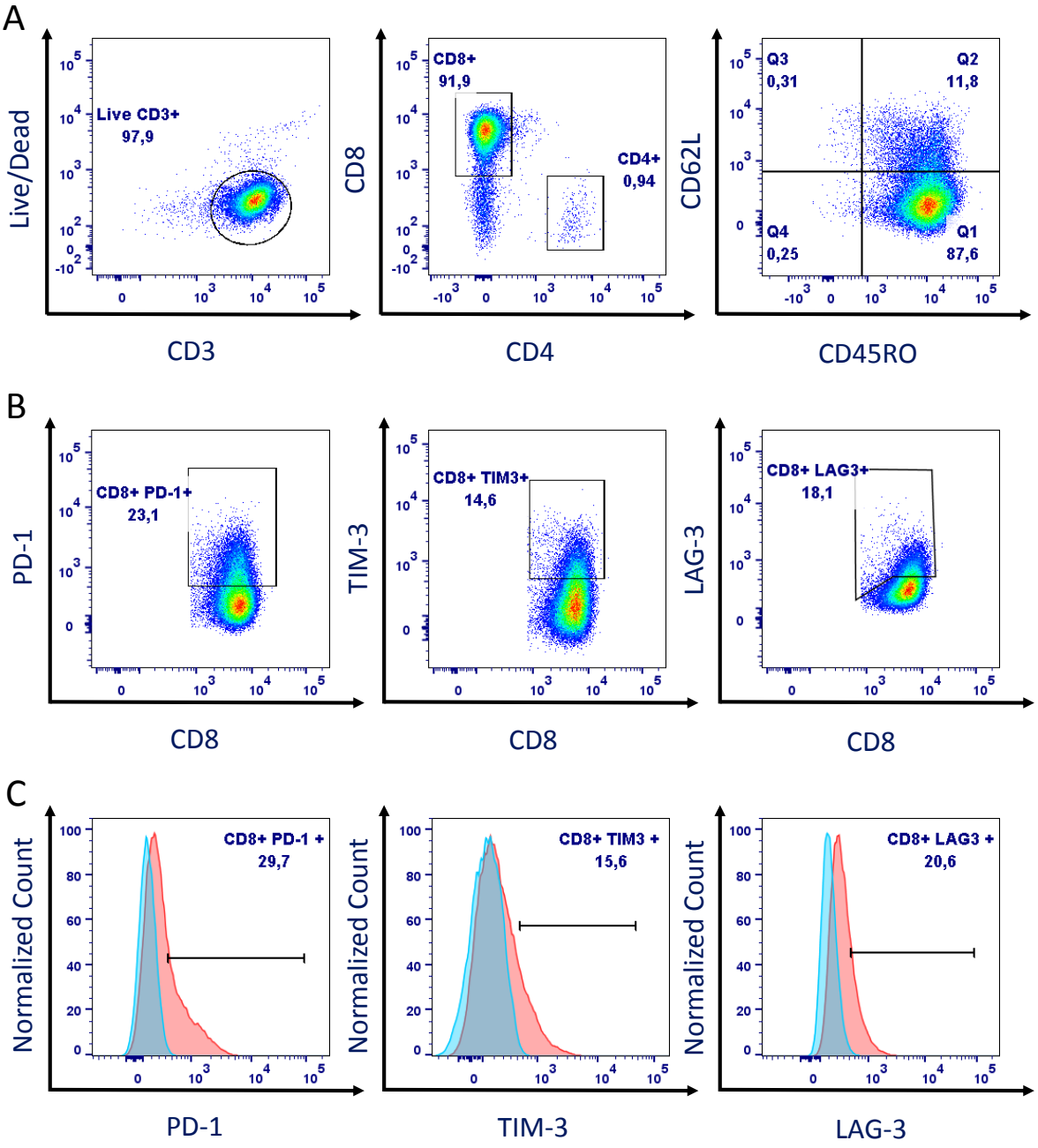

Figure 4: Phenotypical characterization of FluT. (A) Left and middle panel: FACS analysis of CD4 and CD8 expression on CD3⁺ FluT after REP. Right panel: Expression of effector and memory markers CD45RO and CD62L on CD8⁺ FluT. Naïve T cells (TN) are represented by CD62L+, CD45O- expression, central memory (T_{CM}) cells are defined as CD62L+, CD45O+ expression, effector memory (T_{EM}) cells are CD62L-, CD45O+, whereas terminal effector cells (T_{EFF}) are represented by CD62L-, CD45O- population. **(B-C)** FACS analysis for PD-1, TIM-3 and LAG-3 on CD3⁺ CD8⁺ FluT. **(B)** Dot pots and **(C)** histograms showing the expression levels of the exhaustion markers. Blue and red histograms indicate the isotype control and antibody stained samples, respectively.

After phenotypical characterization, the functionality of FluT cells were analyzed. First, the cytotoxic capacity of FluT cells was determined by ^{51}Chromium-release assay. T2

cells either pulsed with 0,5 µg/ml flu peptide for 1h or unpulsed were labelled with ^{51}Cr and co-cultured with FluT cells at effector to target (E:T) ratios in a range of 50:1 to 1:1. 4h after co-culture, supernatant was harvested, ^{51}Cr release was measured and the percent specific lysis was calculated. Pulsed T2 cells were effectively killed by FluT proportional to increased E:T ratios, whereas unpulsed T2 cells were not targeted by FluT. Total lysis of T2 cells was achieved at E:T of 50:1, whereas 20% of pulsed T2 cells were lysed at E:T of 1:1 (Figure 5A).

Next the secretion of IFNγ by FluT cells upon co-culture with T2 cells was assessed. T2 cells were either unpulsed or pulsed with flu peptide concentrations between 0,1 and 0,0001 µg/ml and co-cultured with FluT at E:T ratios of 1:1, 2:1 and 5:1. After 6h of co-culture the supernatant was collected and IFNγ ELISA was performed. Peptide concentrations between 0,1 and 0,001 µg/ml activated FluT similar as PMA/ionomycin stimulation, whereas IFNγ could not be detected in the co-culture of FluT with unpulsed T2 cells indicating only HLA-A2-TCR mediated activation of FluT (Figure 5B).

As next step, the FluT mediated killing of MO3.13-A2-Luc cells was determined and the co-culture conditions for the upcoming HTP screen were optimized. Therefore luciferase-based cytotoxicity assays were performed, where MO3.13-A2-Luc cells were pulsed with flu peptide concentrations between 0,1 µg/ml and 0,0000001 µg/ml and co-cultured with different E:T ratios of FluT. After 20h of co-culture, the remaining luciferase activity was measured. Luciferase activities measured in pulsed samples were normalized to luciferase intensity measured in unpulsed control. An increased killing of MO3.13-A2-Luc cells was detected at E:T of 20:1, between 0,1-0,001 µg/ml peptide concentrations and at E:T of 10:1, with 0,1-0,01 µg/ml peptide concentrations (Figure 5C). Furthermore, the levels of Granzyme B, a cytotoxic protein present in the supernatant upon T cell/tumor cell co-culture, was measured. As expected Granzyme B levels correlated with higher E:T ratio and peptide concentration. Compared to unstimulated FluT, or FluT co-cultured with unpulsed MO3.13-A2-Luc cells, increased levels of Granzyme B were detected only with 0,1 and 0,01 µg/ml peptide concentrations (Figure 5D). In order to study the impact of immune checkpoint molecules in this setup, 0,01 µg/ml peptide concentration and the E:T of 20:1 were used in all of the following co-culture conditions.

In order to show MHC-I restricted killing of oligodendrocytes by FluT cells, MHC-I was blocked with a MHC blocking antibody and cytotoxicity assay was performed using a real-time live-cell microscopy. To this end, pulsed MO3.13-A2 cells were treated either with 60 µg/ml of MHC-I blocking antibody or isotype control and were co-cultured with FluT in the presence of YOYO-1 dye. Apoptotic oligodendrocytes were visualized and quantified using YOYO-1 incorporation into the cells for 25 hours. An increased apoptosis of pulsed MO3.13-A2 treated with isotype over time was observed, whereas the blockade of MHC-I inhibited almost entirely T cell mediated killing (Figure 5E). In order to confirm the necessity of a TCR downstream signaling in FluT mediated killing, we treated T cells with 10 µM of Lck-specific inhibitor (7-Cyclopentyl-5-(4-phenoxyphenyl)-7H-pyrrolo[2,3-d]pyrimidin-4-ylamine) and co-cultured with pulsed oligodendrocytes. The treatment of T cells with the Lck inhibitor completely abrogated the killing of MO3.13-A2 cells, thus indicating the essential role of a TCR downstream signaling in FluT cytotoxicity (Figure 5F).

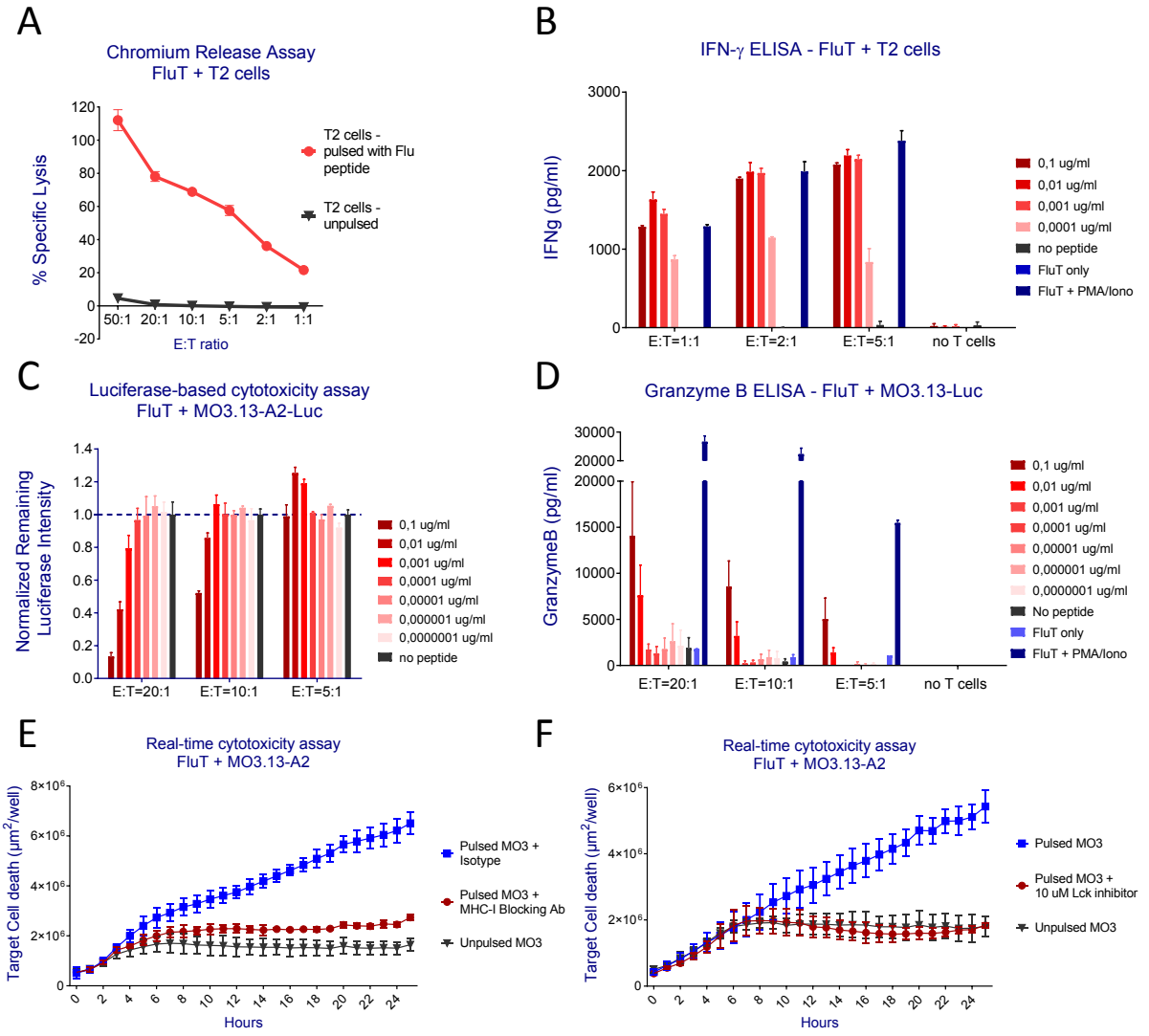

Figure 5: Functional characterization FluT cells. (A) ^{51}Chromium-release assay to measure antigen specific cytolysis of flu-peptide pulsed T2 cells by FluT cells. Pulsed or unpulsed T2 cells were labelled with ^{51}Cr and co-cultured with FluT at different E:T ratios depicted on the x-axis. After 4h of co-culture, ^{51}Cr release was measured and the percentage of specific lysis was calculated. **(B)** ELISA for detecting IFNγ secretion by FluT cells upon co-culture with T2 cells. T2 cells were pulsed with different concentrations of flu-peptide and co-cultured with FluT at different E:T ratios. After 6h of co-culture IFNγ levels in the supernatant were measured by ELISA. PMA/Ionomycin stimulated and unstimulated FluT cells were used as positive and negative controls, respectively. **(C)** Luciferase-based cytotoxicity assay to optimize the co-culture conditions for MO3.13-A2-Luc and FluT cells. MO3.13-A2-Luc were pulsed with diluting concentrations of flu peptide and co-cultured with FluT cells at different E:T ratios. After 20h of co-culture, remaining luciferase activity was measured. Luciferase activities measured in pulsed samples were normalized to luciferase intensity of unpulsed control. **(D)** ELISA for detecting Granzyme B secretion upon co-culture with MO3.13-A2-Luc cells. Granzyme B levels were measured in the supernatant of the luciferase-based cytotoxicity assay as described in C. **(E-F)** Real-time cytotoxicity assay (IncuCyte® ZOOM System) to analyze MHC-I-TCR engagement dependent killing of MO3.13-A2 cells by FluT. **(E)** Blockade of MHC-I. Pulsed MO3.13-A2 cells were co-cultured with FluT in the presence or absence of MHC-I blocking antibody and YOYO®-1 dye for 25 hours. **(F)** Inhibition of Lck. Pulsed MO3.13-A2 cells were co-cultured with FluT in the

presence or absence of a Lck inhibitor. Analysis shows YOYO®-1 dye incorporation for 25 hours. **(E-F)** Incorporation of YOYO®-1 into apoptotic cells were visualized and quantified. Total YOYO-1+ green area per well (µm2/well) indicating killing of MO3.13-A2 cells was indicated on the y-axis. Error bars indicate +/- SD, each sample was prepared in triplicates. Representative data of at least 2 independent experiments.

3.1.4 Optimization of siRNA transfection in human oligodendrocytes

When using RNAi, it is essential to achieve high efficacy without increasing potential off-target effects. In order to optimize the transfection conditions for MO3.13-A2-Luc cells, two different transfection reagents (RNAiMAX and Dharmafect1), two different end points (48h and 72h), as well as different concentrations of siRNA were tested.

Therefore, MO3.13-A2-Luc cells were transfected with 25 or 50 nM of non-targeting siRNA control (Scr) or with a siRNA cocktail targeting genes essential for cell survival (cell death siRNA). Transfection was performed using RNAiMAX or Dharmafect1 transfection reagents and cell viability was visualized and analyzed by means of the IncuCyte ZOOM system for 72h. The transfection reagent RNAiMAX showed a higher transfection efficacy as a reduced number of cells transfected the cell death siRNA remained viable compared to cells transfected with Dharmafect (data not shown). The impact of cell death siRNA on the cell viability showed a better outcome after 72h and 25 nM of siRNA concentration (Figure 6A).

To confirm these observations, additional immune checkpoint genes were knocked down in MO3.13-A2-Luc cells using RNAiMAX and 25 nM of a pool of 4 non-overlapping siRNAs targeting PD-L1 and 4-1BBL. Quantitative real-time PCR (RT-qPCR) analysis showed more than 80% knockdown of PD-L1 and 4-1BBL in target siRNA transfected cells compared to Scr transfection (Figure 6B).

For later validation steps, I aimed at using a pool of 30 siRNAs to reduce potential off-target effects as much as possible. Therefore, the siRNA concentration for the 30pool siRNAs in MO3.13-A2-luc cells was also optimized. Cells were transfected with 1, 5, 10 and 25 nM of 30 pool of non-targeting siRNA or with siRNAs targeting GAPDH and relative GAPDH mRNA levels were analyzed by RT-qPCR. It was observed that 1nM of siRNA concentration already efficiently decreased GAPDH mRNA levels by 98,8%. Higher siRNA concentrations were not able increase the knockdown efficacy further (Figure 6C).

The non-targeting siRNA Scr did not induce a change of the mRNA level of GAPDH at any tested siRNA concentration. Although 1 nM siRNA concentration was found to be sufficient to reduce the levels of GAPDH, 5 nM was selected for optimal and robust gene knockdown with the 30 pool siRNAs based on the results obtained from the knockdown efficiency tests of the siRNAs targeting different genes (data not shown).

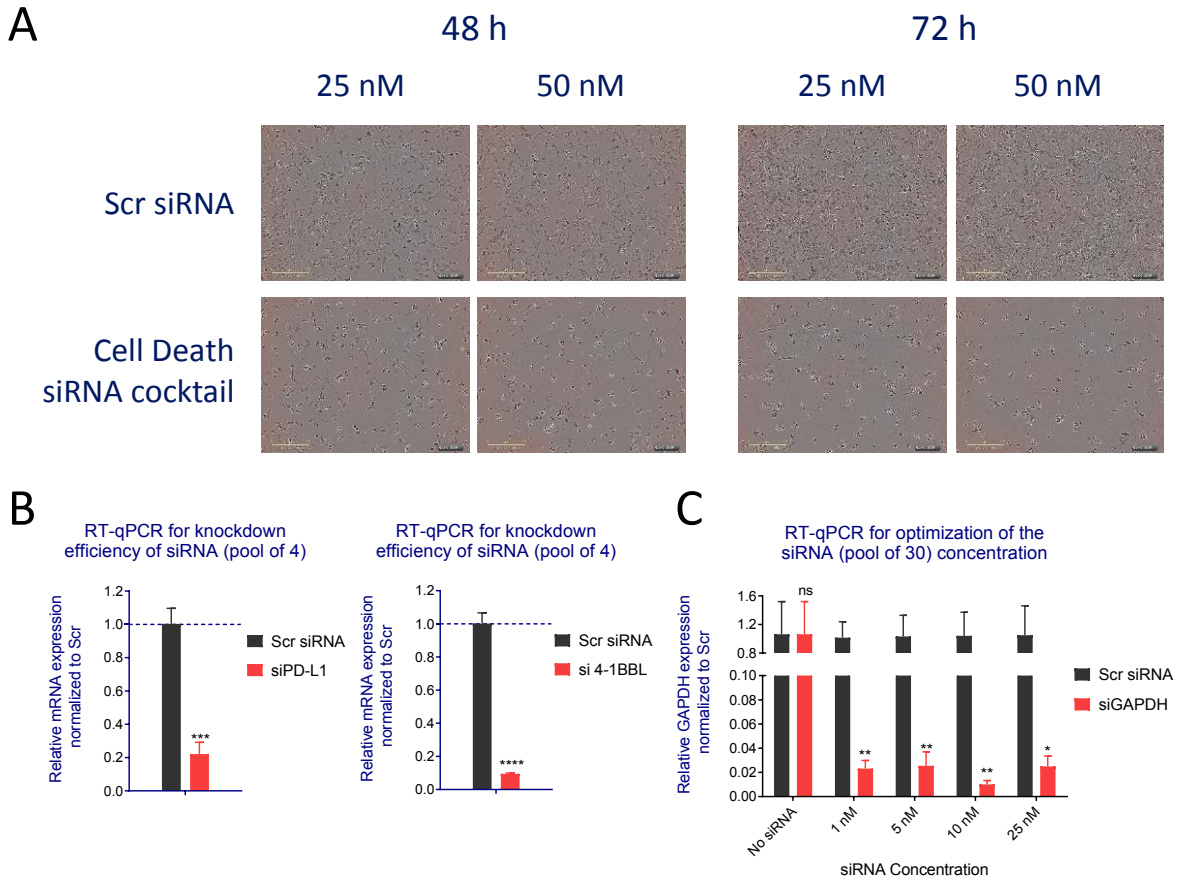

Figure 6: Optimization of reverse transfection protocol for oligodendrocytes. (A) MO3.13-A2-Luc cells were transfected with 25 or 50 nM of non-targeting siRNA control (Scr) or with a siRNA cocktail targeting genes essential for cell survival (cell death siRNA). Viability of transfected cells was visualized via the IncuCyte ZOOM system for 72h. **(B)** Quantitative real-time PCR was performed to analyze the knock-down efficacy of siRNAs targeting PD-L1 and 4-1BBL. cDNA was synthesized from the RNA of MO3.13-A2-Luc cells transfected with 25 nM of pool of 4 non-overlapping siRNAs or Scr control for 72h. **(C)** Quantitative real-time PCR for optimizing the siRNA concentration for 30 pool siRNAs from siTOOLs. MO3.13-A2-Luc cells were transfected with 1, 5, 10 and 25 nM of pool of 30 non-targeting or GAPDH targeting siRNAs. After 72h of transfection relative GAPDH mRNA levels were determined. **(B-C)** Expression of beta-actin was used for normalization. mRNA expression in target samples were normalized to mRNA expression in control siRNA transfection.

3.1.5 Selection of positive and negative controls for the primary HTP screen

Defining co-inhibitory and co-stimulatory immune-checkpoint controls is essential for the reliability and the robustness of the HTP-screen [169]. Appropriate controls enable proper interpretation of the impact of novel immune checkpoint genes on T cell mediated killing and help to identify HITs in the screen.

Non-targeting siRNA sequences (scrambled, Scr) are needed as a negative control for siRNA transfection and serve as a baseline to normalize the impact of gene knockdown in the cytotoxicity and viability settings. In order to select non-targeting siRNA controls that have a similar phenotype as wild type control (WT, mock control; not transfected with any siRNA), two different siRNA sequences (Scr3 and Scr4) were tested. The luciferase-based cytotoxicity assay showed that both sequences did not have an impact on the T cell mediated killing or on MO3.13-A2-Luc cell viability compared to WT samples (Figure 7A and B). Therefore, both negative controls were included in the HTP-screen.

The viability setting is performed to exclude genes whose knockdown has an impact on cell viability. In order to identify appropriate viability controls, genes that are essential for cell survival such as ubiquitin C (UBC) were silenced. “Cell death” siRNA, a cocktail of several siRNAs targeting ubiquitously expressed human genes, was also tested. Viability controls also serve as controls for transfection efficacy. By luciferase readout, it was observed that transfection of MO3.13-A2-Luc cells with siUBC and siCell death completely abrogated luciferase activity indicating an efficient tumor cell death, thus transfection efficacy (Figure 7).

For the cytotoxicity setting, it was needed to establish already known co-inhibitory and co-stimulatory immune checkpoint controls. Therefore the co-inhibitory molecules programmed death ligand 1 (PD-L1), C-C Motif Chemokine Receptor 9 (CCR9) [172], salt-inducible kinase 3 (SIK3) and Connexin 32 (CX32) (novel immune modulators identified by our group in previous pancreatic cancer and melanoma screens) were silenced. As co-stimulatory controls 4-1BBL, OX40L and CD40 were tested. Also caspase 3 (CASP3) was knocked down as a control for apoptosis resistance. Using the luciferase-based cytotoxicity assay, we showed that downregulation of PD-L1, CCR9, SIK3, CX32 and CD40 lead to an increased FluT mediated killing of MO3.13-A2-Luc cells, whereas

downregulation of 4-1BBL decreased FluT mediated killing of the target cells compared to Scr3 and Scr4 transfection. Downregulation of CASP3 did not provide resistance to MO3.13-A2-Luc cells towards T cell attack. Silencing of PD-L1 and OX40 resulted in decreased cell viability, whereas silencing of CCR9, 4-1BBL and SIK3 showed a moderate positive effect or no effect on cell viability (Figure 7). Thus, CCR9 and SIK3 were selected as co-inhibitory controls and 4-1BBL was used as co-stimulatory control in the HTP screen. Although PD-L1, CX32, OX40L did not show strong impacts, they were included in the HTP screen as well.

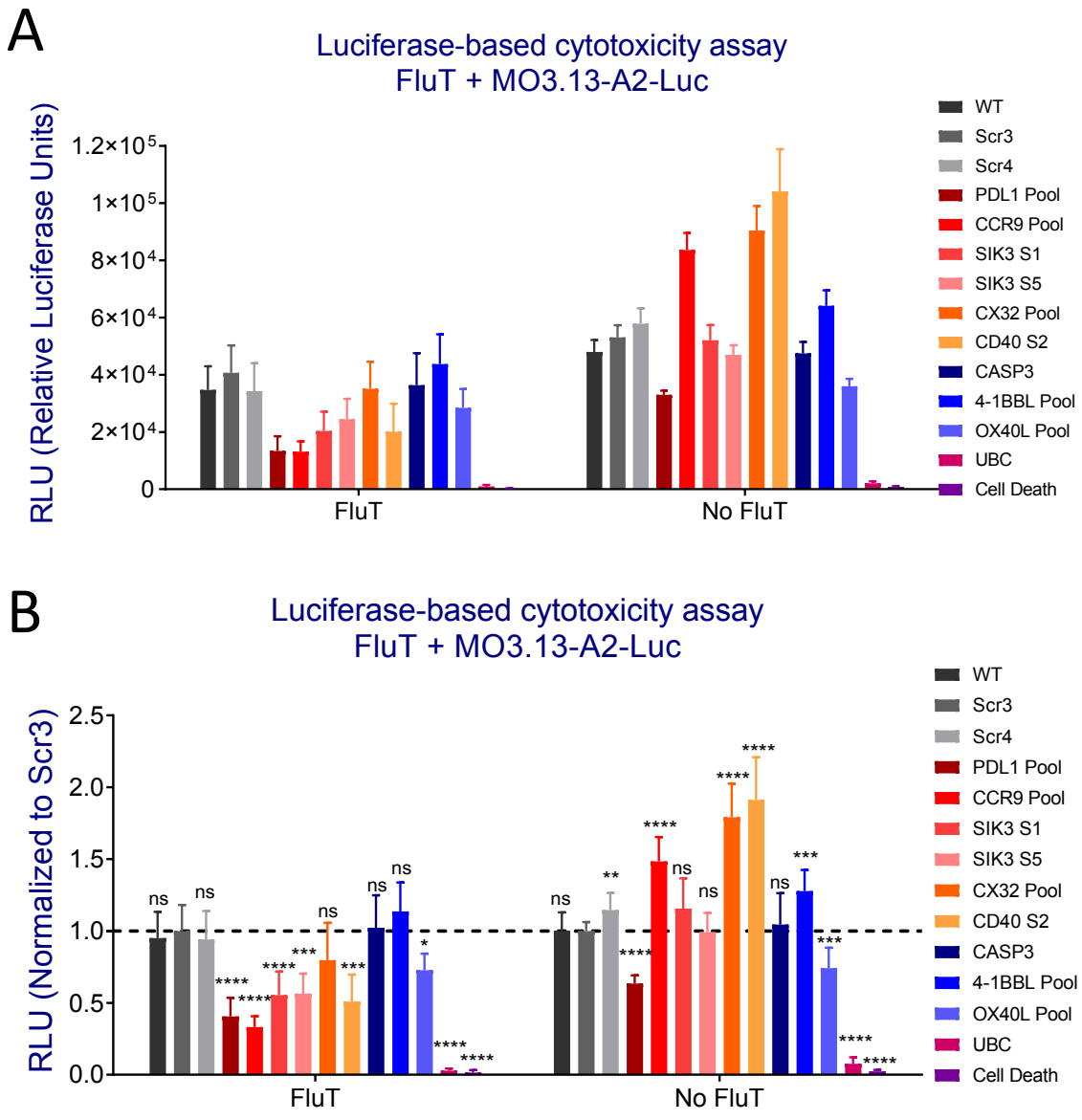

Figure 7: Luciferase-based cytotoxicity assay to determine appropriate controls for the HTP screen. (A-B) MO3.13-A2-Luc cells were transfected with the indicated siRNAs. After 72h of transfection cells are pulsed with flu peptide and cultured either with FluT or plain T cell media. 20h following co-

culture, remaining luciferase activity was measured. **(A)** Raw data showing relative luciferase units (RLU). **(B)** The RLU of each sample was normalized to the RLU of Scr3 transfected sample in the cytotoxicity (FluT) or viability (no FluT, medium) setting to determine the impact of gene knockdown. Cumulative data of two experiments each performed with four replicates per sample. Graphs show mean +/- SD. P-values were calculated using two-tailed student´s t-test. * = $p < 0.05$, ** = $p < 0.01$, *** = $p < 0.005$, **** = $p < 0.001$. Ursula Spirk contributed to generation of the data as a Bachelor`s student under my supervision.

3.2 Performance of the Primary HTP screen

3.2.1 Performance of controls and the primary HTP screen

After setting-up and optimizing appropriate controls, we performed a HTP screen in a 384-well format, using FluT from donor 11 as effector cells and MO3.13-A2-Luc as target cells. MO3.13-A2-Luc cells were transfected with a siRNA library consisting of 4155 genes including the whole surfaceome, different kinases and metabolic proteins. Transfected MO3.13-A2-Luc cells were either co-cultured with FluT three days post-transfection (cytotoxicity setting) or kept in plain medium (viability setting). The screen was conducted using technical duplicates. Luciferase readout was performed 21h after co-culture.

Plate normalization was performed as a first step of the data analysis, to exclude inter-plate variability during the readout (Figure 8A). Next, the performance of the control genes was determined. Non-targeting siRNAs (Scr3 & Scr4) did not show an impact in both cytotoxicity and viability settings. Transfection with UBC and cell death siRNA induced strong cell death. Downregulation of CCR9 did not affect cell viability and increased T cell cytotoxicity thereby resulting to be the strongest ICM among the other controls (Figure 8B). As a measure of technical quality and reproducibility of the screen, the Pearson correlation coefficient (r^2) was calculated for both settings. Pearson correlation coefficient for the replicates in cytotoxicity and viability settings were calculated as $r^2 = 0.94$ and $r^2 = 0.96$ respectively (Figure 8B).

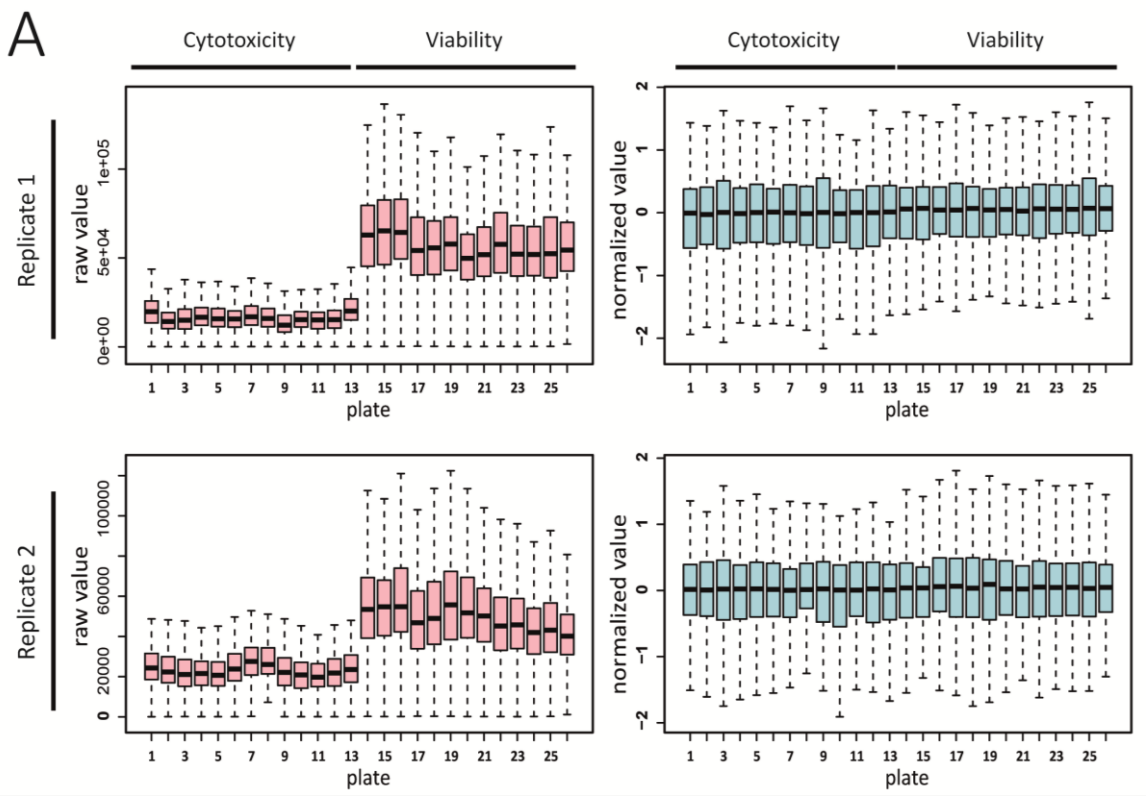
A
Cytotoxicity
Viability
Cytotoxicity
Viability
Replicate 1
raw value
0e+00
5e+04
1e+05
plate
normalized value
Replicate 2
raw value
0
20000
60000
100000
plate
normalized value

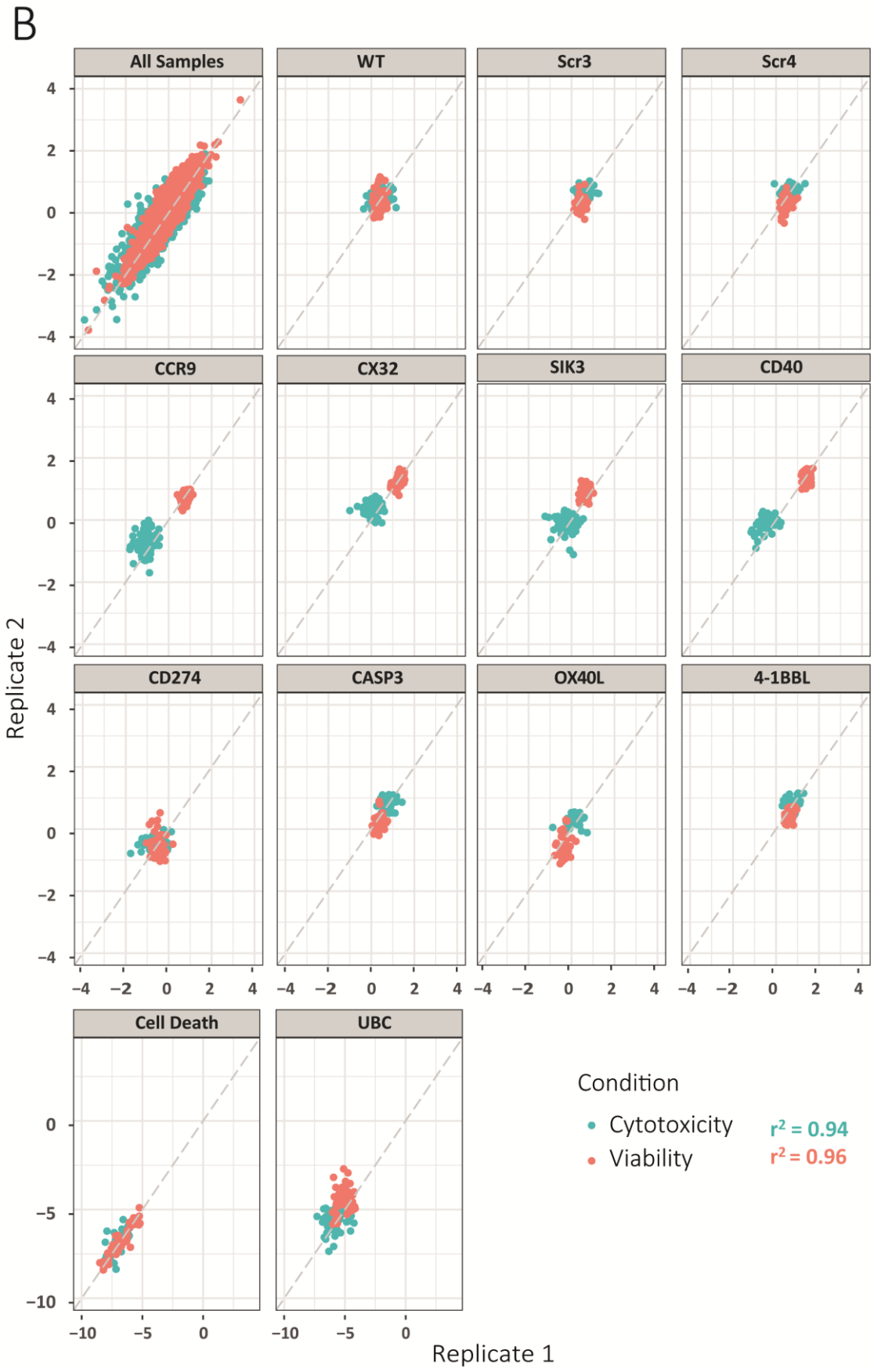

Figure 8: Performance of the controls. (A) Left panel: Raw luciferase activity (RLU) was measured for each well of 52 x 384-well plates. Upper and lower panels show replicate 1 & 2 respectively. Right

panel: To exclude inter-plate variability, RLUs were normalized using the following formula: Normalized RLU $=\log_2 x/M$, where x is the raw RLU from each well and M is the median RLU value in each plate. For each replicate set, plates from 1 to 13 were co-cultured with FluT at E:T = 20:1 (Cytotoxicity), while plates from 14 to 26 were cultured with plain T cell media (Viability) **(B)** Performance of the controls in the HTP-screen. Dot plot shows normalized RLUs after transfection of MO3.13-A2-Luc cells with several control siRNAs. Technical replicates were plotted against each other. Blue dots: cytotoxicity setting (with FluT). Red dots: viability setting (plain medium). Pearson correlation (r2) amongst the 2 replicate values was calculated for each setting (cytotoxicity setting: r^2 = 0.94; viability setting: r^2 = 0.96).

In order to identify novel MS-GBM associated immune-checkpoint molecules, the HTP screen data are analyzed by transforming the RLU values of each gene knockdown into z-scores, which is defined by the number of standard deviations between the corresponding data point and the mean of the plate. Each z-score was then multiplied with -1 for the simplification of the analysis. Thereby positive z scores indicate reduced luciferase intensity. An overview of the results from the primary screen is depicted in Figure 9. In the quadrant plot, each gene is plotted for its impact on cell viability (viability score) on the x-axis and the T cell mediated cytotoxicity (cytotoxicity score) on the y-axis. Scr siRNA served as negative control, since its transfection did not affect cell viability nor T cell cytotoxicity. The knockdown of the previously determined positive control CCR9 resulted in increased T cell cytotoxicity without having a major impact on cell viability. Potential co-inhibitory immune checkpoint molecules are the ones with high cytotoxicity and low viability scores (depicted in the black rectangle) (Figure 9A).

Genes were then ranked according to their differential score; a difference between the cytotoxicity and the viability z-scores using the local regression (LOESS) rank. LOESS-rank enables identification of candidate immune checkpoints whose knockdown shows the strongest immune-mediated phenotype (Figure 9B). The primary screen revealed 126 co-inhibitory HITs that were ranked higher than the best performing control CCR9. Among these HITs, we were able find several published immune modulators such as CEACAM6 (Carcinoembryonic antigen-related cell adhesion molecule 6) and NT5E (5'-nucleotidase, CD73) supporting the reliability of our screen approach [175, 176]. The primary screen also unraveled potential co-stimulatory immune checkpoints, however this project focused on co-inhibitory HITs, since the blockade of this class of proteins has been used as a immunotherapeutic strategy for several different tumor entities [177-181].

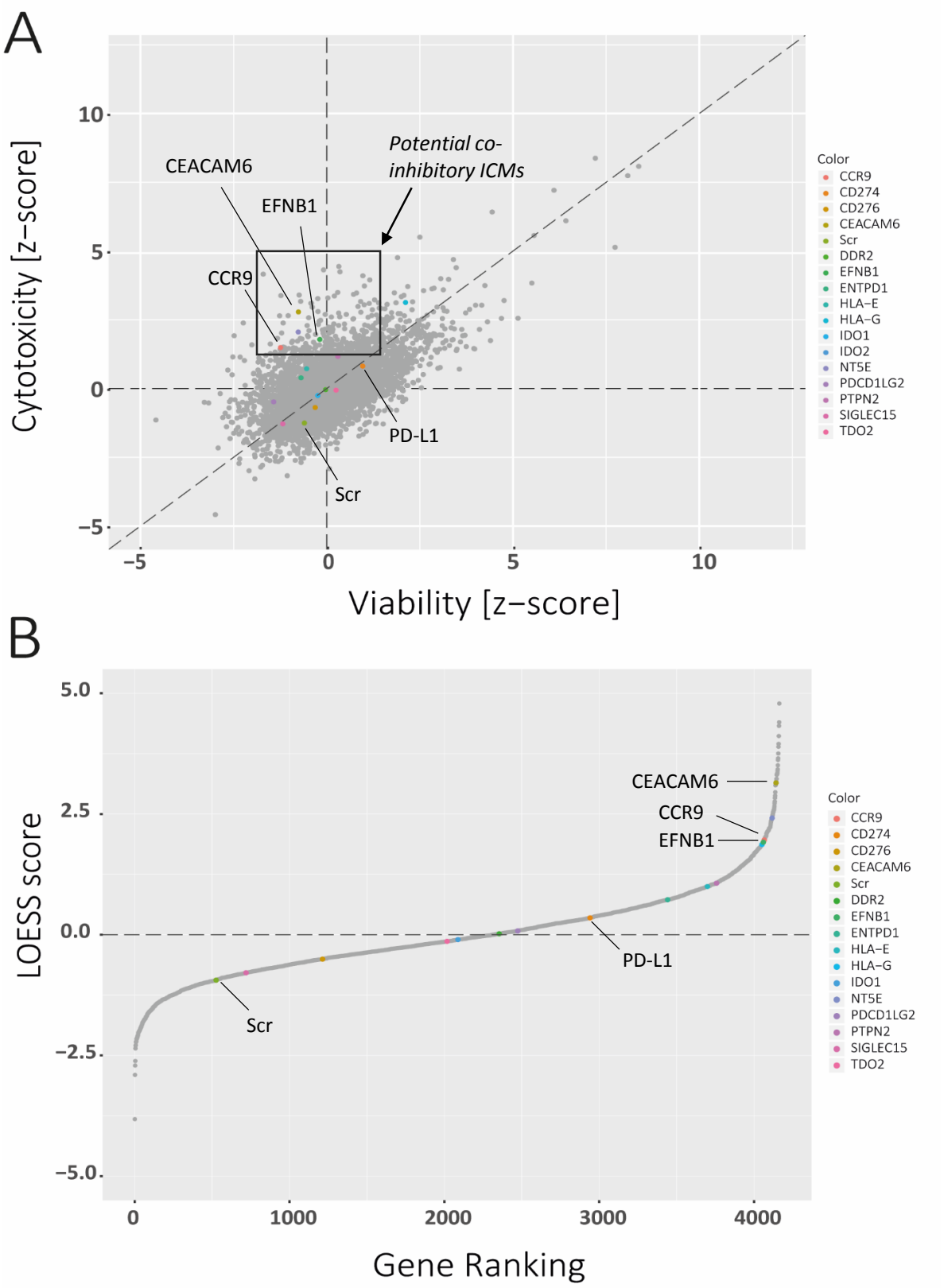

Figure 9: Performance of the HTP screen for the identification of novel MS-GBM-associated ICMs. **(A)** Overview of the results from the primary screen where the quadrant plot depicts the z-scores of the median-normalized luciferase intensity of transfected MO3.13-A2-Luc cells after co-culture with FluT D11 (cytotoxicity score) or with culture medium (viability score), using a siRNA library of 4155 genes plus control genes. The cytotoxicity score indicates the influence of the gene knock-down on

FluT-mediated killing. Positive values indicate decreased tumor cell viability. Potential co-inhibitory immune checkpoint molecules with high cytotoxicity and low viability scores are depicted in a box. **(B)** Gene ranking diagram showing the differential score between the cytotoxicity and viability z-scores using the local regression (LOESS) rank. Potential co-inhibitory immune checkpoints are represented in the ascending arm of the rank, whereas genes ranked in the lower arm could be potential co-stimulatory molecules. **(A-B)** Scores of Scr control, PD-L1, CCR9, CEACAM-6 and the selected HIT EFNB1 are highlighted in the graph. Published immune checkpoint genes were depicted in colored dots.

3.2.2 Selection strategy of candidate immune checkpoint molecules for further HITs validation

The goal for performing the primary HTP screen was to identify potential genes with an unknown role in immuno-oncology. Among the 126 co-inhibitory HITs that showed a stronger impact on T cell cytotoxicity compared to CCR9, 51 genes were selected for further validation based on their results in screen and literature search. Additionally, 5 HITs ranked lower than CCR9 and one potential co-stimulatory molecule (EPHA2) were selected. The selection criteria for the HITs were as following:

- Viability score between 2 > z > -2,0
- Druggability: the long-term aim of the project is to identify novel targets for immunotherapy of MS and glioma that could be easily targeted with antibodies. Therefore genes encoding for proteins associated with the plasma membrane, were prioritized
- Exclusion of cell essential genes such as those involved in translation and transcription mechanisms
- Presence of mouse homologs
- RNA and protein expression in human/mouse oligodendrocytes
- Expression in glioma tissue

I also investigated if the HITs had known disease associations such as mutations or SNPs especially linked with autoimmune diseases. Moreover, I also took advantage of mouse databases to research if knock-in/out resulted in immunological or neurological phenotypes. The names of the selected HITs and their rank in the primary screen are listed in the Table 1.

3.3 HITs selection and validation of selected candidate immune checkpoint molecules

3.3.1 Secondary screens with oligodendrocytes

In order to validate the results of the primary screen, two secondary screens were performed with two different siRNA libraries with 56 selected HITs (Figure 10). The primary screen library contained a pool of 4 non-overlapping siRNAs. By using pooled siRNAs, the possible off-target effect of each single siRNA can be reduced and the sequence coverage of the target mRNA can be increased. To validate the on-target effect of the individual siRNAs, the first secondary screen was performed with a deconvoluted library, where single siRNA sequences and pool of 4 were used separately to transfect MO3.13-A2-Luc cells (Dharmacon library) (Figure 10A). The secondary screens were performed in 96-well format using FluT D11 as effector cells. As in the primary HTP the luciferase-based readout was performed 20h after co-culture and the cytotoxicity and viability RLU values of each HIT were normalized to the RLU values of Scr in each setting. Thresholds for the cytotoxicity and viability ratios were set to reduce the HIT-list for further validation. I selected HITs which showed a viability ratio more than 0.75 (less than 25% viability impact) and a cytotoxicity ratio less than 0.6 (more than 40% increased T cell cytotoxicity) with at least two single siRNA sequences and the pool of four. In the first MO3.13-A2-luc screen, 37 out of 56 HITs were re-validated (Table 1).

In order to exclude potential off-target effects of siRNAs in a more efficient way, another second secondary screen was performed, where MO3.13-A2-Luc cells were transfected with a siRNA library consisting of a pool of 30 siRNA sequences (siTOOLs Biotech library). In this library, only the 37 HITs that were selected from the first secondary screen were included. The same threshold for the cytotoxicity and viability ratios were set as in the first secondary screen and it was observed that 23 HITs fitted to these criteria (Table 1). Excluded HITs from the first secondary screen were depicted in table 1 with a grey box.

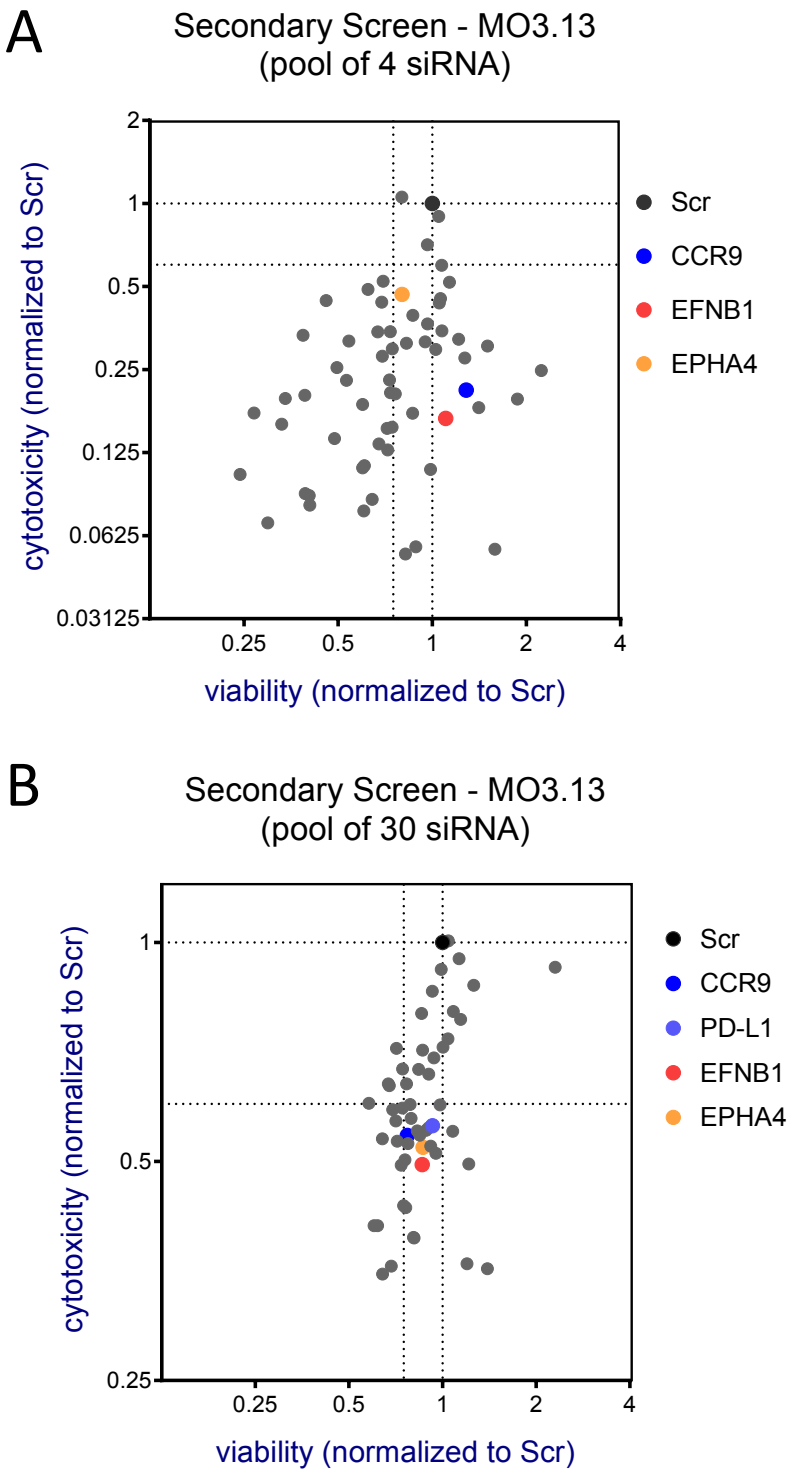

Figure 10: Results of the secondary screen with MO3.13-A2-Luc cells. (A) Secondary screen with pool of 4 siRNA library from Dharmacon (same siRNAs used in the primary HTP screen) Dots depict the values obtained from cells transfected with the pool of 4 siRNA **(B)** Secondary screen with the pool of 30 siRNA library from siTOOLs Biotech. RLU values from cytotoxicity and viability settings were normalized to the Scr control. Cytotoxity and viability ratios of Scr control, PD-L1, CCR9, and the selected HITs (EFNB1 and EPHA4) are depicted in colored dots. Experiments were performed in quadruplicates. (B) Antonia Engelhorn contributed to generation of the data as a Master`s student under my supervision.

3.3.2 Secondary screens with primary glioblastoma cells

MO3.13-A2-Luc cells are immortalized cell line generated by fusing human oligodendrocytes with rhabdomyosarcoma. They express oligodendrocyte markers such as myelin basic protein (MBP) and proteolipid protein (PLP). In order to test the impact of HITs in a more patient-relevant model, two additional screens were performed using primary brain tumor initiating stem cells isolated from a HLA-A2+ glioblastoma patient, RAV27 (Figure 11) (Kindly provided by department of Neurooncology, UKR). Before performing the screens, the same above mentioned optimization steps as for MO3.13-A2-LUC cells (generation of luciferase expressing cells, defining co-culture conditions, optimization of the transfection, identification of proper controls) were also performed for RAV27 cells (data not shown). The same siRNA libraries were used to transfect RAV27-Luc cells and FluT D11 were used as effector cells. Luciferase-based readout was performed 20h after co-culture. Cytotoxicity and viability RLU values of each HIT were normalized to the RLU values of Scr in each setting. For RAV27 cells, different thresholds were set for the cytotoxicity and viability ratios. I selected HITs which showed a viability ratio higher than 0.70 (less than 30% viability impact) and cytotoxicity ratio less than 0.75 (more than 25% increased cytotoxicity) with at least two single siRNA sequences and the pool of 4 regarding the Dharmacon library and fitting the same criteria for the 30 pool siTOOLs library. In the first RAV27 screen, 4 out of 56 HITs (ELFN2, EFNB1, HCN2, CADM4) were fitting the criteria. In table 1 more than 4 HITs are marked in green, since only values from the pool of 4 siRNAs were depicted. On the other hand, 15 out of 37 HITs showed an increased cytotoxicity with a minor impact on cell viability in the secondary screen with the 30 pool library (Table 1).

HITs validated in both MO3.13-A2-Luc screens were highlighted in red, whereas the 3 HITs (EFNB1, HCN2 and CADM4) that were validated in both oligodendrocyte and primary glioblastoma models were underlined in Table 1.

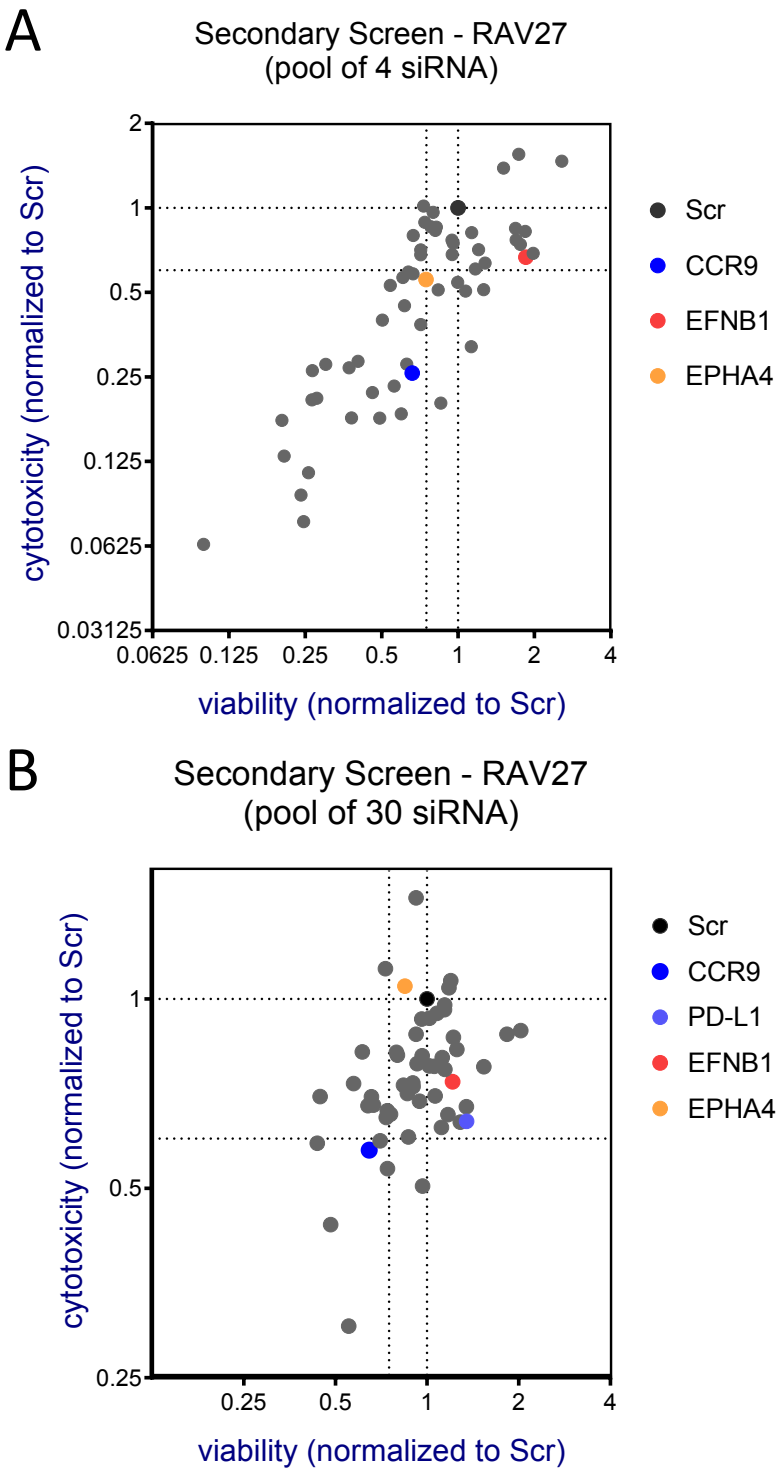

Figure 11: Results of the secondary screen with primary glioblastoma cells RAV27-Luc. (A) Secondary screen with pool of 4 siRNA library from Dharmacon (same siRNAs used in the primary HTP screen) Dots depict the values obtained from cells transfected with pool of 4 siRNA **(B)** Secondary screen with the pool of 30 siRNA library from the siTOOLs Biotech. RLU values from cytotoxicity and viability settings were normalized to the Scr control. Cytotoxicity and viability ratios of Scr control, PD-L1, CCR9, and selected HITs EFNB1 and EPHA4 were depicted in colored dots. Experiments were performed in quadruplicates.

Table 1: Results summary of all 4 secondary screens

Gene	Rank in the 1° screen	Secondary Screen - MO3.13 (Dharmacon - pool 4)		Secondary Screen - MO3.13 (siTOOLs - pool 30)		Secondary Screen - RAV27 (Dharmacon - pool 4)		Secondary Screen - RAV27 (siTOOLs - pool 30)	
		cytx	viab	cytx	viab	cytx	viab	cytx	viab
GPR27	1	0,06	0,89			0,71	1,20		
MLEC	2	0,71	0,96	0,78	1,14	1,39	1,51	1,07	1,20
CD300LG	3	0,49	0,62			0,83	0,81		
ABCA1	4	0,34	0,67	0,64	0,77	1,47	2,56	0,89	2,03
STK11	10	0,08	0,64	0,92	2,30	0,69	1,98	0,88	1,83
EVC2	11	0,13	0,67	0,74	1,04	0,08	0,25	0,50	0,97
HRK	15	0,08	0,60	0,60	0,58	0,51	1,07	0,81	0,80
FFAR1	17	0,07	0,30			0,68	0,95		
GABRB2	18	0,11	0,61			0,26	0,27		
COMT	22	0,13	0,72	0,69	0,94	0,06	0,10	0,65	0,73
CD79A	23	0,17	0,27	0,50	1,21	0,38	0,71	0,93	1,02
KCNH8	24	0,14	0,49	0,51	0,95	0,74	1,76	0,79	0,93
C20orf24	25	0,06	1,59	0,55	0,89	0,56	0,61	0,78	1,06
ISLR2	28	0,18	1,41	0,49	0,74	0,68	0,71	0,68	0,67
PRPS1	30	0,45	1,06	0,54	0,84	0,27	0,37	0,59	0,44
MAT2A	32	0,32	0,54	0,36	1,39	0,21	0,27	1,45	0,92
DISP2	34	0,20	0,34			0,85	0,82		
SYVN1	36	0,39	0,87			0,13	0,21		
ABCA2	38	0,10	0,24	0,59	0,69	0,64	1,28	0,64	1,29
ELFN2	40	0,08	0,41			0,51	1,26		
SLC31A2	42	0,09	0,40			0,59	0,64		

PCDHA9	44	0,25	2,23	0,64	0,67	1,55	1,73	0,66	0,74
LRRC37A2	52	0,32	1,21	0,72	1,00	0,28	0,63	0,73	0,90
HAS1	53	0,23	0,73	0,60	0,98	0,22	0,46	0,73	0,84
GPR12	57	0,09	0,39			0,61	1,17		
CLSTN3	58	0,19	0,60	0,80	1,08	0,54	1,00	0,93	0,96
LAPTM4A	63	0,05	0,82			0,86	0,78		
IGDCC3	69	0,16	0,33	0,36	0,68	0,09	0,24	0,65	1,17
MGAT5B	71	0,11	0,99			0,18	0,20		
LRRN1	74	0,21	0,74	0,39	0,81	0,28	0,40	1,12	0,73
TAAR9	75	0,11	0,60			0,18	0,38		
TMEM220	78	0,33	0,39			0,28	0,30		
RYR2	79	0,52	0,70			0,82	1,13		
C1orf162	80	0,30	1,03	0,66	0,90	0,89	0,74	0,78	1,54
SLC1A3	83	0,20	1,87	0,39	0,81	0,23	0,56	0,30	0,55
GRP	87	0,25	0,50			0,71	0,71		
PLXDC1	88	0,44	0,46			0,45	0,62		
DLL1	94	0,28	0,69	0,71	0,86	0,85	1,68	0,63	1,12
GPR156	96	0,28	1,27			0,77	0,95		
SIGLEC1	100	0,23	0,53	0,50	0,76	0,80	0,67	0,82	0,61
SMIM8	101	0,52	1,13	0,35	0,64	0,80	0,67	0,70	0,66
EFNB1	103	0,17	1,10	0,49	0,86	0,67	1,85	0,74	1,21
HCN2	105	0,30	1,50	0,56	0,90	0,32	1,13	0,71	0,86
IDH1	106	0,31	0,83	0,59	0,74	0,58	0,66	0,87	1,22
CHRNA1	107	0,34	0,73	0,55	1,08	0,82	1,84	0,77	1,14
SLC25A17	109	0,20	0,39	0,67	0,84	0,21	0,28	0,96	1,14
ELOVL7	110	0,32	0,95	0,95	1,13	1,02	0,73	0,66	0,76

TNFRSF1A	115	0,20	0,76	0,41	0,60	0,18	0,60	0,44	0,48
TM2D3	118	0,15	0,74	0,55	0,83	0,77	1,69	0,81	0,96
PDE3B	119	0,60	1,07			0,53	0,54		
NINJ1	121	0,44	0,69			0,18	0,49		
CADM4	128	0,15	0,72	0,54	0,64	0,51	0,83	0,60	0,70
KCNQ2	134	0,17	0,87	0,80	0,86	0,20	0,86	1,04	1,18
HCAR3	173	0,30	0,75	0,53	0,71	0,56	0,75	0,60	0,87
EPHA4	177	0,47	0,80	0,52	0,86	0,75	0,96	1,05	0,84
RAPGEF4	247	0,35	1,07	0,60	0,79	0,11	0,26	0,78	1,02
*EPHA2**	*4066*	1,15	1,30	0,43	0,76	0,59	0,67	0,68	0,64

HITs ranked according to their LOESS rank in the primary screen. The cytotoxicity and viability ratios of the HITs transfected with the pool of 4 or pool of 30 are depicted. Green box indicates ratios fitting to threshold criteria; grey box indicates absence of the HIT in 30pool library. Red marking indicates HITs validated in both MO3.13-A2-Luc screens, whereas underlined HITs were validated also in primary glioblastoma screens (cytx: cytotoxicity ratio, viab: viability ratio).

3.3.3 HITs expression in oligodendrocytes and primary glioblastoma cells

After having performed the secondary screens, the mRNA expression of the selected HITs was analyzed in MO3.13-A2-Luc and RAV27cells by conventional PCR. Apart from RYR2 whose expression could not be detected in RAV27, all tested HITs were found to be expressed at different levels in both cell types.

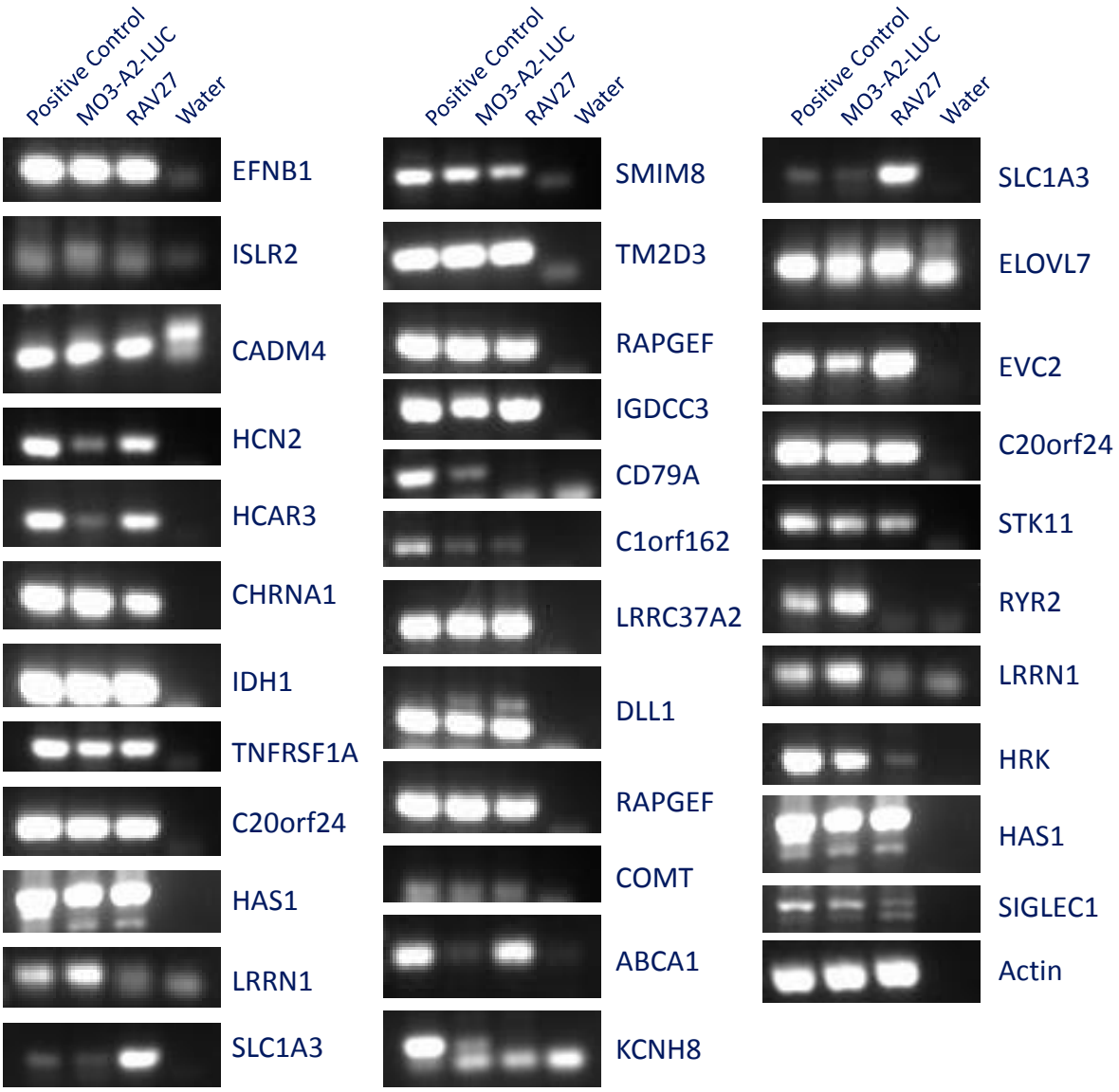

Figure 12: HITs expression in MO3.13-A2-Luc and RAV27 cells. Conventional PCR was performed to detect gene expression of candidate HITs validated in the MO3.13-A2-Luc screens. The positive control is a mixture of cDNAs from different tumor cell lines and PBMCs. β-actin was used as house-keeping gene. H_2O served as no template control.

3.4 EFNB1 regulates the cross-talk between oligodendrocytes and antigen-specific T cells

3.4.1 Selection of EFNB1 for further validation

Based on the outcome of the four secondary screens and on an extensive literature search, I selected EFNB1 (Ephrin-B1; ligand for erythropoietin producing hepatocellular carcinoma (Eph) receptors) for further functional validation. EFNB1 is ubiquitously

expressed [182] in oligodendrocytes as well, and upregulated in different types of cancer including glioma, pancreatic cancer and head and neck cancer. Ephrin ligands are single-pass type I transmembrane proteins and therefore their interaction with cognate receptors can be blocked by antibodies. The role of EFNB1 in neuronal development has been well studied, but so far no clear immuno-oncological function is known. In humans, mutated EFNB1 cause craniofrontonasal syndrome (CFNS), which is a rare X-linked genetic disorder causing facial asymmetry [183]. Mice carrying Efnb1 mutations also develop neurological and facial abnormalities [184]. There is also a study, which links EFNB1 expression on T cells with the immunopathogenesis of MS and EAE [185]. Of note, EPHA4, one of the cognate receptors of EFNB1, was also identified as a co-inhibitory molecule in the primary and secondary oligodendrocyte screens. Due to its above mentioned biological relevance; EFNB1 was selected as a promising, druggable target associated with glioma and MS.

3.4.2 EFNB1 siRNA transfection results in increased T cell mediated target cell killing

In four different secondary screens, the transfection of oligodendrocytes and glioblastoma cells with siRNAs targeting EFNB1 resulted in increased FluT cell mediated tumor cell killing. It was observed that transfection of MO3.13-A2-Luc cells with 3 out of 4 EFNB1-specific single siRNAs (S2, S3, S4) or the pool, increased the cytotoxicity mediated by FluT without having a major impact on cell viability (Figure 13A). Regarding the S2 and the pooled transfection, the observed phenotype was stronger than the knockdown of CCR9. In line with these findings in RAV27 cells, 2 out of 4 EFNB1-targeting siRNAs (S1 and S2) or the pool improved the T cell mediated killing to levels comparable to the knockdown of CCR9 (Figure 13B), however, less efficiently compared to the effect observed in MO3.13-A2-Luc cells.

I was able to validate the phenotype observed with single or pool of 4 siRNAs also with the pool of 30 siRNAs. For the single siRNAs a concentration of 25 nM was used for the transfection of the siRNAs, whereas for the pool of 30 a concentration of 5 nM was sufficient. Transfection of MO3.13-A2-Luc cells with the 30 pool targeting EFNB1 significantly improved the T cell mediated killing even stronger than CCR9 and PD-L1 knockdown (Figure 13C). Although this effect was not significant in RAV27 cells, it was comparable to the impact of PD-L1 downregulation (Figure 13D).

To increase the confidence of the role of EFNB1 on T cell cytotoxicity, chromium release assay was conducted as an independent approach (Figure 13E). For this assay, MO3.13-A2-Luc cells were transfected with the pool of 30 siRNAs targeting EFNB1 and co-cultured with different ratios of FluT cells for 6h. Compared to scramble transfection, modulation of EFNB1 increased the specific lysis to more than 10%. Except for the highest effector to target cell ratio (100:1), the impact of EFNB1 was found to be stronger than the knockdown of PD-L1.

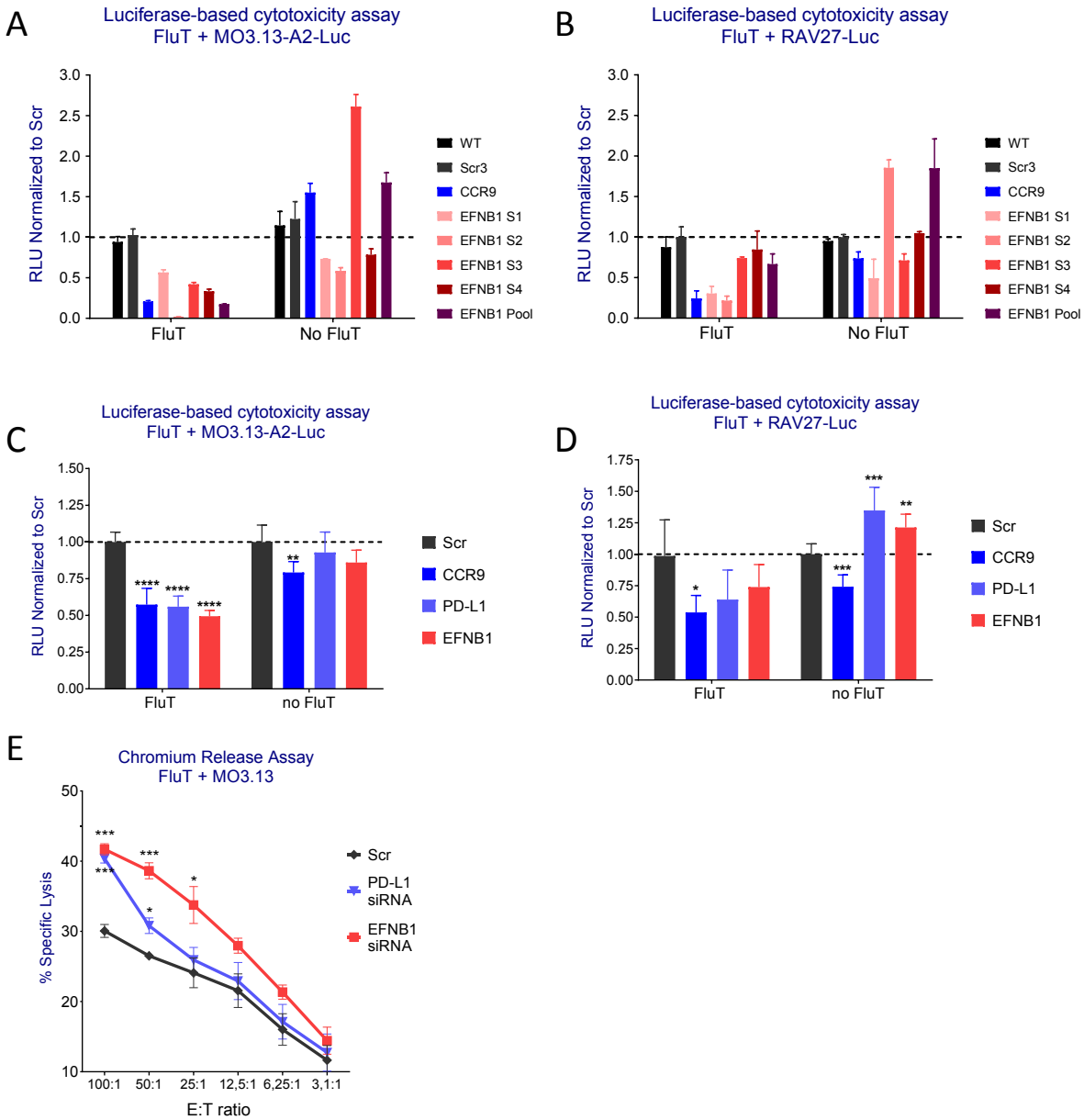

Figure 13: Impact of EFNB1 on T cell mediated glial cell killing. (A-D) Luciferase-based cytotoxicity assay to determine the impact of EFNB1 siRNA transfection in glial cells on FluT mediated killing of MO3.13-A2-Luc and RAV27 cells. **(A)** MO3.13-A2-Luc cells and **(B)** RAV27 cells were transfected with either single or a pool of 4 siRNAs targeting EFNB1. **(C)** MO3.13-A2-Luc cells and **(D)** RAV27 cells

were transfected with the pool of 4 siRNAs targeting EFNB1. After 72h of transfection, the cells are pulsed with a flu peptide and cultured either with FluT or plain T cell media. 20h following co-culture, remaining luciferase activity was measured. CCR9 and PD-L1 downregulation served as positive control, mock (WT) and Scr transfections were used as negative controls. **The** RLU of each sample was normalized to the RLU of Scr transfected samples in the cytotoxicity (FluT) or viability (no FluT, medium) settings to determine the impact of gene knockdown. **(E)** ^{51}Chromium-release assay as an independent kill assay to determine the impact of EFNB1 knockdown on specific cytolysis of MO3.13-A2-Luc cells by FluT cells. Transfected and with flu peptide pulsed cells were labelled with ^{51}Cr and co-cultured with FluT at different effector to target cell ratios (E:T) depicted on the x-axis. After 6h of co-culture, ^{51}Cr release was measured and the percent specific lysis was calculated. Representative data of 2 experiments. Graphs show mean +/- SD. P-values were calculated using two-tailed student´s t-test. * = $p < 0.05$, ** = $p < 0.01$, *** = $p < 0.005$, **** = $p < 0.001$.

3.4.3 EFNB1 levels are elevated in glioma cells and inversely correlated with patient survival

After validating the impact of EFNB1 on the T cell mediated primary glioblastoma cell killing, the expression levels of EFNB1 in different subtypes of glioblastoma tissues with non-neoplastic brain tissues were compared. Therefore, the RNA-Seq data from the TCGA database was analyzed. It was observed that different molecular subtypes of GBM express different levels of EFNB1 and in particular it was overexpressed in all of the subtypes compared to the non-neoplastic brain (Figure 14A). The highest EFNB1 expression was detected in the mesenchymal subtype which is characterized as highly immunogenic. A similar pattern was observed for the expression of PD-L1 in GBM patients [158, 159].

Furthermore, I analyzed the association between the EFNB1 expression and the clinical outcome in low grade glioma (LGG) patients (Figure 14B). I therefore used the web server TIMER (Tumor IMmune Estimation Resource), which enables the performance of correlations between different parameters such as survival and gene expression using the TCGA dataset. Interestingly, high levels of EFNB1 expression were correlated with worse survival of LGG patients compared to those patients who express EFNB1 at low levels. When I narrowed down the analysis and included only 15% of the patients with highest and lowest EFNB1expression, I observed that the impact of EFNB1 on patient survival became stronger (Figure 14B, lower panel). Thus, EFNB1 is a promising immune checkpoint target for the immunotherapy of glioma.

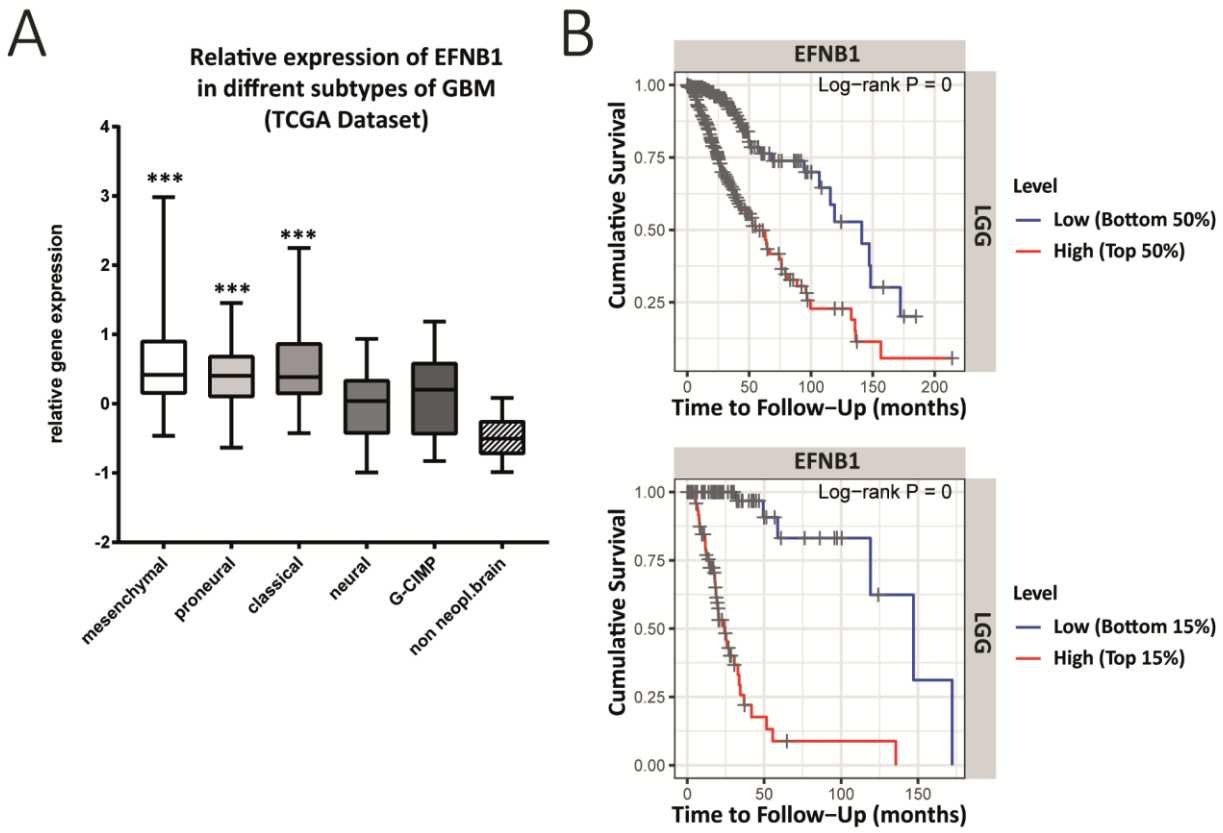

Figure 14: EFNB1 expression in glioma patients. (A) EFNB1 expression in different glioblastoma subtypes compared to the non-neoplastic brain (Data from the TCGA dataset). Relative gene expression of "0" indicates the means of all data sets of all genes included in the analysis. Statistics were performed using One-way ANOVA, Tukey's multiple comparison test. *** = $p < 0.001$. (Analysis was kindly performed by Dr. Tanja Rothhammer-Hampl, Department of Neuropathology, UKR). **(B)** The association between EFNB1 expression and the clinical outcome of low grade glioma (LGG) patients (TCGA dataset). Web server TIMER (Tumor IMmune Estimation Resource) was used for the analysis. Upper Kaplan Kaplan-Meier curve: Survival curve of LGG patients, where patients were stratified for EFNB1 expression as low (bottom 50%, blue) or high (top 50%, red). Lower Kaplan Kaplan-Meier curve: Survival curve of LGG patients, where only 15% of patients with highest (red) or lowest (blue) EFNB1 expression were taken into analysis.

3.4.4 EFNB1 levels are elevated in oligodendrocytes of EAE mice

Since I hypothesized that the HITs identified in oligodendrocytes may play a role in the immunopathology of MS and EAE, I wanted to investigate whether the expression of Efnb1 was differentially regulated in the brain of mice with EAE. Therefore, RNA from total brain of healthy or MOG-induced EAE C57BL/6 mice was isolated. EAE mice with different disease scores were included in the analysis. Conventional PCR showed strong Efnb1 expression in both healthy and diseased mice brain (Figure 15A). In order to quantify and compare the levels of Efnb1, qPCRs were performed. Compared to healthy

mouse brain, Efnb1 levels were decreased in EAE mice and inversely correlated with disease severity.

As mentioned in the section 3.2.2 one of the criteria for HITs selection was the expression of the candidate genes in mouse oligodendrocytes. To this end, I took into account the proteomic and RNA-Seq data published by Sharma *et al*. [186]. In this study Efnb1 was detected in mouse oligodendrocytes at mRNA and protein level. Next, the levels of Efnb1 were analyzed in oligodendrocytes and astrocytes isolated from healthy or MOG-induced EAE mice brain. Oligodendrocyte progenitor cells and astrocyte populations were isolated from dissociated brain by anti-O4+ and anti-ACSA2+ coupled magnetic beads using MACS separation. The remaining non-glial cells containing a mixture of microglia, neurons and potentially immune cells were also included in the analysis. In conventional PCR, Efnb1 was detected in each sample (Figure 15B). Subsequently, qPCRs were performed for relative quantification and normalized Efnb1 levels in oligodendrocytes and astrocytes to the Efnb1 levels in non-glial population. In healthy mice a 70% lower expression of Efnb1 was observed in oligodendrocytes, whereas astrocytes showed a similar expression level compared to non-glial cells (Figure 15D). Interestingly, in EAE mice, Efnb1 expression was strongly induced in oligodendrocytes, whereas astrocytes showed a 40% reduction compared to non-glial cells.

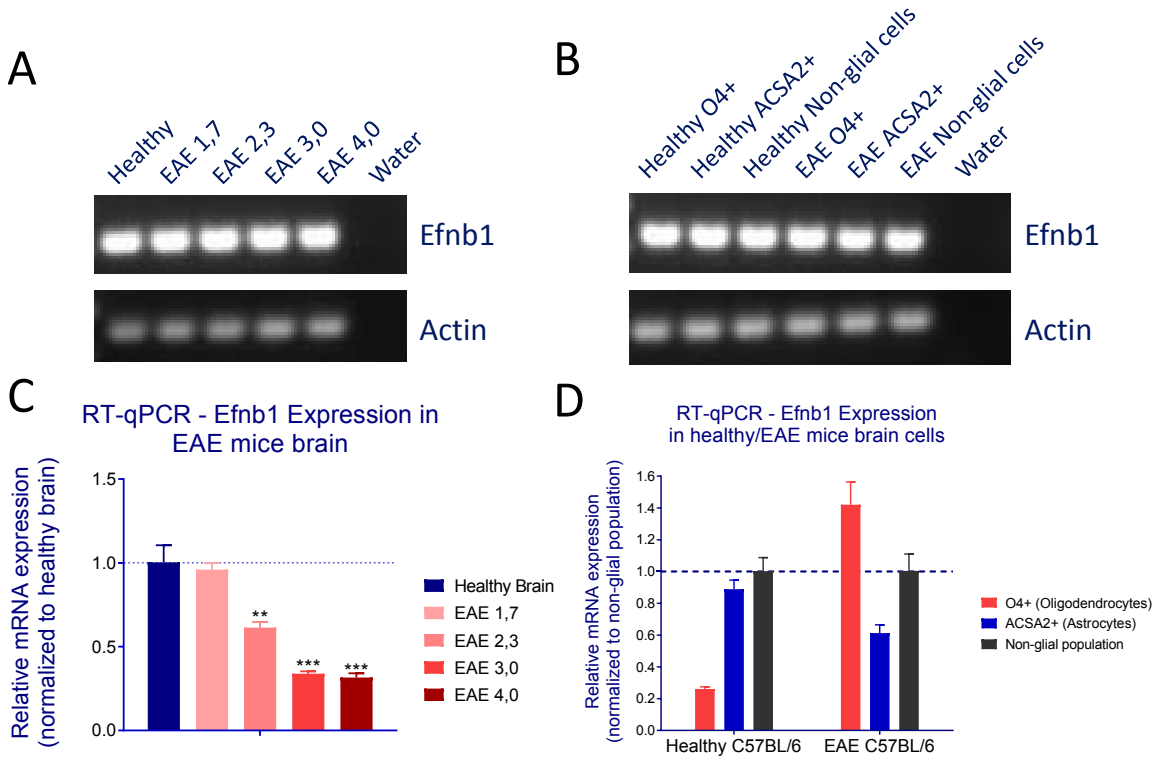

Figure 15: Efnb1 expression in the EAE experienced mice brain. (A) Expression of Efnb1 in total brain isolated from healthy or EAE induced C57BL/6 mice. RNA from the brain of healthy and EAE mice with different disease scores was isolated and converted into cDNA. Efnb1 levels were determined by PCR. **(B)** Expression of Efnb1 in glial and non-glial cells from healthy and MOG-induced EAE C57BL/6 mice. Mouse oligodendrocytes and astrocytes were isolated from the brains of healthy or EAE experienced mice by using MACS separation. Remaining non-glial population of cells was also collected. RNA from each cell population was converted to cDNA to determine Efnb1 expression by PCR. **(C)** Real-time qPCR analysis for relative quantification of Efnb1 levels in mice brain depicted in (A). Expression of beta-actin was used for normalization. mRNA expression in the EAE experienced mouse brains were normalized to the mRNA expression in the healthy brain. **(D)** Real-time qPCR for relative quantification of Efnb1 levels in the mice brain cells depicted in (B). Expression of beta-actin was used for normalization. mRNA expression in the oligodendrocytes and the astrocytes were normalized to the mRNA expression in non-glial cell population. Bars show median and error bars indicate +/- SD. Triplicates were used for qPCR. P-values were calculated using two-tailed student´s t-test. ** = $p < 0.01$, *** = $p < 0.005$. Mice brains were kindly provided by (A&C) Prof. Michael Platten, DKFZ, Heidelberg) and (B&D) Prof. Matthias Mack, UKR, Regensburg).

3.4.5 EFNB1 is expressed in different tumor entities

After the secondary screens, the expression of all selected HITs including EFNB1 was determined in MO3.13-A2-Luc and RAV27 cells. Next, the analysis was broadened to determine EFNB1 expression in different tumor entities and T cell sources. To this end, PCR was performed to determine the expression of EFNB1 in primary glioblastoma cells

from different patients (RAV301, RAV21, RAV232, RAV229), as well as the glioblastoma cell line U-251, the primary melanoma cells M579, the uveal melanoma cell line Mel285, the pancreatic ductal adenocarcinoma (PDAC) cell line PANC-1, the multiple myeloma cell line KMM-1, the breast cancer cell lines MCF-7 and MDA-231, the colon adenocarcinoma cell line SW-480, the lung adenocarcinoma cell line NCI H-23, the embryonic kidney cells 293T and the cervical adenocarcinoma cell line HeLa cells (Figure 16A). Moreover, the EFNB1 mRNA expression was assessed in different T cell sources such as, resting and activated FluT cells, marrow infiltrating lymphocytes (MILs), tumor infiltrating lymphocytes (TILs) isolated from melanoma, pancreatic ductal adenocarcinoma and lung adenocarcinoma tissues. EFNB1 was found to be expressed in all tested tumor and T cell types (Figure 16B).

I confirmed the surface expression of EFNB1 on tumor cells by performing FACS analysis. I stained MO3.13-A2-Luc cells, RAV27, RAV337 (primary glioblastoma cells), M579, PANC-1, KMM-1, KS (Kaposi's sarcoma cell line) and MCF-7 cells with a rabbit antibody recognizing extracellular domain of human EFNB1. In all tested cell types EFNB1 surface expression was detected to range between 50-80% (Figure 16C).

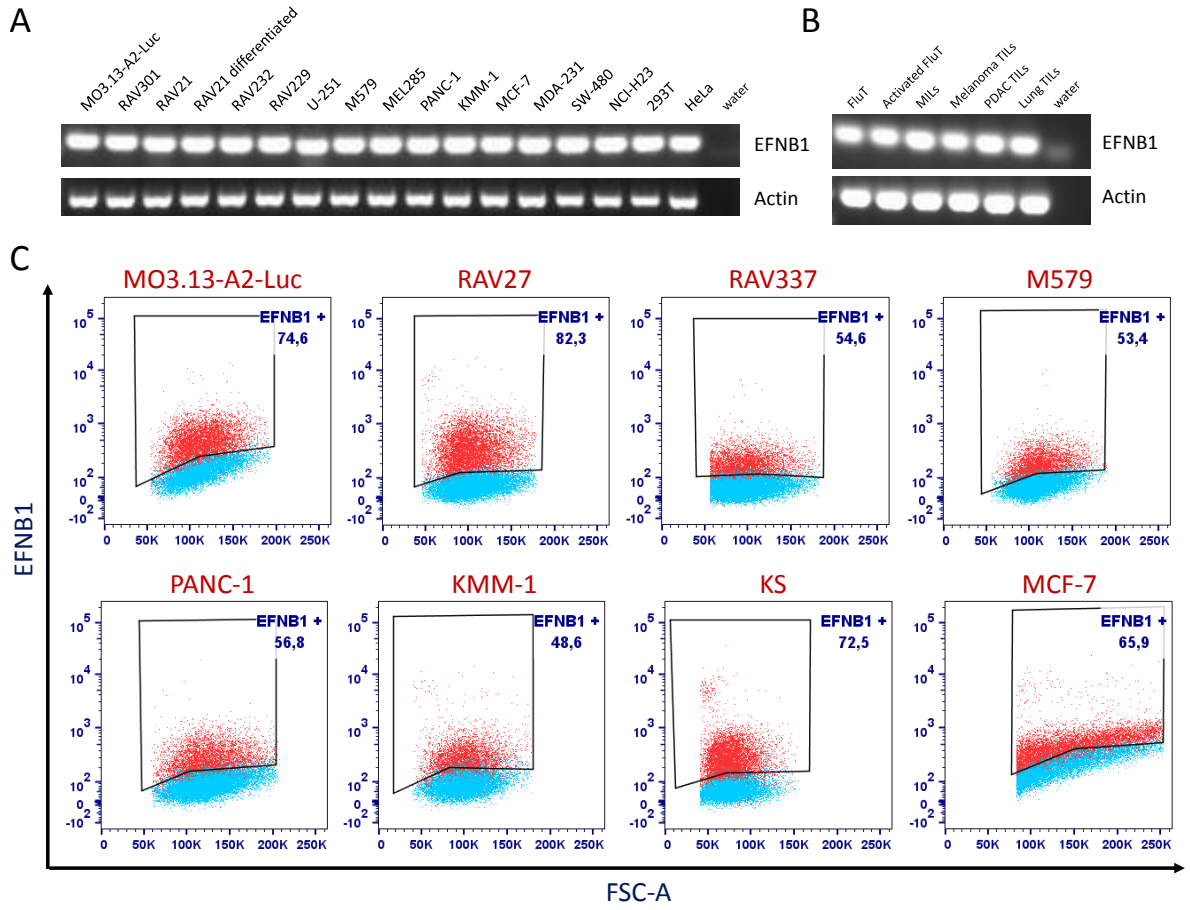

Figure 16: Expression of EFNB1 in different tumor cell lines and T cells. PCR for the detection of EFNB1 expression at mRNA level in **(A)** different human tumor cell lines **(B)** different human T cell sources. **(C)** FACS analysis for the surface expression of EFNB1 in different cell lines and primary cells. Gates indicate the percentage of EFNB1 on living cells. Blue: Negative control with secondary antibody (anti-rabbit - BV421) staining only, red: staining with primary anti-EFNB1 antibody and secondary anti-rabbit - BV421 antibody.

3.4.6 Ephrin receptors are expressed by T cells

After assessing the expression of EFNB1, the expression of Ephrin receptors cognate for EFNB1 (EPHA4, EPHB1-4 & 6) were determined on different T cell sources such as, resting and activated FluT cells, MILs, TILs isolated from melanoma, pancreatic ductal adenocarcinoma and lung adenocarcinoma tissues. All tested receptors were expressed by resting FluT cells. Interestingly, EPHA4 and EPHB6 levels were decreased and EPHB4 was slightly upregulated in activated FluT cells. Except for the lack of EPHB2 expression on MILs, all receptors were expressed at different levels in the tested T cell sources (Figure 17).

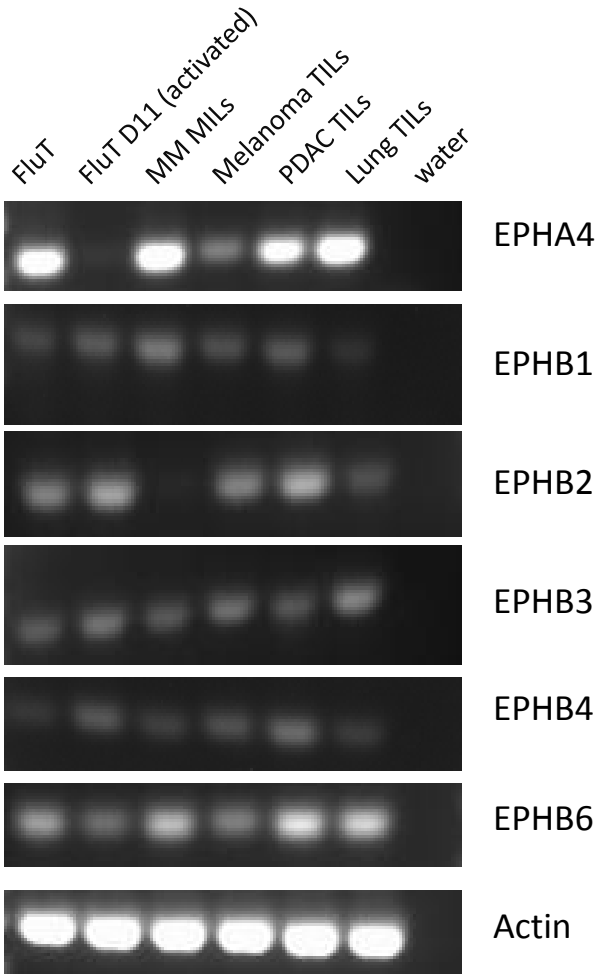

Figure 17: Expression of Ephrin receptors on human T cells. PCR analysis to determine the expression of EPHA4, EPHB1-2-3-4-6 in different human T cell sources at mRNA level. Actin was used as a loading control. Water served as a negative control

3.4.7 EFNB1 mRNA and protein levels inversely correlate following siRNA transfection

Evaluation of the siRNA knockdown efficiency is crucial for the validation of on-target effects. Therefore, the knockdown efficiency of pooled and single EFNB1 siRNA sequences were assessed in MO3.13-A2-Luc and RAV27 cells. First qPCRs were performed to determine the mRNA abundance. It was observed that both the pool of 30 and the pool of four as well as the single siRNA sequences lead to a significant reduction of approximately 80% of EFNB1 mRNA compared to the Scr control. The only exception was the single siRNA sequence S2 which downregulated EFNB1 levels by 50% in MO3.13-A2-Luc cells (Figure 18A-D).

In order to confirm the downregulation also at protein level Western Blot analyses were performed. Surprisingly, an upregulation of the EFNB1 protein was observed in MO3.13-A2-Luc and in the RAV27 cells after the transfection with the 30 pool of siRNAs (Figure 18E). In order to rule out a possible cross-reactivity of the anti-EFNB1 Western Blot antibody, these results were confirmed with two additional antibodies specific for different epitopes (data not shown).

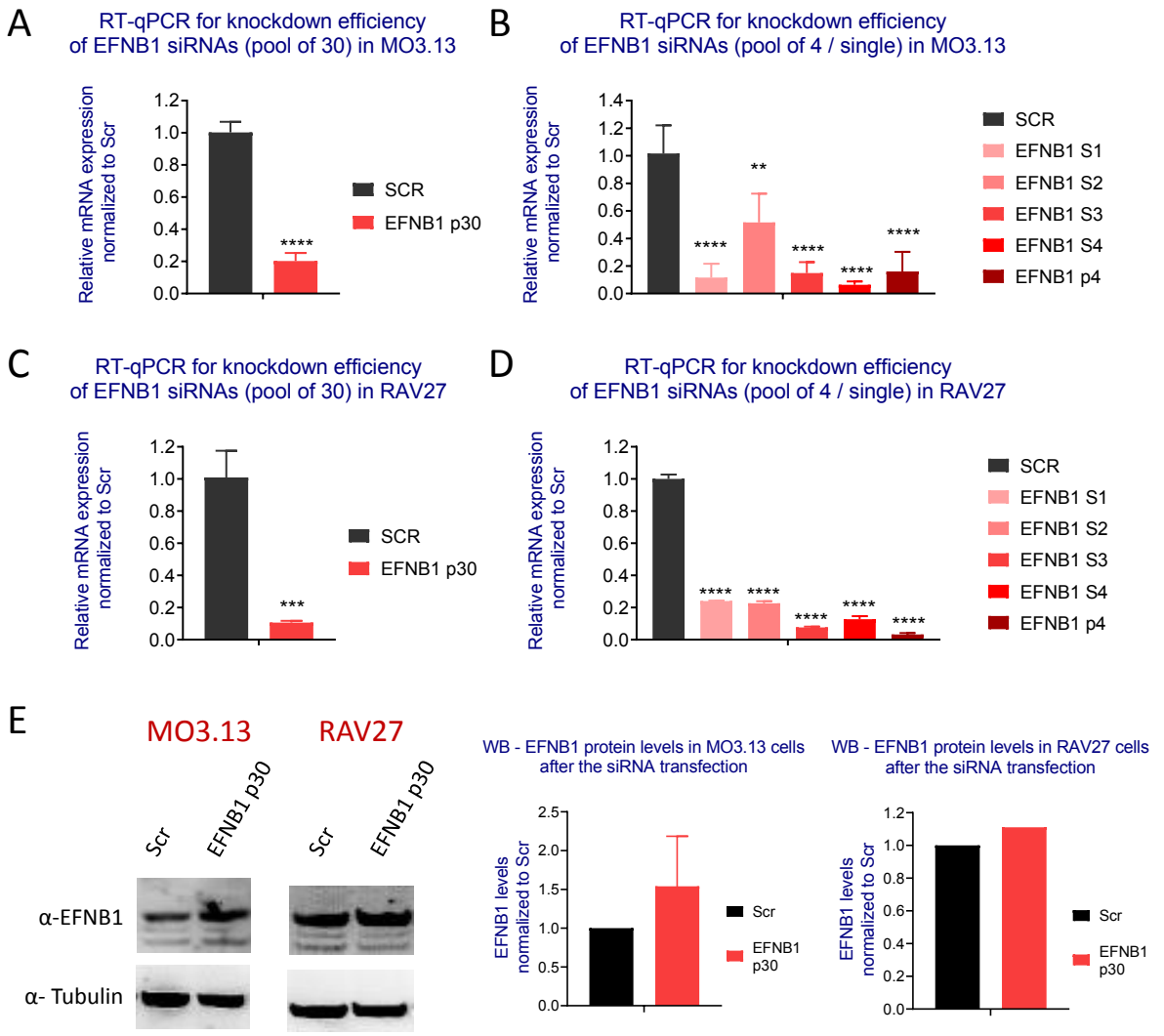

Figure 18: Analysis of EFNB1 siRNA knockdown efficiency by qPCR and western Blot. RT-qPCR was performed to analyze the knock-down efficacy of **(A&C)** pool of 30 siRNA, **(B&D)** single siRNAs and pool of 4 siRNAs from Dharmacon targeting EFNB1 **(A&B)** in MO3.13-A2-Luc cells and **(C&D)** RAV27 cells. Expression of beta-actin was used for the normalization. mRNA expression in the target samples were normalized to the mRNA expression in the Scr control. **(E)** Western Blot was performed to analyze the knock-down efficiency of EFNB1 at protein level. Total protein lysates were prepared from the MO3.13-A2-Luc and the RAV27 cells transfected with the pool of 30 siRNAs targeting EFNB1 or Scr control. Tubulin was used as a loading control. Right graphs: Relative quantification of protein abundance using ImageJ. EFNB1 protein

intensity was first normalized to the tubulin intensity, and then the protein intensity in the EFNB1 p30 sample was normalized to Scr. For MO3.13.13-A2-Luc, cumulative data of 4 experiments, for RAV27 representative graph of two experiments. Bars show median and error bars indicate +/- SD (A, E: n=4, B, C, D: n=2). P-values were calculated using two-tailed student´s t-test. *** = $p < 0.005$, **** = $p < 0.001$. Melanie Gimpl contributed to generation of the data as a Bachelor`s student under my supervision.

In order to validate the results of the Western Blot, FACS analysis was performed to investigate the surface expression of EFNB1 in MO3.13-A2-Luc and RAV27 cells after EFNB1 siRNA transfection. The epitope recognized by FACS antibody was only detected in EFNB1 according to a protein BLAST analysis. It was observed that, except from the single siRNA sequence S4, all EFNB1 siRNA transfections resulted in increased EFNB1 surface expression on MO3.13-A2-Luc cells compared to mock and Scr transfections (Figure 19A). Aligned with the Western Blot data, the increase in EFNB1 expression was not as strong as in RAV27 cells compared to MO3.13-A2-Luc cells. Nevertheless, also in RAV27 cells the pool of 30 siRNAs was not able to downregulate EFNB1 protein levels on the cell surface (Figure 19B).

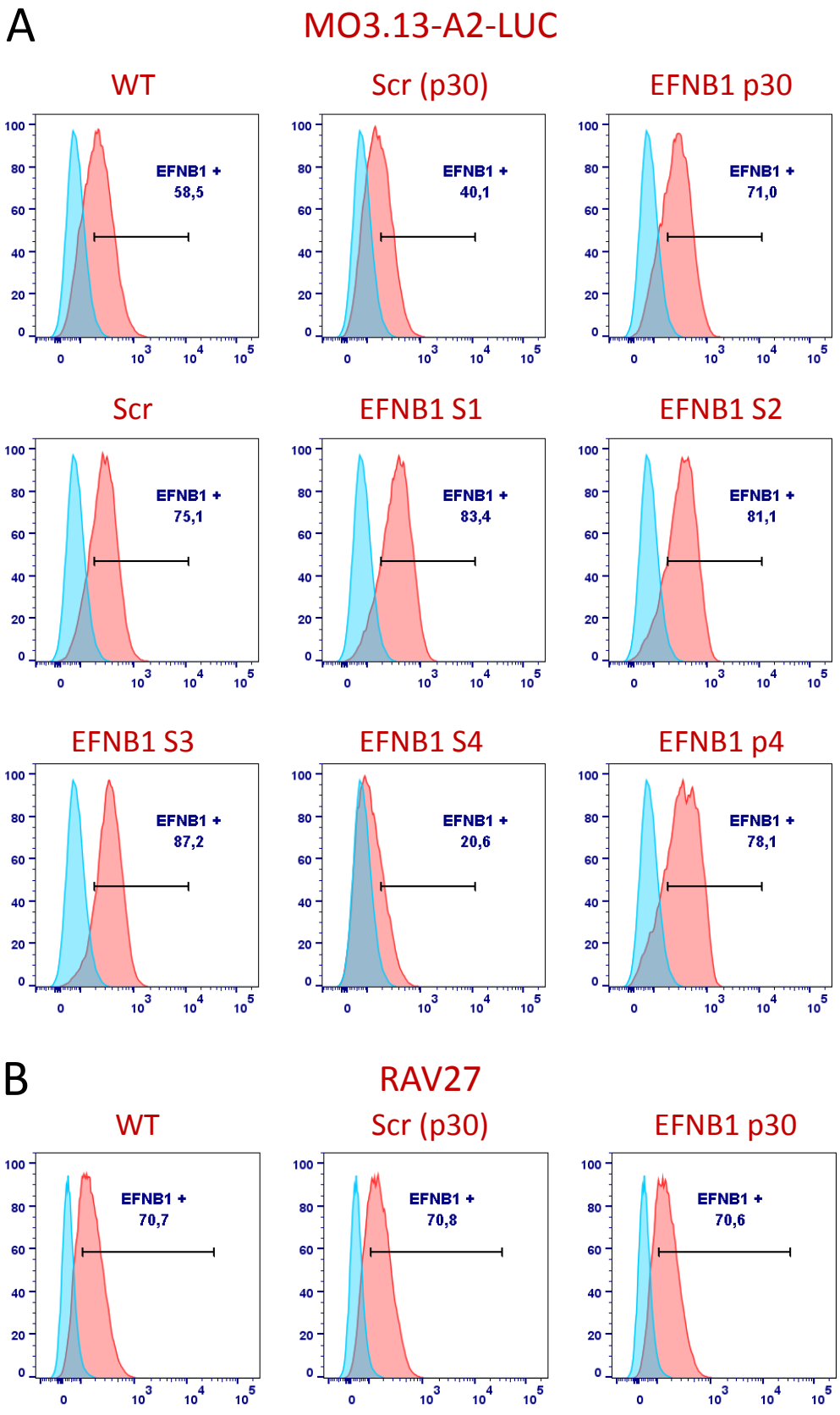

Figure 19: FACS analysis for the surface expression of EFNB1 in (A) MO3.13-A2-Luc and (B) RAV27 cells following EFNB1 siRNA transfection. Gate indicates the percentage of EFNB1 expression on living cells. Blue: Negative control with secondary antibody (anti-rabbit - BV421) staining only, red:

staining with primary anti-EFNB1 antibody and secondary anti-rabbit - BV421 antibody. (WT: mock transfection, Scr: non-targeting control, S1-4: single siRNA sequences, p4: pool of 4, p30: pool of 30). Representative data of three independent experiments.

3.4.8 EFNB1 expression may be regulated by non-coding RNAs

The inverse correlation between the mRNA downregulation and EFNB1 upregulation at protein level could find an explanation in the post-transcriptional and post-translational regulatory mechanisms [187].

One potential mechanism that may lead to a siRNA mediated overexpression of the EFNB1 protein could be the RNAi mediated silencing of non-coding RNAs that are involved in the regulation of EFNB1 expression [188]. To test this hypothesis, RNA-sequencing was performed on Scr and EFNB1 (pool of 30 siRNA) transfected MO3.13-A2-Luc cells. 18 non-coding RNAs were identified that were up- or downregulated more than 2 fold in EFNB1 silenced cells compared to the negative control (Scr). Interestingly, it was observed that the top differentially regulated non-coding RNA belong to the small nuclear RNA (RNA, variant U1 small nuclear 28) family involved in the splicing of pre-mRNA. These were upregulated more than 32-fold in EFNB1 mRNA deficient cells. Also a novel transcript was detected, which was downregulated in EFNB1 siRNA transfected cells more than 28-fold (Table 2).

Table 2: Non-coding RNAs differentially expressed in EFNB1 siRNA transfected MO3.13-A2-Luc cells compared to Scr transfected cells with more than 2-fold difference

ID	log2 Fold Change	chrom	strand	type	gene name	description
ENSG00000277918.1	5,055	chr1	-	snRNA	RF00003	RNA, variant U1 small nuclear 28
ENSG00000253154.2	1,697	chr8	+	lincRNA	AC100801.1	novel transcript
ENSG00000117226.11	1,402	chr1	-	nonsense mediated decay	GBP3	guanylate binding protein 3
ENSG00000259673.5	1,349	chr15	-	lincRNA	IQCH-AS1	IQCH antisense RNA 1
ENSG00000144959.9	1,322	chr3	-	nonsense mediated	NCEH1	neutral cholesterol ester hydrolase 1

				decay		
ENSG00000159588.14	1,319	chr1	-	nonsense mediated decay	CCDC17	coiled-coil domain containing 17
ENSG00000226674.9	1,227	chr2	+	lincRNA	TEX41	testis expressed 41
ENSG00000258311.5	1,227	chr12	+	nonsense mediated decay	BLOC1S1-RDH5	novel protein
ENSG00000284543.1	1,122	chr1	+	processed transcript	LINC01226	long intergenic non-protein coding RNA 1226
ENSG00000248538.7	0,978	chr8	+	lincRNA	AC022784.1	novel transcript
ENSG00000260249.2	0,976	chr16	+	antisense	AC007608.3	novel transcript, antisense to SNX20
ENSG00000269900.3	-1,008	chr9	-	lincRNA	RMRP	RNA component of mitochondrial RNA processing endoribonuclease
ENSG00000173727.12	-1,117	chr11	+	processed transcript	AP000769.1	Finkel-Biskis-Reilly murine sarcoma virus (FBR-MuSV) ubiquitously expressed (FAU) pseudogene
ENSG00000093010.13	-1,244	chr22	+	nonsense mediated decay	COMT	catechol-O-methyltransferase
ENSG00000080947.14	-1,65	chr1	-	processed transcript	CROCCP3	CROCC pseudogene 3
ENSG00000266560.5	-1,864	chrX	-	processed transcript	MAGEA10-MAGEA5	MAGEA10-MAGEA5 readthrough
ENSG00000274026.1	-1,938	chr9	-	processed transcript	FAM27E3	family with sequence similarity 27 member E3
ENSG00000284803.1	-4,84	chr15	-	processed transcript	AC245033.4	novel transcript

3.4.9 EFNB1 activates T cells and leads to increased cytokine secretion

Because of the increased EFNB1 expression after the transfection, I needed to re-interpret the HTP screen data. In contrast to our initial interpretation, EFNB1 could act as a T cell co-stimulatory molecule, since elevated EFNB1 levels on the surface of MO3.13-A2-Luc cells resulted in increased T cell mediated target cell killing. The co-stimulatory role of Efnb1 on mouse T cells was published before [189], but was not shown for human T cells.

In order to test this hypothesis, T cells were stimulated with the EFNB1 ligand tagged with the Fc part of the IgG molecule (EFNB1-Fc). Therefore, 96-well plates were coated overnight with different concentrations of EFNB1-Fc together with 1 µg/ml of anti-CD3 antibody. As a control, the Fc part of the IgG was coated together with the anti-CD3 antibody. IgG-Fc was added to the samples with lower EFNB1-Fc concentrations in order to achieve consistent total concentrations in every sample and to avoid titration of CD3-binding sites on the plate. After overnight coating, 100.000 FluT cells were added per coated 96-well and stimulated for 24-72h. Unstimulated T cells included to monitor the impact of the anti-CD3 activation alone. After stimulation the supernatant of FluT cells was collected and measured for Granzyme B, TNF-α, IFN-γ levels by sandwich ELISA. Compared to IgG-Fc treatment, stimulation of FluT with 10 µg/ml of EFNB1-Fc strongly increased the secretion of Granzyme B, TNF-α and IFN-γ by FluT cells (Figure 20A). Since I could not observe a prominent effect at a concentration of 20 µg/ml and 1,25 µg/ml EFNB1-Fc, I decided to use 10 µg/ml as the highest concentration for future experiments. It was observed that 2,5 µg/ml of EFNB1-Fc was sufficient to induce the same phenotype as 10 µg/ml of EFNB1-Fc (Figure 20A).

In order to investigate whether the induction of cytokine production would change over time, FluT-cells were stimulated for 24h, 48h and 72h and Granzyme B, TNF-α and IFN-γ ELISAs were performed. It was observed that until 72h, the impact of EFNB1 stimulation on the cytokine secretion was consistent (Figure 20B).

These results were confirmed with different T cell sources. The same experiment was performed using TILs isolated from two different glioblastoma patients, TIL337 and TIL339 and MART-1 antigen specific TILs isolated from a melanoma patient. TIL337 cells are composed of 7% and 91,5% of $CD8^+$ and $CD4^+$ cells respectively, whereas TIL339 are composed of 66% and 31% $CD8^+$ and $CD4^+$ T cells respectively. MART-1 specific T cells comprise only $CD8^+$ cells. Also for TILs, the anti-CD3/EFNB1-Fc stimulation significantly increased the cytokine secretion compared to the anti-CD3/IgG-Fc stimulation alone (Figure 21A). The cytokine levels secreted by TIL337 and TIL339 were lower compared to the levels measured by FluT-cells but the impact of EFNB1-Fc on the cytokine production was stronger on the TILs.

For the stimulation of MART-1 TILs, two more conditions were included in the setting. The samples were stimulated with 1 µg/ml anti-CD3 and 10 µg/ml - 2,5 µg/ml EFNB1-Fc

or 10 µg/ml IgG-Fc as described before. In order to asses if EFNB1-Fc stimulation without TCR downstream signaling can activate the T cells, MART1 TILs were treated with a Lck-inhibitor prior to stimulation with 10 µg/ml EFNB1-Fc. Additionally, MART-1 TILs were treated with rhynchophylline, an EPHA4 inhibitor (one of the EFNB1 receptors) and the cells were stimulated with 10 µg/ml EFNB1-Fc. After 24h of stimulation, Granzyme B, TNF-α, IFN-γ secretion was measured by ELISA. MART-1 TILs elevated the cytokine secretion significantly following the stimulation with EFNB1-Fc. Interestingly; this effect was reverted by treating the cells with EPHA4 inhibitor, which indicates that EPHA4 is the cognate receptor of EFNB1 expressed on MART1 TILs. TNF-α and IFN-γ levels in rhynchophylline treated samples were similar to the amounts in IgG-Fc stimulated TILs. Granzyme B secretion was not decreased upon treatment with EPHA4 inhibitor. Lck-inhibitor treatment cells completely abolished the TCR signaling and led to a loss of cytokine secretion. EFNB1-Fc stimulation alone could not induce cytokine secretion, indicating the TCR co-stimulatory role of EFNB1 (Figure 21B).

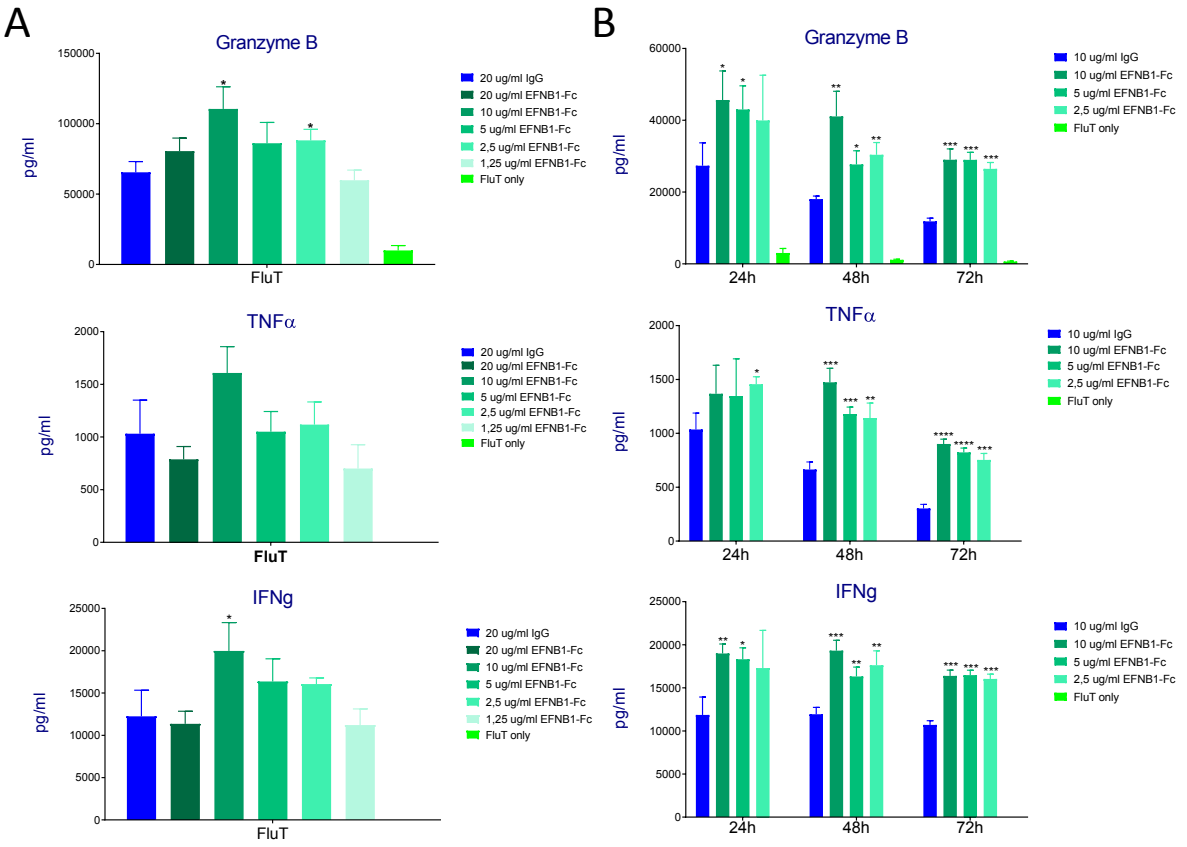

Figure 20: Stimulation of FluT cells with EFNB1 leads to increased cytokine secretion. FluT cells were stimulated with anti-CD3 together with different concentrations of anti-EFNB1-Fc (green) or anti-IgG-Fc (blue) for **(A)** 24h or **(B)** 24, 48 and 72h. After the indicated stimulation period, the

secretion of Granzyme B, TNF-α and Interferon-γ was determined by sandwich ELISA. Unstimulated T cells were included as a control (FluT only). Error bars indicate +/- SD. Significance for anti-CD3/EFNB1-Fc stimulated samples was calculated compared to anti-CD3/IgG-Fc stimulation. Triplicates were used for each sample. P-values were calculated using two-tailed student´s t-test. * = $p < 0.05$, ** = $p < 0.01$, *** = $p < 0.005$, **** = $p < 0.001$. (A) Representative data of four independent experiments. Hannes Linder contributed to generation of the data as a Bachelor`s student under my supervision.

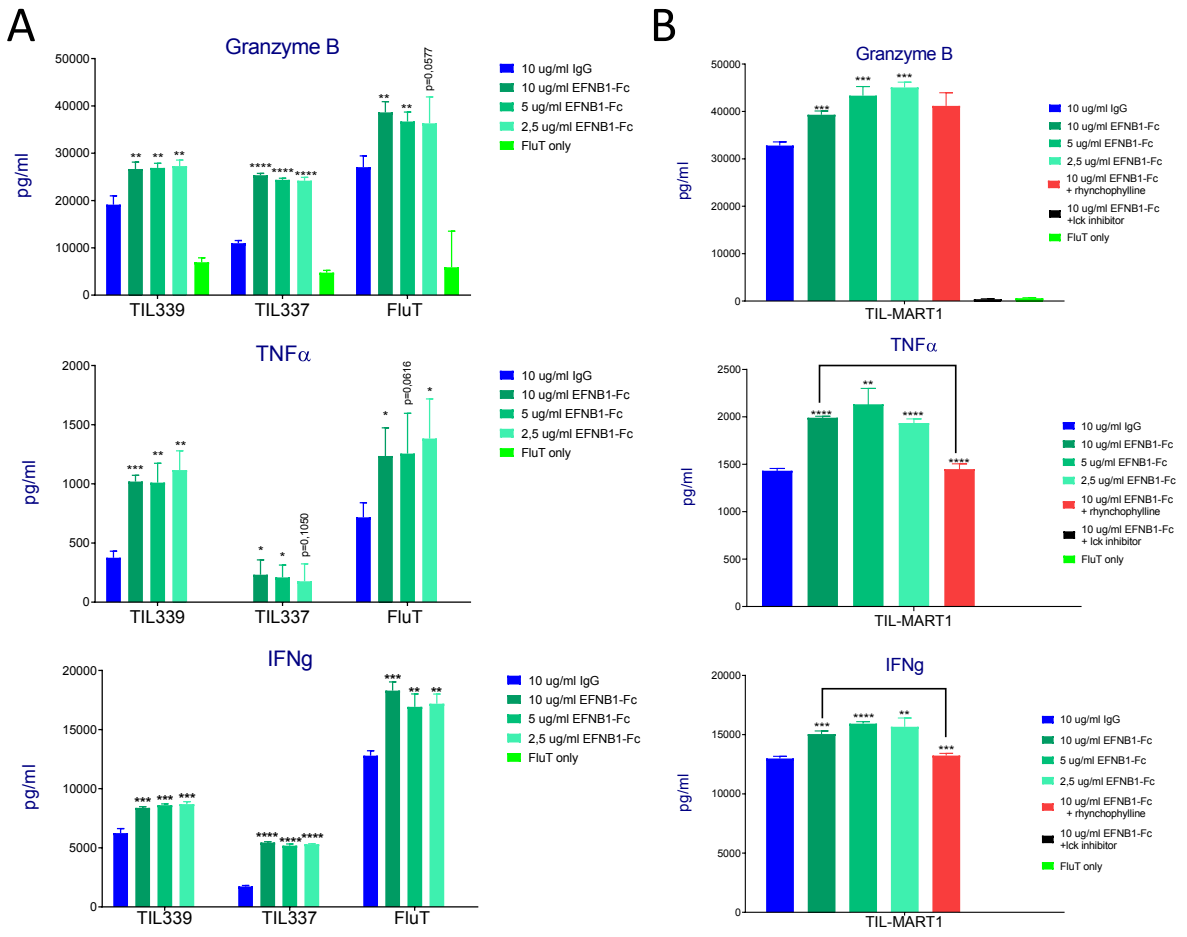

Figure 21: Stimulation of FluT cells and TILs from GBM and melanoma with EFNB1. (A) FluT cells and TILs isolated from two different GBM donors (TIL337 & TIL339) were stimulated with anti-CD3 together with different concentrations of anti-EFNB1-Fc (green) or anti-IgG-Fc (blue) for 24h. After stimulation, secretion of Granzyme B, TNF-α and Interferon-γ were determined by sandwich ELISA. **(B)** MART-1 antigen specific melanoma derived TILs were stimulated with anti-CD3 together with different concentrations of anti-EFNB1-Fc (green) or anti-IgG-Fc (blue) for 24h. Additionally, two samples stimulated with 10µg/ml of EFNB1-Fc were treated with EPHA4 inhibitor rhynchophylline (red) or Lck inhibitor (black). Error bars indicate +/- SD. Significance for anti-CD3/EFNB1-Fc stimulated samples was calculated compared to anti-CD3/IgG-Fc stimulation. Significance for rhynchophylline treated sample was calculated compared to sample stimulated with 10µg/ml of EFNB1-Fc. Triplicates were used for each sample. Representative data of two independent

experiments. P-values were calculated using two-tailed student´s t-test. * = $p < 0.05$, ** = $p < 0.01$, *** = $p < 0.005$, **** = $p < 0.001$.

In order to determine the expression of the activation/exhaustion markers PD-1, LAG-3 and TIM-3, FACS-analysis was performed on T cells following EFNB1 stimulation. For this experiment the same T cells from which the cytokine secretion was assessed were used (described in Figure 21). After 24h of stimulation and harvesting of the supernatant, FluT cells were stained for CD8, PD-1, LAG-3 and TIM3 expression. As expected, expression of activation markers was induced in T cells stimulated with anti-CD3/IgG-Fc compared to unstimulated cells. In concordance with the cytokine secretion data, stimulation of FluT cells with EFNB1-Fc augmented the expression levels of all tested markers and this effect correlated the EFNB1 concentration (Figure 22).

The same FACS analysis was performed on TILs from glioblastoma patients (TIL337 and TIL339) and MART-1 TILs. For the GBM TILs CD4 staining was included to determine if both CD8+ and CD4+ populations could be activated upon EFNB1 stimulation. The results of this FACS-analysis are depicted/summarized in Table 3 (dot plots are not shown). PD-1 and LAG-3 levels were both elevated on EFNB1-Fc stimulated CD4+ and CD8+ TIL337 and TIL339. TIM-3 expression on CD8+ cells showed a similar pattern, whereas it did not change on CD4+ TILs compared to IgG-Fc control. On the other hand, for MART-1 specific TILs, it was observed that already 86,2% of unstimulated cells express PD-1. Upon stimulation with anti-CD3/IgG-Fc only a slight increase in PD-1 expression was observed, which was not further elevated upon anti-CD3/EFNB1-Fc stimulation. LAG-3 expression was also already strongly induced by anti-CD3/IgG-Fc and I observed a 3,6% increase when the cells were stimulated with anti-CD3/EFNB1-Fc. The impact of EFNB1 on TIM-3 upregulation on MART-1 specific TILs was more prominent compared to other markers. In alignment with the ELISA data, treatment of anti-CD3/EFNB1-Fc stimulated MART-1 TILs with EPHA4 inhibitor downregulated the expression of the activation markers to similar levels as on anti-CD3/IgG-Fc stimulated cells. Additionally, inhibition of Lck strongly reduced the levels of activation markers to similar levels of unstimulated cells.

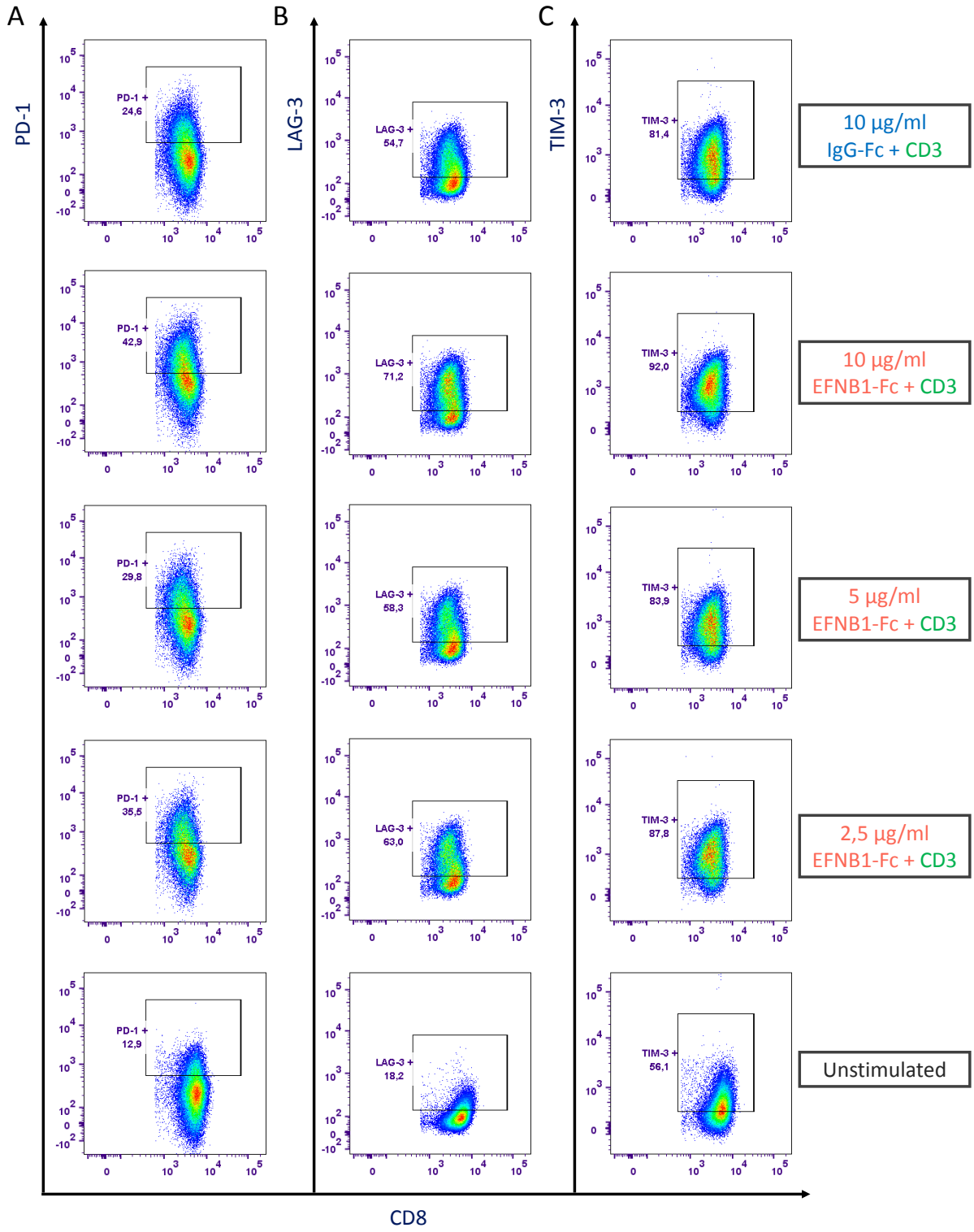

Figure 22: Stimulation of FluT cells with EFNB1 elevated the expression of activation markers. FluT cells were stimulated with anti-CD3 together with different concentrations of anti-EFNB1-Fc or anti-IgG-Fc. After 24h, FACS analysis was performed to determine the expression of **(A)** PD-1, **(B)** LAG-3, **(C)** TIM-3 on $CD8^+$ cells. Gates were set based on the isotype controls. Representative results of three independent experiments.

Table 3: Percentages of PD-1, LAG-3 and TIM-3 expressing FluT cells, TIL337, TIL339 and MART-1 TILs upon stimulation with EFNB1-Fc

FluT		10 ug/ml IgG-Fc	10 ug/ml EFNB1-Fc	5 ug/ml EFNB1-Fc	2,5 ug/ml EFNB1-Fc	No stimulation
PD-1	CD8	24,6 %	42,9 %	29,8 %	35,5 %	12,9 %
LAG-3	CD8	54,7 %	71,2 %	58,3 %	63,0 %	18,2 %
TIM-3	CD8	81,4 %	92,0 %	83,9 %	87,8 %	56,1 %
TIL337		**10 ug/ml IgG-Fc**	**10 ug/ml EFNB1-Fc**	**5 ug/ml EFNB1-Fc**	**2,5 ug/ml EFNB1-Fc**	**No stimulation**
PD-1	CD8	21,7 %	34,8 %	29,4 %	29,7 %	14,7 %
	CD4	37,7 %	43,4 %	40,3 %	40,5 %	31,7 %
LAG-3	CD8	66,7 %	84,0 %	79,5 %	79,1 %	51,7 %
	CD4	23,6 %	35,2 %	31,4 %	32,6 %	19,4 %
TIM-3	CD8	90,3 %	96,3 %	93,8 %	93,2 %	78,5 %
	CD4	75,7 %	75,4 %	73,2 %	71,6 %	69,7 %
TIL339		**10 ug/ml IgG-Fc**	**10 ug/ml EFNB1-Fc**	**5 ug/ml EFNB1-Fc**	**2,5 ug/ml EFNB1-Fc**	**No stimulation**
PD-1	CD8	18,1 %	39,3 %	28,7 %	37,8 %	11,0 %
	CD4	45,5 %	54,5 %	51,0 %	55,1 %	44,3 %
LAG-3	CD8	76,3 %	83,0 %	83,3 %	85,0 %	72,2 %
	CD4	16,8 %	21,7 %	21,7 %	23,1 %	17,6 %
TIM-3	CD8	86,6 %	92,9 %	91,4 %	93,8 %	78,0 %
	CD4	78,0 %	70,3 %	75,1 %	72,1 %	75,8 %
TIL-MART1		**10 ug/ml IgG-Fc**	**10 ug/ml EFNB1-Fc**	**10 ug/ml EFNB1-Fc +rhynchop hylline**	**10 ug/ml EFNB1-Fc + Lck - inhibitor**	**No stimulation**
PD-1	CD8	94,2 %	95,8 %	94,4 %	86,5 %	86,2 %
LAG-3	CD8	86,1 %	89,7 %	88,1 %	51,6 %	58,7 %
TIM-3	CD8	69,5 %	81,2 %	72,5 %	1,8 %	3,6 %

3.4.10 EFNB1 overexpression by oligodendrocytes leads to activation of T cells

After confirming the co-stimulatory role of EFNB1 on T cells, I investigated whether EFNB1 expressed on MO3.13-A2-Luc cells had the same impact on T cell activation. Therefore, EFNB1 overexpressing MO3.13-A2-Luc cells were generated by transfecting them with a mammalian expression plasmid encoding for the open reading frame (ORF) of EFNB1. After 2 weeks of hygromycin selection, the expression of EFNB1 was compared by FACS analysis between transfected cells and untransfected control (WT). It was observed that a strong induction from 58 to 82% of EFNB1 expression on the surface of transfected cells (Figure 23A). Next, EFNB1 overexpressing cells were co-cultured with FluT cells to test if elevated EFNB1 levels on the target cells could stimulate T cells. WT and EFNB1 overexpressing MO3.13-A2-Luc cells were co-cultured with 2500 or 5000 FluT cells and after 20h of co-culture the supernatant was harvested and TNFα ELISA was performed. TNFα secretion by FluT cells was strongly increased upon encountering more EFNB1 on target cells (Figure 23B). Consequently, the co-stimulatory role of EFNB1 could be confirmed in a co-culture model as well.

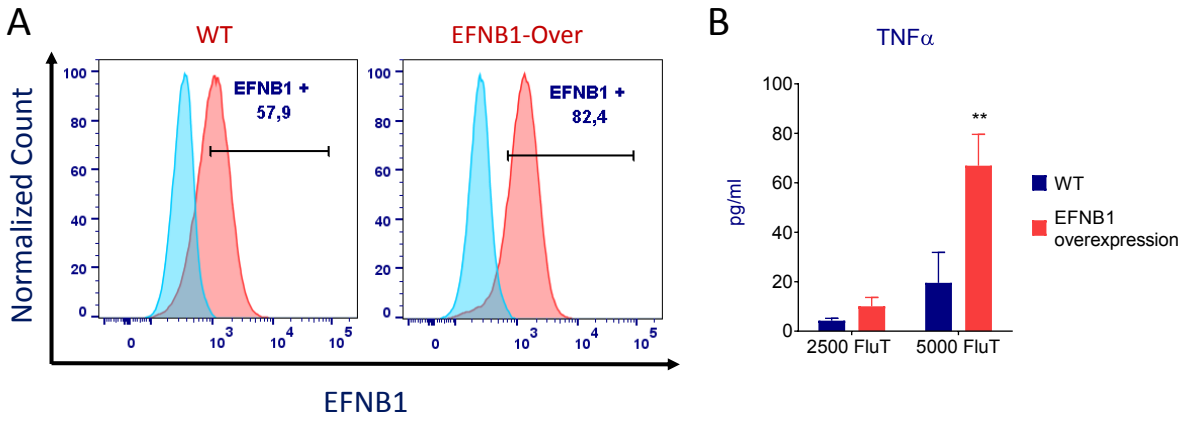

Figure 23: EFNB1 overexpression by oligodendrocytes leads to activation of T cells (A) FACS-analysis for EFNB1 expression on MO3.13-A2-Luc cells transfected with EFNB1 ORF encoding plasmid compared to untransfected (WT) cells after 2 weeks of hygromycin selection. Blue: Negative control with secondary antibody (anti-rabbit - BV421) staining only, red: staining with primary anti-EFNB1 antibody and secondary anti-rabbit - BV421 antibody. **(B)** TNFα secretion by FluT cells upon co-culture with EFNB1-overexpressing or WT MO3.13-A2-Luc cells. 20.000 MO3.13-A2-luc cells were seeded for 24h and were co-cultured with different amounts of FluT cells. After 20h of co-culture ELISA was performed to detect TNFα levels in the supernatant. Error bars indicate +/- SD. P-values were calculated using two-tailed student´s t-test. ** = $p < 0.01$. Representative data of 2 independent experiments.

3.4.11 EPH forward signaling stimulates T cells through Akt-mTOR pathway

Next, I wanted to investigate the mode of action of EFNB1 in mediating co-stimulation to T cells. I performed literature research to determine the key players in the ephrin receptor downstream pathway (forward signaling). As described in the section 1.1.1. CD28 is one the most prominent T cell co-stimulatory molecule and acts through phosphoinositide 3-kinase (PI3K) and protein kinase B (Akt). Ligation of CD28 with its cognate ligands CD80/CD86 leads to phosphorylation of Akt, which in turn activates several transcription factors through additional downstream molecules such as mTOR. Among these transcription factors, NF-κB induces gene expression of various cytokines, which in turn promotes T-cell effector functions [190, 191]. Interestingly, I observed that ephrin receptors use the common pathway (PI3K/Akt) with CD28 (Figure 24A) [192, 193]. Thus I hypothesized that ligation of ephrin receptors with EFNB1 on T cells may mimic the CD28/CD80 signaling pathway thereby stimulating T cells.

To test this hypothesis, FluT cells were stimulated with plate coated anti-CD3/EFNB1-Fc or anti-CD3/IgG-Fc (as described in 3.4.9) for 30 min and Western Blot was performed to determine the phosphorylation levels of Akt and mTOR in FluT cells. Additionally, the pan-Akt levels were determined to confirm that the changes in phospho-Akt were caused by a differential phosphorylation activity and not by a modified expression of Akt. It was observed that the stimulation of FluT with anti-CD3/EFNB1-Fc resulted in almost 3-fold increase in Akt and mTOR phosphorylation compared to anti-CD3/IgG-Fc stimulation (Figure 24B). This confirms that Eph receptors on FluT cells transduce downstream signaling through the Akt-mTOR pathway upon EFNB1-mediated stimulation.

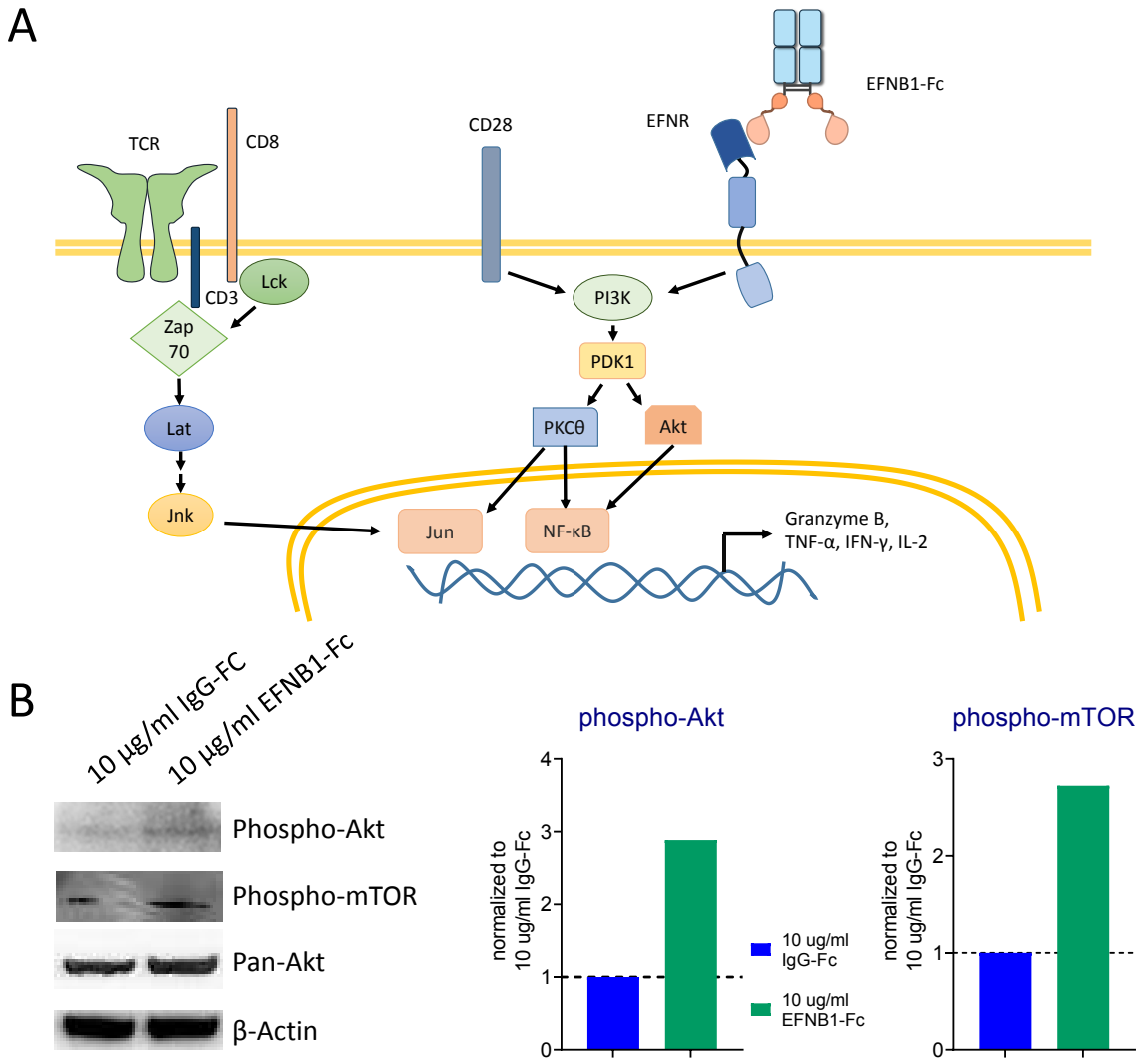

Figure 24: Mode of action analysis of EFNB1-Ephrin receptor (EFNR) forward signaling. (A) Overview of Ephrin receptor downstream pathway. EFN-Eph forward signaling shares common nodes with B7/CD28 downstream pathway such as PI3K and Akt. Phosphorylation of Akt leads to nuclear translocation of NF-κB which in turn promotes T cell activation by inducing the expression of effector cytokines. **(B)** Determination of Akt - mTOR phosphorylation in FluT cells upon stimulation with EFNB1-Fc. FluT cells were stimulated with plate-coated anti-CD3 antibody together with either EFNB1-Fc or IgG-Fc for 30 min. After stimulation, protein lysates were generated to determine phosphorylation levels of Akt and mTOR by western Blot. Left panel: Image of the blot incubated with phosho-Akt, phospho-mTOR, pan-Akt and β-Actin antibodies. Right panel: Abundance of phospho-Akt and phospho-mTOR in anti-CD3/EFNB1-Fc stimulated FluT cells normalized to anti-CD3/IgG-Fc stimulated cells. phospho-Akt and phospho-mTOR expression was first normalized to β-Actin. Representative data of two independent experiments.

3.4.12 EFNB1 reverse signaling induces pSTAT3 levels in oligodendrocytes

The ephrin - ephrin receptor interaction induces a bi-directional signaling [194]. As described in the section 3.4.11, signaling induced in Ephrin receptor expressing cells is called "forward signaling", whereas ephrin ligand expressing cells are triggered by "reverse signaling". Ligation of EFNB1 with one of its Eph receptors resulted in recruitment of the tyrosine kinase Src through SH2 domain of EFNB1. Src phosphorylates JAK2, which later phosphorylates STAT3 thereby inducing STAT3 dimerization and nuclear translocation [195, 196]. STAT3 is also phosphorylated by MAPK or mTOR at a different residue to become fully active in transcription [197, 198]. As a consequence, expression of STAT3 target genes are induced following ephrin mediated reverse signaling (Figure 25A) [196].

Upon interaction, Ephrin - Eph molecules cluster on the cell surface thereby increasing the strength of a downstream signaling. Based on our findings on siRNA-mediated overexpression of EFNB1, I wanted to investigate whether the elevated EFNB1 expression on oligodendrocytes triggers a reverse signaling by binding to Ephrin receptors on neighboring oligodendrocytes. Therefore, Western Blot analysis was performed to detect phospho-STAT3 levels in MO3.13-A2-Luc cells that were transfected with EFNB1 siRNA or Scr control. Additionally, total STAT3 levels were determined to ensure that the changes in phosho-STAT3 were caused by differential phosphorylation activity and not by a dysregulated expression of STAT3. The Western Blot analysis showed that phospho-STAT3 levels were increased by 60% in EFNB1 siRNA transfected cells compared to Scr transfected cells (Figure 25B).

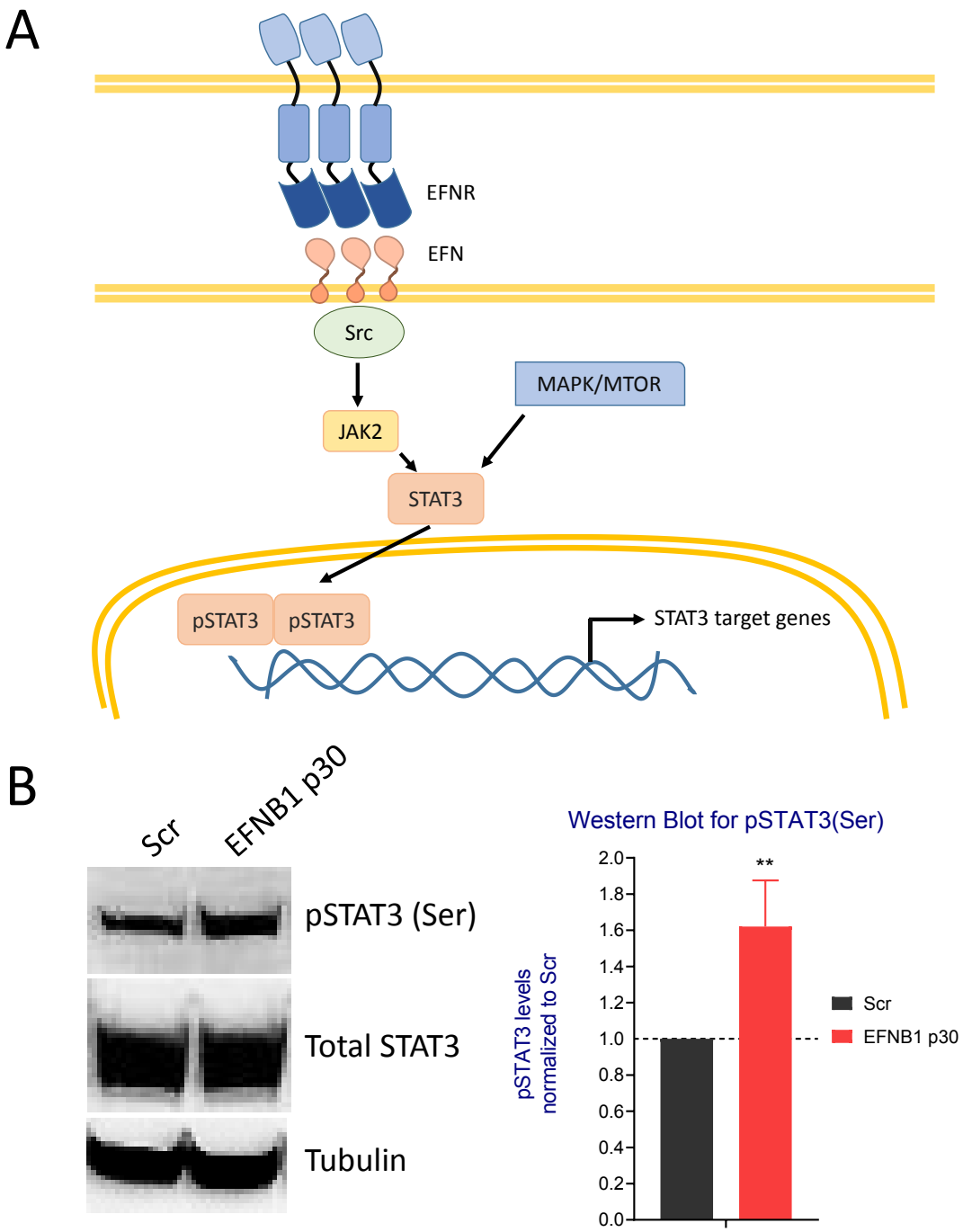

Figure 25: Mode of action analysis for Ephrin receptor (EFNR) - EFNB1 reverse signaling. (A) Overview of EFNB1 downstream pathway. Upon ligation with its cognate ephrin receptor, EFNB1 activates the JAK2/STAT3 signaling pathway and thereby induces the expression of STAT target genes. **(B)** Western blot analysis of phospho-STAT3 levels in MO3.13-A2-Luc cells transfected with Scr or EFNB1 p30 siRNA. Three days after transfection protein lysates were prepared to determine pSTAT3 and total STAT3 levels. For analysis, pSTAT3 of each sample was first normalized to tubulin and then pSTAT3 level in EFNB1 p30 sample was normalized to Scr control. Error bars indicate +/- SD. P-values were calculated using two-tailed student´s t-test. ** = $p < 0.01$. Cumulative data of four experiments.

3.4.13 EFNB1 reverse signaling induces PD-L1 expression and regulates other intrinsic tumor resistance mechanisms against T cell attack

STAT2/3 are key transcription factors involved in IFNγ mediated upregulation of PD-L1 in tumor cells [199]. In order to investigate if the increased phosho-STAT3 levels in EFNB1 siRNA transfected oligodendrocytes also elevated PD-L1 expression as a resistance mechanism I checked the RNASeq data from section 3.4.8. It was observed that EFNB1 siRNA transfection altered gene signature of MO3.13-A2-Luc cells. The multidimensional scaling (MDS) plot for replicate RNAseq data sets showed that Scr and EFNB1 siRNA transfection separate samples by at least 4 dimensions (Figure 26A). Particularly, two-dimensional hierarchical clustering analysis showed that 78 genes were more than 2 fold up- and 31 genes were down-regulated in EFNB1 siRNA transfected oligodendrocytes (Figure 27 and 28). As it was highlighted in volcano plot, PD-L1 (CD274) is one the genes that was strongly upregulated in EFNB1 siRNA transfected cells, potentially due to elevated EFNB1 protein and subsequently increased phospho-STAT3 levels (Figure 26B).

Next, I aimed to validate the RNAseq results for PD-L1 both at mRNA and protein level. Therefore, RT-qPCR, Western Blot and FACS analyses were performed to compare PD-L1 expression in EFNB1 and Scr siRNA transfected MO3.13-A2-Luc cells. As a control, PD-L1 p30 siRNA transfection was included. In alignment with the RNAseq data, the RT-qPCR analysis showed a 3-fold upregulation of PD-L1 mRNA in EFNB1 siRNA transfected oligodendrocytes compared to Scr transfected control (Figure 29A). The induction in PD-L1 expression at protein level was also confirmed by western blot and FACS analyses (Figure 29B and C). Interestingly the co-transfection of EFNB1 and PD-L1 siRNAs also increased PD-L1 expression compared to PD-L1 knockdown alone.

Our group performed different HTP-screens to identify novel immune checkpoint molecules and immune resistance mechanisms in breast cancer, melanoma, pancreatic ductal adenocarcinoma (PDAC), multiple myeloma, lung adenocarcinoma tumor cells and oligodendrocytes (MS-Glioma screen). These six screens revealed 550 candidate immune modulators (HITs) in total. I investigated the expression of these HITs via RNAseq data to understand whether EFNB1 could regulate the expression of immune resistance genes other than PD-L1. I also included known immune checkpoints such as ICOSLG and CEACAM6 in the analysis. In total, 65 genes were observed to be

differentially regulated in EFNB1 siRNA transfected MO3.13-A2-Luc cells. Among them, five were more than 2-fold upregulated and four were more than 2 fold downregulated (Table 4). Differentially expressed HITs from the MS-Glioma screen were highlighted in red. Importantly, four of the MS-Glioma HITs other than EFNB1 were validated in two different secondary screens with MO3.13-A2-Luc cells. These HITs are CADM4 (cell adhesion molecule 4, log2 = -0,864), PRPS1 (phosphoribosyl pyrophosphate synthetase 1, log2 = -0,22), LRRN1 (leucine rich repeat neuronal 1, log2 = 0,612) and CHRNA1 (cholinergic receptor nicotinic alpha 1 subunit, log2 = 0,263). CADM4 was also validated in secondary screens with primary glioblastoma cells (Table 1).

Another interesting observation that was obtained from the RNAseq results was the upregulation of TGF-beta and many related genes as well as the downregulation of TGF-alpha in EFNB1 p30 siRNA transfected MO3.13-A2-Luc cells (Table 5). Upregulation of TGF-beta together with its receptor and regulators may indicate another immune resistance mechanism triggered by EFNB1-reverse signaling in oligodendrocytes.

Taken together, these results identify EFNB1 as a novel immune checkpoint with a dual role in T cell co-stimulation, as well as glial cell's resistance towards T cell attack.

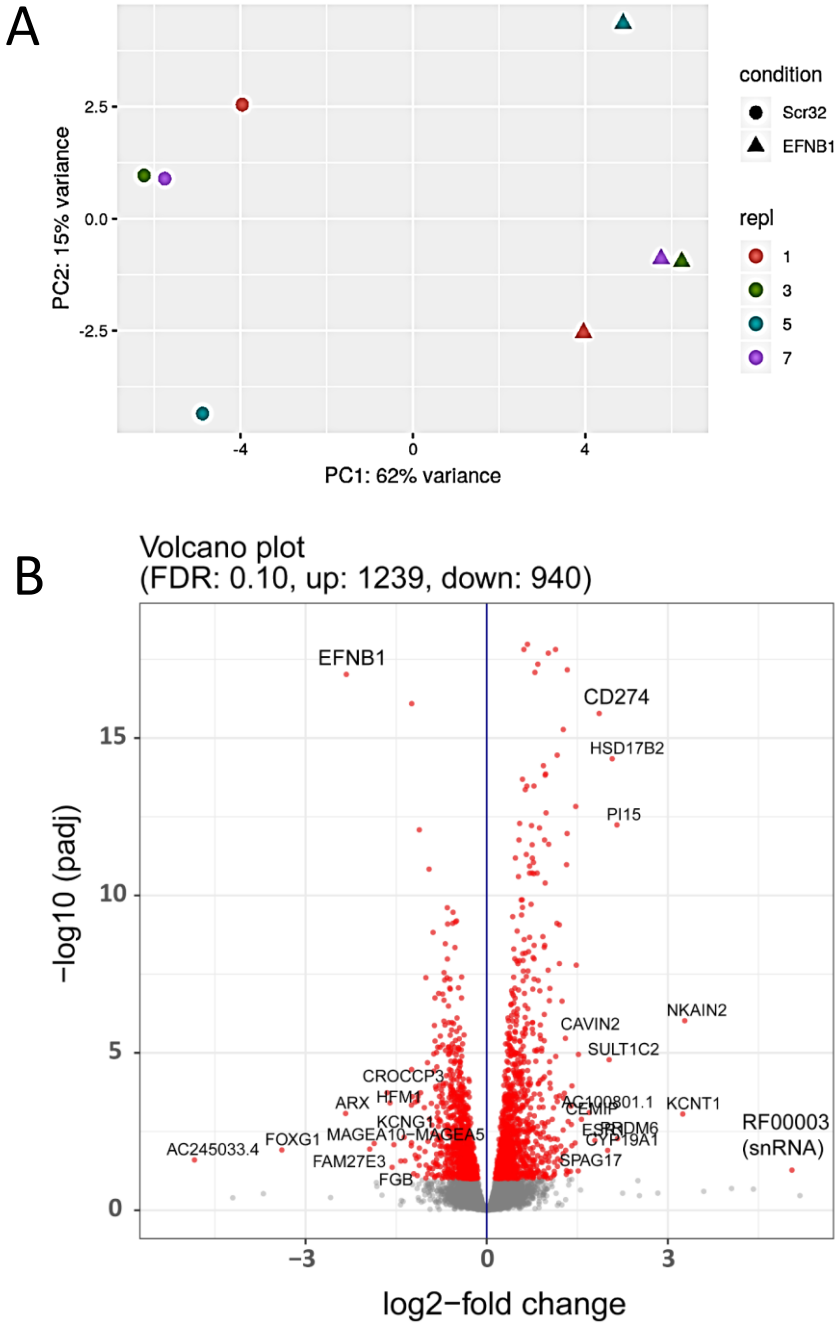

Figure 26: Impact of EFNB1 p30 siRNA transfection on basal gene expression in oligodendrocytes. MO3.13-A2-Luc cells were transfected with EFNB1 p30 and Scr siRNAs. After 72h of transfection, gene expression levels were determined using RNAseq. **(A)** The multidimensional scaling (MDS) plot illustrating the distances between all samples. The x-axis represents the dimension (similar to principal component) showing the variance in the dataset, followed by the dimension 2 (y-axis). Gene expression in Scr and EFNB1 p30 siRNA transfected samples were depicted in circle and triangle respectively. Sequencing was performed on quality verified total RNA from 4 independent experiments. The MDS plot was generated using the plotMDS function of edgeR for R. **(B)** Volcano Plot highlighting differentially expressed genes after EFNB1 p30 siRNA transfection (fold change ≥ 2, FDR ≤ 0.1). Red dots = genes with significant differential expression Experiments and data analysis were conducted in collaboration with Prof. Michael Rehli, Dr. Nicholas Strieder and Dr. Claudia Gebhard (RCI).

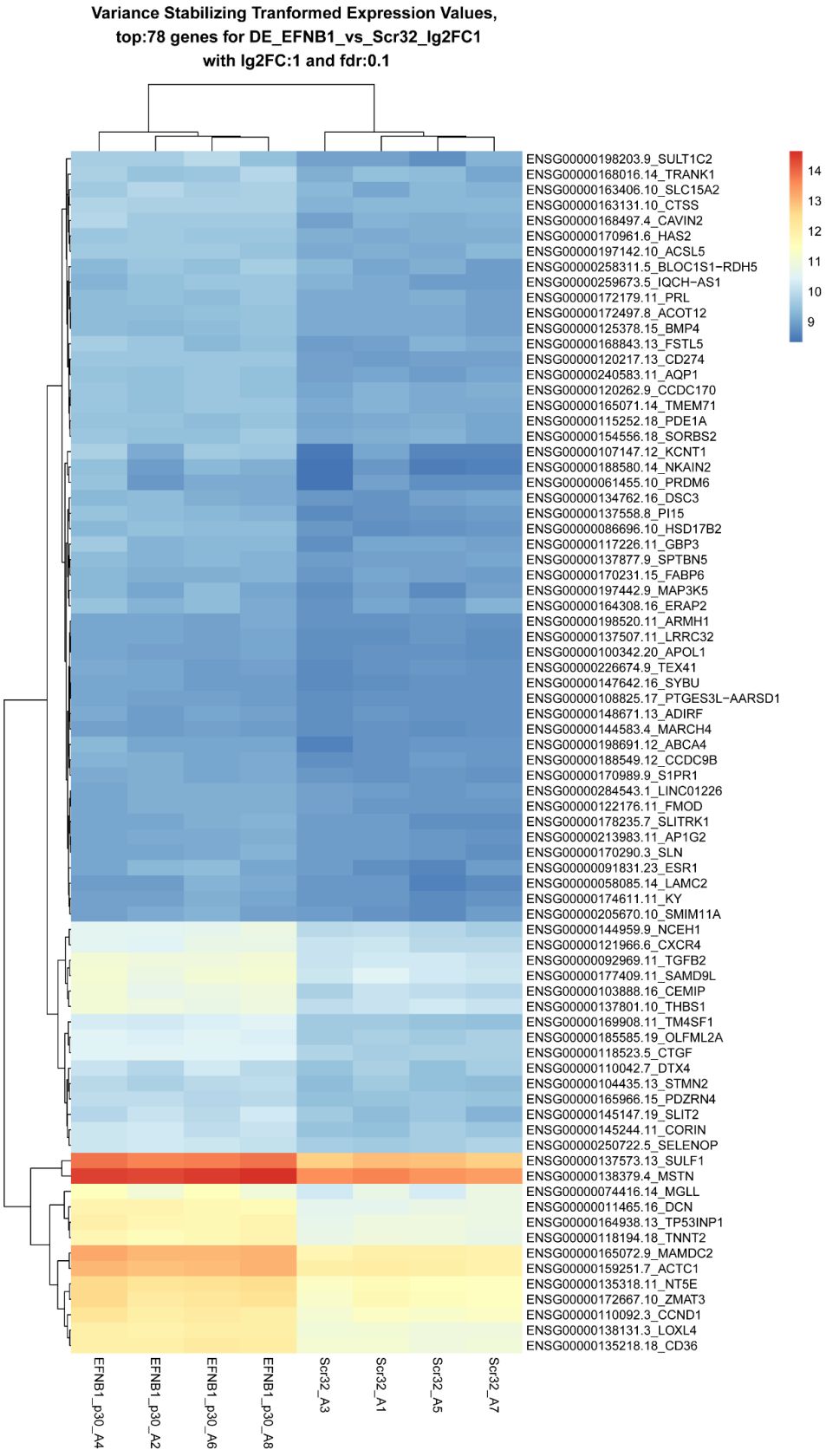

Figure 27: Two-dimensional hierarchical clustering indicating 78 genes that were more than 2 fold upregulated in EFNB1 p30 siRNA transfected MO3.13-A2-Luc cells.

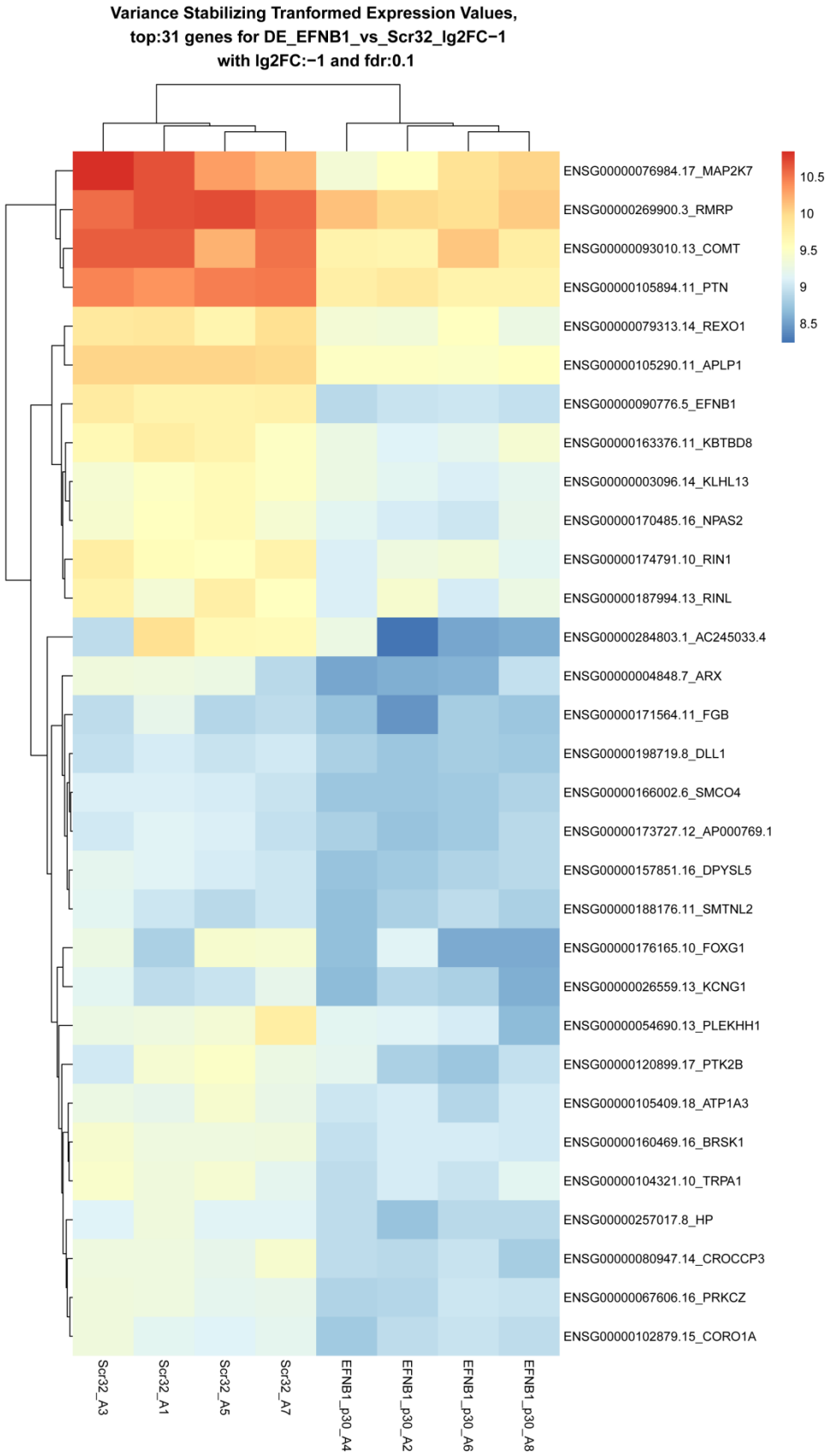

Figure 28: Two-dimensional hierarchical clustering indicating 31 genes that were more than 2 fold downregulated in EFNB1 p30 siRNA transfected MO3.13-A2-Luc cells.

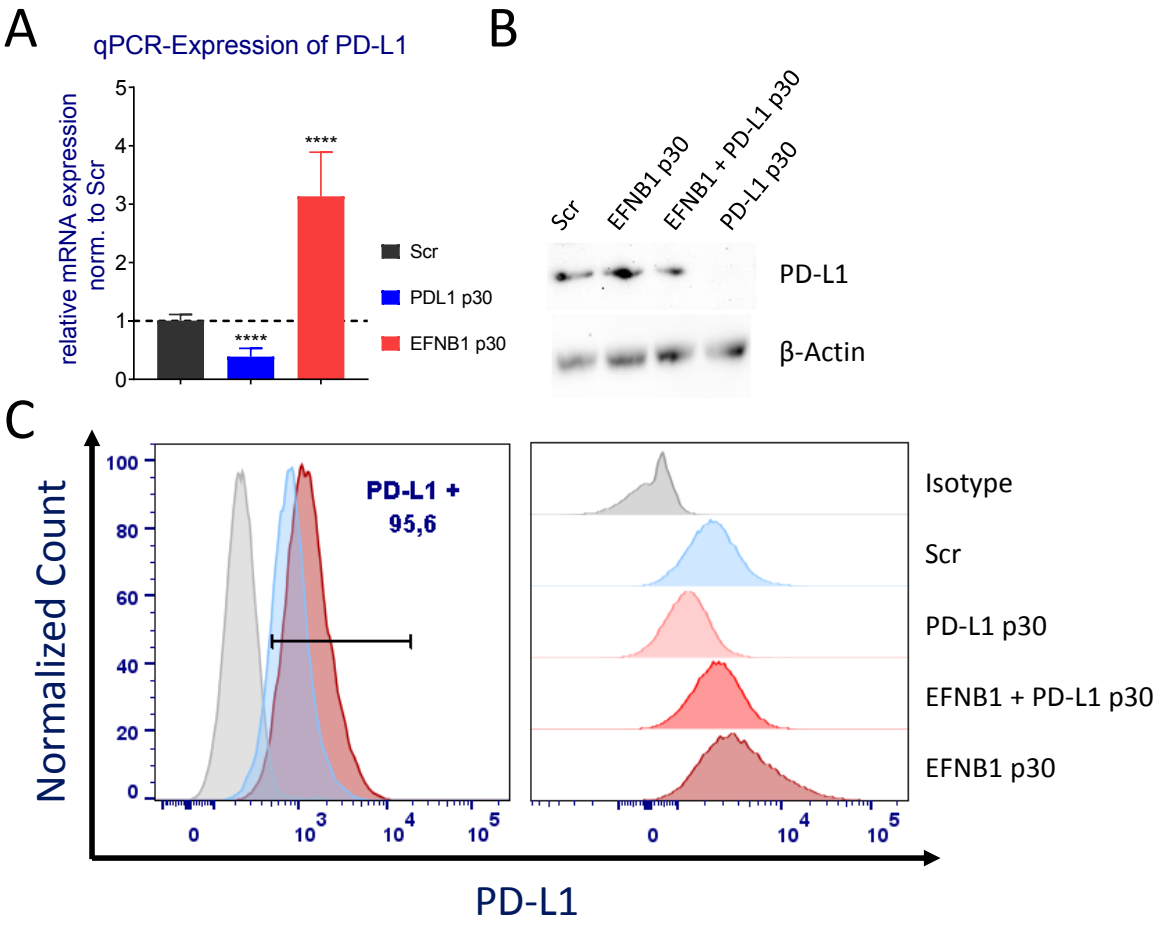

Figure 29: EFNB1 reverse signaling induces PD-L1 expression. (A) Validation of RNAseq results by RT-qPCR. MO3.13-A2-Luc cells were transfected with EFNB1 p30, PD-L1 p30 and Scr siRNAs. mRNA expression of PD-L1 was determined in transfected cells by RT-qPCR. Expression of beta-actin was used for normalization. mRNA expression in target samples was normalized to mRNA expression in Scr sample. Bars show median and error bars indicate +/- SD. Cumulative data of 3 independent experiments. P-values were calculated using two-tailed student´s t-test. **** = $p < 0.001$. **(B)** Western blot analysis, **(C)** FACS analysis for PD-L1 expression in Scr, EFNB1 p30, PD-L1 p30 and EFNB1-PD-L1 p30 double transfected MO3.13-A2-Luc cells. Left panel: Overlay of histograms of isotype staining (grey), and PD-L1 staining on Scr (blue) and EFNB1 p30 (dark red) transfected cells. Right panel: Comparison of PD-L1 histograms of each sample. Representative data of three independent experiments.

Table 4: Log2 fold changes of candidate cancer-associated immune checkpoint genes in EFNB1 p30 siRNA transfected MO3.13-A2-Luc cells.

Gene name	log2 Fold Change	Description	Identified Screen
CD274	1,863	CD274 molecule	
S1PR1	1,275	sphingosine-1-phosphate receptor 1	Melanoma
NT5E	1,14	5'-nucleotidase ecto	MS-Glioma
TMEM71	1,042	transmembrane protein 71	Lung adenocarcinoma
CXCR4	1,038	C-X-C motif chemokine receptor 4	MS-Glioma
ACTN2	0,968	actinin alpha 2	PDAC
TG	0,966	thyroglobulin	PDAC
ICOSLG	0,85	inducible T cell costimulator ligand	
IL7R	0,842	interleukin 7 receptor	Multiple myeloma
PIK3IP1	0,84	phosphoinositide-3-kinase interacting protein 1	MS-Glioma
ADGRG6	0,836	adhesion G protein-coupled receptor G6	Multiple myeloma
TAS1R1	0,673	taste 1 receptor member 1	MS-Glioma
LRRN1	0,612	leucine rich repeat neuronal 1	MS-Glioma
MYL4	0,57	myosin light chain 4	Melanoma
TPM1	0,493	tropomyosin 1	Melanoma
LGR4	0,49	leucine rich repeat containing G protein-coupled receptor 4	breast
CLSTN3	0,446	calsyntenin 3	MS-Glioma
LGALS3BP	0,433	galectin 3 binding protein	PDAC
CDKN2B	0,414	cyclin dependent kinase inhibitor 2B	Melanoma
PRKCE	0,414	protein kinase C epsilon	Multiple myeloma
PLPPR2	0,406	phospholipid phosphatase related 2	Lung adenocarcinoma
SORT1	0,388	sortilin 1	PDAC
JAK2	0,384	Janus kinase 2	Melanoma, PDAC
IGF2	0,38	insulin like growth factor 2	Multiple myeloma
MAP1A	0,378	microtubule associated protein 1A	Melanoma

NEK11	0,357	NIMA related kinase 11	PDAC
THBS2	0,357	thrombospondin 2	Multiple myeloma
TPM2	0,355	tropomyosin 2	Multiple myeloma
DUSP4	0,353	dual specificity phosphatase 4	Multiple myeloma
PKM	0,343	pyruvate kinase M1/2	Multiple myeloma
FAT1	0,329	FAT atypical cadherin 1	PDAC
RGS7	0,316	regulator of G protein signaling 7	PDAC
ITGB1	0,311	integrin subunit beta 1	Multiple myeloma
SQSTM1	0,311	sequestosome 1	PDAC
DMPK	0,287	DM1 protein kinase	PDAC
SLC29A1	0,287	solute carrier family 29 member 1	MS-Glioma, Lung adenocarcinoma
LAPTM4A	0,276	lysosomal protein transmembrane 4 alpha	MS-Glioma
AKAP11	0,271	A-kinase anchoring protein 11	PDAC
CHRNA1	0,263	cholinergic receptor nicotinic alpha 1 subunit	MS-Glioma, Lung adenocarcinoma
HLA-E	0,255	major histocompatibility complex, class I, E	Multiple myeloma
CD44	0,25	CD44 molecule	Melanoma
COPB2	0,232	coatomer protein complex subunit beta 2	Multiple myeloma, PDAC
NCOA2	0,184	nuclear receptor coactivator 2	Melanoma
RPN2	0,172	ribophorin II	Lung adenocarcinoma
EEF1A1	0,161	eukaryotic translation elongation factor 1 alpha 1	MS-Glioma, Lung adenocarcinoma
RPS2	-0,199	ribosomal protein S2	Lung adenocarcinoma
PRPS1	-0,22	phosphoribosyl pyrophosphate synthetase 1	MS-Glioma
TCOF1	-0,234	treacle ribosome biogenesis factor 1	PDAC
AKAP1	-0,298	A-kinase anchoring protein 1	PDAC
AURKA	-0,309	aurora kinase A	PDAC
PLK4	-0,314	polo like kinase 4	PDAC
ATP1A1	-0,322	ATPase Na+/K+ transporting subunit alpha 1	MS-Glioma
KIF15	-0,389	kinesin family member 15	Melanoma
SIK3	-0,421	SIK family kinase 3	Melanoma, PDAC

KIF20A	-0,441	kinesin family member 20A	Melanoma
RRM1	-0,464	ribonucleotide reductase catalytic subunit M1	MS-Glioma, Lung adenocarcinoma
CHAF1B	-0,477	chromatin assembly factor 1 subunit B	Multiple myeloma
RGS2	-0,509	regulator of G protein signaling 2	breast
MELK	-0,524	maternal embryonic leucine zipper kinase	Multiple myeloma
HRK	-0,634	harakiri, BCL2 interacting protein	MS-Glioma, Lung adenocarcinoma
CADM4	-0,864	cell adhesion molecule 4	MS-Glioma
DLL1	-1,163	delta like canonical Notch ligand 1	MS-Glioma
COMT	-1,244	catechol-O-methyltransferase	MS-Glioma, Lung adenocarcinoma
PTK2B	-1,423	protein tyrosine kinase 2 beta	Multiple myeloma
EFNB1	-2,326	ephrin B1	MS-Glioma

Table 5: Log2 fold changes of TGFB and related genes in EFNB1 p30 siRNA transfected MO3.13-A2-Luc cells.

Gene name	log2 Fold Change	Type	Description
LRRC32	1,41	protein_coding	leucine rich repeat containing 32 (Regulator of TGFB1, TGFB2 and TGFB3)
TGFB2	1,331	protein_coding	transforming growth factor beta 2
TGFB2-OT1	0,906	3´prime overlapping ncRNA	TGFB2 overlapping transcript 1
TGFBI	0,624	protein_coding	transforming growth factor beta induced
SMURF2	0,486	protein_coding	SMAD specific E3 ubiquitin protein ligase 2
TGFBRAP1	0,405	protein_coding	transforming growth factor beta receptor associated protein 1
SMAD1	0,397	protein_coding	SMAD family member 1
TGFBR2	0,348	protein_coding	transforming growth factor beta receptor 2
SMAD5	0,188	protein_coding	SMAD family member 5
TGFA	-0,594	protein_coding	transforming growth factor alpha

4 Discussion

One of the major challenges in the immunotherapy of cancer and autoimmune diseases is to fine-tune the balance in the immune checkpoint signaling. This challenge is even more prominent for glioma and multiple sclerosis, due to the restricted self-renewal capacity of the CNS [137]. So far developed strategies could not achieve safe and effective treatment, emphasizing the need for the identification of novel molecular targets involved in the immunopathology of glioma and MS.

In this study, I established an *in-vitro* co-culture model for MS and glioma to identify novel ICMs that play a role in the antigen-specific $CD8^+$ T cell mediated glial cell killing. I performed a high-throughput screen by co-culturing Flu-specific $CD8^+$ T cells with the human oligodendrocyte cell line MO3.13-A2-Luc that were transfected with a siRNA library consisting of 4155 genes. Out of the top 126 HITs I selected 56 HITs based on literature search and subsequently performed secondary screens using both MO3.13-A2-Luc and primary glioma cells. Among the identified HITs, EFNB1 was selected for further validation. EFNB1 is overexpressed in glioma patients and oligodendrocytes of EAE experienced mice. Surprisingly, I observed an overexpression of EFNB1 at protein level after siRNA transfection and performed RNA-Seq to identify the non-coding RNAs potentially regulating the expression of EFNB1. I demonstrated that EFNB1 on glial cells activates effector cytokine secretion by T cells and increases the T cell mediated target cell killing. At the same time, I showed that EFNB1 reverse signaling induces PD-L1 expression and upregulates TGFβ pathway as immune resistance mechanisms in oligodendrocytes.

4.1 RNAi screen for the identification of MS & glioma associated immune checkpoints

4.1.1 High-throughput screen design and rationale

In this study, I adapted the HTP RNAi screen method established in our division by Dr. Nisit Khandelwal to identify novel immune checkpoint molecules involved in the cross-talk between oligodendrocytes and antigen specific $CD8^+$ T cells [172]. The below mentioned modifications were applied according to the aim of the study:

Target cells: A human oligodendrocyte cell line was used instead of a breast cancer cell line. More than 75% of gliomas in adults originate from astrocytes, whereas less than

10% of the patients develop oligodendroglial tumors [200]. However, in MS, oligodendrocytes are targeted by myelin-antigen reactive $CD8^+$ T cells [201, 202]. Previous screens conducted in our division using different tumor models revealed a unique list of candidate immune modulatory genes, indicating the heterogeneity between each tumor entity. Since I aimed at identifying immune resistance mechanisms relevant for both MS and glioma, I decided to take advantage of oligodendrocytes as target cells in this HTP screen. In order to verify the relevance of the selected HITs for glioma patients, I performed additional secondary validation screens using primary glioma cells.

Effector T cell source: Instead of polyclonally stimulated PBMCs, Flu-antigen specific CD8 T^+ cells (FluT) from a HLA-$A2^+$ healthy donor were used as effector cells. Thereby I could mimic the HLA/TCR interaction between oligodendrocytes and autoreactive myelin-antigen specific $CD8^+$ T cells infiltrated into the CNS of MS patients. FluT cells from donor #11 expressed in the resting state low levels of exhaustion markers PD-1, TIM-3 and LAG-3, indicating their cytotoxic potential and capacity for further activation. Importantly, the potency of FluT mediated target cell killing can be adjusted by optimizing the peptide concentration used to pulse target cells. This enabled us to define the optimal window to study how siRNA-mediated knockdown of co-stimulatory and co-inhibitory molecules on target cells affects T cell functionality.

The siRNA library: The initial breast cancer screen targeted in total 520 GPCRs. In this study, the library was expanded to target the whole surfaceome and to identify immune checkpoints that are potentially involved in the immunological synapse in a broader manner. Catalog of 3702 cell surface proteins used in the library were bioinformatically defined in a previous study [203]. As candidate HITs localizing at the target cell surface may directly modulate T cell function by interacting with cognate ligand/receptor expressed on T cells. These interactions could be suitable targets for an antibody-mediated blockade. Additional to surface molecules, siRNAs targeting 453 different cytoplasmic protein kinases and metabolic proteins were included. The previous PDAC screen performed in our group by Dr. Antonio Sorrentino identified salt-inducible kinase 3 (SIK3) as a novel tumor intrinsic resistance gene involved in TNFα mediated cytotoxicity (manuscript in preparation). Another screen for multiple myeloma associated ICMs performed by Dr. Valentina Volpin revealed CamV1 (masked name) as a

key modulator of tumor resistance towards FasL-mediated apoptosis induced by marrow infiltrating lymphocytes (manuscript submitted). Moreover, the activity of kinases can be blocked by small molecule inhibitors and clinical combination of such tyrosine kinase inhibitors with cancer immunotherapy improved antitumor efficacy [204]. Taken together, we enlarged the siRNA library to target 4155 genes comprising 3702 surface (89%) and 453 kinases and metabolic proteins (11%) in the HTP screen in order to broaden the spectrum of candidate immune checkpoint molecules that could potentially improve cancer immunotherapy.

4.1.2 The performance of the HTP screen and interpretation of the results

The reliability and robustness of RNAi-based screens for novel immune checkpoint molecules are dependent on multiple parameters. The outcome of the crosstalk between effector and target cells can only be analyzed if proper quality controls have been set. As first step, the conditions for oligodendrocyte - FluT cell co-culture were optimized. Therefore, I performed luciferase-based cytotoxicity assays where I tested different E:T ratios and Flu-peptide concentrations. Since I later aimed to assess the impact of immune checkpoint knockdown on T cell mediated target cell killing, this step was crucial to define a window for the luciferase readout. The optimum co-culture conditions were identified with the E:T of 20:1 and 0,01 µg/ml peptide concentration, which resulted in 60% FluT mediated oligodendrocyte killing. I also confirmed that cytotoxicity of FluT is MHC-I restricted and dependent on the activation of TCR signaling.

Next, the siRNA transfection conditions for MO3.13-A2-Luc cells were optimized in order to achieve a high knock-down efficacy without increasing potential off-target effects. Therefore, different transfection reagents, time points, siRNA concentrations and compositions were tested. For MO3.13-A2-Luc cells, I determined RNAiMAX mediated delivery of 25nM siRNAs for 72h as the optimal condition for gene knockdown. The siRNA library for the HTP screen consisted of a pool of 4 non-overlapping siRNAs. To reduce off-target effects, in later validation experiments I also used a pool of 30 siRNAs [205]. With the pool of 30 siRNAs, already 5 nM was sufficient for potent on-target gene silencing. Due to the lack of a whole surfaceome library, I was not able to use the pool of 30 siRNAs for HTP screen.

As a control for the transfection efficiency and cell viability, siRNAs targeting genes essential for cell survival (UBC and "cell death" siRNA cocktail) were included and a strong reduction in luciferase intensity following transfection could be observed in the both viability and cytotoxicity settings. To exclude a sequence independent effect of siRNAs such as induction of IFNγ response, I selected non-targeting Scr3 and Scr4 siRNAs as negative controls. Previously, the impact of 4 different scrambled sequences (Scr1-4) on the expression levels of oligodendrocyte marker genes such as MOG and PLP were tested and similar expressions between mock transfected and Scr3-4 transfected cells were observed. Negative controls are also needed for setting up a baseline to normalize luciferase intensity measured in the cytotoxicity and viability settings upon target gene knockdown.

For a reliable interpretation of the HITs as candidate immune checkpoint molecules in the HTP-screen, I needed to validate already characterized co-inhibitory and co-stimulatory controls. Ideally, positive controls should cover a range of strength that enable identification of both weak and strong HITs [169]. I could show that, downregulation of CCR9, which was previously identified as a co-inhibitory molecule in breast cancer cells, increased FluT cell mediated killing of oligodendrocytes. Another co-inhibitory control was SIK3, a novel immune modulator identified in our previous pancreatic screen. In pancreatic cancer cells, SIK3 is involved in tumor cell intrinsic resistance against TNFα triggered apoptosis. Downregulation of SIK3 in oligodendrocytes also resulted in increased target cell killing potentially due to loss of resistance against TNFα secreted by FluT. As mentioned in the introduction, the co-inhibitory role of PD-L1 in many cancer and autoimmune diseases including MS and glioma is already well-known. However, in our model, I observed a strong decrease in cell viability when PD-L1 was silenced in oligodendrocytes. This phenotype may be due to an off-target effect of the pool of 4 siRNAs, since I did not observe the same effect when the cells were transfected with the pool of 30 siRNAs targeting PD-L1. As a co-stimulatory control, I was able to show that knockdown of 4-1BBL decreased FluT mediated target cell killing compared to the negative control. Ligation of the cognate receptor 4-1BB expressed on T cells with 4-1BBL promotes T cell survival, expansion and differentiation by upregulating BCL-2 and Akt-pathway [206].

The HTP-screen was performed in two settings where I co-cultured transfected oligodendrocytes with FluT cells to assess cytotoxicity (plates 1-13) or cultured without FluT cells to measure the impact of gene knockdown on cell viability (plates 14-26). Each setting was performed in duplicates, by targeting each gene in two wells on different plates. As first quality measurement, we evaluated the Pearson correlation coefficient (r^2) for the replicates in the cytotoxicity and viability settings and observed a high correlation between duplicates (0.94 for cytotoxicity and 0.96 for viability, respectively). Another important indicator for the high quality of the data is the performance of the controls. We could successfully identify CCR9 and 4-1BBL as co-inhibitory and co-stimulatory immune checkpoints, respectively. In this project, I focused mainly on co-inhibitory molecules for later functional validation. For the identification of co-inhibitory HITs, cytotoxicity and viability LOESS scores of CCR9 served as cut-off values. In the primary screen, CCR9 showed a weak impact on T cell cytotoxicity, as downregulation of 126 genes exerted a stronger phenotype. Notably, several recently identified immune modulators such as CEACAM6 (Carcinoembryonic antigen-related cell adhesion molecule 6) and NT5E (5'-nucleotidase, CD73) were found among the HITs whose knockdown improved FluT mediated oligodendrocyte killing compared to CCR9 knockdown. The role of CEACAM6 in regulating $CD8^+$ T cell responses against multiple myeloma was previously described by our group [176]. Blockade of CEACAM6 restored autologous T cell reactivity against myeloma cells. Interestingly, CEACAM6 expression is upregulated in many epithelial malignancies such as pancreatic cancer and correlates with poor survival. CEACAM6 downstream signaling triggers oncogenic and immune resistance pathways such as TGFβ, SRC, AKT and FAK [207]. Here I showed for the first time that CEACAM6 acts as a co-inhibitory immune checkpoint in oligodendrocytes as well.

In the field of cancer immunotherapy ectonucleotidases have emerged as novel therapeutic targets to improve anti-tumor immune responses. Extracellular ATP induces inflammation by purinergic signals and plays an important role in anti-tumor immunity. Conversely, breakdown of ATP into immunosuppressive adenosine by ectonucleotidases acts as a negative-feedback mechanism to prevent tissue damage. One of such ectonucleotidases NT5E (CD73) is expressed on healthy epithelial, stromal and immune cells and is even overexpressed in solid tumors and certain leukemias. Pre-clinical data in mice showed a synergistic effect of CD73 blockade in anti-CTLA-4, anti-PD-1 and anti-

TIM3 treated mice. Currently one anti-CD73 mAb phase I clinical trial for advanced cancers such as triple negative breast cancer is ongoing [175, 208]. In line with published data, I identified NT5E as an inhibitory immune regulator in oligodendrocytes.

In addition to novel co-inhibitory immune checkpoints, the established HTP-screen also revealed potential co-stimulatory molecules. Targeting co-stimulatory receptors such as 4-1BB, OX40 and CD28 by agonistic antibodies or recombinant cognate ligands elicited high potentials in pre-clinical tumor models [209]. Conversely, blockade of such molecules can be used to reduce excessive immune reactions in autoimmune diseases. However, in this study I focused on novel co-inhibitory molecules and selected 51 genes among 126 co-inhibitory HITs for further validation. Additionally, I included five inhibitory HITs ranked lower than CCR9 and one potential co-stimulatory HIT (EPHA2).

4.2 Rationale for HIT selection

In order to identify reliable immune checkpoint genes among the HITs ranked higher than CCR9, I applied an extensive validation strategy. Out of 126 top co-inhibitory HITs, 51 genes were selected for further validation based on their performance in the primary screen and literature search. For the first line of selection, I applied the criteria described in 3.2.2. HITs were excluded that i) displayed strong viability effects, ii) those are not expressed in both human and mouse oligodendrocytes and iii) HITs with essential functions such as those involved in the translation and transcription machinery. Additionally, I searched for autoimmune disease association (polymorphisms or mutations), HIT knockout mouse phenotype and expression in glioma and different tumor entities.

An essential step for target selection and validation is the exclusion of false-positive results that can arise due to off-target effects of siRNAs. Off-target effects are one of the major drawbacks of RNAi-based approaches and can cause target-unrelated phenotypes in a sequence dependent and independent mechanism [210, 211]. Four main mechanisms can cause off-target effects [212]: i) partial or complete sequence complementarity between a siRNA and an unrelated mRNA, ii) RNAi machinery in the cells cannot differentiate between siRNAs and microRNAs iii) the partial binding of the seed sequence of the siRNA (from 2nd to 7th/8th nucleotide) to the 3'UTR of multiple unrelated mRNAs causes their degradation and as an intrinsic defense mechanism

against exogenous oligonucleotides, mammalian cells can exhibit IFNγ response upon siRNAs transfection and iv) importantly, both strands of the siRNA duplex can induce gene silencing.

As it was used in the primary screen, the pooled siRNA approach dilutes potential off-target effects of individual siRNAs without decreasing the knockdown efficiency for target mRNAs [213]. However, further validation is necessary to confirm the on-target effect. Therefore, I performed secondary screens with oligodendrocytes using two different types of siRNA libraries. The first library (deconvoluted library) consists of 4 individual siRNAs together with the pool of 4 as it was used in the primary screen. The probability that different non-overlapping siRNAs share the same off-target effect is very low, therefore the observation of the same RNAi-induced phenotype using at least 2 distinct siRNAs supports and validates the on-target effect and thereby the gene-specific phenotype [210]. In the first secondary screen in oligodendrocytes, the phenotype of 37 out of 56 HITs could be validated with 2 or more siRNA sequences. To further dilute sequence-specific off-target effects, I performed a second validation screen using siRNA pool of 30 (siPools) from siTOOLs Biotech [205]. In this screen I only included 37 validated HITs from the first secondary screen. The impact of 23 out of 37 HITs on the T cell mediated oligodendrocyte killing could be reproduced when I used the pool of 30 siRNAs. Considering the results of both screens, 40% of the HITs were validated, indicating the importance of validation experiments to exclude false-positive results before performing further functional assays.

Since MO3.13-A2-Luc cells are an immortalized hybridoma cell line, I tested the same HITs in a primary brain tumor initiating stem cells from a HLA-A2+ glioblastoma patient, RAV27 (Table 1, Figure 11). I identified 3 HITs (EFNB1, HCN2 and CADM4) that were validated in the four secondary screens. HCN2 (hyperpolarization-activated cyclic nucleotide–gated channel 2) is a voltage-gated channel mainly expressed in the heart and the nervous system. HCN2 is activated by cAMP and conducts K+ and Na+ ions. HCN channels (HCN1-4) are involved in the regulation of neuronal excitability and synaptic transmission. Dysfunction of these channels is associated with neurodegenerative diseases such as epilepsy, neuropathic and inflammatory pain [214]. CADM4 (cell adhesion molecule 4, or TSLL2/IGSF4C) belongs to the immunoglobulin (Ig) superfamily and is involved in cell adhesion. It is expressed at the cell-cell attachment sites in the

brain, kidney, bladder and prostate. Its potential role as a tumor suppressor was shown in mouse prostate cancer models [215]. In the brain, CADM4 mediates the contact between oligodendrocytes and axons thereby regulating the myelination process [216].

Among these three common oligodendroctye-glioma cell HITs, I selected EFNB1 (Ephrin-B1; ligand for erythropoietin producing hepatocellular carcinoma (Eph) receptors) for further functional validation because of its strength in the HTP screen and its biological relevance as it was described in the section 3.4.1.

4.3 EFNB1 as a novel co-stimulatory immune checkpoint target on glial cells

4.3.1 Structure and function of ephrin ligands & Eph receptors

Erythropoietin producing hepatocellular carcinoma (Eph) receptors and their ligands, the ephrins (Eph receptors interacting proteins, EFNs), are the major coordinators of contact-dependent cell-cell communication required to guide cells to their proper destination during developmental processes [192]. Bi-directional signaling mediated by Eph-Ephrins orchestrate tissue boundary formation, cell repulsion, cell adhesion and migration [194]. They are ubiquitously expressed in developing embryos and regulate tissue patterning, axon guidance, cardiovascular and skeletal development [195].

Eph receptors belong to the largest family of receptor tyrosine kinases (RTKs), with 14 receptors subdivided into 2 classes: EphA (EPHA1-8 and EPHA10) and EphB (EPHB1-4 and EPHB6). Ephrins are also divided into two types: ephrin-A1-5 (EFNA1-5) and ephrin-B1-3 (EFNB1-3) [192]. Preferentially A-type receptors promiscuously bind ephrin-A ligands, while EphBs bind ephrin-B ligands [217]. Exceptionally, EPHA4 can bind all ephrin-B ligands and EPHB2 can bind ephrin-A5 [218, 219]. Eph receptors can have overlapping functions and due to their promiscuous interactions with ephrin ligands, loss of one receptor can be compensated by other members of the family [220]. Two distinct features make Eph-Ephrin signaling unique: (1) both, receptor and ligand expressing cells transduce signal upon interaction, (2) the functional outcome of the signaling induced by the same Eph-Ephrin can be opposite or different depending on the cell type. Moreover, by interacting with other RTKs, proteases and adhesion molecules they are involved in complex signaling networks [192].

Structurally, all Eph receptors have a N-terminal extracellular domain composed of a globular ligand-binding domain (LBD), Cys-rich domain (which itself contains sushi and epidermal growth factor (EGF)-like motifs) and two fibronectin domains. A transmembrane (TM) domain connects the extracellular part with the cytoplasmic signaling part, which contains the Tyr kinase (TK) domain, the sterile alpha motif (SAM) and the PDZ domain. On the other hand, ephrins are composed of a receptor-binding domain (RBD), where ephrin-As are linked to the membrane via a glycophosphatidylinositol (GPI), whereas the B-type ligands have a transmembrane and an intracellular PDZ domain [194].

Eph-Ephrin interaction can transduce signals in multiple ways. Signaling into Eph receptor expressing cells is defined as "forward signaling", whereas signaling from Ephs to ephrins is referred as "reverse signaling". Simultaneous activation of both pathways can transduce a bi-directional, parallel or anti-parallel signaling depending on the distribution of the Ephs and Ephrins on the interacting cells [194]. Upon ligand binding, Eph signaling is initiated through autophosphorylation of multiple tyrosine residues (e.g. Y576 and 602) in the juxtamembrane region. Phosphorylated tyrosines have a regulatory function in kinase activity and serve as docking sites for downstream signaling proteins such as Ras GTPase-activating protein (RasGAP), the p85 subunit of phosphatidylinositol 3-kinase (PI3K) and Src family kinases [221]. In reverse signaling, following receptor ligation, the intracellular domains of ephrin-B ligands are also phosphorylated by Src family kinases [222]. The strength of downstream signaling elevates upon clustering of the receptors and ligands on the cell membrane [223, 224]. It was also shown that Ephs and Ephrins can interact in *cis* (on the surface of the same cell) which in turn can block the formation of Eph clusters and attenuates downstream signals [225, 226].

Eph-Ephrins are essential not only during embryonic development, but also for neuronal plasticity, homeostasis and normal physiology of adult organs [227]. Upon discovery in the erythropoietin-producing hepatoma cell line, the involvement of Eph-Ephrin signaling in physiological and pathological conditions has been extensively studied [227, 228]. Dysregulation of Eph-Ephrin signaling has been found in all types of cancer cells [229, 230]. Frequently, Ephs and ephrins are upregulated in tumors and are involved in metastasis, invasion and angiogenesis [231, 232]. The outcome of Eph-Ephrin signaling

can be controversial dependent on the cellular context. The same molecules can act as a tumor promoter and suppressor within the same or in neighboring tissues [233].

4.3.2 Role of Eph-Ephrin signaling in glioma

Similar to other cancer types, imbalances in Eph-Ephrin signaling has been associated with glioma growth, invasion and bad prognosis [234]. Among Eph-Ephrin interactions, EPHA2-EFNA1 signaling has been described by many studies for glioma tumorigenesis [235-237]. In GBM patients, EPHA2 overexpression was associated with poor prognosis and inversely correlated with survival [238, 239], whereas EFNA1 expression was strongly downregulated [235, 240]. As a feedback mechanism, prolonged interaction between EPHA2 and EFNA1 resulted in downregulation of EPHA2 expression. Therefore, downregulation of EFNA1 in GBM cells accounts for the persistent EPHA2 overexpression [238, 240]. EPHA2 acts as tumor suppressor upon ligation with EFNA1 by inhibiting pathways involved in cell migration and proliferation such as Akt and Ras/mitogen-activated protein kinase (MAPK) pathways (ligand-dependent signaling) [235]. Interestingly, EPHA2 can be converted to a tumor promoter when phosphorylated by Akt (ligand-independent signaling) [241, 242]. Other than EPHA2, EPHA4-5-7 are also upregulated in GBM and associated with poor prognosis, whereas other ephrin-A type ligands are downregulated similar to EFNA1 [234]. Of note, EPHA4 and EPHA2 were identified as co-inhibitory and co-stimulatory HITs in our primary screen. The impact of EPHA4 on FluT mediated oligodendrocyte killing was validated in the secondary screens. Interestingly, although it displayed a co-stimulatory phenotype in the primary screen with oligodendrocytes, in the secondary screens with primary glioblastoma cells EPHA2 acted as a co-inhibitory molecule (Table 1). Taken the complex Ephrin-Eph signaling into account and redundancy between receptor and ligands, the exact role of EPHA4 and EPHA2 in glial cells still needs to be further investigated.

In contrast to the negative feedback mechanism between EPHAs and EFNAs, both EPHBs and EFNBs are upregulated in the glioma tissue. Although their role in glioma is less characterized than that of EPHA/EFNA, EPHB/EFNB signaling is linked to increased migration and invasion [243]. Upon binding to EFNB2 and EFNB3, EPHB2 forward signaling activates R-Ras and thereby promotes GBM cell invasion [243-245]. The same interaction also promotes invasion by activating Rac1 GTPase in EFNB2/3 expressing cells (reverse signaling) [244].

The RNA-Seq data from the TCGA database was analyzed to compare the expression of EFNB1 in different subtypes of glioblastoma tissues. EFNB1 was upregulated in all different GBM subtypes, where the highest expression level was detected in the highly immunogenic mesenchymal subtype. Furthermore, LGG patients with higher EFNB1 levels, showed a worse survival rate. The differential expression of EFNB1 in GBM tissues compared to non-neoplastic brain as well as its involvement in patient survival, underline the role of EFNB1 as a potential therapeutic target for glioma.

4.3.3 The role of Eph-Ephrin signaling in MS and EAE

Despite extensive researches in the CNS development, the involvement of Eph-Ephrin signaling has been shown by only few studies in MS and its mouse model EAE so far. Epha4 knockout mice exhibited better axonal regeneration and functional recovery after spinal cord injury [246]. Based on these findings Munro *et. al.* showed a potential involvement of Epha4 in the development of EAE [247]. Epha4 knockout mice delayed the onset of the MOG peptide-induced EAE and attenuated the clinical course. Additionally, blockade of Epha4 signaling by soluble Epha4-Fc as a decoy receptor attenuated the EAE response in wildtype mice. In this study, T cell and macrophage infiltration were found to be equivalent in both genotypes however, Epha4 knockout mice showed a decreased axonal pathology. Transfer of autoreactive T cells from wildtype and Epha4 knockout mice into naïve mice both induced diseases of comparable severity indicating a non-inflammatory role of Epha4 in that context [247]. As it will be discussed in detail in section 4.4.6, I indirectly revealed the role of EPHA4 in T cell activation. Treatment of MART-1 antigen specific melanoma-derived TILs with the EPHA4 inhibitor rhynchophylline reduced T cell activation following the stimulation with EFNB1 (Figure 21, Table 3). In the above-mentioned study, global Epha4 knockout mice were used in EAE experiments. The exact immunological role of Epha4 should still be investigated in T cell specific knockout mice models.

EFNB1 and EFNB2 expressed on T cells were also associated with the immunopathogenesis of MS and EAE [185]. In this study, T cell specific double knockout (dKO) of Efnb1/2 reduced proliferation of mice T cells in response to their cognate peptide. This resulted in defective Th1 and Th17 differentiation by reducing IFNγ and IL-17 secretion and lowered the clinical score of MOG-induced EAE. Double KO T cells also showed defective capacity to migrate to the CNS. In alignment with the EAE mice

data, Th1 and Th17 cells with high EFNB1 and EFNB2 expression were detected among immune infiltrates in MS lesions. Stimulation of EFNB1 and B2 reverse signaling increased the migration of Th17 cells across human BBB epithelial cells *in vitro* [185]. An extensive comparative analysis for Eph receptor expression on autoreactive T cells in MS patients and healthy donors can provide therapeutically relevant insights about the role of Eph-Ephrin signaling in MS.

4.3.4 Post-transcriptional regulation of Eph-Ephrin expression by non-coding RNAs

I first identified EFNB1 as a co-inhibitory immune checkpoint, since the transfection of oligodendrocytes with EFNB1 targeting siRNAs resulted in increased FluT mediated killing. However, when the siRNA knockdown efficiency was analyzed, I observed an inverse correlation between the EFNB1 mRNA and protein levels following transfection in oligodendrocytes. At mRNA level different siRNAs reached 50-80% knockdown efficiency, whereas EFNB1 protein levels were upregulated by all tested siRNAs except from S4. To exclude a cross-reactivity of the anti-EFNB1 Western Blot antibody these results were validated with 2 additional antibodies specific for different epitopes. Besides, I analyzed the epitope recognized by anti-EFNB1 FACS antibody by using the BLAST program and was not able to find a similar epitope bearing protein that might be recognized unspecifically by the EFNB1 antibody.

There are multiple mechanisms involved in protein stability, post-transcriptional and post-translational regulation, which can cause low or inverse correlation between mRNA levels and protein abundance [187]. There is also a possibility that EFNB1 stored in vesicles can translocate to the cell surface to maintain EFNB1 signaling. Besides, as a negative feedback mechanism, EFNB1 mRNA could increase ribosome occupancy and thereby the translational efficiency after siRNA transfection [248].

One potential explanation for the siRNA mediated gene overexpression can be the presence of long and short non-coding RNAs (lncRNAs and miRNAs) that regulate EFNB1 expression. LncRNAs consist of RNA species longer than 200 nucleotides (nt) that lack protein-coding potential. They exist in diverse forms such as mRNA-like intergenic transcripts (lincRNAs), natural anti-sense transcripts (NATs) of protein-coding genes, derivatives of excised introns (snoRNA ended lncRNAs) and circular RNAs

(circRNAs). LncRNAs regulate gene expression by controlling chromatin accessibility, mRNA stability, translation and post-transcriptional modifications [249]. They can regulate mRNA turnover by different mechanisms. First, lncRNAs can function as miRNA sponges, compete with mRNAs for miRNA binding, and thereby de-repress miRNA targets [250, 251]. Second, lncRNAs can recruit proteins to degrade mRNAs. As an example, lncRNAs containing *Alu* elements can induce Staufen 1 (STAU1)-mediated mRNA decay (SMD) in trans. mRNAs containing *Alu* elements within the 3'-UTRs can base pair with complementary *Alu* in lncRNA and thereby can be recognized and targeted by SMD [252, 253]. Third, lncRNAs can act as decoy for RNA binding proteins (RBPs) involved in mRNA decay. For instance, the lncRNA NORAD (noncoding RNA activated by DNA damage) function as a reservoir of PUMILIO 1 and PUMILIO 2 (PUM1/2) and limit their availability to degrade mRNA targets [254]. Other than mRNA stability, lncRNAs can also regulate translation by associating with ribosomes [255]. As an example, association of lincRNA-p21 with HuR (a RNA binding protein) leads to the recruitment of let-7/Ago2 to destabilize lincRNA-p21. In the absence of HuR, lincRNA-p21 accumulates and base pair with mRNA targets to suppress their translation by recruiting the translation repressor Rck [256]. Another mechanism by which lncRNAs can regulate the gene expression is interfering with post-translational modifications (PTMs). Several lncRNAs can mask the PTM sites or the binding sites for PTM enzymes. One of such example is Lnc-DC, which can bind STAT3 to prevent binding of protein tyrosine phosphatase SHP1 and thereby promotes phosphorylation of STAT3 on Tyr705 [257].

So far, no long noncoding RNAs were characterized as a regulator for EFNB1 expression; however the expression of several members of the Eph-Ephrin family were shown to be regulated by miRNAs and lncRNAs [188]. For instance, EPHB4 expression is upregulated by lncRNA BC005927 under hypoxia in gastric cancer cells [258]. The same group also identified two lncRNAs, *GMAN* (gastric cancer metastasis associated long noncoding RNA) and the anti-sense transcript *GMAN-AS,* that are transcribed from the EFNA1 genomic locus. GMAN-AS is complementary to both GMAN and EFNA1 and can directly bind both transcripts, whereas GMAN only binds to GMAN-AS and not EFNA1. In this study, the authors found that GMAN promotes the translation of EFNA1 by competitively binding GMAN-AS [259]. In other studies expression of EFNA3 and EPHB2 was shown to be regulated by anti-sense lncRNAs [260, 261].

Taken together, siRNAs targeting EFNB1 or the complemetary strands of the siRNAs can target a repressor lncRNA as well thereby increasing the translation rate of the remaining EFNB1 mRNAs [262]. In order to discover potential lncRNAs involved in the siRNA-mediated overexpression of EFNB1, I performed RNA sequencing of Scr and EFNB1 p30 siRNA transfected oligodendrocytes. I was not able to identify a novel anti-sense transcript encoded within the EFNB1 genomic locus. However, we identified several lncRNAs that were differentially expressed between Scr and EFNB1 p30 siRNA transfected cells (Table 2). Interestingly, a novel transcript AC245033.4 was about 29-fold downregulated in EFNB1 siRNA transfected cells compared to Scr control. On the other hand, a snRNA (RNA, variant U1 small nuclear 28) was more than 32-fold up-regulated upon EFNB1 siRNA transfection. Human U1 small nuclear (sn) RNA are required for splicing of pre-mRNAs. Transcriptome analysis where snRNA variant U1.8 is blocked by antisense oligonucleotides showed 116 differentially expressed genes more than 2-fold up or downregulated in HeLa cells. Interestingly, EFNB2 was one of these differentially expressed genes and upregulated 2,5-fold when snRNA U1.8 was blocked [263]. snRNA variants function in a cell and gene specific manner, therefore upregulation of RNA, variant U1 small nuclear 28 may have regulatory roles on EFNB1 expression. In this study, I did not characterize the role of candidate lncRNAs on EFNB1 expression. However, it is worth to analyze in detail how EFNB1 expression is regulated.

4.3.5 EFNB1 promotes T cell mediated glial cell killing by activating the Akt-mTOR pathway in T cells

Because of the unexpected siRNA mediated overexpression of EFNB1, I needed to re-interpret the primary and secondary screen results. Following siRNA transfection, oligodendrocytes elevate EFNB1 levels on the surface and this resulted in increased T cell cytotoxicity. I revisited our hypothesis as EFNB1 function as a co-stimulatory immune checkpoint rather than being co-inhibitory. The increased EFNB1 protein levels in primary glioblastoma cells was not as strong as in oligodendrocytes; still this was enough to induce a similar impact on T cell cytotoxicity.

In a previous study, the co-stimulatory role of Efnb1 on mouse splenocytes was shown [189]. Stimulation of CD4+ and CD8+T cells from BALB/c mice with plate bound EFNB1 and agonistic anti-CD3 antibody enhanced T cell proliferation similar levels to CD28-mediated stimulation. Additionally, EFNB1-Fc mediated co-stimulation increased IFN-γ

secretion and enhanced T cell mediated target cell lysis [189]. In order to test a direct EFNB1 mediated co-stimulation of human T cells, I switched to a simpler model than target-T cell co-culture where I stimulated T cells with plate bound recombinant EFNB1 together with anti-CD3 agonist antibody (Figure 20 & 21). Compared to anti-CD3 stimulation alone (IgG-Fc control), stimulation of FluT cells as well as glioblastoma-derived TILs and MART-1 antigen specific melanoma-derived TILs strongly elevated the secretion of the effector cytokines Granzyme B, TNF-α and IFN-γ. This impact was lost when the TCR downstream signaling was blocked by Lck inhibitor in MART-1 TILs, indicating EFNB1 alone is not sufficient to activate T cells but rather function as a TCR co-stimulator. As described in the section 4.3.1, EFNB1 can bind Eph-B type receptors as well as EPHA4, which was also identified as a HIT in the primary screen. Blockade of EPHA4 with the small molecule inhibitor rhynchophylline completely reverted EFNB1-mediated stimulation in MART-1 TILs. This phenotype was not observed by other T cell sources, potentially because of the involvement of Eph-B type receptors in those T cells rather than EPHA4.

As a second approach to test T cell activation, I confirmed the upregulation of exhaustion markers PD-1, LAG-3 and TIM-3 following the stimulation with EFNB1. The exhaustion markers are expressed on T-cells upon activation as a negative feedback mechanism. Therefore, upregulation of exhaustion markers is an indicator of T cell activation. Especially during chronic infections or inside the tumor tissue, constant antigen exposure induces T cell exhaustion [264, 265]. Of note, both $CD8^+$ and $CD4^+$ T cell populations in GBM-TILs could be activated upon EFNB1 stimulation.

Previous studies already showed the involvement of Eph receptors in TCR co-stimulation [266, 267]. Indeed, both EphA and EphB type receptors are highly expressed on thymocytes as well as detected on peripheral $CD4^+$ and $CD8^+$ T cells. Eph receptors co-localize with activated T cell receptors in lipid rafts [266, 267]. Activation of EphB receptors with ephrin-B Fc ligands promotes T cell proliferation, IFN-γ secretion and cytotoxic T cell activity by upregulating p38 and p42/44 MAP kinases [268, 269]. Among the different Eph family members, EPHB6 is the most characterized one showing an immune modulatory function [266]. Stimulation of T cells with anti-EPHB6 antibodies or ephrin-B ligands resulted in tyrosine phosphorylation and increased signaling. Although EPHB6 lacks kinase activity, it can be phosphorylated by other co-

clustered EPHB receptors. The impact of EPHB6 on T cell co-stimulation is due to common downstream signaling proteins, such as the adapter and ubiquitin ligase Cbl, with the TCR [227]. In line, EPHA type receptors also modulate TCR downstream signals. EFNA1 mediated stimulation of $CD4^+/CD8^+$ double positive thymocytes triggers apoptosis induced by strong TCR activation. This indicates the role of EPHA receptors on the negative selection of self-reactive thymocytes [227]. Interestingly, Eph receptors and the co-stimulatory molecule CD28 share common downstream signaling molecules such as PI3K and Akt [192, 193]. Upon binding to CD80, CD28 recruits PI3K thereby inducing the phosphorylation of Akt (protein kinase B) [190]. Phosphorylated Akt activates the regulatory protein mTOR (mammalian target of rapamycin) which in turn activates multiple transcription factors such as NFκB. Nuclear NF-κB induces the expression of its target genes, which promote T cell proliferation, activation and effector function [191, 270]. Since EPHA/B receptors can also transduce signals through the PI3K/Akt pathway. Indeed, I analyzed the phosphorylation of Akt and mTOR in T cells and observed a clear activation of these signaling molecules following 30 min after the stimulation with EFNB1. Additionally, mTOR can phosphorylate the transcription factor T-bet, which is one of the key inducer of type-I immunity associated genes such as IFNγ [271, 272]. Taken together EFNB1-Eph forward downstream signaling augments T cell activation by mimicking the B7/CD28 axis.

4.3.6 EFNB1 reverse signaling induces PD-L1 expression and TGFβ pathway in the oligodendrocytes as immune resistance mechanisms

As described in section 4.4.1, ephrin-Eph interaction can transduce signals bi-directionally. Previous HTP screens performed in our department using PDAC, multiple myeloma and lung models, identified novel tumor intrinsic resistance genes involved in TNFα, FasL and TRAIL mediated cytotoxicity. Therefore, I examined whether EFNB1 reverse signaling in oligodendrocytes induce such resistance mechanisms as well. One of the key downstream transcription factors activated by EFNB1 reverse signaling is STAT3, which drives the expression of genes important for oncogenic signaling in tumor cells [228]. Phosphorylation of EFNB1 in response to ligation with Eph receptors, leads to the recruitment and activation of the Src kinase. Src later phosphorylates JAK2, which in turn phosphorylates STAT3 and thereby induces STAT3 dimerization and nuclear translocation [195, 196]. STAT3 needs an additional phosphorylation by MAPK or mTOR

to be fully transcriptionally active [197, 198]. Therefore, I examined STAT3 phosphorylation in Scr and EFNB1 siRNA transfected oligodendrocytes. The upregulation of EFNB1 levels on oligodendrocytes following transfection indeed increased phosho-STAT3 levels indicating that an interaction between neighboring oligodendrocytes can promote reverse signaling. I also confirmed the activation of STAT by RNA-Seq data, since 33 STAT2/3 target genes were upregulated following siRNA-mediated overexpression of EFNB1. Interestingly among these genes, I detected PD-L1 as one of STAT target genes which was upregulated 3,6-fold in EFNB1 siRNA transfected cells compared to negative control (top 9th differentially upregulated gene). It is important to note that, in tumor cells PD-L1 is mainly upregulated in response to IFNγ. Similar to EFNB1 reverse signaling, IFNγ receptors also transduce downstream signals via the JAK-STAT pathway, thereby inducing PD-L1 expression [199]. In this study, for the first time I demonstrated the EFNB1 mediated regulation of PD-L1.

Another important immunosuppressive mechanism found to be induced in EFNB1 upregulated cells is the TGFβ (transforming growth factor beta) pathway (Table 5). Interestingly, TGFβ2, its receptor TGFβR2 and receptor associated protein (TGFBRAP1), downstream effectors SMURF2 and SMAD1/5 and the TGFβ activator LRRC32 (leucine rich repeat containing 32) were upregulated in oligodendrocytes upon increased EFNB1-Eph signaling. In a previous study, the role of Ephrin-Eph signaling in TGFβ-mediated immunosuppression was disclosed using the interaction between T cells and human mesenchymal stem cells (MSC) [273]. MSCs are bone-marrow derived multipotential cells which exhibit immunosuppressive properties to suppress allogeneic reactions. Nguyen et al. showed that, ligation of EPHB2 and EFNB2 expressed by MSCs with EFNB1 and EPHB4 on T cells respectively, induced the expression of TGFβ1, indolamine 2,3-dioxygenease (IDO) and inducible nitric oxide synthase (NOS2) by MSCs, which in turn suppress T-cell proliferation [273]. Of note, I found a 1,6-fold upregulated of NOS3 also in EFNB1 overexpressing cells via RNA-Seq.

Other than PD-L1 and TGFβ, EFNB1 reverse signaling also regulated the expression of many candidate co-inhibitory immune checkpoints identified in the previous HTP screens performed in our department. Further characterization of these co-inhibitory HITs identified in the MS-glioma screen can provide deeper insights about the synergistic or antagonist signaling pathways interfering with the EFNB1-Eph signaling.

Taken together, EFNB1-Eph receptor forward signaling activates on the hand T cells, while the reverse signaling on the other hand induces immune resistance mechanisms in oligodendrocytes. Nevertheless, the upregulation of PD-L1 and TGFβ was not sufficient to suppress EFNB1-Eph driven co-stimulation and cannot prevent T cell mediated oligodendrocyte killing.

4.4 Translational implications of EFNB1 and Ephs as targets for MS and glioma immunotherapy

The major aim of this work was to identify novel immune modulatory molecules that could be used as potential targets for the immunotherapy of multiple sclerosis and glioma. MS and glioma are two different CNS diseases with potentially similar mechanisms involved in the disease immunopathology.

The multiple-domain structure of Eph receptors provides a plenty selection of specific target regions. In recent years many approaches such as antibodies, peptides and soluble fragments of the receptors/ligands, small molecule inhibitors of protein-protein interactions, kinase inhibitors and siRNAs have been developed to target the Eph/ephrin signaling [274]. However, only few of these therapeutic tools have entered clinical trials [275]. So far, EFNB1 has not been targeted for the immunotherapy of cancer and autoimmune diseases.

In the current study, I describe the co-stimulatory role of EFNB1-Eph forward signaling on T cells as well as the reverse signaling inducing immune resistance mechanisms such as the upregulation of PD-L1 and TGFβ. For MS and glioma inverse therapeutic strategies need to be developed to suppress autoreactive T cell activity on the one hand and stimulate tumor reactive T cells on the other hand. Therefore, I first need to characterize the specific Eph receptor(s) through which EFNB1 signal to antigen-specific $CD8^+$ T cells and glioma tumor infiltrating lymphocytes (TILs). Antagonistic antibodies targeting the cognate receptor of EFNB1 can be used to suppress autoreactive T cells in MS patients, whereas agonistic antibodies can increase cytotoxic activity of TILs in glioma patients. As a current approach, adoptive T cell therapy using CAR-T cells engineered to secrete single chain variable fragment (scFv) are a promising strategy [276]. For glioma CAR-T cells secreting anti-PD-1/anti-PD-1 together with agonistic anti-Eph scFv can be applied for the immunotherapy of glioma, whereas CAR-Tregs

secreting agonist anti-Eph may reduce autoimmune reactions in MS patients more effective than CAR-Treg therapy alone [277]. Second and third generation CAR-T cells have been developed with CD28 or 4-1BB cytoplasmic domains to transduce co-stimulatory downstream signal upon target recognition [278]. As previously mentioned, Eph receptors share common downstream signaling nodes with CD28. Therefore, CAR-T cells engineered with the cytoplasmic domain of Eph instead of CD28 may exhibit a safer profile. Another potential therepeutical strategy is the use of soluble EFNB1-Fc to trigger Eph signaling in glioma TILs.

Although EFNB1 is a promising target, several concerns have to be considered when modulating its activity. EFNB1 is widely expressed in adult tissues and plays important roles in neuronal plasticity and maintenance. Another concern is the redundancy and context dependent interaction of ephrin-Eph signaling. Blockade of EFNB1-Eph interaction can potentially be compensated by EFNB2 and EFNB3 and several Eph receptors such as EphB2, B4 and A4. In addition, the outcome of the interaction between EFNB1 and a particular Eph receptor can be different depending on the type of downstream signaling used by communicating cells. Therefore, better understanding of this complex and paradoxical signaling is crucial for the development of effective and safe immunotherapeutic strategies against cancer and autoimmune diseases.

5 Conclusion

One of the key goals of immunotherapeutic strategies against cancer and autoimmune diseases is the fine-tuning of the balance between T cell cytotoxicity and target cell resistance. In brain, dysregulated T cell co-stimulation or co-inhibition can contribute to the MS immunopathology or glioma immune evasion depending on which direction the balance was shifted. Blockade of so far identified immune checkpoint molecules demonstrated limited efficacy in glioma patients. Current therapeutic strategies for MS have shown serious side effects and are not able to prevent the disease progression so far.

In this study, I aimed at discovering novel MS and glioma relevant molecular mechanisms which regulate the crosstalk between cytotoxic T cells and glial cells. By taking advantage of a HTP screen, I identified EFNB1 as a novel co-stimulatory molecule which may involve in the immunopathology of glioma and MS. I showed that, EFNB1 expressed on glial cells activates effector cytokine secretion by T cells and increases T cell mediated target cell killing *in vitro*. At the same time, EFNB1 reverse signaling modulates glial cell intrinsic immune resistance by inducing PD-L1 expression and the TGFβ pathway. In this context, this work contributes to a better understanding for opposite dual mechanisms exerted by immune checkpoint signaling and underlines the importance of combinatorial therapies. Understanding bi-directional signals between target cells and immune cells is necessary for the development of an effective anti-tumor immunity and for the re-stabilizing of self-tolerance.

6 Materials

6.1 Laboratory equipment

Instrument	Company
Agilent 2100 Bioanalyzer	Agilent Technologies
Bolt Mini Gel Tank	Life Technologies
FACS Lyrics	BD
FACSARIA II cell sorter	BD
IBL 437C Blood Irradiator	CIS Bio International
Gamma Counter	PerkinElmer
gentleMACS™ Octo Dissociator	Miltenyi Biotech
IncuCyte ZOOM	ESSEN BioScience
MultiDrop Combi I	Thermo Fisher Scientific
myECL documentation system	Thermo Fisher Scientific
NextSeq 550	Illumina
Owl EasyCast B2 Mini Gel Electrophoresis Systems	Thermo Fisher Scientific
Power Ease 3000W	Life technologies
QuantStudio 3 Real-Time PCR System	Thermo Fisher Scientific
SimpliAmp thermal cycler	Thermo Fisher Scientific
Spark 10M multimode microplate reader	Tecan
Spectrometer Scan Drop 250	Analytic Jena
ThermoMixer C	Eppendorf

6.2 Chemicals and reagents

Material	Company
1 kb DNA Ladder (GeneRuler)	Thermo Fisher Scientific
100 bp Ladder (GeneRuler)	Thermo Fisher Scientific
50 bp Ladder (GeneRuler)	Thermo Fisher Scientific
7-Cyclopentyl-5-(4-phenoxyphenyl)-7H-pyrrolo[2,3-d]pyrimidin-4-ylamine (Lck Inhibitor)	Sigma-Aldrich
Accutase	Sigma-Aldrich
Adenosine 5′-monophosphate disodium salt	Sigma-Aldrich
Adenosine 5′-triphosphate disodium salt hydrate	Sigma-Aldrich
Agarose NEEO Ultra-Quality	Roth
Ampicillin	Thermo Fisher Scientific
Aqua ad iniectabilia	B. Braun
Assay Diluent	BD
Beta-mercaptoethanol	Sigma-Aldrich
Biocoll separating solution	Millipore
Bovine serum albumin (BSA)	Sigma-Aldrich
Buffer RDD	Qiagen
Cell signaling lysis buffer	Millipore
Chromium-51 Radionuclide, 5mCi (185MBq), Sodium Chromate in Normal Saline (pH 8-10)	Perkin Elmer
Collagenase type 4	Worthington
DharmaFECT1	Dharmacon, GE Healthcare
D-Luciferin	Biosynth
DNase I	Roche

Dynabeads Human T-Activator CD3/CD28	Thermo Fisher Scientific
Ethanol absolute	Sigma-Aldrich
GelRed 10000x	Biotium
GelRed Nucleic Acid Gel Stain	Biotium
HBSS with calcium, with magnesium	Sigma-Aldrich
HBSS without calcium, without magnesium	Sigma-Aldrich
Ionomycin calcium salt	Sigma-Aldrich
Isopropanol	Fluka
Jet-PEI	Polyplus-transfection
Kiovig	Baxter
Lipofectamine 3000	Thermo Fisher Scientific
Lipofectamine RNAiMAX	Thermo Fisher Scientific
Loading dye solution (6x)	Thermo Fisher Scientific
Methanol	Sigma-Aldrich
Nuclease free water	Ambion
NuPAGE 4-12% Bis-Tris Gels	Thermo Fisher Scientific
NuPAGE LDS Sample Buffer	Thermo Fisher Scientific
NuPAGE, MES SDS Running Buffer (20x)	Thermo Fisher Scientific
Oxalic acid	Sigma-Aldrich
PageRuler Prestained Protein Ladder	Thermo Fisher Scientific
Phenylacetic acid	Sigma-Aldrich
Phorbol 12-myristate 13-acetate (PMA)	Sigma-Aldrich
Phosphatase inhibitor III	Sigma-Aldrich
Pierce 1-Step Transfer Buffer	Thermo Fisher Scientific

Ponceau S solution	Sigma-Aldrich
Protease Inhibitor Cocktail Set III, EDTA-Free	Calbiochem
Rhynchophylline	MCE (MedChemExpress)
RNAlater RNA Stabilization Reagent	Qiagen
RNase-Free DNase Set	Qiagen
SDS polyacrylamide gels (4-12% Bis/Tris)	Life Technologies
Skimmed milk powder	Carl Roth
TAE Buffer (Tris-acetate-EDTA) (50X)	Thermo Fischer Scientific
Triton X-100	Fluka
Trypan blue solution (0.4 %)	Fluka
Trypsin-EDTA (1x)	Lonza
Tween 20	Sigma-Aldrich
YOYO-1 Iodide (491/509) - 1 mM Solution in DMSO	Thermo Fisher Scientific
Zombie Aqua Fixable Viability Kit	BioLegend
Zombie NIR Fixable Viability Kit	BioLegend

6.3 Assay kits

Kits	Company
2x MyTaq HS Red Mix	Bioline
Adult Brain Dissociation Kit	Miltenyi
Anti-O4 MicroBeads	Miltenyi
CD8+ T Cell Isolation Kit, human	Miltenyi
ELISA development kit for human Granzyme B	MabTech
ELISA development kit for TNFα, IFNγ	BD Bioscience

EndoFree Plasmid Maxi Kit	Qiagen
Myelin Removal Beads II human, mouse, rat	Miltenyi
NextSeq 500/550 High Output Kit v2.5 (75 Cycles)	Illumina
OptEIA TMB Substrate Reagent Set	BD Bioscience
Pierce BCA Protein Assay Kit	Thermo Fisher Scientific
QuantiFast SYBR Green PCR Kit	Qiagen
QuantiTect Reverse Transcription Kit	Qiagen
RNAeasy Lipid Tissue Mini Kit	Qiagen
RNeasy Mini Kit	Qiagen
Trident femto Western HRP Substrate	GeneTex

6.4 siRNAs, siRNA libraries, plasmids, lentiviral particles

Material	Company
AllStars Hs Cell Death Control siRNA	Qiagen
CMV-Luciferase (firefly)-2A-GFP (Puro) (LVP020)	GenTarget Inc - Amsbio
Customized EFNB1 overexpression plasmid (pCDNA3.1 backbone)	GenScript
Customized HLA-A2 plasmid (pCDNA3.1 backbone)	GenScript
Customized siRNA library for the secondary screen (LP-47592 RNAi Cherry Pick Library)	Horizon (formerly: Dharmacon, GE Healthcare)
EF1a-Luciferase (firefly)-2A-GFP (Bsd) (LVP436)	GenTarget Inc - Amsbio
ON-TARGETplus Non-targeting siRNA #3	Horizon (formerly: Dharmacon, GE Healthcare)
ON-TARGETplus Non-targeting siRNA #4	Horizon (formerly: Dharmacon, GE Healthcare)

siGENOME set of four against SIK3, CCR9, 4-1BBL, CD40, CX-32, PD-L1	Horizon (formerly: Dharmacon, GE Healthcare)
siGENOME SMARTpool against PD-L1, CCR9, 4-1BBL, CD40, CASP3, SIK3, CX-32, OX-40L, UBC	Horizon (formerly: Dharmacon, GE Healthcare)
siRNA library - 30 pool	siTOOLs Biotech
Sub-library of the siGENOME library for the primary screen	Horizon (formerly: Dharmacon, GE Healthcare)

6.5 Primers

Primer	Sequence	Company
Human β-Actin	F AGAAAATCTGGCACCACA R: GGGGTGTTGAAGGTCTCAAA	Sigma-Aldrich
Human EFNB1	F: GGCTGAACTCCTGGAACTTG R: GTTGGTCACCTGCAATAGGC	Sigma-Aldrich
Mouse β-Actin	F: GGAGGGGGTTGAGGTGTT R: GTGTGCACTTTTATTGGTCTCAA	Sigma-Aldrich
Mouse EFNB1	F: CTCTTCCTGGTTCACAGTCTCA R: CCAAGCAAGGAGTCAGACAA	Sigma-Aldrich
RT^2 qPCR Primer Assay for Human CD274 (PD-L1)	N.A.	Qiagen

6.6 Consumables

Material	Company
24 Channel Aspiration or Dispensing Wand on 4.5 mm centers and 11 mm long for Microplates, PolyCarbonate Barrel	V & P Scientific, Inc.
Cell strainer 100µm	Omnilab
Conical centrifuge tubes (15 and 50 ml)	TPP

Coolcell LX	VWR
Cryogenic vials (2 ml)	Corning
FACS tubes	Falcon
Flat bottom plates (6 and 96 wells)	TPP
GentleMACS C Tubes	Mitenyi
LumaPlates	Perkin Elmer
MACS Seperation Colums, LS / MS	Miltenyi
MACS SmartStrainers (70 µm)	Miltenyi
magnetic MACS separator frame	Miltenyi
MicroAmp Optical 96-Well Reaction Plate	Thermo Fisher Scientific
NUNC MaxiSorp 96 wells ELISA plates	Thermo Fisher Scientific
OptiPlate-384 white opaque	Greiner
OptiPlate-96 white opaque	Perkin Elmer
PCR micro test tube	Nerbe plus
Pipette filter tips (10 µl - 1000 µl)	Thermo Fisher Scientific
Polysorp 96 wells plates	Thermo Fisher Scientific
Polystyrene round bottom tubes with caps	Falcon
Polyvinylidene diflouride (PVDF) membrane	Millipore
Reservoir 10-25ml sterile	INTEGRA Biosciences
Round-bottom plate (96 well)	TPP

Safe-lock tubes (0.5, 1.5, 2.0 ml)	Eppendorf
Syringe filter units (0.22 µm-pores)	Millipore
Tissue culture flask/filter cap (25, 75, 150 cm^2)	TPP
Vakuumtitration 500 „rapid“-Filtermax	TPP
Whatman 3 mm gel blot paper	Sigma-Aldrich

6.7 Buffers

Buffer	Ingredients	Volume
B2 Buffer	ddH_2O DDT (415 mM) ATP (33 mM) AMP (0,996)	85 ml 6,4 g 1,82 g 0,035 g
BL Buffer	ddH_2O HEPES (50 mM) EDTA (0,5 mM) Phenylacetic acid (0,33 mM) Oxalic acid (0,07 mM) pH	84,8 ml 5 ml 0,1 ml 0,033 ml 0.07 ml 7,6
FACS buffer	FCS PBS	2 % 500 ml
Immunoblot blocking solution	TBS-T BSA	100 ml 5 g
Immunoblot washing solution (TBS-T)	TBS (10x) ddH_2O Tween-20	100 ml 900 ml 0.5 ml
Luciferase assay buffer	BL buffer B2 buffer D-Luciferase (10mg/ml) 1M $MgSO_4$	44,35 ml 5 ml 0,65 ml 751 µL

Lysis buffer for the luciferase-based cytotoxicity assay	BL buffer 10% Triton-X-100	48,5 ml 1,5 ml
Phosphate saline buffer (PBS)	PBS 10x (Sigma-Aldrich) ddH_2O	100 ml 900 ml
SDS-PAGE running buffer	MES SDS running buffer (20x) ddH_2O	50 ml 950 ml
Tris Buffer Saline (TBS)	TBS 10x (Sigma-Aldrich) ddH_2O	100 ml 900 ml
Tris-acetate-EDTA (TAE) buffer (50x)	Tris Glacial acetic acid 0.5 M EDTA ddH_2O pH	242 g (2 M) 57.1 ml 100 ml 1 L 8.5

6.8 Cell media and supplements

Material	Company
AB serum (heat-inactivated), human	Valley Biomedical
AIM V Medium	Thermo Fischer Scientific
AIM-V with L-glutamine, streptomycin sulfate, gentamycin sulfate	Gibco
Beta-mercaptoethanol (50 mM)	Gibco
Blasticidin	Thermo Fischer Scientific
Dimethyl sulfoxide (DMSO)	Sigma-Aldrich
DMEM; high glucose (4.5 g/l), L-glutamine, sodium pyruvate, $NaHCO_3$	Sigma-Aldrich
DMEM-High Glucose (4.5 g/l), without sodium pyruvate	Sigma-Aldrich

Dulbecco-PBS without Ca^{2+}, $MgCl_2$ (1x)	Sigma-Aldrich
EDTA 1% (w/v) without Mg^{2+}	Biochrom
FBS	Biochrom
Fetal calf serum (FCS) (heat-inactivated)	Biochrom
Fungizone	Gibco
Geneticin sulfate (G418)	Gibco
HEPES buffer (1 M)	PAA
Hepes Buffer (1M)	Sigma-Aldrich
Human EGF, premium grade	Miltenyi
Human FGF-2, premium grade	Miltenyi
Hygromycin	Thermo Fischer Scientific
IL-15	R&D
IL-2 (human, recombinant)	Novartis
Opti-MEM	Thermo Fischer Scientific
Penicillin/Streptomycin (P/S; 100X)	PAA
PROLEUKIN (rHuIL2)	Novartis Pharma
Puromycin (10 mg/ml)	GIBCO
Recombinant Golden Nuclease/Benzonase Protein	Speed BioSystems
RHB-A Neural Stem Cell Culture Media	Takara
RPMI 1640 with L-glutamine	Gibco

RPMI 1640 with L-glutamine and $NaHCO_3$	Sigma-Aldrich

Medium	Component	Amount
Complete DMEM (without sodium pyruvate)	DMEM	500 ml
	FCS	50 ml
	P/S	5 ml
Complete lymphocyte medium (CLM)	RPMI	500 ml
	AB serum	50 ml
	P/S	5 ml
	HEPES	5 ml
	Beta-mercaptoethanol	50 µL
Complete RHB-A	RHB-A	50 ml
	EGF	20 ng/ml
	FGF-2	20 ng/ml
	P/S	500 µL
DMEM Transfection medium (w/o sodium pyruvate)	DMEM	500 ml
	FCS	50 ml
FluT / MO3.13 freezing medium A	FCS Serum	60 %
	RPMI	40 %
FluT / MO3.13 freezing medium B	FCS Serum	80 %
	DMSO	20 %
FluT expansion medium	CLM	50 %
	AIM-V	50 %
FluT expansion medium with feeder cells	CLM	50 %
	AIM-V	50 %
	Feeder cells	100x TILs
	OKT3	30 ng/ml
	rHuIL-2	3,000 U/ml
Freezing Medium for Tumor Cells	FCS	90 %
	DMSO	10 %

RHB-A Transfection medium	RHB-A EGF FGF-2	50 ml 20 ng/ml 20 ng/ml
TIL freezing medium A	AB Serum RPMI	60 % 40 %
TIL freezing medium B	AB Serum DMSO	80 % 20 %

6.9 Cell lines and primary cells

Cell Line	Origin	Culture medium
FluT	Healthy donor PBMCs	CLM
MO3.13	Human Oligodendrocytic cell line (Tebu-Bio)	Complete DMEM (without sodium pyruvate)
MO3.13-A2	""	Complete DMEM (without sodium pyruvate), 0,8 mg/ml G418
MO3.13-A2-eLuc-EFNB1over	""	Complete DMEM (without sodium pyruvate), 0,8 mg/ml G418, 1 µg/ml blasticidin, 0,5 mg/ml Hygromycin
MO3.13-A2-Luc	""	Complete DMEM (without sodium pyruvate), 0,8 mg/ml G418, 0,6 µg/ml puromycin
RAV27	Human primary glioblastoma tissue	Complete RHB-A
RAV27-Luc	""	Complete RHB-A, 0,2 µg/ml puromycin
TILs (GBM), MART-1 TILs	Human primary glioblastoma tissue	CLM

6.10 Antibodies, recombinant proteins and peptides

6.10.1 Western blot antibodies

Specificity	Size (kDa)	Species	Isotype	Conjugate	Company	Dilution
Anti-Akt	60	Mouse	IgG1	-	Cell Signaling Technology (CST)	1:2000
Anti-EFNB1 (LS-C332134)	37	Rabbit	IgG	-	LS Bio (Life Span Biosciences)	1:1000
Anti-PD-L1	50	Mouse	IgG2a	-	R&D systems	1:500
Anti-phospho STAT3 (Ser727)	86	Rabbit	IgG	-	Cell Signaling Technology (CST)	1:1000
Anti-Phospho-Akt (S473)	60	Rabbit	IgG	-	Cell Signaling Technology (CST)	1:1000
Anti-Phospho-mTOR (S2448)	289	Rabbit	IgG	-	Cell Signaling Technology (CST)	1:1000
Anti-STAT3	86	Mouse	IgG2a	-	Cell Signaling Technology (CST)	1:1000
Anti-α-Tubulin	50	Mouse	IgG1	-	Santa Cruz	1:1000
Anti-β-Actin	42	Mouse	IgG1	-	Abcam	1:5000
Secondary anti-mouse	-	Goat	IgG	HRP	Santa Cruz	1:5000
Secondary anti-rabbit	-	Goat	IgG	HRP	Santa Cruz	1:5000

6.10.2 FACS antibodies

Specificity	Species	Isotype	Conjugate	Company	Dilution
Anti-human CD223 (LAG-3)	Mouse	IgG1κ	FITC	Biolegend	1:100
Anti-human CD274 (PD-L1)	Mouse	IgG2b	APC	Biolegend	1:40
Anti-human CD279 (PD-1)	Mouse	IgG1κ	APC	Biolegend	1:40
Anti-human CD3	Mouse	IgG1κ	AF700	Biolegend	1:40
Anti-Human CD4	Mouse	IgG1κ	PerCP-Cy5.5	BD	1:200
Anti-human CD45RO	Mouse	IgG2a	APC-Cy7	Biolegend	1:66
Anti-human CD62L	Mouse	IgG1κ	BV605	Biolegend	1:100
Anti-human CD8	Rat	IgG1κ	V450	BD	1:200
Anti-human Ephrin-B1 (extracellular)	Rabbit	IgG	-	Alomone Labs	20 µg/ml
Anti-human HLA-A2	Mouse	IgG2b	APC	BD	1:50
Anti-human TIM-3 (CD366)	Mouse	IgG1κ	PE/Cy7	eBioscience	1:20
Anti-mouse ACSA-2	Rat	IgG2b	PE	Miltenyi	1:10
Anti-O4 (human, mouse, rat)	Recombinant	human IgG1	APC	Miltenyi	1:50
Anti-rabbit IgG	Goat	IgG	BV421	BD	10 µg/ml
Flu Pentamer (A*02:01 - GILGFVFTL, Influenza A MP 58-66)	-	-	APC	ProImmune	1:10

Isotype control	Mouse	IgG2b	APC	BD	1:50
Isotype control	Mouse	IgG1κ	FITC	Biolegend	1:100
Isotype control	Mouse	IgG2a	APC-Cy7	Biolegend	1:66
Isotype control	Mouse	IgG1κ	PE/Cy7	eBioscience	1:20
Isotype control	Mouse	IgG1κ	BV605	Biolegend	1:100
Isotype control	Mouse	IgG1κ	APC	eBioscience	1:20
REA Control (I)	Recombinant	Human IgG1	APC	Miltenyi	1:50

6.10.3 Antibodies for functional assays, recombinant proteins and peptides

Antibody/Protein/Peptide	Company	Working concentration
Anti-human CD3 (clone: OKT3)	eBioscience	30 ng/ml for REP, 1 µg/ml for coating
Ephrin-B1 Protein, Human, Recombinant (His & Fc Tag)	Sino Biological	20 - 1,25 µg/ml
IgG1 Protein, Human, Recombinant (103 Cys/Ser)	Sino Biological	20 - 1,25 µg/ml
Mouse, IgG2a Isotype	Prof. Moldenhauer (DKFZ – Heidelberg)	60 µg/ml
Anti-MHC-I (Cone W6/32) mouse, IgG2a	Prof. Moldenhauer (DKFZ – Heidelberg)	60 µg/ml
Matched peptide A*02:01-GILGFVFTL	ProImmune	Assay dependent

6.11 Software

Software	Developer
Adobe Illustrator	Adobe system
cellHTS2	Boutros et al. [279]
Endnote (X7)	Adept Scienctific
FlowJo	Tree Star
Graph Pad Prism (8)	GraphPad Software
ImageJ	Wayane Rasband
Microsoft Office 2013	Microsoft, USA
R Studio	RStudio, Inc.

7 Methods

7.1 Cell culture methods

7.1.1 Cell lines and primary cells

7.1.1.1 MO3.13

Human glial (oligodendrocytic) hybrid cell line (MO3.13) was purchased from Tebu-Bio. MO3.13 cells were cultured in high glucose DMEM media (Sigma-Aldrich, D5796) supplemented with 10% fetal calf serum, 1% P/S. Cells were detached by trypsin and splitted 1:10 when they reached 80% confluency. Cells were frozen in freezing media A and B (1:1) containing FCS.

7.1.1.2 RAV27

The primary glioblastoma cells (RAV27) were cultured in RHB-A media supplemented with 1% P/S, 20 ng/ml human EGF and 20 ng/ml human FGF-2. Cells were detached by accutase, washed and splitted 1:3 when they reach 80% confluency. Cells were frozen by resuspending the cell pellet in 900 µl plain RHB-A media and subsequently adding 100 µl DMSO dropwise.

7.1.1.3 FluT cells and TILs

FluT cells and TILs were thawn 6h prior to performing experiments and cultured in plain CLM medium at a concentration of 1 x 10^6 cells/ml. After 6h of resting, T cells were resuspended in fresh CLM, counted again and diluted in CLM for the desired concentration of cells according to the experimental set-up.

7.1.2 Generation of stable HLA-A2 and Luciferase-GFP expressing MO3.13 and RAV27 cells

MO3.13 cells were transfected with a customized plasmid vector pcDNA 3.1 from Genscript encoding HLA-A2 and a resistance gene for Geniticin 418. JetPEI was used as transfection reagent according to the manufacturer´s instructions. Transfected cells were selected for 14 days with G418-containing medium (0,8 mg/ml). The optimal concentration of G418 was established by titration of the toxic dosage of G418 in MO3.13 cells. Afterwards MO3.13 cells were sorted by flow cytometry based on the HLA-A2 expression and cultured in the presence of 0,8 mg/ml G418.

For the generation of stably luciferase expressing cells, MO3.13 and RAV27 cells were transduced with lentiviral vector (CMV-Luciferase (firefly)-2A-GFP (Puro)) encoding firefly luciferase coupled to GFP through a self-cleaving 2A element driven under a strong constitutive CMV promoter. Puromycin resistance gene under a viral RSV promoter served for selection purposes. 200.000 MO3.13-A2 cells and 400.000 RAV27 cells were seeded 24h prior to transduction. Lentiviral particles were added dropwise to the cells with a multiplicity of infection of 1 (MOI 1). The following day, the medium was exchanged and the selection was started by adding 0,6 µg/ml and 0,2 µg/ml puromycin for MO3.13-A2 and RAV27 cells respectively. The optimal concentration of puromycin for each cell type was determined by titration curve for 14 days. After 2 weeks of selection transduced MO3.13-A2 and RAV27 cells were sorted for GFP expression by flow cytometry and cultured in the presence of the above mentioned puromycin concentration. All cell sorting experiments were conducted in collaboration with the RCI's central FACS facility (Irina Fink, Dr. Rüdiger Eder), using the FACSARIA II cell sorter (BD).

7.1.3 Generation of EFNB1 over-expressing MO3.13-A2-Luc

For the generation of EFNB1 over-expressing MO3.13-A2-Luc cells, cells were transfected with a customized plasmid encoding an open-reading frame of EFNB1 (GenScript). 200.000 cells were seeded in a 6-well plate 24h prior to transfection. Lipofectamine 3000 was used as transfection reagent according to the manufacturer´s instructions. Transfected cells were cultured under selection pressure in hygromycin-containing medium (0,5 mg/ml). After 14 days of selection EFNB1 mRNA levels and surface expression was determined by RT-qPCR and flow cytometry respectively.

7.2 Generation of FluT cells

7.2.1 Isolation of peripheral blood mononuclear cells (PBMCs)

PBMCs were isolated from buffy coats of healthy donors via Biocoll density gradient centrifugation (Biochrome). Briefly, buffy coats were diluted 1:10 in RPMI (3,5 ml blood + 31,5 ml RPMI) and added to 50mL conical centrifuge tubes, containing 15 ml of Biocoll solution. Density gradient centrifugation was performed at 2000 rpm for 20 min at room temperature using low brake. Afterwards PBMCs were collected, washed twice with RPMI and frozen in aliquots of 5 x 10^7 cells per vial using freezing media A-B (1:1) containing FCS.

7.2.2 Antigen specific expansion (ASE) of FluT

For the generation of influenza (Flu)-specific CD8+ T (FluT) cells, PBMCs from HLA-A*02+ healthy donors were isolated. A minimum of 5 x 10^7 PBMCs were used for sorting total CD8+ T cells using a CD8+ Isolation Kit (Miltenyi) according to the manufacturer´s protocol. Subsequently, total CD8+ T cells were expanded in the presence of A2-matched Flu peptide (GILGFVFTL, ProImmune, Oxford, UK) for 14 days. The autologous CD8- fraction was irradiated and used as feeder cells for 1 week and were then substituted with irradiated T2 cells. On day 1 and day 8, 100 U/ml of IL-2 and 5 ng/µl of IL-15 were added. Cells were expanded in expansion medium composed of 50% CLM and 50% AIM-V medium. Some cells were kept without adding Flu peptide as a negative control. The percentage of Flu-antigen specific T cells were determined by pentamer staining on day 7 and 14. After antigen-specific expansion cells were frozen in aliquots of 5 x 10^6 cells per vial. Later, FluT cells were sorted by FACS and expanded further for 14 days by using a rapid expansion protocol.

7.2.3 Rapid expansion protocol (REP) for FluT

To increase the total number of CD8+ FluT cells, the cells obtained from ASE were further expanded according to the protocol from *Rosenberg et al* [173]. Prior to expansion FluT from ASE were stained with Flu-Pentamer (section 7.4.9.1) and sorted by FACS. Meanwhile, PBMCs isolated from three healthy donors as described above were irradiated with 60 Gray (IBL 437C Blood Irradiator). Irradiated PBMCs were used as feeder cells to support FluT expansion. 1 x 10^6 sorted FluT cells were co-cultured with irradiated PBMCs at a ratio of 1:200 in 150 ml of expansion medium supplemented with 3000 U/ml IL-2 and 30ng/ml anti-CD3 (clone: OKT3) antibody in a T175 flask. After 5 days of incubation, 100 ml of supernatant was changed with 150 ml of fresh medium and IL-2 was replenished to keep the concentration at 3000 U/ml. On day 7, 9 and 11, 2/3 of old expansion medium was discarded, cells were counted, and cell concentration was adjusted to 0,6 x 10^6 cells/ml with fresh expansion medium containing IL-2 as much as to keep the concentration 3000 U/ml. On the final day of REP- day 14- 300.000 cells were taken for a FACS Pentamer staining to check the percentage of CD8+ FluT cells in the expansion. Finally, cells were frozen in aliquots of 5-10 x 10^6 cells per vial in freezing media A and B (1:1).

7.3 Isolation and expansion of TILs from glioma tissue

7.3.1 Tumor digestion

Fresh tumor pieces were cut in small pieces using two scalpels. Pieces were transferred into a single well of a 24-well plate and digested in expansion medium containing 0,38 µg/ml Fungizone, 400 µg/ml Dnase I and 400 U/ml collagenase type 4 for 2h at 37°C, 5% CO_2. After 2h, tumor digest was mixed with using a 1000 µl pipette, passed through a 100 µm cell strainer, and washed with expansion medium by centrifuging 10 min at 1400 rpm. The pelleted cells were then used for expansion (7.3.2).

7.3.2 Rapid expansion protocol (REP) for TILs

TILs from the digested tumor were expanded using the REP described in 7.2.3 with some adjustments. Tumor digest was co-cultured with 2 x 10^7 of irradiated PBMCs in 20 ml expansion medium supplemented with Fungizone, 3000 U/ml IL-2 and 30ng/ml anti-CD3 (clone: OKT3) antibody in a T25 flask. On days 5, 7, 9 and 11, IL-2 was replenished as described above. On day 14, an aliquot of TIL was used for a FACS staining to check CD3, CD4, CD8, CD45RO, CD62L, PD-1, LAG-3 and TIM-3 expression. Finally, cells were frozen in aliquots of 5-20 x 10^6 cells per vial in freezing media A and B (1:1).

7.4 Molecular biology techniques

7.4.1 Transformation of bacteria with plasmids

Competent one Shot Top-10 *E.coli* bacteria were transformed with 100 ng of plasmids encoding HLA-A2 or EFNB1. Bacteria were incubated for 10 min on ice, were then exposed to a heat-shock at 42°C for 45 seconds and subsequently incubated for another 2 min on ice. 200 µl of SOC media was added and 50µl of bacteria suspension was plated on LB agar plates containing 100 µg/ml ampicillin and incubated overnight at 37°C. The following day, a single colony was picked, transferred to 5 ml LB medium supplemented with 100 µg/ml Ampicillin and incubated on the shaker in a 15ml falcon. 8h later, 500µl of the starter culture was transferred to 100ml LB medium containing 100 µg/ml ampicillin and incubated overnight shaking at 37°C. The next day, bacteria were harvested by centrifugation at 4700 rpm for 45 minutes; at 4°C and plasmids were isolated by performing a MaxiPrep (Qiagen) according to the manufacturer´s protocol.

7.4.2 RNA isolation and reverse transcription

Total RNA was isolated from cell pellets using the RNeasy Mini Kit (Qiagen) according to the manufacturer's guidelines. RNA isolation from total mouse brain was performed using RNeasy Lipid Tissue Mini Kit (Qiagen). RNA quality and concentration was analyzed using the Scan Drop (AnalytikJena). 1 µg of RNA from each sample was reversely transcribed to complementary DNA (cDNA) using the QuantiTect Reverse Transcription Kit (Qiagen) according to the manufacturer's protocol (including gDNA digestion). Briefly, 1 µg (= x µL) of RNA was incubated with 12-x µL H_2O and 2 µL gDNAse for 3 min. Subsequently, the master mix consisting of 4 µL buffer, 1 µL primer and 1 µL reverse transcriptase (RT) was added. To investigate genomic DNA contamination, water was added instead of reverse transcriptase (-RT controls). The mix was incubated for 20 min at 42°C and finally incubated for 3 min at 95°C for enzyme inactivation. cDNA was stored at -20°C.

7.4.3 PCR

Gene expression was measured using end-point PCR. Synthesized cDNA was amplified using conventional PCR. PCR samples were set up in a total volume of 25 µL using 2x MyTaq HS Red Mix (Bioline), 500 nM of gene-specific primer mix (list of primers in section 6.5) and 100 ng of template cDNA. Water was added to the reaction mix instead of cDNA for contamination controls. The PCR program was set as the following: 95°C for 3 min, 35 cycles of 3 repetitive steps of denaturation (95°C for 30 s), annealing (60°C for 30 s) and extension (72°C for 30 s), and a final step at 72°C for 5 min. PCR products were run on a 2% agarose gel in 1X TAE buffer using a gel electrophoresis system (Thermo Fisher Scientific) and DNA bands were visualized using UV light of myECL Imager (Thermo Fisher Scientific).

7.4.4 Real-time quantitative PCR (RT-qPCR)

Knockdown efficiency of siRNA sequences was measured by quantitative PCR. 10 ng of template cDNA, 2x QuantiFast SYBR Green PCR mix (Qiagen) and 300 nM of gene-specific primer mix was used per 20 µL reaction and each sample was prepared in triplicates. Reactions were run using the QuantStudio 3 (Applied Biosystems). Expression of target genes were normalized to the expression of β-actin gene and the analysis was performed using comparative Ct method. For gene-specific primer list see section 6.5.

7.4.5 Western blot

7.4.5.1 Preparation of protein lysates

Frozen cell pellets were resuspended in Miliplex Lysis buffer supplemented with 1:100 protease inhibitor and 1:100 phosphatase inhibitor. The amount of lysis buffer was adjusted to the size of pellet. Afterwards, samples were incubated in the fridge for 15 min under continuous rotation. Subsequently, the samples were centrifuged at 17.000 g at 4°C for 15 minutes. Then the supernatants were collected in fresh tubes and an aliquot was diluted 1:5 in water for a bicinchoninic acid assay (BCA). For that the BCA-standards were pipetted into a 96-well plate together with the diluted samples. BCA solution A and B were mixed 50:1 and 200 µl of this mix was added to each well. After 30 min of incubation at 37°C, the absorbance at 562 nm was measured with the TECAN reader and the protein concentration of the samples was calculated using the standard curve.

7.4.5.2 SDS Gel-electrophoresis

50 µg of protein lysates were denaturated in NuPAGE LDS Sample Buffer (containing 10% β-mercaptoethanol) (Thermo Fisher Scientific) at 95°C for 10 min and separated on the NuPAGE 4-12% Bis-Tris Gels (Thermo Fisher Scientific) using 1X MES running buffer.

7.4.5.3 Semi-dry blotting

After the electrophoresis, the gel was briefly washed with water and placed in Pierce 1-Step Transfer Buffer. A PVDF membrane was incubated in methanol for 1 min before equilibrating it together with 4 Whatman papers in Pierce 1-Step Transfer Buffer for 10 min. To transfer the proteins from the gel to the PVDF membrane, semi-dry blotting was performed. For that a stack of two Whatman papers, PVDF membrane, gel and again two Whatman papers was assembled directly on top of the anode plate. Then, the stack was covered with the cathode plate. Blotting was performed by using a "Thermo-Fisher Scientific Pierce G2 Fast Blotter".

7.4.5.4 Membrane development

After blotting, the membrane was washed with TBS and blocked with 5% BSA/TBS-T for 2 h. After blocking the membrane was incubated with the desired primary antibody (diluted in 5% BSA/TBS-T) overnight at 4°C, rotating. On the next day, the membrane

was washed 3 times with 1% BSA/TBS-T for 10 min and then incubated with suitable HRP-conjugated secondary antibody for 1h at RT (see the list of antibodies in section 6.10.1). This step was followed by washing three times for 10 min first with 1% BSA/TBS-T, then TBS-T and finally TBS. Trident femto Western HRP Substrate (GeneTex) A and B were mixed 1:1 (500 µl of each per membrane) and pipetted on top of the membrane. After incubating for 3 min in the dark, the chemiluminescent signal was detected using the MY ECL Imager (Thermo Fisher Scientific).

7.4.6 Reverse siRNA Transfection

To knock-down target HITs, 200 µl of 50 nM (for 30 pool siRNAs from siTOOLs) or 250 nM (for siRNAs from Dharmacon/Horizon) of siRNA solution was added per 6-well. 4 µl of RNAiMAX (Invitrogen) transfection reagent was diluted in 200 µl final volume of RPMI (Sigma-Aldrich) and incubated for 10 min at RT. 400 µl of additional RPMI was added and 600 µl of RNAiMAX-RPMI mix was pipetted to the siRNA coated well and incubated for 30 min at RT. $2x10^5$ MO3.13 oligodendrocytes were resuspended in 1,2 ml of antibiotic-free DMEM culture medium supplemented with 10% FCS and seeded into the siRNA-RNAiMAX containing wells and incubated for 72 h at 37 °C. For reverse transfection in 96-well and 384-well plates, the described protocol was proportionally reduced adjusting the final siRNA concentration to 5 or 50 nM and the cell number to 2,5 x 10^3 and 1 x 10^3 cells respectively. For RAV27 cells, 400.000 and 4000 cells were seeded per 6- and 96-well respectively. Instead of DMEM, 10% FCS, RHB-A medium supplemented with 20 ng/ml EGF and FGF-2 was used.

7.5 Immunological techniques

7.5.1 Luciferase-based cytotoxicity assay

For the luciferase-based kill assay, cells were reversely transfected as depicted in 7.4.5. After 3 days, media was exchanged to CLM supplemented with Flu peptide at a final concentration of 0,01 µg/ml and 0,001 µg/ml for MO3.13-A2-Luc and RAV27-Luc cells respectively. After 1 h of incubation, the pulsing medium was removed and the appropriate amount of FluT cells was added in 100 µl CLM to the wells. After 20 h of co-culture, the media was removed and the remaining cells were lysed with 40 µl of lysis buffer for 15 min at RT. Finally, 60 µl of luc-buffer containing luciferin reagent was pipetted to the wells and the luciferase signal was immediately measured at the TECAN Reader (see section 6.7 for the lysis and luc buffer compositions).

7.5.2 ^{51}Chromium-release assay

MO3.13-A2-Luc cells were transfected with siRNAs as described before. After 3 days, cells were detached with PBS-EDTA. After washing cells were resuspended in 1 ml CLM containing 0,01 µg/ml Flu-peptide and labelled with 100µl $^{51}Cr/10^6$cells for 1h at 37°C. Later, labelled and pulsed cells were washed once with CLM and incubated in PBS-EDTA (1:20 dilution) for 10 min at 37°C to prevent clumping. To remove excess chromium, two more additional washing steps were performed. Then, cells were counted and the desired number of cells were plated in 96U-well plates and co-cultured with FluT cells at effector to target ratios ranging from 100:1 to 3.125:1. After 6h of co-culture at 37°C, plates were centrifuged for 5 min at 500 g and 100 µl of the supernatant was transferred to 96-well Luma plates. Finally, Luma plates were dried overnight and the remaining chromium activity was measured in the gamma counter. For the evaluation of the data, the spontaneous release of ^{51}Cr was determined by measuring the wells with target cells that were not co-cultured with FluT cells and the maximum ^{51}Cr release was determined by measuring the release from target cells that were lysed with Triton-X-100. Finally, the percent specific lysis was calculated using the formula:

$$\%\ specific\ lysis = \frac{experimental\ release - spontaneous\ release}{maximum\ release - spontaneous\ release} x\ 100$$

7.5.3 Real-time live-cell imaging system

IncuCyte ZOOM live-cell imaging and analysis system (Essen BioScience), an incubator with integrated microscope, was used to measure the cytotoxicity of FluT cells co-cultured with MO3.13 oligodendrocytes. Therefore, MO3.13-A2 cells were seeded on transparent flat-bottomed 96-well plates and pulsed with Flu-peptide. After removing peptide containing media, MO3.13-A2 cells were incubated with 60 µg/ml of MHC-I blocking antibody or isotype control for 30 min and then co-cultured with FluT cells as described for Luc-assays (7.4.6). For Lck-inhibition, FluT cells were treated with 10 µM of Lck-inhibitor before setting up the co-culture. When adding FluT cells to MO3.13 cells, the cell-suspension was additionally supplemented with YOYO-1 Iodide dye at a final dilution of 1:10000 to visualize dying cells. Samples were directly put into the IncuCyte analyzer, where cells were co-cultured for 25h at 37°C, 5% CO_2. As YOYO-1 dye can only enter dying cells that lose their membrane-integrity and emits green light when it is bound to double-stranded DNA, registered green signals over time were used as a

reference value for cells killed by FluT cells. Therefore pictures of the co-culture plates were taken by the IncuCyte in defined intervals and total green object area per well (μm^2/well) was calculated by the IncuCyte-software for each time-point.

7.5.4 Flow cytometry

7.5.4.1 Pentamer and antibody staining of FluT cells

In order to detect proteins expressed on the cell surface and to assess the percentage of CD8+ Flu-specific T cells within a cell population, FACS analysis was performed. FluT cells were resuspended in FACS buffer and distributed in FACS tubes (3 x 10^5 cells/sample). Afterwards, cells were incubated with Kiovig (Baxter) for 20 min on ice, to reduce unspecific antibody binding. After blocking, cells were washed once in cold FACS buffer and stained for live/dead cell determination with the Zombie Aqua dye (1:1000 in 100 µL PBS) for 15 min in the dark at RT. Before adding the Flu Pentamer, it was centrifuged at 14.000 g for 5 min in order to remove protein aggregates. After a washing step with FACS buffer, cells were stained with the pentamer for 10 min in the dark at RT. After another washing step, cells were stained with fluorophore-conjugated antibodies or isotype controls at the concentrations indicated in section 6.10.2 for 20 min on ice in the dark. The cells were washed one last time, centrifuged and resuspended in 300 µl FACS-buffer and acquired with the FACSLyric machine (BD). Data were analyzed using the FlowJo software.

7.5.4.2 Surface staining for oligodendrocytes and tumor cells

Surface expression of proteins on oligodendrocytes and tumor cells were detected by FACS analysis. Adherent cells were detached from plates using PBS-EDTA and centrifuged at 500 g for 5 min. Cells were re-suspended in FACS buffer and distributed in FACS tubes (2 x 10^5 cells/sample). Cells were then stained as described for FluT cells, excluding the step for the pentamer staining (7.4.10.1). For indirect flow cytometry (EFNB1 staining), samples were incubated with the primary (unconjugated) antibody for 30 min as described above and subsequently stained with the BV421-conjugated secondary antibody for 30 minutes on ice in the dark. Samples were washed, filtered and acquired.

7.5.5 Stimulation of T cells with plate-bound recombinant proteins

PolySorp Nunc plates (Thermo Fisher) were coated with recombinant EFNB1 with a Fc tag (EFNB1-Fc), IgG-Fc and anti-CD3 antibody (clone OKT3) in 50 µl of PBS simultaneously at the concentrations described in the table below and incubated at 4°C overnight. Lower concentrations of EFNB1-Fc were compensated with IgG-Fc to avoid titration of CD3 binding sites. Additionally, some wells were kept with plain PBS overnight as an unstimulated control.

Table 7.4.11: Concentrations of EFNB1-Fc and IgG-Fc for the stimulation of T cells

EFNB1-Fc	0 µg/ml	1,25 µg/ml	2,5 µg/ml	5 µg/ml	10 µg/ml	20 µg/ml
IgG-Fc	20 µg/ml	18,75 µg/ml	17,5 µg/ml	15 µg/ml	10 µg/ml	0 µg/ml
Anti-CD3	1 µg/ml	1 µg/ml	1 µg/ml	1 µg/ml	1 µg/ml	1 µg/ml

On the next day the wells were washed with 200 µl of PBS and $1x10^5$ FluT cells or TILs were seeded in 200 µl CLM per well. After 24-72 h of incubation at 37°C, 5% CO_2, supernatants were collected and frozen at -20°C, until they were used for ELISA. The cells were pelleted in a 96-well plate (U-bottom) and either stored at -20°C for later protein isolation or used for FACS analysis.

7.5.6 Sandwich ELISA

Supernatants from MO3.13-A2-Luc-FluT cell co-culture, or EFNB1-Fc stimulated FluT cells were harvested after the above indicated period of time for the detection of IFN-γ, TNF-α (Human IFN-γ, Human TNF-α ELISA Set; BD OptEIA™), and granzyme B (Human Granzyme B ELISA development kit; Mabtech). Experiments were performed according to the manufacturer's instructions. PMA/Ionomycin stimulation was used as positive control. PMA was used at final concentration of 50ng/ml and Ionomycin at final concentration of 1 µg/ml. Absorbance was measured at λ = 450 nm, taking λ = 570 nm as reference wavelength using the TECAN reader.

7.6 High-throughput RNAi screen

7.6.1 Primary RNAi screen

The primary RNAi screening was conducted using a sub-library of the genome-wide siRNA library siGENOME (Horizon, formerly: Dhamacon, GE Healthcare) which

comprised 4155 genes. The library was prepared in iOmx Therapeutics (Martinsried, Munich, Germany) as described in [279]. Each gene was targeted by a SMARTpool (siGENOME) consisting pool of four non-overlapping synthetic siRNA duplexes (arrayed screen approach). The screen procedure was adopted from *Khandelwal et al.* [172]. The screen was performed in duplicates. Positive and negative siRNA controls were added in empty wells of each 384-well plate. For each well, reverse siRNA transfection was performed as follows: 0,05 µL of RNAiMAX were mixed with 4,95 µL of RPMI for 10 min. Afterwards 10 µL of RPMI were added and the diluted transfection regent was added to each siRNA-containing well for 30 min. Next, 1000 MO3.13-A2-Luc cells were resuspended in 30 µL of DMEM with 10 % FCS and cell suspension was added to the wells and incubated at 37°C, 5% CO_2. The final siRNA pool concentration was 25 nM. 72h after siRNA transfection, cells were pulsed with 0,01 µg/ml Flu-peptide for 1h. After pulsing, peptide containing medium was removed and oligodendrocytes were either co-cultured with medium containing FluT D11 cells resuspended in 50 µL at an E:T ratio of 20:1 (cytotoxicity setting) or with 50 µL of plain CLM (viability setting). 20 h after co-culture, the supernatant was removed and 20 µL of the lysis buffer (section 6.7) was added for 15 min at RT. Afterwards, 30 µL of the luciferase assay buffer (section 6.7) was added and luminescence was measured using the TECAN reader with an integration time of 100 ms.

7.6.2 Screening analysis

Screening data was analyzed using the cellHTS2 and Bioconductor packages for R [279]. The general R script for the first screen was kindly provided by Dr. Marco Breinig (DKFZ, Heidelberg). Raw luciferase intensity data was logarithmic transformed and per-plate normalized using the median method. The replicates were scored using the Z score method:

$$x_{ki}^{z} = \frac{x_{ki} - \mu_i}{\sigma_i}$$

Here the Z score for each *k*-th value (x) within the *i*-th result file (replicate plate) is calculated by subtracting the plate average (μ_i) from each value (x_{ki}) divided by the according standard deviation (σ_i) estimated from all values on the plate .

As an induction of FluT cell-mediated killing (or apoptosis by gene knock-down) results in a decrease in luciferase intensity compared to the average of the plate (assuming normal distribution), the option 'sign = -' is used. Therefore, reduced luciferase intensity results in a higher Z score. In order to distinguish genes impacting the FluT-mediated oligodendrocyte lysis but not the cell viability per se, the cytotoxicity Z scores were fitted to the viability Z scores using the LOESS method (LOcal regrESSion) included in R. The function normalizeQuantileRank from the aroma.light package in R was used to perform quantile normalization on the Z scores. The resulting LOESS score was used to rank the genes, taking into consideration the ranges of the according cytotoxicity and viability Z scores.

The thresholds for HIT calling were set according to the immune checkpoint control (CCR9) and viability controls (UBC and cell death). HITs with a viability score of $-z > 2{,}0$ or $-z < -2{,}0$ were excluded. Negative control siRNA 3 and 4 served as negative controls, which should not impact cytotoxicity or viability. Finally, remaining genes which had a LOESS score above 1 were considered potential negative immune checkpoints, whereas genes with a LOESS score below -1 were considered potential immune activators. Data analysis was performed by Tillman Michels (RCI, Regensburg).

7.6.3 Secondary screens

For the first set of secondary screens, a customized deconvoluted siRNA library (containing 4 single and pool of 4 siRNA) targeting 57 genes from the primary screening was distributed in several 96-well plates along with positive and negative siRNA controls. For the second set of secondary screens, a siRNA library consisting of pool of 30 siRNAs targeting 36 HITs validated by the first set of secondary secreens was used. Reverse transfection was performed as described in section 7.4.6 with MO3.13-A2-Luc and RAV27-Luc cells. For the cytotoxicity setting FluT D11 cells (E:T ratio of 20:1 and 5:1 for MO3.13-A2-Luc and RAV27-Luc cells respectively) were added to the transfected target cells. Plain CLM medium was added to the wells designated for the viability setting. After 20 h, luciferase based read-out was performed as described in section 7.4.7.

Cytotoxicity and viability RLU values of each HIT were normalized to the RLU values of Scr in each setting. For the MO3.13-A2-Luc screens, thresholds for the normalized

cytotoxicity and viability values were set as follows; viability ratio more than 0,75 (less than 25% viability impact) and cytotoxicity ratio less than 0,6 (more than 40% increase in cytotoxicity) with at least two single siRNA sequences and the pool of 4 and pool of 30. For RAV27 cells, the threshold for the viability ratio was kept the same whereas the one for the cytotoxicity ratio was increased to 0,75.

7.7 Isolation of mouse oligodendrocytes and astrocytes

Brains isolated from healthy or EAE experienced mice were dissociated using Adult Brain Dissociation Kit (Miltenyi) according to the manufacturer's protocol. Enzymatic digestion was coupled to mechanical digestion by using the gentleMAC Octo Dissociator with Heaters (Miltenyi). After brain dissociation, myelin sheath was removed by Myelin Removal Beads II (Miltenyi) and primary adult mouse oligodendrocyte progenitor cells and astrocytes were isolated by performing MACS separation using Anti-O4 MicroBeads and Anti-ACSA-2 MicroBead Kit (Miltenyi) respectively. Purity of isolated cell populations was determined by FACS analysis. After isolation cells were used for RNA isolation and cDNA synthesis as described in 7.4.2.

7.8 RNA sequencing

MO3.13-A2-Luc cells were reverse transfected either with Scr or with EFNB1 p30 siRNAs in a 6-well plate as described in 7.4.6. After 72h of transfection, oligodendrocytes were harvested in RLT buffer and RNA was isolated using the RNeasy mini kit (Qiagen) according to the manufacturer´s instructions. RNA-seq libraries were generated using the ScriptSeq Complete Kit (Illumina) according to the manufacturer's instructions. Libraries were sequenced paired-end (2 x 75bp) on a NextSeq 550 (Illumina) at the NGS Core facility of RCI. First, ".bcl" files, containing scanned images from the flowcell were converted to ".fastq" files containing cDNA sequence information applying bcl2fastq (v2.20.0.422, Illumina Inc.). Raw ".fastq" data was quality controlled using FastQC (http://www.bioinformatics.babraham.ac.uk/projects/fastqc/) [FastQC v0.11.7] and mapped to the annotated GRCh38 [gencode release29] assembly of the human genome using Salmon [280] within the SnakePipes analysis pipeline [281]. Differentially expressed genes were analyzed using DESeq2 [282] and visualized using software packages in R [283]. Gene set enrichment analyses were done using EnrichR [284]. Library preparation was performed by Dr. Claudia Gebhard (RCI) and the bioinformatic analysis was performed by Dr. Nicholas Strieder (RCI).

7.9 Statistical evaluation

For statistical analysis GraphPad Prism 8 software was used. Statistical differences between the control and the test groups were determined by using two-tailed unpaired Student's *t*-test. In all cases, *p*-value ≤ 0.05 was taken as significant, with * = $p < 0.05$, ** = $p < 0.01$, *** = $p < 0.005$, ****.

8 References

1. Zhang, Q. and D.A. Vignali, *Co-stimulatory and Co-inhibitory Pathways in Autoimmunity.* Immunity, 2016. **44**(5): p. 1034-51.
2. Chen, L. and D.B. Flies, *Molecular mechanisms of T cell co-stimulation and co-inhibition.* Nat Rev Immunol, 2013. **13**(4): p. 227-42.
3. Zhu, Y., S. Yao, and L. Chen, *Cell surface signaling molecules in the control of immune responses: a tide model.* Immunity, 2011. **34**(4): p. 466-78.
4. Paluch, C., et al., *Immune Checkpoints as Therapeutic Targets in Autoimmunity.* Front Immunol, 2018. **9**: p. 2306.
5. Schnell, A., et al., *The yin and yang of co-inhibitory receptors: toward anti-tumor immunity without autoimmunity.* Cell Res, 2020.
6. Anderson, M.S., et al., *Projection of an immunological self shadow within the thymus by the aire protein.* Science, 2002. **298**(5597): p. 1395-401.
7. Derbinski, J., et al., *Promiscuous gene expression in medullary thymic epithelial cells mirrors the peripheral self.* Nat Immunol, 2001. **2**(11): p. 1032-9.
8. Richards, D.M., B. Kyewski, and M. Feuerer, *Re-examining the Nature and Function of Self-Reactive T cells.* Trends Immunol, 2016. **37**(2): p. 114-125.
9. Rudd, C.E., A. Taylor, and H. Schneider, *CD28 and CTLA-4 coreceptor expression and signal transduction.* Immunol Rev, 2009. **229**(1): p. 12-26.
10. Boomer, J.S. and J.M. Green, *An enigmatic tail of CD28 signaling.* Cold Spring Harb Perspect Biol, 2010. **2**(8): p. a002436.
11. Janardhan, S.V., et al., *Evidence implicating the Ras pathway in multiple CD28 costimulatory functions in CD4+ T cells.* PLoS One, 2011. **6**(9): p. e24931.
12. Yao, S., et al., *B7-h2 is a costimulatory ligand for CD28 in human.* Immunity, 2011. **34**(5): p. 729-40.
13. Driessens, G., J. Kline, and T.F. Gajewski, *Costimulatory and coinhibitory receptors in anti-tumor immunity.* Immunol Rev, 2009. **229**(1): p. 126-44.
14. Simpson, T.R., S.A. Quezada, and J.P. Allison, *Regulation of CD4 T cell activation and effector function by inducible costimulator (ICOS).* Curr Opin Immunol, 2010. **22**(3): p. 326-32.
15. Rudd, C.E. and H. Schneider, *Unifying concepts in CD28, ICOS and CTLA4 co-receptor signalling.* Nat Rev Immunol, 2003. **3**(7): p. 544-56.
16. Croft, M., *The role of TNF superfamily members in T-cell function and diseases.* Nat Rev Immunol, 2009. **9**(4): p. 271-85.
17. Croft, M., *Co-stimulatory members of the TNFR family: keys to effective T-cell immunity?* Nat Rev Immunol, 2003. **3**(8): p. 609-20.
18. Wang, C., et al., *Immune regulation by 4-1BB and 4-1BBL: complexities and challenges.* Immunol Rev, 2009. **229**(1): p. 192-215.
19. Yokosuka, T., et al., *Spatiotemporal basis of CTLA-4 costimulatory molecule-mediated negative regulation of T cell activation.* Immunity, 2010. **33**(3): p. 326-39.
20. Saito, T. and S. Yamasaki, *Negative feedback of T cell activation through inhibitory adapters and costimulatory receptors.* Immunol Rev, 2003. **192**: p. 143-60.
21. Wolchok, J.D. and Y. Saenger, *The mechanism of anti-CTLA-4 activity and the negative regulation of T-cell activation.* Oncologist, 2008. **13 Suppl 4**: p. 2-9.
22. Topalian, S.L., C.G. Drake, and D.M. Pardoll, *Immune checkpoint blockade: a common denominator approach to cancer therapy.* Cancer Cell, 2015. **27**(4): p. 450-61.

23. Tivol, E.A., et al., *Loss of CTLA-4 leads to massive lymphoproliferation and fatal multiorgan tissue destruction, revealing a critical negative regulatory role of CTLA-4.* Immunity, 1995. **3**(5): p. 541-7.
24. Agata, Y., et al., *Expression of the PD-1 antigen on the surface of stimulated mouse T and B lymphocytes.* Int Immunol, 1996. **8**(5): p. 765-72.
25. Chemnitz, J.M., et al., *SHP-1 and SHP-2 associate with immunoreceptor tyrosine-based switch motif of programmed death 1 upon primary human T cell stimulation, but only receptor ligation prevents T cell activation.* J Immunol, 2004. **173**(2): p. 945-54.
26. Parry, R.V., et al., *CTLA-4 and PD-1 receptors inhibit T-cell activation by distinct mechanisms.* Mol Cell Biol, 2005. **25**(21): p. 9543-53.
27. Yokosuka, T., et al., *Programmed cell death 1 forms negative costimulatory microclusters that directly inhibit T cell receptor signaling by recruiting phosphatase SHP2.* J Exp Med, 2012. **209**(6): p. 1201-17.
28. Sheppard, K.A., et al., *PD-1 inhibits T-cell receptor induced phosphorylation of the ZAP70/CD3zeta signalosome and downstream signaling to PKCtheta.* FEBS Lett, 2004. **574**(1-3): p. 37-41.
29. Hannier, S., et al., *CD3/TCR complex-associated lymphocyte activation gene-3 molecules inhibit CD3/TCR signaling.* J Immunol, 1998. **161**(8): p. 4058-65.
30. Huard, B., et al., *Characterization of the major histocompatibility complex class II binding site on LAG-3 protein.* Proc Natl Acad Sci U S A, 1997. **94**(11): p. 5744-9.
31. Long, L., et al., *The promising immune checkpoint LAG-3: from tumor microenvironment to cancer immunotherapy.* Genes Cancer, 2018. **9**(5-6): p. 176-189.
32. Grosso, J.F., et al., *LAG-3 regulates CD8+ T cell accumulation and effector function in murine self- and tumor-tolerance systems.* J Clin Invest, 2007. **117**(11): p. 3383-92.
33. Goldberg, M.V. and C.G. Drake, *LAG-3 in Cancer Immunotherapy.* Curr Top Microbiol Immunol, 2011. **344**: p. 269-78.
34. Workman, C.J., et al., *Lymphocyte activation gene-3 (CD223) regulates the size of the expanding T cell population following antigen activation in vivo.* J Immunol, 2004. **172**(9): p. 5450-5.
35. Wolf, Y., A.C. Anderson, and V.K. Kuchroo, *TIM3 comes of age as an inhibitory receptor.* Nat Rev Immunol, 2019.
36. Clayton, K.L., et al., *T cell Ig and mucin domain-containing protein 3 is recruited to the immune synapse, disrupts stable synapse formation, and associates with receptor phosphatases.* J Immunol, 2014. **192**(2): p. 782-91.
37. Rangachari, M., et al., *Bat3 promotes T cell responses and autoimmunity by repressing Tim-3-mediated cell death and exhaustion.* Nat Med, 2012. **18**(9): p. 1394-400.
38. Lee, J., et al., *Phosphotyrosine-dependent coupling of Tim-3 to T-cell receptor signaling pathways.* Mol Cell Biol, 2011. **31**(19): p. 3963-74.
39. Davidson, D., B. Schraven, and A. Veillette, *PAG-associated FynT regulates calcium signaling and promotes anergy in T lymphocytes.* Mol Cell Biol, 2007. **27**(5): p. 1960-73.
40. Tada, Y., et al., *Role of the costimulatory molecule CD28 in the development of lupus in MRL/lpr mice.* J Immunol, 1999. **163**(6): p. 3153-9.
41. Tada, Y., et al., *CD28-deficient mice are highly resistant to collagen-induced arthritis.* J Immunol, 1999. **162**(1): p. 203-8.

42. Oliveira-dos-Santos, A.J., et al., *CD28 costimulation is crucial for the development of spontaneous autoimmune encephalomyelitis.* J Immunol, 1999. **162**(8): p. 4490-5.
43. Chang, T.T., et al., *Studies in B7-deficient mice reveal a critical role for B7 costimulation in both induction and effector phases of experimental autoimmune encephalomyelitis.* J Exp Med, 1999. **190**(5): p. 733-40.
44. Iwai, H., et al., *Amelioration of collagen-induced arthritis by blockade of inducible costimulator-B7 homologous protein costimulation.* J Immunol, 2002. **169**(8): p. 4332-9.
45. Gwyer Findlay, E., et al., *OX40L blockade is therapeutic in arthritis, despite promoting osteoclastogenesis.* Proc Natl Acad Sci U S A, 2014. **111**(6): p. 2289-94.
46. Yoshioka, T., et al., *Contribution of OX40/OX40 ligand interaction to the pathogenesis of rheumatoid arthritis.* Eur J Immunol, 2000. **30**(10): p. 2815-23.
47. Weinberg, A.D., et al., *Selective depletion of myelin-reactive T cells with the anti-OX-40 antibody ameliorates autoimmune encephalomyelitis.* Nat Med, 1996. **2**(2): p. 183-9.
48. Carboni, S., et al., *CD134 plays a crucial role in the pathogenesis of EAE and is upregulated in the CNS of patients with multiple sclerosis.* J Neuroimmunol, 2003. **145**(1-2): p. 1-11.
49. Ndhlovu, L.C., et al., *Critical involvement of OX40 ligand signals in the T cell priming events during experimental autoimmune encephalomyelitis.* J Immunol, 2001. **167**(5): p. 2991-9.
50. Martinez Gomez, J.M., et al., *Development of experimental autoimmune encephalomyelitis critically depends on CD137 ligand signaling.* J Neurosci, 2012. **32**(50): p. 18246-52.
51. Waterhouse, P., et al., *Lymphoproliferative disorders with early lethality in mice deficient in Ctla-4.* Science, 1995. **270**(5238): p. 985-8.
52. Klocke, K., et al., *Induction of autoimmune disease by deletion of CTLA-4 in mice in adulthood.* Proc Natl Acad Sci U S A, 2016. **113**(17): p. E2383-92.
53. Karandikar, N.J., et al., *CTLA-4: a negative regulator of autoimmune disease.* J Exp Med, 1996. **184**(2): p. 783-8.
54. Luhder, F., et al., *Cytotoxic T lymphocyte-associated antigen 4 (CTLA-4) regulates the unfolding of autoimmune diabetes.* J Exp Med, 1998. **187**(3): p. 427-32.
55. Ueda, H., et al., *Association of the T-cell regulatory gene CTLA4 with susceptibility to autoimmune disease.* Nature, 2003. **423**(6939): p. 506-11.
56. Nishimura, H., et al., *Autoimmune dilated cardiomyopathy in PD-1 receptor-deficient mice.* Science, 2001. **291**(5502): p. 319-22.
57. Nishimura, H., et al., *Development of lupus-like autoimmune diseases by disruption of the PD-1 gene encoding an ITIM motif-carrying immunoreceptor.* Immunity, 1999. **11**(2): p. 141-51.
58. Wang, J., et al., *Establishment of NOD-Pdcd1-/- mice as an efficient animal model of type I diabetes.* Proc Natl Acad Sci U S A, 2005. **102**(33): p. 11823-8.
59. Prokunina, L., et al., *A regulatory polymorphism in PDCD1 is associated with susceptibility to systemic lupus erythematosus in humans.* Nat Genet, 2002. **32**(4): p. 666-9.
60. Lee, Y.H., et al., *Meta-analysis of genetic polymorphisms in programmed cell death 1. Associations with rheumatoid arthritis, ankylosing spondylitis, and type 1 diabetes susceptibility.* Z Rheumatol, 2015. **74**(3): p. 230-9.
61. Kroner, A., et al., *A PD-1 polymorphism is associated with disease progression in multiple sclerosis.* Ann Neurol, 2005. **58**(1): p. 50-7.

62. Yaghoobi, E., et al., *TIM-3 Rs10515746 (A/C) and Rs10053538 (C/A) Gene Polymorphisms and Risk of Multiple Sclerosis.* Iran J Public Health, 2016. **45**(5): p. 644-9.
63. Chae, S.C., et al., *The polymorphisms of Th1 cell surface gene Tim-3 are associated in a Korean population with rheumatoid arthritis.* Immunol Lett, 2004. **95**(1): p. 91-5.
64. Sanchez-Fueyo, A., et al., *Tim-3 inhibits T helper type 1-mediated auto- and alloimmune responses and promotes immunological tolerance.* Nat Immunol, 2003. **4**(11): p. 1093-101.
65. Monney, L., et al., *Th1-specific cell surface protein Tim-3 regulates macrophage activation and severity of an autoimmune disease.* Nature, 2002. **415**(6871): p. 536-41.
66. Koguchi, K., et al., *Dysregulated T cell expression of TIM3 in multiple sclerosis.* J Exp Med, 2006. **203**(6): p. 1413-8.
67. Boivin, N., et al., *Interferon-beta suppresses murine Th1 cell function in the absence of antigen-presenting cells.* PLoS One, 2015. **10**(4): p. e0124802.
68. Kanai, Y., et al., *Impaired expression of Tim-3 on Th17 and Th1 cells in psoriasis.* Acta Derm Venereol, 2012. **92**(4): p. 367-71.
69. Liu, Y., et al., *Increased Tim-3 expression on peripheral lymphocytes from patients with rheumatoid arthritis negatively correlates with disease activity.* Clin Immunol, 2010. **137**(2): p. 288-95.
70. Shi, F., et al., *Dysregulated Tim-3 expression and its correlation with imbalanced CD4 helper T cell function in ulcerative colitis.* Clin Immunol, 2012. **145**(3): p. 230-40.
71. Lee, J., et al., *TIM polymorphisms--genetics and function.* Genes Immun, 2011. **12**(8): p. 595-604.
72. Bettini, M., et al., *Cutting edge: accelerated autoimmune diabetes in the absence of LAG-3.* J Immunol, 2011. **187**(7): p. 3493-8.
73. Dunn, G.P., L.J. Old, and R.D. Schreiber, *The three Es of cancer immunoediting.* Annu Rev Immunol, 2004. **22**: p. 329-60.
74. Leach, D.R., M.F. Krummel, and J.P. Allison, *Enhancement of antitumor immunity by CTLA-4 blockade.* Science, 1996. **271**(5256): p. 1734-6.
75. Sotomayor, E.M., et al., *In vivo blockade of CTLA-4 enhances the priming of responsive T cells but fails to prevent the induction of tumor antigen-specific tolerance.* Proc Natl Acad Sci U S A, 1999. **96**(20): p. 11476-81.
76. Sckisel, G.D., et al., *Late administration of murine CTLA-4 blockade prolongs CD8-mediated anti-tumor effects following stimulatory cancer immunotherapy.* Cancer Immunol Immunother, 2015. **64**(12): p. 1541-52.
77. Huang, P.Y., et al., *Tumor CTLA-4 overexpression predicts poor survival in patients with nasopharyngeal carcinoma.* Oncotarget, 2016. **7**(11): p. 13060-8.
78. Roncella, S., et al., *CTLA-4 in mesothelioma patients: tissue expression, body fluid levels and possible relevance as a prognostic factor.* Cancer Immunol Immunother, 2016. **65**(8): p. 909-17.
79. Hodi, F.S., et al., *Improved survival with ipilimumab in patients with metastatic melanoma.* N Engl J Med, 2010. **363**(8): p. 711-23.
80. Strome, S.E., et al., *B7-H1 blockade augments adoptive T-cell immunotherapy for squamous cell carcinoma.* Cancer Res, 2003. **63**(19): p. 6501-5.
81. Blank, C., et al., *PD-L1/B7H-1 inhibits the effector phase of tumor rejection by T cell receptor (TCR) transgenic CD8+ T cells.* Cancer Res, 2004. **64**(3): p. 1140-5.

82. Brahmer, J.R., et al., *Phase I study of single-agent anti-programmed death-1 (MDX-1106) in refractory solid tumors: safety, clinical activity, pharmacodynamics, and immunologic correlates.* J Clin Oncol, 2010. **28**(19): p. 3167-75.
83. Juneja, V.R., et al., *PD-L1 on tumor cells is sufficient for immune evasion in immunogenic tumors and inhibits CD8 T cell cytotoxicity.* J Exp Med, 2017. **214**(4): p. 895-904.
84. Ren, D., et al., *Predictive biomarkers and mechanisms underlying resistance to PD1/PD-L1 blockade cancer immunotherapy.* Mol Cancer, 2020. **19**(1): p. 19.
85. Salmaninejad, A., et al., *PD-1 and cancer: molecular mechanisms and polymorphisms.* Immunogenetics, 2018. **70**(2): p. 73-86.
86. Fourcade, J., et al., *PD-1 and Tim-3 regulate the expansion of tumor antigen-specific CD8(+) T cells induced by melanoma vaccines.* Cancer Res, 2014. **74**(4): p. 1045-55.
87. Sakuishi, K., et al., *Targeting Tim-3 and PD-1 pathways to reverse T cell exhaustion and restore anti-tumor immunity.* J Exp Med, 2010. **207**(10): p. 2187-94.
88. Zhang, Y., et al., *TIM-3 is a potential prognostic marker for patients with solid tumors: A systematic review and meta-analysis.* Oncotarget, 2017. **8**(19): p. 31705-31713.
89. Cai, C., et al., *T-cell immunoglobulin- and mucin-domain-containing molecule 3 gene polymorphisms and renal cell carcinoma.* DNA Cell Biol, 2012. **31**(7): p. 1285-9.
90. Tong, D., et al., *T cell immunoglobulin- and mucin-domain-containing molecule 3 gene polymorphisms and susceptibility to pancreatic cancer.* Mol Biol Rep, 2012. **39**(11): p. 9941-6.
91. Bai, J., et al., *T-cell immunoglobulin- and mucin-domain-containing molecule 3 gene polymorphisms and prognosis of non-small-cell lung cancer.* Tumour Biol, 2013. **34**(2): p. 805-9.
92. He, Y., et al., *TIM-3, a promising target for cancer immunotherapy.* Onco Targets Ther, 2018. **11**: p. 7005-7009.
93. Demeure, C.E., et al., *T Lymphocytes infiltrating various tumour types express the MHC class II ligand lymphocyte activation gene-3 (LAG-3): role of LAG-3/MHC class II interactions in cell-cell contacts.* Eur J Cancer, 2001. **37**(13): p. 1709-18.
94. Wierz, M., et al., *Dual PD1/LAG3 immune checkpoint blockade limits tumor development in a murine model of chronic lymphocytic leukemia.* Blood, 2018. **131**(14): p. 1617-1621.
95. Woo, S.R., et al., *Immune inhibitory molecules LAG-3 and PD-1 synergistically regulate T-cell function to promote tumoral immune escape.* Cancer Res, 2012. **72**(4): p. 917-27.
96. Michot, J.M., et al., *Immune-related adverse events with immune checkpoint blockade: a comprehensive review.* Eur J Cancer, 2016. **54**: p. 139-148.
97. Filippi, M., et al., *Multiple sclerosis.* Nat Rev Dis Primers, 2018. **4**(1): p. 43.
98. Koch-Henriksen, N. and P.S. Sorensen, *The changing demographic pattern of multiple sclerosis epidemiology.* Lancet Neurol, 2010. **9**(5): p. 520-32.
99. Niland, B., et al., *CD8+ T cell-mediated HLA-A*0201-restricted cytotoxicity to transaldolase peptide 168-176 in patients with multiple sclerosis.* J Immunol, 2005. **175**(12): p. 8365-78.
100. Olsson, T., L.F. Barcellos, and L. Alfredsson, *Interactions between genetic, lifestyle and environmental risk factors for multiple sclerosis.* Nat Rev Neurol, 2017. **13**(1): p. 25-36.

101. Baranzini, S.E. and J.R. Oksenberg, *The Genetics of Multiple Sclerosis: From 0 to 200 in 50 Years.* Trends Genet, 2017. **33**(12): p. 960-970.
102. International Multiple Sclerosis Genetics, C., et al., *Analysis of immune-related loci identifies 48 new susceptibility variants for multiple sclerosis.* Nat Genet, 2013. **45**(11): p. 1353-60.
103. Cotsapas, C. and M. Mitrovic, *Genome-wide association studies of multiple sclerosis.* Clin Transl Immunology, 2018. **7**(6): p. e1018.
104. De Jager, P.L., et al., *Meta-analysis of genome scans and replication identify CD6, IRF8 and TNFRSF1A as new multiple sclerosis susceptibility loci.* Nat Genet, 2009. **41**(7): p. 776-82.
105. Lublin, F.D. and S.C. Reingold, *Defining the clinical course of multiple sclerosis: results of an international survey. National Multiple Sclerosis Society (USA) Advisory Committee on Clinical Trials of New Agents in Multiple Sclerosis.* Neurology, 1996. **46**(4): p. 907-11.
106. Brownlee, W.J., et al., *Diagnosis of multiple sclerosis: progress and challenges.* Lancet, 2017. **389**(10076): p. 1336-1346.
107. McDonald, W.I., *Relapse, remission, and progression in multiple sclerosis.* N Engl J Med, 2000. **343**(20): p. 1486-7.
108. Polman, C.H., et al., *Diagnostic criteria for multiple sclerosis: 2010 revisions to the McDonald criteria.* Ann Neurol, 2011. **69**(2): p. 292-302.
109. Lublin, F.D., et al., *Defining the clinical course of multiple sclerosis: the 2013 revisions.* Neurology, 2014. **83**(3): p. 278-86.
110. Minagar, A. and J.S. Alexander, *Blood-brain barrier disruption in multiple sclerosis.* Mult Scler, 2003. **9**(6): p. 540-9.
111. Ortiz, G.G., et al., *Role of the blood-brain barrier in multiple sclerosis.* Arch Med Res, 2014. **45**(8): p. 687-97.
112. Lucchinetti, C., et al., *Heterogeneity of multiple sclerosis lesions: implications for the pathogenesis of demyelination.* Ann Neurol, 2000. **47**(6): p. 707-17.
113. Frohman, E.M., M.K. Racke, and C.S. Raine, *Multiple sclerosis--the plaque and its pathogenesis.* N Engl J Med, 2006. **354**(9): p. 942-55.
114. Harlow, D.E., J.M. Honce, and A.A. Miravalle, *Remyelination Therapy in Multiple Sclerosis.* Front Neurol, 2015. **6**: p. 257.
115. Lassmann, H., *Multiple Sclerosis Pathology.* Cold Spring Harb Perspect Med, 2018. **8**(3).
116. Goldschmidt, T., et al., *Remyelination capacity of the MS brain decreases with disease chronicity.* Neurology, 2009. **72**(22): p. 1914-21.
117. Dendrou, C.A., L. Fugger, and M.A. Friese, *Immunopathology of multiple sclerosis.* Nat Rev Immunol, 2015. **15**(9): p. 545-58.
118. Kebir, H., et al., *Preferential recruitment of interferon-gamma-expressing TH17 cells in multiple sclerosis.* Ann Neurol, 2009. **66**(3): p. 390-402.
119. Huber, M., et al., *IL-17A secretion by CD8+ T cells supports Th17-mediated autoimmune encephalomyelitis.* J Clin Invest, 2013. **123**(1): p. 247-60.
120. van Langelaar, J., et al., *T helper 17.1 cells associate with multiple sclerosis disease activity: perspectives for early intervention.* Brain, 2018. **141**(5): p. 1334-1349.
121. Niland, B., et al., *CD8+ T Cell-Mediated HLA-A*0201-Restricted Cytotoxicity to Transaldolase Peptide 168-176 in Patients with Multiple Sclerosis.* The Journal of Immunology, 2005. **175**(12): p. 8365-8378.

122. Zang, Y.C.Q., et al., *Increased CD8+ Cytotoxic T Cell Responses to Myelin Basic Protein in Multiple Sclerosis.* The Journal of Immunology, 2004. **172**(8): p. 5120-5127.
123. Baecher-Allan, C., B.J. Kaskow, and H.L. Weiner, *Multiple Sclerosis: Mechanisms and Immunotherapy.* Neuron, 2018. **97**(4): p. 742-768.
124. Johnson, K.P., et al., *Copolymer 1 reduces relapse rate and improves disability in relapsing-remitting multiple sclerosis: results of a phase III multicenter, double-blind placebo-controlled trial. The Copolymer 1 Multiple Sclerosis Study Group.* Neurology, 1995. **45**(7): p. 1268-76.
125. Montalban, X., et al., *ECTRIMS/EAN Guideline on the pharmacological treatment of people with multiple sclerosis.* Mult Scler, 2018. **24**(2): p. 96-120.
126. Polman, C.H., et al., *A randomized, placebo-controlled trial of natalizumab for relapsing multiple sclerosis.* N Engl J Med, 2006. **354**(9): p. 899-910.
127. Rudick, R.A., et al., *Natalizumab plus interferon beta-1a for relapsing multiple sclerosis.* N Engl J Med, 2006. **354**(9): p. 911-23.
128. Willis, M.A. and J.A. Cohen, *Fingolimod therapy for multiple sclerosis.* Semin Neurol, 2013. **33**(1): p. 37-44.
129. Kappos, L., et al., *A placebo-controlled trial of oral fingolimod in relapsing multiple sclerosis.* N Engl J Med, 2010. **362**(5): p. 387-401.
130. Calabresi, P.A., et al., *Safety and efficacy of fingolimod in patients with relapsing-remitting multiple sclerosis (FREEDOMS II): a double-blind, randomised, placebo-controlled, phase 3 trial.* Lancet Neurol, 2014. **13**(6): p. 545-56.
131. Lublin, F., et al., *Oral fingolimod in primary progressive multiple sclerosis (INFORMS): a phase 3, randomised, double-blind, placebo-controlled trial.* Lancet, 2016. **387**(10023): p. 1075-1084.
132. Kapoor, R., et al., *Effect of natalizumab on disease progression in secondary progressive multiple sclerosis (ASCEND): a phase 3, randomised, double-blind, placebo-controlled trial with an open-label extension.* Lancet Neurol, 2018. **17**(5): p. 405-415.
133. Havrdova, E., D. Horakova, and I. Kovarova, *Alemtuzumab in the treatment of multiple sclerosis: key clinical trial results and considerations for use.* Ther Adv Neurol Disord, 2015. **8**(1): p. 31-45.
134. Sorensen, P.S. and M. Blinkenberg, *The potential role for ocrelizumab in the treatment of multiple sclerosis: current evidence and future prospects.* Ther Adv Neurol Disord, 2016. **9**(1): p. 44-52.
135. Alcantara Llaguno, S.R. and L.F. Parada, *Cell of origin of glioma: biological and clinical implications.* Br J Cancer, 2016. **115**(12): p. 1445-1450.
136. Weller, M., et al., *Glioma.* Nat Rev Dis Primers, 2015. **1**: p. 15017.
137. Lucca, L.E. and D.A. Hafler, *Co-inhibitory blockade while preserving tolerance: checkpoint inhibitors for glioblastoma.* Immunol Rev, 2017. **276**(1): p. 9-25.
138. Porter, K.R., et al., *Prevalence estimates for primary brain tumors in the United States by age, gender, behavior, and histology.* Neuro Oncol, 2010. **12**(6): p. 520-7.
139. Ostrom, Q.T., et al., *CBTRUS statistical report: primary brain and central nervous system tumors diagnosed in the United States in 2007-2011.* Neuro Oncol, 2014. **16 Suppl 4**: p. iv1-63.
140. Connelly, J.M. and M.G. Malkin, *Environmental risk factors for brain tumors.* Curr Neurol Neurosci Rep, 2007. **7**(3): p. 208-14.
141. Network, T.C., *Corrigendum: Comprehensive genomic characterization defines human glioblastoma genes and core pathways.* Nature, 2013. **494**(7438): p. 506.

142. Aldape, K., et al., *Glioblastoma: pathology, molecular mechanisms and markers.* Acta Neuropathol, 2015. **129**(6): p. 829-48.
143. Noushmehr, H., et al., *Identification of a CpG island methylator phenotype that defines a distinct subgroup of glioma.* Cancer Cell, 2010. **17**(5): p. 510-22.
144. Stupp, R., et al., *Radiotherapy plus concomitant and adjuvant temozolomide for glioblastoma.* N Engl J Med, 2005. **352**(10): p. 987-96.
145. Gilbert, M.R., et al., *A randomized trial of bevacizumab for newly diagnosed glioblastoma.* N Engl J Med, 2014. **370**(8): p. 699-708.
146. Dunn, G.P., I.F. Dunn, and W.T. Curry, *Focus on TILs: Prognostic significance of tumor infiltrating lymphocytes in human glioma.* Cancer Immun, 2007. **7**: p. 12.
147. Dix, A.R., et al., *Immune defects observed in patients with primary malignant brain tumors.* J Neuroimmunol, 1999. **100**(1-2): p. 216-32.
148. Fecci, P.E., et al., *Increased regulatory T-cell fraction amidst a diminished CD4 compartment explains cellular immune defects in patients with malignant glioma.* Cancer Res, 2006. **66**(6): p. 3294-302.
149. Preusser, M., et al., *Prospects of immune checkpoint modulators in the treatment of glioblastoma.* Nat Rev Neurol, 2015. **11**(9): p. 504-14.
150. Tran, T.T., et al., *Inhibiting TGF-beta signaling restores immune surveillance in the SMA-560 glioma model.* Neuro Oncol, 2007. **9**(3): p. 259-70.
151. Wainwright, D.A., et al., *Durable therapeutic efficacy utilizing combinatorial blockade against IDO, CTLA-4, and PD-L1 in mice with brain tumors.* Clin Cancer Res, 2014. **20**(20): p. 5290-301.
152. Muller, C., et al., *Hematogenous dissemination of glioblastoma multiforme.* Sci Transl Med, 2014. **6**(247): p. 247ra101.
153. Aspelund, A., et al., *A dural lymphatic vascular system that drains brain interstitial fluid and macromolecules.* J Exp Med, 2015. **212**(7): p. 991-9.
154. Chen, D.S. and I. Mellman, *Oncology meets immunology: the cancer-immunity cycle.* Immunity, 2013. **39**(1): p. 1-10.
155. Berghoff, A.S., et al., *Programmed death ligand 1 expression and tumor-infiltrating lymphocytes in glioblastoma.* Neuro Oncol, 2015. **17**(8): p. 1064-75.
156. Weber, J.S., et al., *Safety, efficacy, and biomarkers of nivolumab with vaccine in ipilimumab-refractory or -naive melanoma.* J Clin Oncol, 2013. **31**(34): p. 4311-8.
157. Velcheti, V., et al., *Programmed death ligand-1 expression in non-small cell lung cancer.* Lab Invest, 2014. **94**(1): p. 107-16.
158. Doucette, T., et al., *Immune heterogeneity of glioblastoma subtypes: extrapolation from the cancer genome atlas.* Cancer Immunol Res, 2013. **1**(2): p. 112-22.
159. Bhat, K.P.L., et al., *Mesenchymal differentiation mediated by NF-kappaB promotes radiation resistance in glioblastoma.* Cancer Cell, 2013. **24**(3): p. 331-46.
160. Avril, T., et al., *Distinct effects of human glioblastoma immunoregulatory molecules programmed cell death ligand-1 (PDL-1) and indoleamine 2,3-dioxygenase (IDO) on tumour-specific T cell functions.* J Neuroimmunol, 2010. **225**(1-2): p. 22-33.
161. Wintterle, S., et al., *Expression of the B7-related molecule B7-H1 by glioma cells: a potential mechanism of immune paralysis.* Cancer Res, 2003. **63**(21): p. 7462-7.
162. Bloch, O., et al., *Gliomas promote immunosuppression through induction of B7-H1 expression in tumor-associated macrophages.* Clin Cancer Res, 2013. **19**(12): p. 3165-75.
163. McGranahan, T., et al., *Current State of Immunotherapy for Treatment of Glioblastoma.* Curr Treat Options Oncol, 2019. **20**(3): p. 24.

164. Fecci, P.E., et al., *Systemic CTLA-4 blockade ameliorates glioma-induced changes to the CD4+ T cell compartment without affecting regulatory T-cell function.* Clin Cancer Res, 2007. **13**(7): p. 2158-67.
165. Zeng, J., et al., *Anti-PD-1 blockade and stereotactic radiation produce long-term survival in mice with intracranial gliomas.* Int J Radiat Oncol Biol Phys, 2013. **86**(2): p. 343-9.
166. Belcaid, Z., et al., *Focal radiation therapy combined with 4-1BB activation and CTLA-4 blockade yields long-term survival and a protective antigen-specific memory response in a murine glioma model.* PLoS One, 2014. **9**(7): p. e101764.
167. Leitinger, M., et al., *Fatal Necrotizing Encephalopathy after Treatment with Nivolumab for Squamous Non-Small Cell Lung Cancer: Case Report and Review of the Literature.* Front Immunol, 2018. **9**: p. 108.
168. Dorsett, Y. and T. Tuschl, *siRNAs: applications in functional genomics and potential as therapeutics.* Nat Rev Drug Discov, 2004. **3**(4): p. 318-29.
169. Boutros, M. and J. Ahringer, *The art and design of genetic screens: RNA interference.* Nat Rev Genet, 2008. **9**(7): p. 554-66.
170. Elbashir, S.M., et al., *Duplexes of 21-nucleotide RNAs mediate RNA interference in cultured mammalian cells.* Nature, 2001. **411**(6836): p. 494-8.
171. Hannon, G.J., *RNA interference.* Nature, 2002. **418**(6894): p. 244-51.
172. Khandelwal, N., et al., *A high-throughput RNAi screen for detection of immune-checkpoint molecules that mediate tumor resistance to cytotoxic T lymphocytes.* EMBO Mol Med, 2015. **7**(4): p. 450-63.
173. Jin, J., et al., *Simplified method of the growth of human tumor infiltrating lymphocytes in gas-permeable flasks to numbers needed for patient treatment.* J Immunother, 2012. **35**(3): p. 283-92.
174. Wherry, E.J., *T cell exhaustion.* Nat Immunol, 2011. **12**(6): p. 492-9.
175. Allard, B., et al., *The ectonucleotidases CD39 and CD73: Novel checkpoint inhibitor targets.* Immunol Rev, 2017. **276**(1): p. 121-144.
176. Witzens-Harig, M., et al., *Tumor cells in multiple myeloma patients inhibit myeloma-reactive T cells through carcinoembryonic antigen-related cell adhesion molecule-6.* Blood, 2013. **121**(22): p. 4493-4503.
177. Brahmer, J.R., et al., *Safety and activity of anti-PD-L1 antibody in patients with advanced cancer.* N Engl J Med, 2012. **366**(26): p. 2455-65.
178. Mellman, I., G. Coukos, and G. Dranoff, *Cancer immunotherapy comes of age.* Nature, 2011. **480**(7378): p. 480-9.
179. Slovin, S.F., et al., *Ipilimumab alone or in combination with radiotherapy in metastatic castration-resistant prostate cancer: results from an open-label, multicenter phase I/II study.* Ann Oncol, 2013. **24**(7): p. 1813-21.
180. Topalian, S.L., et al., *Safety, activity, and immune correlates of anti-PD-1 antibody in cancer.* N Engl J Med, 2012. **366**(26): p. 2443-54.
181. Yang, J.C., et al., *Ipilimumab (anti-CTLA4 antibody) causes regression of metastatic renal cell cancer associated with enteritis and hypophysitis.* J Immunother, 2007. **30**(8): p. 825-30.
182. Beckmann, M.P., et al., *Molecular characterization of a family of ligands for eph-related tyrosine kinase receptors.* EMBO J, 1994. **13**(16): p. 3757-62.
183. Wieland, I., et al., *Twenty-six novel EFNB1 mutations in familial and sporadic craniofrontonasal syndrome (CFNS).* Hum Mutat, 2005. **26**(2): p. 113-8.

184. Babbs, C., et al., *Duplication of the EFNB1 gene in familial hypertelorism: imbalance in ephrin-B1 expression and abnormal phenotypes in humans and mice.* Hum Mutat, 2011. **32**(8): p. 930-8.
185. Luo, H., et al., *EphrinB1 and EphrinB2 regulate T cell chemotaxis and migration in experimental autoimmune encephalomyelitis and multiple sclerosis.* Neurobiol Dis, 2016. **91**: p. 292-306.
186. Sharma, K., et al., *Cell type- and brain region-resolved mouse brain proteome.* Nat Neurosci, 2015. **18**(12): p. 1819-31.
187. Liu, Y., A. Beyer, and R. Aebersold, *On the Dependency of Cellular Protein Levels on mRNA Abundance.* Cell, 2016. **165**(3): p. 535-50.
188. Arvanitis, D.N. and A. Davy, *Regulation and misregulation of Eph/ephrin expression.* Cell Adh Migr, 2012. **6**(2): p. 131-7.
189. Yu, G., et al., *EphrinB1 is essential in T-cell-T-cell co-operation during T-cell activation.* J Biol Chem, 2004. **279**(53): p. 55531-9.
190. Kane, L.P., et al., *Akt provides the CD28 costimulatory signal for up-regulation of IL-2 and IFN-gamma but not TH2 cytokines.* Nat Immunol, 2001. **2**(1): p. 37-44.
191. Cheng, J., A. Montecalvo, and L.P. Kane, *Regulation of NF-kappaB induction by TCR/CD28.* Immunol Res, 2011. **50**(2-3): p. 113-7.
192. Gucciardo, E., N. Sugiyama, and K. Lehti, *Eph- and ephrin-dependent mechanisms in tumor and stem cell dynamics.* Cell Mol Life Sci, 2014. **71**(19): p. 3685-710.
193. Boyd, A.W., P.F. Bartlett, and M. Lackmann, *Therapeutic targeting of EPH receptors and their ligands.* Nat Rev Drug Discov, 2014. **13**(1): p. 39-62.
194. Kania, A. and R. Klein, *Mechanisms of ephrin-Eph signalling in development, physiology and disease.* Nat Rev Mol Cell Biol, 2016. **17**(4): p. 240-56.
195. Arvanitis, D. and A. Davy, *Eph/ephrin signaling: networks.* Genes Dev, 2008. **22**(4): p. 416-29.
196. Bong, Y.S., et al., *ephrinB1 signals from the cell surface to the nucleus by recruitment of STAT3.* Proc Natl Acad Sci U S A, 2007. **104**(44): p. 17305-10.
197. Wen, Z., Z. Zhong, and J.E. Darnell, Jr., *Maximal activation of transcription by Stat1 and Stat3 requires both tyrosine and serine phosphorylation.* Cell, 1995. **82**(2): p. 241-50.
198. Yokogami, K., et al., *Serine phosphorylation and maximal activation of STAT3 during CNTF signaling is mediated by the rapamycin target mTOR.* Curr Biol, 2000. **10**(1): p. 47-50.
199. Sun, C., R. Mezzadra, and T.N. Schumacher, *Regulation and Function of the PD-L1 Checkpoint.* Immunity, 2018. **48**(3): p. 434-452.
200. Wesseling, P., M. van den Bent, and A. Perry, *Oligodendroglioma: pathology, molecular mechanisms and markers.* Acta Neuropathol, 2015. **129**(6): p. 809-27.
201. Ruijs, T.C., et al., *Human oligodendrocytes are susceptible to cytolysis by major histocompatibility complex class I-restricted lymphocytes.* J Neuroimmunol, 1990. **27**(2-3): p. 89-97.
202. Jurewicz, A., W.E. Biddison, and J.P. Antel, *MHC class I-restricted lysis of human oligodendrocytes by myelin basic protein peptide-specific CD8 T lymphocytes.* J Immunol, 1998. **160**(6): p. 3056-9.
203. da Cunha, J.P., et al., *Bioinformatics construction of the human cell surfaceome.* Proc Natl Acad Sci U S A, 2009. **106**(39): p. 16752-7.
204. Kwilas, A.R., et al., *Immune consequences of tyrosine kinase inhibitors that synergize with cancer immunotherapy.* Cancer cell & microenvironment, 2015. **2**(1): p. e677.

205. Hannus, M., et al., *siPools: highly complex but accurately defined siRNA pools eliminate off-target effects.* Nucleic Acids Res, 2014. **42**(12): p. 8049-61.
206. Lieping Chen, D.B.F., *Molecular mechanisms of T cell co-stimulation and co-inhibition*, in *Nature Reviews, Immunology*. 2013. p. 13: 227-242.
207. Johnson, B. and D. Mahadevan, *Emerging Role and Targeting of Carcinoembryonic Antigen-related Cell Adhesion Molecule 6 (CEACAM6) in Human Malignancies.* Clin Cancer Drugs, 2015. **2**(2): p. 100-111.
208. Allard, D., et al., *Targeting the CD73-adenosine axis in immuno-oncology.* Immunol Lett, 2019. **205**: p. 31-39.
209. Sanmamed, M.F., et al., *Agonists of Co-stimulation in Cancer Immunotherapy Directed Against CD137, OX40, GITR, CD27, CD28, and ICOS.* Semin Oncol, 2015. **42**(4): p. 640-55.
210. Echeverri, C.J., et al., *Minimizing the risk of reporting false positives in large-scale RNAi screens.* Nat Methods, 2006. **3**(10): p. 777-9.
211. Echeverri, C.J., et al., *Minimizing the risk of reporting false positives in large-scale RNAi screens.* Nature Methods, 2006. **3**(10): p. 777-779.
212. Sharma, S. and A. Rao, *RNAi screening: tips and techniques.* Nature immunology, 2009. **10**(8): p. 799-804.
213. Jackson, A.L. and P.S. Linsley, *Recognizing and avoiding siRNA off-target effects for target identification and therapeutic application.* Nat Rev Drug Discov, 2010. **9**(1): p. 57-67.
214. Chang, X., et al., *Hyperpolarization-Activated Cyclic Nucleotide-Gated Channels: An Emerging Role in Neurodegenerative Diseases.* Front Mol Neurosci, 2019. **12**: p. 141.
215. Williams, Y.N., et al., *Cell adhesion and prostate tumor-suppressor activity of TSLL2/IGSF4C, an immunoglobulin superfamily molecule homologous to TSLC1/IGSF4.* Oncogene, 2006. **25**(10): p. 1446-53.
216. Elazar, N., et al., *Axoglial Adhesion by Cadm4 Regulates CNS Myelination.* Neuron, 2019. **101**(2): p. 224-231 e5.
217. Barquilla, A. and E.B. Pasquale, *Eph receptors and ephrins: therapeutic opportunities.* Annu Rev Pharmacol Toxicol, 2015. **55**: p. 465-87.
218. Pasquale, E.B., *Eph receptor signalling casts a wide net on cell behaviour.* Nat Rev Mol Cell Biol, 2005. **6**(6): p. 462-75.
219. Himanen, J.P., et al., *Repelling class discrimination: ephrin-A5 binds to and activates EphB2 receptor signaling.* Nat Neurosci, 2004. **7**(5): p. 501-9.
220. Liang, L.Y., et al., *Eph receptor signalling: from catalytic to non-catalytic functions.* Oncogene, 2019. **38**(39): p. 6567-6584.
221. Binns, K.L., et al., *Phosphorylation of tyrosine residues in the kinase domain and juxtamembrane region regulates the biological and catalytic activities of Eph receptors.* Mol Cell Biol, 2000. **20**(13): p. 4791-805.
222. Palmer, A., et al., *EphrinB phosphorylation and reverse signaling: regulation by Src kinases and PTP-BL phosphatase.* Mol Cell, 2002. **9**(4): p. 725-37.
223. Egea, J., et al., *Regulation of EphA 4 kinase activity is required for a subset of axon guidance decisions suggesting a key role for receptor clustering in Eph function.* Neuron, 2005. **47**(4): p. 515-28.
224. Himanen, J.P., et al., *Architecture of Eph receptor clusters.* Proc Natl Acad Sci U S A, 2010. **107**(24): p. 10860-5.
225. Carvalho, R.F., et al., *Silencing of EphA3 through a cis interaction with ephrinA5.* Nat Neurosci, 2006. **9**(3): p. 322-30.

226. Kao, T.J. and A. Kania, *Ephrin-mediated cis-attenuation of Eph receptor signaling is essential for spinal motor axon guidance.* Neuron, 2011. **71**(1): p. 76-91.
227. Pasquale, E.B., *Eph-ephrin bidirectional signaling in physiology and disease.* Cell, 2008. **133**(1): p. 38-52.
228. Pasquale, E.B., *Eph receptors and ephrins in cancer: bidirectional signalling and beyond.* Nat Rev Cancer, 2010. **10**(3): p. 165-80.
229. Ireton, R.C. and J. Chen, *EphA2 receptor tyrosine kinase as a promising target for cancer therapeutics.* Curr Cancer Drug Targets, 2005. **5**(3): p. 149-57.
230. Noren, N.K. and E.B. Pasquale, *Paradoxes of the EphB4 receptor in cancer.* Cancer Res, 2007. **67**(9): p. 3994-7.
231. Surawska, H., P.C. Ma, and R. Salgia, *The role of ephrins and Eph receptors in cancer.* Cytokine Growth Factor Rev, 2004. **15**(6): p. 419-33.
232. Merlos-Suarez, A. and E. Batlle, *Eph-ephrin signalling in adult tissues and cancer.* Curr Opin Cell Biol, 2008. **20**(2): p. 194-200.
233. Noberini, R. and E.B. Pasquale, *Proliferation and tumor suppression: not mutually exclusive for Eph receptors.* Cancer Cell, 2009. **16**(6): p. 452-4.
234. Nakada, M., Y. Hayashi, and J. Hamada, *Role of Eph/ephrin tyrosine kinase in malignant glioma.* Neuro Oncol, 2011. **13**(11): p. 1163-70.
235. Wykosky, J., et al., *EphA2 as a novel molecular marker and target in glioblastoma multiforme.* Mol Cancer Res, 2005. **3**(10): p. 541-51.
236. Wykosky, J., D.M. Gibo, and W. Debinski, *A novel, potent, and specific ephrinA1-based cytotoxin against EphA2 receptor expressing tumor cells.* Mol Cancer Ther, 2007. **6**(12 Pt 1): p. 3208-18.
237. Wykosky, J. and W. Debinski, *The EphA2 receptor and ephrinA1 ligand in solid tumors: function and therapeutic targeting.* Mol Cancer Res, 2008. **6**(12): p. 1795-806.
238. Liu, F., et al., *A genome-wide screen reveals functional gene clusters in the cancer genome and identifies EphA2 as a mitogen in glioblastoma.* Cancer Res, 2006. **66**(22): p. 10815-23.
239. Wang, L.F., et al., *Increased expression of EphA2 correlates with adverse outcome in primary and recurrent glioblastoma multiforme patients.* Oncol Rep, 2008. **19**(1): p. 151-6.
240. Liu, D.P., et al., *Ephrin-A1 is a negative regulator in glioma through down-regulation of EphA2 and FAK.* Int J Oncol, 2007. **30**(4): p. 865-71.
241. Miao, H., et al., *EphA2 mediates ligand-dependent inhibition and ligand-independent promotion of cell migration and invasion via a reciprocal regulatory loop with Akt.* Cancer Cell, 2009. **16**(1): p. 9-20.
242. Chen, J., et al., *Eph receptors and Ephrins in cancer: common themes and controversies.* Cancer Res, 2008. **68**(24): p. 10031-3.
243. Nakada, M., et al., *The phosphorylation of ephrin-B2 ligand promotes glioma cell migration and invasion.* Int J Cancer, 2010. **126**(5): p. 1155-65.
244. Nakada, M., et al., *Ephrin-B3 ligand promotes glioma invasion through activation of Rac1.* Cancer Res, 2006. **66**(17): p. 8492-500.
245. Nakada, M., et al., *EphB2/R-Ras signaling regulates glioma cell adhesion, growth, and invasion.* Am J Pathol, 2005. **167**(2): p. 565-76.
246. Goldshmit, Y., et al., *Axonal regeneration and lack of astrocytic gliosis in EphA4-deficient mice.* J Neurosci, 2004. **24**(45): p. 10064-73.

247. Munro, K.M., et al., *EphA4 receptor tyrosine kinase is a modulator of onset and disease severity of experimental autoimmune encephalomyelitis (EAE).* PLoS One, 2013. **8**(2): p. e55948.
248. Maier, T., M. Guell, and L. Serrano, *Correlation of mRNA and protein in complex biological samples.* FEBS Lett, 2009. **583**(24): p. 3966-73.
249. Yao, R.W., Y. Wang, and L.L. Chen, *Cellular functions of long noncoding RNAs.* Nat Cell Biol, 2019. **21**(5): p. 542-551.
250. Salmena, L., et al., *A ceRNA hypothesis: the Rosetta Stone of a hidden RNA language?* Cell, 2011. **146**(3): p. 353-8.
251. Poliseno, L., et al., *A coding-independent function of gene and pseudogene mRNAs regulates tumour biology.* Nature, 2010. **465**(7301): p. 1033-8.
252. Kim, Y.K., et al., *Mammalian Staufen1 recruits Upf1 to specific mRNA 3'UTRs so as to elicit mRNA decay.* Cell, 2005. **120**(2): p. 195-208.
253. Gong, C. and L.E. Maquat, *lncRNAs transactivate STAU1-mediated mRNA decay by duplexing with 3' UTRs via Alu elements.* Nature, 2011. **470**(7333): p. 284-8.
254. Zamore, P.D., J.R. Williamson, and R. Lehmann, *The Pumilio protein binds RNA through a conserved domain that defines a new class of RNA-binding proteins.* RNA, 1997. **3**(12): p. 1421-33.
255. Ingolia, N.T., L.F. Lareau, and J.S. Weissman, *Ribosome profiling of mouse embryonic stem cells reveals the complexity and dynamics of mammalian proteomes.* Cell, 2011. **147**(4): p. 789-802.
256. Yoon, J.H., et al., *LincRNA-p21 suppresses target mRNA translation.* Mol Cell, 2012. **47**(4): p. 648-55.
257. Wang, P., et al., *The STAT3-binding long noncoding RNA lnc-DC controls human dendritic cell differentiation.* Science, 2014. **344**(6181): p. 310-3.
258. Liu, X., et al., *Long noncoding RNA BC005927 upregulates EPHB4 and promotes gastric cancer metastasis under hypoxia.* Cancer Sci, 2018. **109**(4): p. 988-1000.
259. Zhuo, W., et al., *Long Noncoding RNA GMAN, Up-regulated in Gastric Cancer Tissues, Is Associated With Metastasis in Patients and Promotes Translation of Ephrin A1 by Competitively Binding GMAN-AS.* Gastroenterology, 2019. **156**(3): p. 676-691 e11.
260. Gomez-Maldonado, L., et al., *EFNA3 long noncoding RNAs induced by hypoxia promote metastatic dissemination.* Oncogene, 2015. **34**(20): p. 2609-20.
261. Modarresi, F., et al., *Inhibition of natural antisense transcripts in vivo results in gene-specific transcriptional upregulation.* Nat Biotechnol, 2012. **30**(5): p. 453-9.
262. Weinberg, M.S. and K.V. Morris, *Long non-coding RNA targeting and transcriptional de-repression.* Nucleic Acid Ther, 2013. **23**(1): p. 9-14.
263. O'Reilly, D., et al., *Differentially expressed, variant U1 snRNAs regulate gene expression in human cells.* Genome Res, 2013. **23**(2): p. 281-91.
264. Joller, N. and V.K. Kuchroo, *Tim-3, Lag-3, and TIGIT.* Curr Top Microbiol Immunol, 2017. **410**: p. 127-156.
265. Oestreich, K.J., et al., *NFATc1 regulates PD-1 expression upon T cell activation.* J Immunol, 2008. **181**(7): p. 4832-9.
266. Wu, J. and H. Luo, *Recent advances on T-cell regulation by receptor tyrosine kinases.* Curr Opin Hematol, 2005. **12**(4): p. 292-7.
267. Freywald, A., et al., *EphA receptors inhibit anti-CD3-induced apoptosis in thymocytes.* J Immunol, 2006. **176**(7): p. 4066-74.
268. Yu, G., et al., *Ephrin-B1 is critical in T-cell development.* J Biol Chem, 2006. **281**(15): p. 10222-9.

269. Alfaro, D., et al., *EphrinB1-EphB signaling regulates thymocyte-epithelium interactions involved in functional T cell development.* Eur J Immunol, 2007. **37**(9): p. 2596-605.
270. Smith-Garvin, J.E., G.A. Koretzky, and M.S. Jordan, *T cell activation.* Annu Rev Immunol, 2009. **27**: p. 591-619.
271. Kim, E.H., et al., *Signal integration by Akt regulates CD8 T cell effector and memory differentiation.* J Immunol, 2012. **188**(9): p. 4305-14.
272. Chornoguz, O., et al., *mTORC1 Promotes T-bet Phosphorylation To Regulate Th1 Differentiation.* J Immunol, 2017. **198**(10): p. 3939-3948.
273. Nguyen, T.M., et al., *EphB and Ephrin-B interactions mediate human mesenchymal stem cell suppression of activated T-cells.* Stem Cells Dev, 2013. **22**(20): p. 2751-64.
274. Saha, N., et al., *Therapeutic potential of targeting the Eph/ephrin signaling complex.* Int J Biochem Cell Biol, 2018. **105**: p. 123-133.
275. Charmsaz, S. and A.W. Boyd, *Eph receptors as oncotargets.* Oncotarget, 2017. **8**(47): p. 81727-81728.
276. Rafiq, S., et al., *Targeted delivery of a PD-1-blocking scFv by CAR-T cells enhances anti-tumor efficacy in vivo.* Nat Biotechnol, 2018. **36**(9): p. 847-856.
277. Zhang, Q., et al., *Chimeric Antigen Receptor (CAR) Treg: A Promising Approach to Inducing Immunological Tolerance.* Front Immunol, 2018. **9**: p. 2359.
278. June, C.H., et al., *CAR T cell immunotherapy for human cancer.* Science, 2018. **359**(6382): p. 1361-1365.
279. Boutros, M., L.P. Brás, and W. Huber, *Analysis of cell-based RNAi screens.* Genome Biology, 2006. **7**(7): p. R66-R66.
280. Patro, R., et al., *Salmon provides fast and bias-aware quantification of transcript expression.* Nat Methods, 2017. **14**(4): p. 417-419.
281. Bhardwaj, V., et al., *snakePipes: facilitating flexible, scalable and integrative epigenomic analysis.* Bioinformatics, 2019. **35**(22): p. 4757-4759.
282. Love, M.I., W. Huber, and S. Anders, *Moderated estimation of fold change and dispersion for RNA-seq data with DESeq2.* Genome Biol, 2014. **15**(12): p. 550.
283. CoreTeam, R. *R: A language and environment for statistical computing.* 2013; Available from: http://www.R-project.org/.
284. Chen, E.Y., et al., *Enrichr: interactive and collaborative HTML5 gene list enrichment analysis tool.* BMC Bioinformatics, 2013. **14**: p. 128.

9 Abbreviations & Definitions

A

AB	Human serum type AB
ACT	Adoptive cell transfer
Akt	RAC-alpha serine/threonine-protein kinase (Protein kinase B)
APC	Antigen presenting cell
ASE	Antigen specific expansion
ATCC	American type culture collection
ATP	Adenosine triphosphate

B

BCL-2	B-cell lymphoma-2
BCL-xL	B-cell lymphoma-extra large
BD	Becton Dickinson
bp	Base pair
BSA	Bovine serum albumin

C

CAR	Chimeric antigen receptors
Casp	Caspase
CCR9	C-C chemokine receptor type 9
CD	Cluster of differentiation
cDNA	Complementary DNA
CEACAM6	Carcinoembryonic antigen related cell adhesion molecule 6
CLM	Complete lymphocyte medium
CO_2	Carbon dioxide
CREB	cAMP response element-binding protein
CSF	Cerebrospinal fluid
CTL	Cytotoxic T lymphocyte
CTLA-4	Cytotoxic T-lymphocyte protein 4

D

DC	Dendritic cell
DMEM	Dulbecco´s modified Eagle´s medium
DNA	Deoxyribonucleic acid

E

e. g.	Latin "exempli gratia" - "for example"
E:T	Effector to target ratio
EAE	Experimental autoimmune encephalomyelitis
ECL	Enhanced chemiluminescent
EDTA	Ethylenediaminetetraacetic acid
ELISA	Enzyme-linked Immunosorbent Assay
EMT	Epithelial-mesenchymal transition
Eph	Erythropoietin producing hepatocellular carcinoma receptor
Ephrin	Eph-related receptor tyrosine kinase ligand
et al.	Latin "et ali" - "and others"

F

FACS	Fluorescence-activated cell sorting
Fas	Fas cell surface death receptor/TNFRSF6
FasL	Fas ligand
FCS	Fetal calf serum
FDA	US Food and Drug Administration
FITC	Fluoerescein isothiocyanate
Fluc	Firefly luciferase
FluT	Flu-antigen specific CD8+ T cells

G

g	Gram
G418	Geneticin sulfate
GBM	Glioblastoma multiform
gDNA	Genomic DNA
GFP	Green fluorescent protein
GM-CSF	Granulocyte macrophage colony-stimulating factor
GPCR	G-protein coupled receptor

H

h	Hours
HEPES	4-(2-hydroxyethyl)-1-piperazineethanesulfonic acid
HLA	Human leukocyte antigen

HRP	Horseradish peroxidase
HTP	High-throughput

I

IDO	Indoleamine 2,3-dioxygenase
IgG	Immunoglobulin G
IgSF	Immunoglobulin super family
IL	Interleukin
IFNγ	Interferon-gamma
irAEs	Immune related adverse events
ITIM	Immunoreceptor Tyrosine-based inhibitory motif
ITSM	Immunoreceptor Tyrosine-based Switch Motif

J

JAK	Janus kinase
JNK	C-Jun N-terminal protein kinase

K

kb	Kilobase
KD	Knockdown
kDA	Kilodalton
KO	Knockout

L

L	Liter
LAG-3	Lymphocyte activation gene 3
Lck	Tyrosine-protein kinase Lck
LincRNA	Long intergenic RNA
LncRNA	Long non-coding RNA
LOESS	LOcal regrESSion
luc	Luciferase

M

M	Molar
mA	Milliampere
mAb	Monoclonal antibody

MACS	Magnetic-activated cell sorting
MAPK	Mitogen-activated protein kinase
MART-1	Melanoma-associated antigen recognized by T cells
MDSC	Myeloid-derived suppressor cell
MFI	Mean fluorescence intensity
mg	Milligram
MHC-I	Class I major histocompatibility molecules
MHC-II	Class II major histocompatibility molecules
MIL	Marrow infiltrating lymphocyte
min	Minutes
miRNA	Micro RNA
ml	Milliliter
MM	Multiple Myeloma
mM	millimolar
mRNA	Messenger RNA
MS	Multiple sclerosis
mTEC	Medullary thymic epithelial cells
mTOR	The mammalian target of rapamycin

N

NF-κB	Nuclear factor-kappa B
NFAT	Nuclear factor of activated T-cells
NK	Natural killer
NOD	Non-obese diabetic
ns	Not significant
nt	Nucleotide

O

OKT-3	Muronomab-CD3
OX40	TNFRSF4

P

p	Phosphorylation
P/S	Penicillin/Streptomycin
p53	Tumor protein p53
PAGE	Polyacrylamide gel electrophoresis

PBMC	Peripheral blood mononuclear cell
PBS	Phosphate buffer saline
PCR	Polymerase chain reaction
PD-1	Programmed death 1
PDAC	Pancreatic ductal adenocarcinoma
PD-L1	Programmed death ligand 1
PE	Phycoerythrin
pH	Latin "poteintia hydrogenii"
PI3K	Phosphatidylinositol-4,5-bisphosphate 3-kinase
PKC	Protein kinase C
PMA	Phorbol 12-myristate 13-acetate
PPMS	Primary progressive MS
PRMS	Progressive relapsing MS

Q

qPCR	Quantitative PCR

R

RA	Rheumatoid arthritis
RCI	Regensburg Center for Interventional Immunology
REP	Rapid expansion protocol
rHu	Recombinant human
RLU	Relative luminescence unit
RNA	Ribonucleic acid
RNAi	RNA interference
RNA-Seq	RNA sequencing
ROS	Reactive oxygen species
RRMS	Relapsing-remitting MS
RT	Room temperature

S

Scr	Scramble, non-coding siRNA sequence
SD	Standard deviation
SDS	Sodium dodecyl sulfate
SD	Standard deviation
SHP-2	SH2-domain containing tyrosine phosphatase 2

siCD	"Cell Death" siRNA cocktail
SIK3	Salt-inducible kinase 3
siRNA	Small interfering RNA
SLE	Systemic lupus erythematosus
SPMS	Secondary progressive MS
STAT	Signal transducer and activator of transcription

T

TRADD	TNFR-I-associated death domain protein
T1D	Type-I Diabetes
TAA	Tumor-associated antigen
TAE	Tris-Acetate-EDTA
TBS	Tris buffer saline
TBS-T	Tris-buffered saline with Tween 20
TCGA	The cancer genome atlas
Tcm	Central memory T cell
TCR	T cell receptor
Tem	Effector memory T cell
TGF-β	Transforming growth factor beta
Th	T helper
TIGIT	T cell immunoreceptor with Ig and ITIM domains
TILs	Tumor infiltrating lymphocytes
TIM-3	T cell immunoglobulin mucin 3
TKI	Tyrosine kinase inhibitor
™	Trademark
TME	Tumor microenvironment
TNF	Tumor necrosis factor
TNFRSF	TNF receptor superfamily members
TRAF	TNF receptor associated factor
TRAIL	TNF-related apoptosis inducing ligand
T_{reg}	Regulatory T cells

U

U	Unit
UBC	Ubiquitin C

UC	Ulcerative colitis
UV	Ultraviolet

V

V	Volt
VEGF	Vascular endothelial growth factor

W

WB	Western blot

X

X	X-fold

Other

α	Alpha
β	Beta
θ	Theta
β2m	β-2 microglobulin
γ	Gamma
δ	delta
κ	Kappa
%	Percentage
°C	Degree Celsius
µg	Microgram
µl	Microliter
µm	Micrometer
4-1BB	TNFRSF9